ACTA UNIVERSITATIS SZEGEDIENSIS

ACTA PHYSICA ET CHEMICA

NOVA SERIES

TOMUS XX

FASCICULI 1—2

AUSHAF 20(1—2) 1—188 (1974)
HU ISSN 0001—6721

SZEGED, HUNGARIA
1974

ACTA UNIVERSITATIS SZEGEDIENSIS

ACTA PHYSICA ET CHEMICA

NOVA SERIES

TOMUS XX

FASCICULI 1—2

AUSHAF 20(1—2) 1—188(1974)

HU ISSN 0001—6721

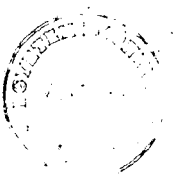

SZEGED, HUNGARIA
1974

Adiuvantibus

M. BARTÓK, L. CSÁNYI, P. FEJES, F. GILDE, P. HUHN, I. KETSKEMÉTY, F. MÁRTA, L. SZALAY et F. SZÁNTÓ

redigit

KÁLMÁN KOVÁCS

Edit

Facultas Scientiarum Naturalium Universitatis Szegediensis de Attila József nominate

Editionem curant

J. ANDOR, G. BERNÁTH et Á. SÜLI

Nota

Acta Phys. et Chem. Szeged

Szerkeszti

KOVÁCS KÁLMÁN

A szerkesztő bizottság tagjai:

BARTÓK M., CSÁNYI L., FEJES P., GILDE F., HUHN P., KETSKEMÉTY I., MÁRTA F., SZALAY L. és SZÁNTÓ F.

Kiadja

a József Attila Tudományegyetem Természettudományi Kara
(Szeged, Aradi Vértanúk tere 1.)

Szerkesztőbizottsági titkárok:

ANDOR J., BERNÁTH G. és SÜLI Á.

Kiadványunk rövidítése:
Acta Phys. et Chem. Szeged

EIN WEITERER BEITRAG ZU DEN QUANTENMECHANISCHEN UNTERSUCHUNGEN DES WASSERSTOFFMOLEKÜLS

Von

F. BERENCZ

Institut für Theoretische Physik der József-Attila-Universität
Szeged

(Eingegangen am 15. Dezember 1973)

Es wurde die Elektronenergie des tiefsten angeregten $1s2s\,^1\Sigma_g^+$-Zustandes des Wasserstoffmoleküls der Annahme gemäss berechnet, dass sie einer $(1\sigma_g 2\sigma_g)$-Bahn-Konfiguration entstammt und bei dem angeregten $2\sigma_g$-Zustand auch die Hybride der $2s$- und $2p$-Zustände erlaubt ist.

In einer früheren Arbeit [1] wurde die Elektronenenergie des tiefsten angeregten $1s2s^1\Sigma_g^+$-Zustandes des Wasserstoffmoleküls der Annahme gemäß berechnet, daß sie einer $(1\sigma_g 2\sigma_g)$-Bahn-Konfiguration entstammt, d.h. einer solchen Konfiguration, bei welcher sich das erste Elektron im Grundzustand und das zweite Elektron im angeregten Zustand befindet. Demgemäß haben die Molekülbahnen der einzelnen Elektronen nach der LCAO-MO-Methode die folgende Gestalt:

$$1\sigma_g(1) = [1s_A(1) + 1s_B(1)]/\sqrt{2(1+S_1)}, \tag{1}$$

$$2\sigma_g(2) = [2s_A(2) + 2s_B(2)]/\sqrt{2(1+S_2)}, \tag{2}$$

wo

$$S_i = \langle is_A | is_B \rangle, \quad i = 1, 2, \tag{3}$$

und is_A und is_B die Wasserstoffeigenfunktionen der is-Zustände sind. Die Eigenfunktion des $1s2s^1\Sigma_g^+$-Zustandes des Wasserstoffmoleküls nimmt also die folgende Gestalt an:

$$\psi = 1\sigma_g(1)2\sigma_g(2)\frac{1}{\sqrt{2}}(\alpha_1\beta_2 - \alpha_2\beta_1). \tag{4}$$

Auf Grund der Molekülbahn von (4) erhielten wir als Elektronenergie 0,68086 atomare Einheit.

In einer folgenden Arbeit [2] erweiterten wir die Molekülbahn von (4) durch den Korrelationsfaktor $(1+pr_{12})$ und mit der korrelationsmäßigen Molekülbahn von der Gestalt

$$\psi_{\text{Korr}} = 1\sigma_g(1)2\sigma_g(2)(1+pr_{12})\frac{1}{\sqrt{2}}(\alpha_1\beta_2 - \alpha_2\beta_1) \tag{5}$$

ergab sich für die Elektronenergie der Wert 0,70221 atomare Einheit.

R. S. MULLIKEN [3] und G. HERZBERG [4] haben aber darauf hingewiesen, daß bei dem angeregten $2\sigma_g$-Zustand auch die Hybride der $2s$- und $2p$-Zustände erlaubt ist. Demgemäß kann die Näherungsfunktion von folgender gestalt angenommen

werden:

$$\psi_{MH} = 1\sigma_g(1)2\sigma'_g(2)\frac{1}{\sqrt{2}}(\alpha_1\beta_2 - \alpha_2\beta_1), \tag{6}$$

wo

$$2\sigma'_g(2) = \{[2s_A(2)+2s_B(2)]+\lambda[2p_A(2)+2p_B(2)]\}/\sqrt{2[(1+S_2)+\lambda^2(1+S_3)}, \tag{7}$$

und

$$S_3 = \langle 2p_A|2p_B\rangle; \tag{8}$$

$2p_A$ und $2p_B$ sind die Wasserstoffeigenfunktionen der $2p$-Zustände.

Die Elektronenergie wurde in üblicher Weise auf Grund des Variationsverfahrens mit Minimalisierung der Energie erhalten. Bei der Berechnung der Molekülintegrale wurde die Methode von M. KOTANI [5] u. A. benützt. Bei λ=0,98765 ergab sich für die Elektronenergie der Wert 0,68456 atomare Einheit.

Ähnliche Berechnungen mit ähnlichen Ergebnissen sind auch bei J. T. ZUNG und A. B. F. DUNCAN [6] zu finden, aber mit dem Unterschied, daß ihre Berechnungen mit den von J. C. SLATER [7] eingeführten knotenlosen Eigenfunktionen durchgeführt wurden.

Die mit den Näherungsfunktionen (4), (5) und (6) erhaltenen Elektronenergien sollen miteinander verglichen werden.

Nach (4) und (5) kann festgestellt werden, daß auf Grund der Erweiterung der Molekülbahn (4) durch den Korrelationsfaktor $(1+pr_{12})$ sich eine energiekorrektion mit dem Wert von 0,02135 atomare einheit ergibt. Von (4) und (6) kann es aber konstatiert werden, daß durch die Einführung der Hybride der $2s$- und $2p$-Zustände bei dem angeregten $2\sigma_g$-Zustand nur eine Energiekorrektion mit dem Wert von 0,00370 atomare Einheit auftritt. Diese letztere ist also um eine Größenordnung kleiner als die vorige. Aus dieser Tatsache kann wieder die Schlußfolgerung gezogen werden, — wie wir schon mehrmals festgestellt haben — daß der Korrelationsfaktor $(1+pr_{12})$ bei dem Aufbau der Näherungsfunktionen eine sehr wichtige Rolle spielt.

* * *

Fräulein A. BOLDIZSÁR möchte ich für Hilfe bei den numerischen Rechnungen auch an dieser Stelle meinen Dank aussprechen.

Literatur

[1] *Berencz, F:* Acta Phys. Hung. **16**, 49 (1963).
[2] *Berencz, F:* Acta Phys. Hung. **27**, 131 (1969).
[3] *Mulliken, R. S:* Revs. Modern Phys. **4**, 63 (1932).
[4] *Herzberg, G:* Spectra of Diatomic Molecules, D. Van Nostrand Company, Inc., Princeton, New Jesey, 1950.
[5] *Kotani, M., A. Amemya, T. Simose:* Proc. Phys. Mat. Soc. Japan **20**, extra No 1, (1938); **22**, extra No. 1940.
[6] *Zung, J. T., A. B. F. Duncan:* J. Chem. Phys. **36**, 2140 (1962).
[7] *Slater, J. C:* Phys. Rev **36**, 57 (1930).

НОВЫЙ ВКЛАД В КВАНТОВОМЕХАНИЧЕСКИЕ ИССЛЕДОВАНИЯ МОЛЕКУЛЫ ВОДОРОДА

Ф. Беренц

Определяется электронная энергия первого возбужденного состояния $1s\,2s\,{}^1\Sigma_g^+$ молекулы водорода предполагая что она возникает из орбитальной конфигурации $(1\sigma_g\,2\sigma_g)$ и при возбужденном состоянии $2\sigma_g$ гибрид состояний $2s$ и 2_p тоже допущен.

SEMI-EMPIRICAL MOLECULAR ORBITAL CALCULATIONS OF BINUCLEAR COBALT COMPLEXES

By
V. MARÁZ
Institute of Theoretical Physics, Attila József University, Szeged

(Received December 15, 1973)

In this paper the energy levels, molecular orbitals, orbital and bond overlap populations and transitions of the $[(NH_3)_4Co(OH)_2Co(NH_3)_4]^{4+}$ and of the $[(NH_3)_3Co(OH)_3Co(NH_3)_3]^{3+}$ binuclear complex ions are calculated by the LCAO-MO method using the half-empirical formula of WOLFSBERG and HELMHOLTZ.

The binuclear complex compounds $[(NH_3)_4Co(OH)_2Co(NH_3)_4]^{4+}$ (denoted in the following by K_1) and $[(NH_3)_3Co(OH)_3Co(NH_3)_3]^{3+}$ (K_2) are theoretically investigated by a simple semiempirical LCAO-MO method. In these complexes the central cobalt ions are surrounded by ligands of approximately "bi-octahedral" symmetry (D_{2h} and D_{3h}). The two octahedra have in the case of K_1 a common edge and in the case of K_2 a common face. The Co ions are in the centres of the octahedra, the OH ions are along the common edge (K_1) and along the common face (K_2), and the NH_3 molecules are on the other vertices of the octahedra. If we disregard the distortions of the octahedra on the basis of Pauling's ions radii [1] we obtain 1,88 Å, 1,92 Å and 2,66 Å for the bond distances of Co-O, Co-N and Co-Co bonds, respectively.

Computational details

In the calculations we neglect the influences of the H atoms on the complex compounds and we do not take into account the electrons in the closed shells of Co, O and N atoms, taking into account only the six valence electrons of the Co ions, the four valence electrons of the OH ions and the two valence electrons of the NH_3 molecules (36 electrons for each of both complexes). For the LCAO-MO treatment of complex ions we take into account the five $3d$, one $4s$ and three $4p$ atomic orbitals of Co atoms, the three $2p$ orbitals of O atoms and one $2p$ orbital of N atoms. The $2p$ and $3d$ atomic orbitals are represented by SLATER type orbitals, and the radial wave function of $4s$, $4p$ orbitals is approximated by

$$\psi_{\text{approx}} = \sum_{k=1}^{4} c_k r^k e^{-\alpha r}$$

where $\alpha = 2.60$ and

$$c_1 = -0.047\,530\,507$$
$$c_2 = 0.360\,145\,640$$
$$c_3 = 0.728\,294\,860$$
$$c_4 = -0.041\,616\,865$$

The coefficients c_k are calculated from the equation

$$\int (\psi - \psi_{\text{approx}})^2 d\tau = \min.$$

where ψ is a SLATER type $4s$, $4p$ radial wave function.

The energy levels and molecular orbitals have been calculated by means of group theoretical considerations, which give

$$\Gamma_1 = 7A_{1g} + 7B_{1u} + 4B_{2g} + 4B_{3u} + 4B_{2u} + 3B_{3g} + 2B_{1g} + A_{1u}$$

$$\Gamma_2 = 6E' + 5E'' + 5A_1' + 5A_2'' + A_2'$$

reducible representations for the complexes. The bases of the irreducible representations are presented in Table I.

The group overlap integrals S_{ij} have been calculated exactly, the group integrals

Table I (K_1)

	Co	O	N
A_{1g}	$d_{z^2}(1)+d_{z^2}(2)$ $d_{x^2-y^2}(1)+d_{x^2-y^2}(2)$ $s(1)+s(2)$ $p_z(1)+p_z(2)$	$p_x(1)+p_y(1)+p_x(2)+p_y(2)$	$p_z(1)+p_z(2)+p_z(3)+p_z(4)$ $p_z(5)+p_z(6)+p_z(7)+p_z(8)$
A_{1u}	$d_{xy}(1)+d_{xy}(2)$		
B_{1g}	$d_{xy}(1)-d_{xy}(2)$	$p_z(1)+p_z(2)$	
B_{1u}	$d_{z^2}(1)-d_{z^2}(2)$ $d_{x^2-y^2}(1)-d_{x^2-y^2}(2)$ $s(1)-s(2)$ $p_z(1)-p_z(2)$	$-p_x(1)+p_y(1)-p_x(2)+p_y(2)$	$p_z(1)+p_z(2)-p_z(3)-p_z(4)$ $p_z(5)+p_z(6)-p_z(7)-p_z(8)$
B_{2g}	$d_{xz}(1)-d_{xz}(2)$ $p_x(1)-p_x(2)$	$-p_x(1)+p_y(1)+p_x(2)-p_y(2)$	$p_z(1)-p_z(2)+p_z(3)-p_z(4)$
B_{2u}	$d_{yz}(1)-d_{yz}(2)$ $p_y(1)-p_y(2)$	$p_z(1)-p_z(2)$	$p_z(5)-p_z(6)-p_z(7)+p_z(8)$
B_{3g}	$d_{yz}(1)+d_{yz}(2)$ $p_y(1)+p_y(2)$		$p_z(5)-p_z(6)+p_z(7)-p_z(8)$
B_{3u}	$d_{xz}(1)+d_{xz}(2)$ $p_x(1)+p_x(2)$	$p_x(1)+p_y(1)-p_x(2)-p_y(2)$	$p_z(1)-p_z(2)-p_z(3)+p_z(4)$

Table I (K_2)

	Co	O	N
A_1'	$d_{z^2}(1)+d_{z^2}(2)$ $s(1)+s(2)$ $p_z(1)+p_z(2)$	$p_x(1)+p_y(1)+p_x(2)+$ $+p_y(2)+p_x(3)+p_y(3)$	$p_z(1)+p_z(2)+p_z(3)+$ $+p_z(4)+p_z(5)+p_z(6)$
A_2'		$p_z(1)+p_z(2)+p_z(3)$	
A_2''	$d_{z^2}(1)-d_{z^2}(2)$ $s(1)-s(2)$ $p_z(1)-p_z(2)$	$p_x(1)+p_x(2)+p_x(3)-$ $-p_y(1)-p_y(2)-p_y(3)$	$p_z(1)+p_z(2)+p_z(3)-$ $-p_z(4)-p_z(5)-p_z(6)$
E'	$d_{x^2-y^2}(1)+d_{x^2-y^2}(2)$ $d_{xz}(1)+d_{xz}(2)$ $p_x(1)+p_x(2)$	$-2p_x(1)-2p_y(1)+p_x(2)+$ $+p_y(2)+p_x(3)+p_y(3)$ $p_z(3)-p_z(2)$	$p_z(2)+p_z(3)+p_z(5)+$ $+p_z(6)-2p_z(1)-2p_z(4)$
	$d_{xy}(1)-d_{xy}(2)$ $d_{yz}(2)-d_{yz}(1)$ $p_y(2)-p_y(1)$	$p_x(2)+p_y(2)-p_x(3)-p_y(3)$ $p_z(2)+p_z(3)-2p_z(1)$	$p_z(3)+p_z(6)-p_z(2)-p_z(5)$
E''	$d_{xy}(1)+d_{xy}(2)$ $d_{yz}(1)+d_{yz}(2)$ $p_y(1)+p_y(2)$	$p_x(2)+p_y(3)-p_y(2)-p_x(3)$	$p_z(2)+p_z(6)-p_z(3)-p_z(5)$
	$d_{x^2-y^2}(2)-d_{x^2-y^2}(1)$ $d_{xz}(1)-d_{xz}(2)$ $p_x(1)-p_x(2)$	$2p_x(1)-2p_y(1)-$ $-p_x(2)-p_x(3)+p_y(2)+p_y(3)$	$p_z(2)+p_z(3)-p_z(5)-$ $-p_z(6)-2p_z(1)+2p_z(4)$

$H_{ij}(i\neq j)$ have been determined by the approximation formula of WOLFSBERG and HELMHOLTZ [2]

$$H_{ij} = 0{,}5F_xS_{ij}(H_{ii}+H_{jj}),$$

where the empirical factor F_x was chosen to be 2.20 for σ bonds and 2.62 for π bonds [3]. The integrals H_{ii} were substituted by the ionization potentials: in the case of Co ions for $4s$ orbitals -7.84 eV, for $4p$ orbitals -4.08 eV, for $3d$ orbitals -9.38 eV [4], in the case of NH_3 molecules for $2p$ orbitals -13.81 eV and in the case of OH for $2p\sigma$ orbitals -11.24 eV and for $2p\pi$ orbitals -10.54 eV [5], respectively.

Results and discussion

The energy values of the MO's are summarized in Table II. The 36 electrons occupy these energy levels according to Pauli's principle. In the ground state of the complexes the highest filled MO of K_1 is $2b_{2u}$ (-8.357 eV), that of K_2 is $3e''$ (-9.208 eV). The lowest empty MO's are $1b_{1g}$ and $3e'$, respectively. On the basis

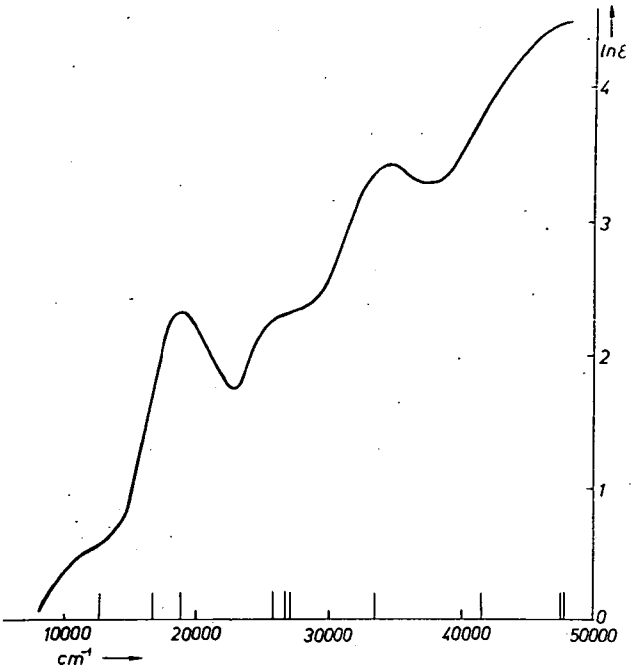
lnε
4
3
2
1
0
10000
20000
30000
40000
50000
cm⁻¹

Fig. 1

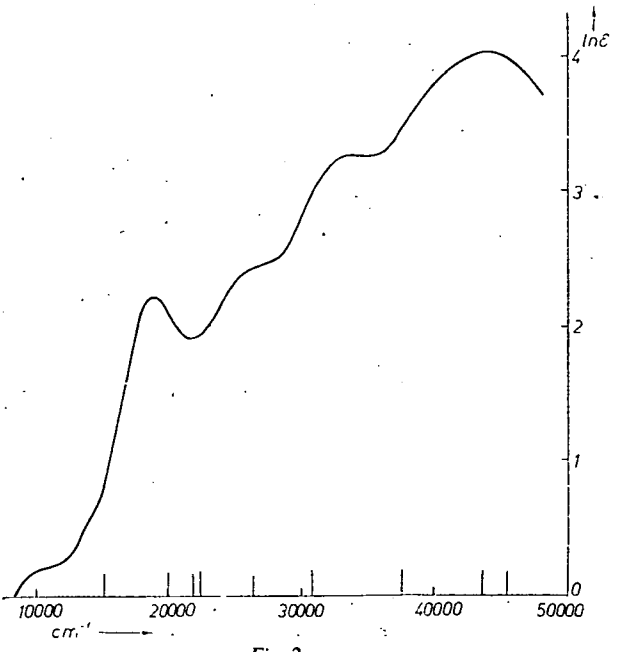
lnε
4
3
2
1
0
10000
20000
30000
40000
50000
cm⁻¹

Fig. 2

of Bohr's frequency rule the allowed electron transitions can be easily calculated with respect to the selection rules summarized in Table III. The most important transitions (in cm^{-1}) are given in Table IV. and are indicated in Figs. 1 and 2, which show the experimental absorption spectra of the complexes [6]. The figures show that the agreement between the experimental and theoretical results is fairly good.

Table II

K_1

A_{1g}	B_{1u}	B_{2g}	B_{3u}	B_{2u}	B_{3g}	B_{1g}	A_{1u}
−0.259	+59.168	+3.940	−3.373	−1.561	+1.881	−8.344	−9.343
−6.004	−1.417	−6.021	−7.211	−8.357	−9.110	−11.374	
−6.766	−5.905	−12.264	−11.919	−11.927	−14.136		
−9.275	−8.328	−14.718	−14.754	−14.107			
−12.622	−12.160						
−14.883	−14.794						
−15.331	−15.207						

K_2

A_1'	A_2'	A_2''	E'	E''
+1.158	−10.54	+49.096	−2.886	+2.375
−5.772		−0.315	−6.723	−5.953
−9.470		−8.472	−8.670	−9.208
−12.881		−11.920	−11.368	−12.328
−15.199		−14.923	−12.185	−14.679
			−14.678	

Table III

K_1

$A_{1g} \leftrightarrow B_{1u}$	$A_{1u} \leftrightarrow B_{2g}$	$B_{1g} \leftrightarrow B_{2u}$
$A_{1g} \leftrightarrow B_{2u}$	$A_{1u} \leftrightarrow B_{3g}$	$B_{2u} \leftrightarrow B_{3g}$
$A_{1g} \leftrightarrow B_{3u}$	$B_{2g} \leftrightarrow B_{3u}$	$B_{1u} \leftrightarrow B_{3g}$
$A_{1u} \leftrightarrow B_{1g}$	$B_{1g} \leftrightarrow B_{3u}$	$B_{1u} \leftrightarrow B_{2g}$

K_2

$A_1' \leftrightarrow A_2''$	$E' \leftrightarrow E'$	$A_2' \leftrightarrow E'$
$A_1' \leftrightarrow E'$	$E' \leftrightarrow E''$	$A_2'' \leftrightarrow E''$
	$E'' \leftrightarrow E''$	

Table IV

K_1		K_2	
7 641	27 190	5 938	22 164
12 840	33 588	6 455	26 262
16 653	41 572	8 052	30 797
18 988	47 583	15 088	37 477
25 857	47 616	20 050	43 690
26 803	47 720	21 768	45 150

Table V (K_1)

MO	energy (eV)	Co			O	N
		3d	4s	4p	2p	2p
$1b_{3u}$	−3.373	22	0	38	10	30
$3b_{1u}$	−5.905	44	1	3	16	36
$2a_{1g}$	−6.004	41	12	7	2	38
$2b_{2g}$	−6.021	40	0	7	24	30
$3a_{1g}$	−6.766	21	18	7	33	20
$2b_{3u}$	−7.211	34	0	18	34	14
$4b_{1u}$	−8.328	57	4	2	25	12
$1b_{1g}$	−8.344	59	0	0	41	0
$2b_{2u}$	−8.357	50	0	10	32	8
$2b_{3g}$	−9.110	89	0	5	0	6
$4a_{1g}$	−9.275	62	9	7	12	10
a_{1u}	−9.343	100	0	0	0	0
$2b_{1g}$	−11.374	39	0	0	60	0
$3b_{3u}$	−11.919	15	0	4	58	24
$3b_{2u}$	−11.928	32	0	8	45	14
$5b_{1u}$	−12.160	23	5	3	51	18
$3b_{2g}$	−12.264	14	0	11	60	16
$5a_{1g}$	−12.622	18	7	8	48	20
$4b_{2u}$	−14.107	2	0	10	4	84
$3b_{3g}$	−14.136	0	0	12	0	88
$4b_{2g}$	−14.718	19	0	5	8	68
$4b_{3u}$	−14.753	20	0	4	11	66
$6b_{1u}$	−14.794	15	9	4	8	64
$6a_{1g}$	−14.883	19	7	2	7	66
$7b_{1u}$	−15.207	19	12	0	1	68
$7a_{1g}$	−15.331	12	15	2	3	68

In Table V the atomic orbital percentage of occupied and of some empty molecular orbitals are listed, and in Table VI the total gross populations on atoms [7] are summarized. Table VII shows the subtotal overlap populations between atoms.

According to these results the first and the second bands arise from Co-O bonding orbitals $2b_{2u}$, $2b_{3g}$, $3e''$ in both complexes and the remaining two bands are assigned according to our calculations to the MO's $2b_{1g}$, $3b_{3u}$, $4a_{1g}$, a_2', $4e'$ respectively, which are mainly of Co-O bonding character and correlate with O orbitals in origin. The orbital and bond overlap populations are similar in both complexes, but in the case of K_1 the orbital population on Co $3d$ orbital is higher than in the case of K_2 and the overlap population between Co atoms in the case of K_1 is less than that of K_2. The electron charge densities on Co atoms are also higher in K_1 than in K_2. According to our calculations the resultant electron configurations of Co atoms are

$$(3d)^{5.5}(4s)^{0.6}(4p)^{0.6} \quad \text{for} \quad K_1 \quad \text{and} \quad (3d)^{4.6}(4s)^{0.8}(4p)^{0.6} \quad \text{for} \quad K_2.$$

* * *

The author wishes to express his thanks to Dr. F. J. GILDE, Director of the Institute of Theoretical Physics, for helpful discussions

Table V (K_2)

MO	energy (eV)	Co			O	N
		3d	4s	4p	2p	2p
$2a_1'$	−5.772	16	17	6	41	20
$7e''$	−5.953	43	0	7	24	26
$2e''$	−5.953	46	0	7	22	24
$8e'$	−6.723	25	0	5	42	18
$2e'$	−6.723	34	0	4	42	20
$3a_2''$	−8.472	52	4	1	31	12
$9e'$	−8.670	48	0	13	30	8
$3e'$	−8.670	49	0	13	29	10
$3e''$	−9.208	84	0	1	10	6
$8e''$	−9.208	82	0	1	11	6
$3a_1'$	−9.470	44	26	10	6	14
a_2'	−11.24	0	0	0	100	0
$4e'$	−11.368	13	0	4	70	14
$10e'$	−11.368	13	0	4	71	12
$4a_2''$	−11.920	12	8	2	64	14
$5e'$	−12.185	24	0	6	56	14
$11e'$	−12.185	25	0	6	56	12
$4e''$	−12.328	20	0	9	53	18
$9e''$	−12.328	19	0	8	55	18
$4a_1'$	−12.881	14	5	8	50	22
$6e'$	−14.678	22	0	3	10	66
$12e'$	−14.678	24	0	3	10	62
$5e''$	−14.679	24	0	4	10	62
$10e''$	−14.679	22	0	4	10	64
$5a_2''$	−14.923	4	13	5	14	70
$5a_1'$	−15.199	7	16	4	12	62

Table VI

	Co	O	N
K_1	6.673	4.574	1.688 and 1.692
K_2	5.906	4.684	1.689

Table VII

	Co–Co	Co–O	Co–N
K_1	0.178	0.387	0.277 and 0.278
K_2	0.327	0.369	0.273

References

[1] *Pauling, L.:* The Nature of the Chemical Bond. Cornell University Press, New York, 1939.
[2] *Wolfsberg, M., L. Helmholtz:* J. Chem. Phys. **20**, 837 (1952).
[3] *Gilde, F.:* Dissertation, Szeged, 1958.
[4] *Landolt—Börnstein:* Zahlenwerte und Funktionen. Atom und Molekularphysik I (Springer, Berlin, 1954.)
[5] *Mulliken, R. S.:* J. Chem. Phys. **2**, 792 (1934).
[6] *Császár, J.:* Private communication.
[7] *Fraga, S., G. Malli:* Many-Electron Systems: Properties and Interactions W. B. Saunders Company, Philadelphia, London and Toronto, 1968.

ПОЛУЭМПИРИЧЕСКИЕ ВЫЧИСЛЕНИЯ НА ДВУЯДЕРНЫХ КОМПЛЕКСАХ КОБАЛЬТА МЕТОДОМ МОЛЕКУЛЯРНЫХ ОРБИТ

В. Мараз

В данной работе рассчитаны энергии, молекулярные орбиты, орбитальные и перекрытные популации и электронные переходы с помощью метода ЛКАО-МО с использованием полуэмпирической формулы Волфсберга — Гельмгольца.

WOLFSBERG—HELMHOLTZ CALCULATIONS ON $[Fe(phen)_3]^{2+}$ AND $[Fe(phen\text{-}(OH)_2)_3]^{2+}$ COMPLEXES

By

GY. PAPP

Institute of Theoretical Physics, Attila József University, Szeged, Hungary

(Received December 15, 1973)

WOLFSBERG—HELMHOLTZ calculation has been performed for $[Fe(phen)_3]^{2+}$ and $[Fe(phen\text{-}(OH)_2)_3]^{2+}$ complexes. The bond between the metal and the ring and the modification caused by the OH radicals built in have been studied in this approximation.

In this paper we attempt to move one step forward in understanding the electronic structure of $[Fe(phen)_3]^{2+}$ and $[Fe(phen\text{-}(OH)_2)_3]^{2+}$. The molecules have significance in redox processes; $[Fe(phen)_3]^{2+}$ is applicable as a redox indicator. During the past years a model, known as the extended HÜCKEL model, or the WOLFSBERG—HELMHOLTZ model [1] has been used to study the molecular orbitals of all electrons in large molecules. The molecules we are dealing with are complicated, so we must neglect a great number of orbitals, especially the σ orbitals of C atoms and the s orbitals of H atoms.

Method

We try to find the solution of the equation

$$H_{\text{eff}}\psi_j = \varepsilon_j\psi_j$$

where the MO-s ψ_j are expanded in the minimal system of atomic orbitals:

$$\psi_j = \sum_p \varphi_p c_{pj}$$

The MO energies ε_j and the coefficients c_{pj} are solutions of the equation

$$\mathbf{Hc} = \varepsilon\mathbf{Sc} \tag{1}$$

In Eq. (1) **H** and **S** are the matrices of the effective Hamiltonian and the so-called overlap matrix, with the matrix elements

$$H_{pq} = (\varphi_p, H_{\text{eff}}\varphi_q), \quad S_{pq} = (\varphi_p, \varphi_q),$$

respectively. Instead of the calculated values, WOLFSBERG and HELMHOLTZ [1] suggested to use the ionization potential values of the atomic orbitals φ_p of the free atom for the diagonal elements H_{pp}, and the values

$$\frac{1}{2}KS_{pq}(H_{pp}+H_{qq})$$

for the off-diagonal elements H_{pq}, where K is an appropriate interaction parameter.

We expand ψ_j in terms of five $3d$, one $4s$ and three $4p$ orbitals of the central ion and one $2s$, two $2p$ orbitals of N atoms, as well as of the $2p_z$ orbitals of C and O atoms.

Model and geometry

The $[Fe(phen)_3]^{2+}$ complex ion is formed by a central Fe^{++} ion and by three phenantroline molecules (Fig. 1). The nitrogens of phenantroline molecules (A, B

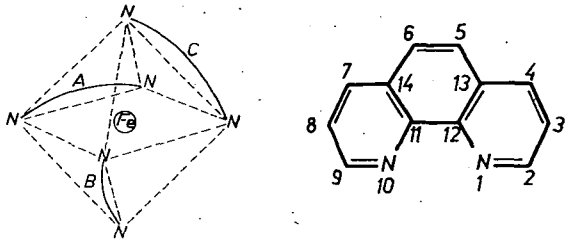

Fig. 1. Schematic structure of iron-phenantroline

and C) in position 1 and 10 occupy the vertices of the octahedra around the central ion. In the other ion, *i. e.* in the $[Fe(phen\text{-}(OH)_2)_3]^{2+}$ complex, the hydrogens bonded to C atoms in position 4 and 7 of the phenantroline molecules are substituted by OH radicals.

X-ray diffraction studies [2] led to a bond distance of 1.97 Å between metal and nitrogen. We assumed the C-C, C-N distances to be 1.39 Å, and the C-O distance 1.08 Å. Numerical calculations have been done by means of a MINSK-22 computer. In order to reduce computation time we have taken into account the symmetry properties of the molecules [3]. The symmetry group of molecules considered is D_3.

Choice of parameters

For computing the overlap integrals we have used single orbitals of SLATER type:

$$\varphi(n, l, m) = Nr^{n-1} \exp(-\xi r) Y_l^m(\Theta, \Phi)$$

where N is a normalizing coefficient, n is the effective quantum number, which can be determined according SLATER's prescription and ξ is a parameter depending on the nuclear charge. CLEMENTI [4] proposed for ξ a higher value than that of SLATER. Computations by ZERNER and GOUTERMAN [5] for systems physically similar to our molecules have shown that a very satisfactory picture of the ligand field can be obtained by the following choice of ξ (Table I). These values of ξ lie between those given by SLATER and CLEMENTI. Using the parameter values of Table I, we have computed the overlap integrals shown in Table II.

Table I

*Basis Set Exponentials**

	s	*p*	*d*
Fe	1.370	1.370	2.722
N	1.9237	1.9170	
C		1.5679	
O		1.2266	

* Ref. [5]

Table II

Overlap integrals

Overlap Type	$(2s, 4s)$	$(2p_\sigma, 4s)$	$(2p_\sigma, 3d_{z^2})$	$(2s, 3d_{x^2-y^2})$	$(2p_\sigma, 3d_{x^2-y^2})$
	0.38808	0.25276	0.03882	0.04903	0.06743
Overlap Type	$(2s, 3d_{z^2})$	$(2p_z, 3d_{xz})$	$(2p_\pi^C, 2p_\pi^N)$	$(2p_\pi^C, 2p_\pi^C)$	$(2p_\pi^C, 2p_\pi^O)$
	0.02567	0.02682	0.2249	0.25102	0.2409

Table III

H_{pp} for Fe, N, C *and* O* *Potential in* eV

	s	*d*	*d*
Fe	$d^6s^2 \rightarrow d^6s - 7.90$	$d^6sp \rightarrow d^6s - 4.55$	$d^6s^2 \rightarrow d^5s^2 - 10.82$
N	$s^2xyz \rightarrow sxyz - 25.17$	$s^2xyz \rightarrow s^2xy + (p) - 14.158$	
C		$s^2xyz \rightarrow s^2xy + (p) - 11.316$	
O		$s^2x^2yz \rightarrow s^2xyz + (p) - 15.863$	

* Numbers in this table are from Ref. [8]

The ionization potentials of valence electrons of the free atoms used in the calculations are presented in Table III. HOFFMANN [6] proposed the value 1,75 for the interaction parameter, and we accept the same value for the π-π bond. For the H_{pq} values between central ion and nitrogen we used $K=1.89$ [5].

Results

The formation of metal-phenantroline bond mainly depends on the atoms of phenantroline. Comparing the obtained energies of orbitals (Tables IV and V), it can seen that the substitution of OH radicals results in changes in the energies of the E orbitals.

By means of the components c_{pj} obtained from the matrix equation, a so-called population analysis [7] has been performed. Results are presented in Tables VI and VII.

The π electron densities at the N atom are 1.3225 and 1.4081 in the first and second molecule, respectively. The electron density at O atoms is 1.7815, the values for C atoms are shown in Table VIII.

Table IV

Molecular-orbital energies of $[Fe(phen)_3]^{2+}$ *in* eV

A_1	A_2	E	
−25.3341	−25.1618	−25.2342	−10.8936
−15.1388	−15.9441	−25.1613	−10.8183
−14.1521	−14.8581	−15.9928	−10.6337
−13.3673	−14.3211	−15.2817	−9.7981
−12.4468	−13.3619	−15.0711	−7.8781
−11.1087	−10.4607	−14.2339	−7.6562
−10.6681	−9.4342	−14.1611	−6.2707
−8.8528	−7.4593	−13.7598	−4.5182
−7.5032	−2.7258	−13.6096	−4.2295
−2.4381	−1.7348	−12.8571	−0.6301
−0.3861		−12.1058	

Table V

Molecular-orbital energies of $[Fe\ (phen\text{-}(OH)_2)_3]^{2+}$ *in* eV

A_1	A_2	E	
−25.3341	−25.21618	−25.4491	−12.0464
−16.7525	−16.8557	−25.1638	−10.7329
−15.1349	−15.8484	−16.7668	−10.6108
−14.1521	−14.6166	−16.7652	−10.5605
−12.6964	−14.3211	−15.9927	−9.2405
−12.8428	−13.0487	−15.2458	−7.6264
−12.4212	−11.2148	−15.0678	−7.4691
−10.6868	−8.5651	−14.2533	−6.2054
−10.6681	−7.4574	−14.1613	−3.0532
−8.1227	−2.7258	−13.6141	−2.9192
−7.4796	−0.3384	−12.9563	−0.4106
−0.3861		−12.2662	

Table VI

Total electronic populations of $[Fe\ (phen)_3]^{2+}$

Fe_2+	$4s$	$4p$	$3d$	Total	Net
	0.453	0.0893	5.8074	6.3497	+0.3497
N	$2s$	$2p_\sigma$	$2p_\pi$		
	1.8653	1.8925	1.3235	5.0813	+0.0813

Table VII

Total electronic populations of $[Fe\ (phen\text{-}(OH)_2)_3]^{2+}$

Fe_2+	4*s*	4*p*	3*d*	Total	Net
	0.453	0.0568	5.7437	6.2535	+0.2535
N	2*s*	$2p_\sigma$	$2p_\pi$		
	1.8048	1.8719	1.4081	5.1848	+0.1848

Table VIII

π electron densities of C′ atoms

	$C_{(2)}$	$C_{(3)}$	$C_{(4)}$	$C_{(5)}$	$C_{(11)}$	$C_{(13)}$
$[Fe\ (phen)_3]^{2+}$	1.0156	0.9566	0.9907	0.9793	1.0186	0.9713
$[Fe\ (phen\text{-}(OH)_2)_3]^{2+}$	0.9944	1.0712	0.7168	1.0181	0.9634	0.9724

As it can be seen, the charge density at nitrogens is transferred to the π orbitals, a more intensive part in the bonds. 4*s* orbitals of Fe^{++} have a considerable charge density in both cases. Substitution of the OH radicals is indicated by the changes in the charge density of the surrounding C atoms, as well as in the distribution of 3*d* and 4*p* orbitals of the Fe^{++} ion.

***

We are indebted to Dr. F. J. Gilde for his kind interest and valuable discussions.

References

[1] *Wolfsberg, M. L. Helmholtz:* J. Chem. Phys. **20**, 837 (1952).
[2] *Templeton, D. H., A. Zalkin, T. Ueki:* Acta Crystallographica **21**, A 154 (1966).
[3] *Papp Gy.:* Doctoral dissertation, Szeged, 1973 (in Hungarian).
[4] *Clementi, E., D. L. Raimondi:* J. Chem. Phys. **38**, 2686 (1963).
[5] *Zerner, M., M. Gouterman:* Theoret. chim. Acta (Berlin) **4**, 44 (1966).
[6] *Hoffmann, R.:* J. Chem. Phys. **39**, 1937 (1963).
[7] *Mullikan, R. S.:* J. Chem. Phys. **23**, 1883 (1955).
[8] *Pilcher, G. H. A. Skinner:* J. Inorg. Nucl. Chem. **24**, 937 (1962).

ВЫЧИСЛЕНИЕ ПО ВОЛФСБЕРГУ—ГЕЛЬМГОЛЬЦУ НА КОМПЛЕКСАХ $[Fe(phen)_3]^{2+}$ и $[Fe(phen\text{-}(OH)_2)_3]^{2+}$

Г. Папп

Мы провели вычисление по Волфсбергу—Гельмгольцу на комплексах $[Fe(phen)_3]^{2+}$ и $[Fe(phen\text{-}(OH)_2)_3]^{2+}$. При таком приближении исследовали связь между металлом и кольцами, и какие изменения дает в распределении электронов встроение радикалов OH.

THE VIBRATIONAL TEMPERATURE OF ORGANIC MOLECULES AND THE RELATIONSHIP BETWEEN ABSORPTION AND FLUORESCENCE SPECTRA IN SOLUTIONS

By

A. RINGLER and L. SZALAY

Institute of Biophysics, Attila József University, Szeged

(Received January 22, 1974)

The vibrational temperature as a function of the band widths and the Stokes-shift was determined for electron exitation spectra of Gaussian distribution in case of mirror simmetry of different kinds and of asimmetry of absorption and fluorescence. An approximate formula is given for the rapid determination of the vibrational temperature from the spectrum characteristics.

Introduction

If complicated molecules are optically excited with frequencies greater than those of the pure electronic transition, the excess energy is degraded by radiationless processes and may appear as local heat; this can cause translational diffusion of the photodissociation products [1], rotational diffusion in condensed systems [2], change in the "photoorientation" of molecules excited by polarized light [3] and the depolarization of fluorescence in solutions [4]. ALBRECHT [5] suggested a very quick dissipation of the local heat while JABŁOŃSKI [6] assumed a quick and a slow mechanism of dissipation, in the picosecond and the nanosecond range, respectively. KOZMA *et. al.* [7] offered a thermodynamical interpretation of the dissipation of heat, assuming a weak thermal interaction between the "hot", excited molecule and its environment. This approach has been corroborated by studying the dependence of the local heat on temperature [8] and solvent [9].

The problem of local heat around a "hot", excited molecule in solution is closely connected with a relationship between the absorption $k(\nu)$ and fluorescence energy spectra $f_e(\nu)$ already studied several decades ago [10]. The following form of this relationship was proposed by STEPANOV [11]:

$$f_e(\nu)/k(\nu) = D(T)\,\nu^3 \exp(-h\nu/kT) \tag{1}$$

where $D(T)$ is a constant independent of the frequency of light ν, T is the temperature of the solution, and h and k are the Planck and Boltzmann constants, respectively. KETSKEMÉTY *et. al.* [12] gave a more generally valid formula containing also the frequency-dependent relative yield of fluorescence and the refractive index of the solution. The relationship was studied by several authors [13], and found to be valid. However, in the majority of cases, the temperature T^* calculated from equation (1) in the knowledge of the other quantities was higher than the ambient tempera-

ture T originally introduced into (1). The higher temperature was explained by assuming that a part of the excess electronic excitation energy is not transferred to the environment within the mean life-time of the excited state. In vapours this occurs very easily and permits the vibrational specific heat to be determined experimentally [14]. Since a T^* higher than T is obtained from (1) in many cases, the distribution of the molecules among the different vibrational levels in these cases corresponds to a local or vibrational temperature T^*. Therefore, the excited molecules act as "thermometers", revealing the vibrational temperature at the instant of emission. The reading of this molecular temperature indicator is given in (1) through the shapes, the overlap and the relative intensity distributions of the fluorescence and absorption spectra.

In this paper the influence of the band widths and the Stokes-shifts of the fluorescence and absorption spectra on the local temperature was studied for different model systems.

Methods

The calculations were based on the linearized form of (1):

$$F(\nu) \equiv \ln\left[D(T)\,\nu^3\,\frac{k(\nu)}{f_e(\nu)}\right] = \frac{h}{kT}\,\nu. \tag{2}$$

From the slope of the straight line $F(\nu)$, $T \equiv T^*$ was calculated. For $k(\nu)$ and $f_e(\nu)$ different distributions were taken, assuming different symmetries (and also asymmetries) between these distributions. This is an allowed procedure, since the slope of the function $F(\nu)$ depends only on the relative spectra. The calculation of T^* was performed easily and quickly with a Minsk-22 computer by means of a simple computer program.

The local temperature and the shapes and locations of the absorption and fluorescence spectra

1. *Gaussian distribution of spectra*

(a) *The case of Levshin mirror symmetry* [15]. The relationship (2) should be written for the fluorescence quantum spectrum $f_q(\nu)$, by using the relationship $f_e(\nu) = h\nu f_q(\nu)$:

$$2\ln\nu + \ln\frac{k(\nu)_{\text{rel}}}{f_q(\nu)_{\text{rel}}} + \text{const} = \frac{h}{kT}\,\nu. \tag{3}$$

In the case of Gaussian distribution

$$k(\nu)_{\text{rel}} = \exp\left[-(\nu - m)^2/2\sigma_a^2\right] \tag{4}$$

and

$$f_q(\nu)_{\text{rel}} = \exp\left[-(\nu - n)^2/2\sigma_e^2\right] \tag{5}$$

where m, n and σ_a, σ_e are the locations and standard deviations of the absorption and fluorescence spectra, respectively. (Further, the band width will be given in

terms of standard deviations.) If these representations with $\sigma_a = \sigma_e = \sigma$ are substituted into (3) and the values of the constants are considered, we obtain

$$2 \ln \nu + \frac{m-n}{\sigma^2} \nu + \text{const} = \frac{4800}{T} \nu. \tag{6}$$

The function $G(\nu) = 2 \ln \nu + \frac{m-n}{\sigma^2} \nu$ is used now for the determination of $T^* \equiv T$ (linearity dues not hold over a greater interval of ν due to the presence of $\ln \nu$). With $m = 4.5 \cdot 10^{14}$ Hz (666.7 nm) and $\sigma = 0.1 \cdot 10^{14}$ Hz ($\cong 15$ nm), the dependence of T^* on the Stokes-shift $m-n$ and on σ is shown in Fig. 1.

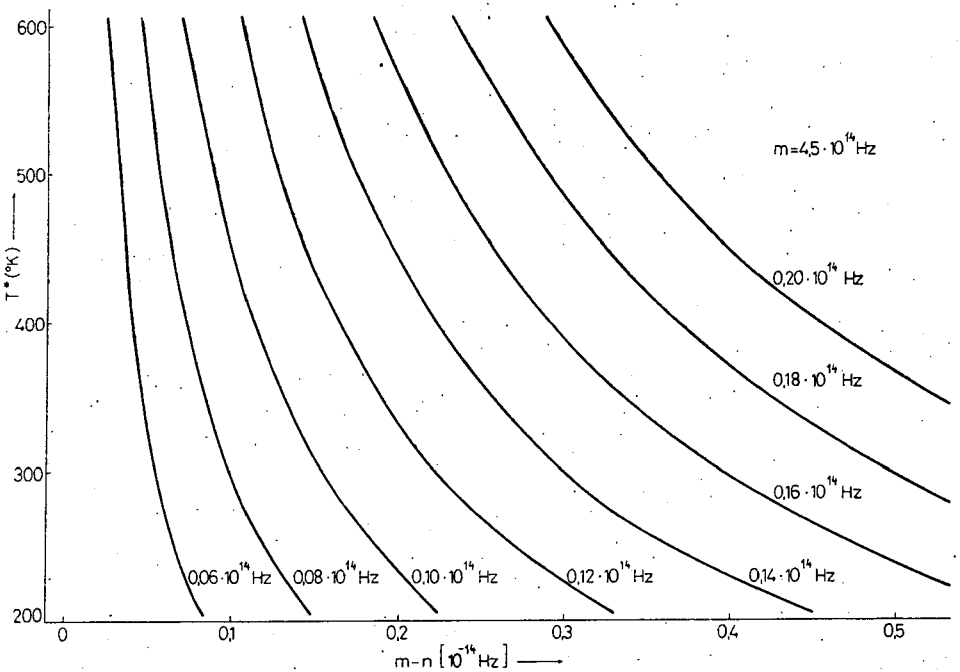

Fig. 1. Dependence of the vibrational temperature T^* on the Stokes-shift m—n at different standard deviations σ of the absorption and fluorescence bands of Gaussian distribution

(b) *The case of Blohintsev mirror symmetry* (16).

$$k(\nu)_{\text{rel}} = \exp\left[-(\nu - m)^2 / 2\sigma^2\right]$$

and

$$f_q(\nu)_{\text{rel}} = \text{const} \frac{\nu^3}{2\nu_0 - \nu} \exp\left[-(2\nu_0 - m)^2 / 2\sigma^2\right]$$

should be substituted into (3). ν_0 is the mirror frequency. The result is

$$\ln \frac{2\nu_0 - \nu}{\nu} - \frac{2(\nu_0 - m)}{\sigma^2}\nu + \text{const} = \frac{4800}{T}\nu. \tag{7}$$

The function $G(\nu) \equiv \ln(2\nu_0 - \nu)/\nu - 2(\nu_0 - m)\nu/\sigma^2$ is used for the determination of T^*. The result of the calculations is in accordance with that obtained for Levshin mirror symmetry; only small quantitative deviations were observed.

(c) *The case of non-symmetry.* In this case the representations (4) and (5) should be substituted into (3); the result is:

$$2\ln \nu + \frac{(\nu - n)^2}{2\sigma_e^2} - \frac{(\nu - m)^2}{2\sigma_a^2} + \text{const} = \frac{4800}{T}\nu. \tag{8}$$

With $m = 4.5 \cdot 10^{14}$ Hz (666,7 nm), $\sigma_a = 0.2 \cdot 10^{14}$ Hz ($\cong 31$ nm) and $n = 4.1 \cdot 10^{14}$ Hz (731.7 nm) and different values of σ_e, T^* was calculated and plotted as a function

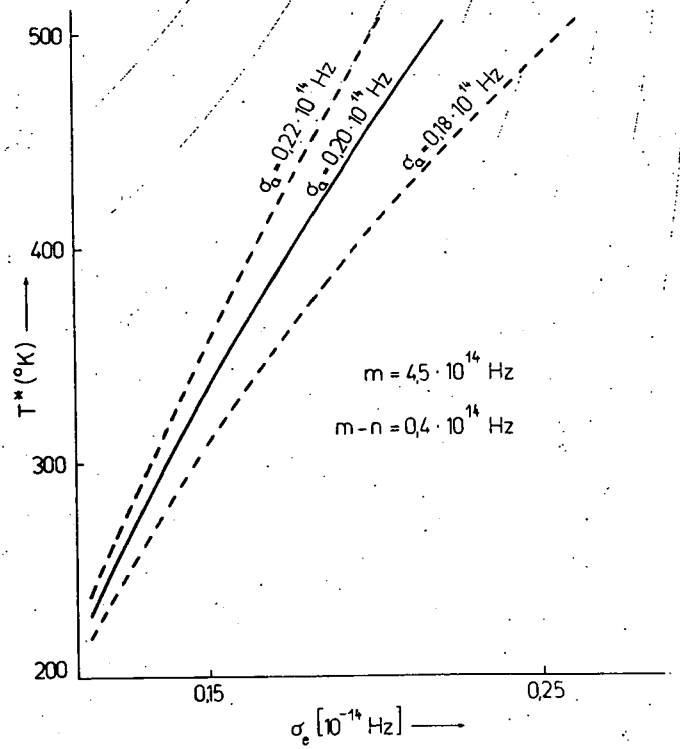

Fig. 2. Dependence of the vibrational temperature T^* on the standard deviation σ_e of the fluorescence band of Gaussian distribution with absorption maximum at $m = 4.5 \cdot 10^{14}$ Hz and Stokes-shift $m - n = 0.4 \cdot 10^{14}$ Hz at different standard deviations σ_a of the absorption band

of σ_e (Fig. 2, solid line). With $\sigma_a = 0.18 \cdot 10^{14}$ Hz (28 nm) and $0.22 \cdot 10^{14}$ Hz (34 nm) the dependence of T^* on σ_e is somewhat different (Fig. 2, broken lines). If $m = 5.5 \cdot 10^{14}$ Hz (545.5 nm), the functions $T^*(\sigma_e)$ (σ_a=const) will be enhanced by a maximum of only 1%. If $m = 4.5 \cdot 10^{14}$ Hz and $\sigma_a = 0.2 \cdot 10^{14}$ Hz, the dependence of T^* on σ_e at different locations of the fluorescence maximum is shown in Fig. 3.

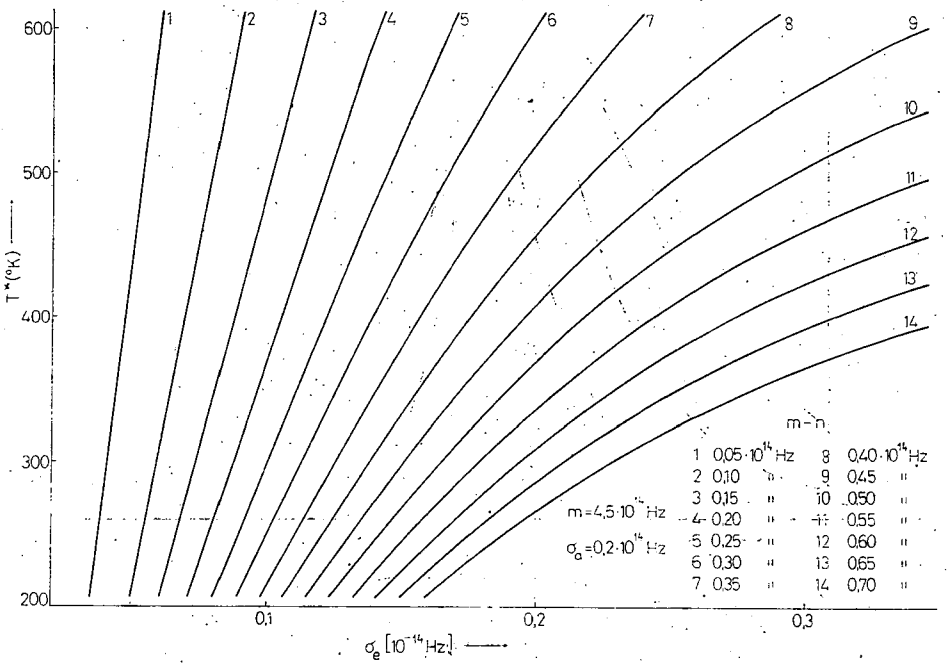

Fig. 3. Dependence of the vibrational temperature T^* on the standard deviation σ_e of the fluorescence band of Gaussian distribution with absorption maxiumum at $m = 4.5 \cdot 10^{14}$ and a standard deviation σ_a of the absorption band at different Stokes-shifts $m-n$ of the fluorescence and absorption bands

2. *Analytical forms of absorption and fluorescence.* DOMBI *et. al.* [17] derived analytical expressions for the active absorption and fluorescence spectra. According to their results

$$f_q(\nu) = B\nu^3 \operatorname{ch}^{-1}[a(\nu - \nu_0)] \exp(-b\nu) \tag{9}$$

$$k(\nu) = A\nu \operatorname{ch}^{-1}[a(\nu - \nu_0)] \exp(b\nu) \tag{10}$$

With proper choice of the parameters a and b, the analytical and experimental fluorescence spectra coincide. If the analytical spectra are substituted into (1), we obtain b=const $h/2kT$. According to SZALAY *etal.* [13], a=const $h/2kT$, too. Using this dependence of the parameters on the temperature, the temperature-

dependence of the absorption and fluorescence spectra can be established. For 300 and 500°K at $\nu_0 = 5.33 \cdot 10^{14}$ Hz (=563 nm), this dependence is shown in Fig. 4. In the anti-Stokes region the spectra can be well approximated with Gaussian distributions.

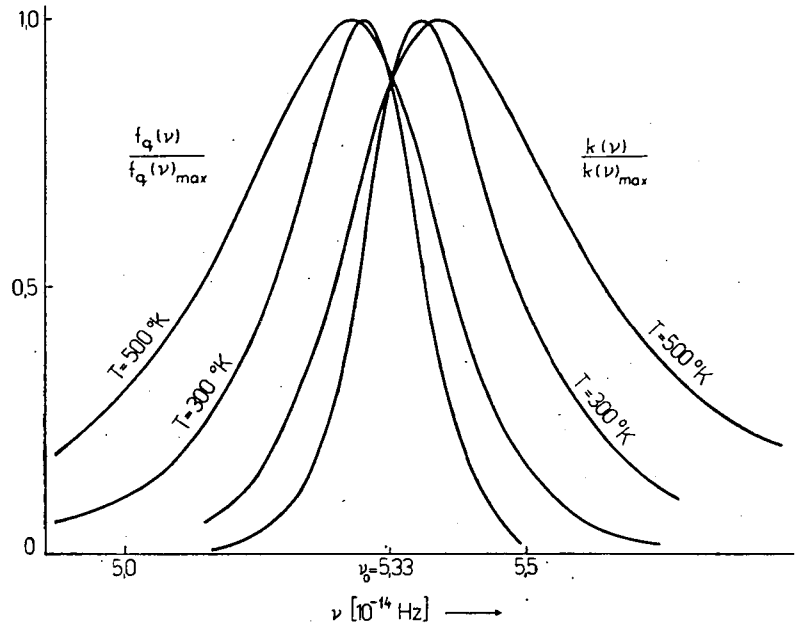

Fig. 4. Relative absorption and fluorescence spectra calculated with the analytical expressions (9) and (10) for 300 and 500°K

Approximate relationship between the vibrational temperature and the spectral characteristics

Figs 1—4. show that the vibrational temperature T^* depends on the widths of absorption and fluorescence (σ_a and σ_e), the distance of absorption and fluorescence peaks ($m-n$, Stokes-shift) and (to a smaller extent) on the location of the absorption maximum. According to Figs 1—3. it can be supposed that $T^* \sim \sigma_a$ and $\sim \sigma_e$, and further $\sim 1/(m-n)$, so that finally $T^* \sim \sigma_a \sigma_e/(m-n)$.

For the values of our parameters, the proportionality factor is approximately $h/k \cdot 1.04$. Therefore

$$T^* \cong \frac{1}{1 \cdot 04} \frac{h}{k} \frac{\sigma_a \sigma_e}{m-n} = 4615 \frac{\sigma_a \sigma_e}{m-n} \text{°K}. \tag{11}$$

(Here the quantities σ_a, σ_e and $m-n$ are considered without the factor 10^{14}.) If the standard deviations of the Gaussian distributions are replaced by half band widths, this expression can easily be rewritten in a form reminiscent of equation (6) of KAZACHENKO's paper [18]. With equation (11) T^* is easily calculated, but a high precision of the quantities is necessary.

If the spectra are plotted as functions of the wavelength λ, and the accuracy of the wavelength λ, and the accuracy of the determination of the locations of maxima is 0.5 nm, the value of T^* can be given as $T^* \pm 16°$ K (with an accuracy of 1 nm, $T^* \pm 28°$ K is obtained). Fig. 5 shows the accuracy of the approximation of T^* calculated with (11).

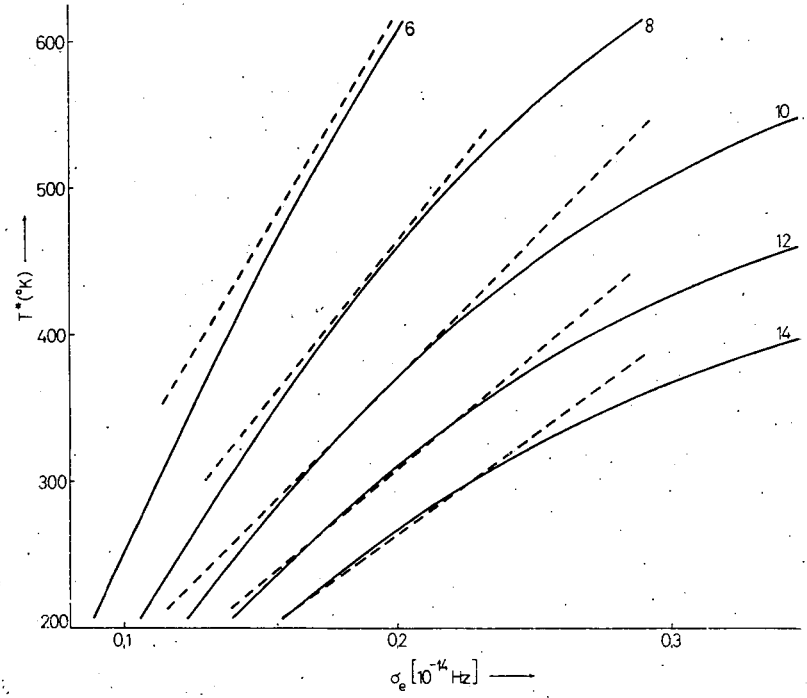

Fig. 5. Selected curves from Fig. 3 approximated by curves (broken lines) calculated with (11)

The deviation from symmetry of the absorption and fluorescence bands

In the case of Levshin symmetry [15] $\nu_a - \nu_e = 2(\nu_0 - \nu_e)$. If both the absorption and the fluorescence bands are of Gaussian distribution, the difference $\nu_a - \nu_e$ as a function of $\nu_0 - \nu_e$ yields a straight line with a slope k different from 2; it is defined in $\nu_a - \nu_0 = k(\nu_0 - \nu_e)$. The dependence of k on the standard deviations σ_e and σ_a is shown in Fig. 6. If the fluorescence band is narrower than the absorption band, k is smaller than 2; in the reverse case k is greater than 2. In all cases the intercept of the straight lines is found at 1. All straight lines in Fig. 6 can therefore be given by the equation

$$\nu_a - \nu_0 = \left(\frac{\sigma_e}{\sigma_a} + 1\right)(\nu_0 - \nu_e) \tag{12}$$

(otherwise in the case of $\sigma_a=\sigma_e$, k could not have the value 2). This means that of course, the slopes of the straight lines in Fig. 6 can be determined by means of the standard deviations only for spectra of Gaussian distribution. If $k(v)$ and

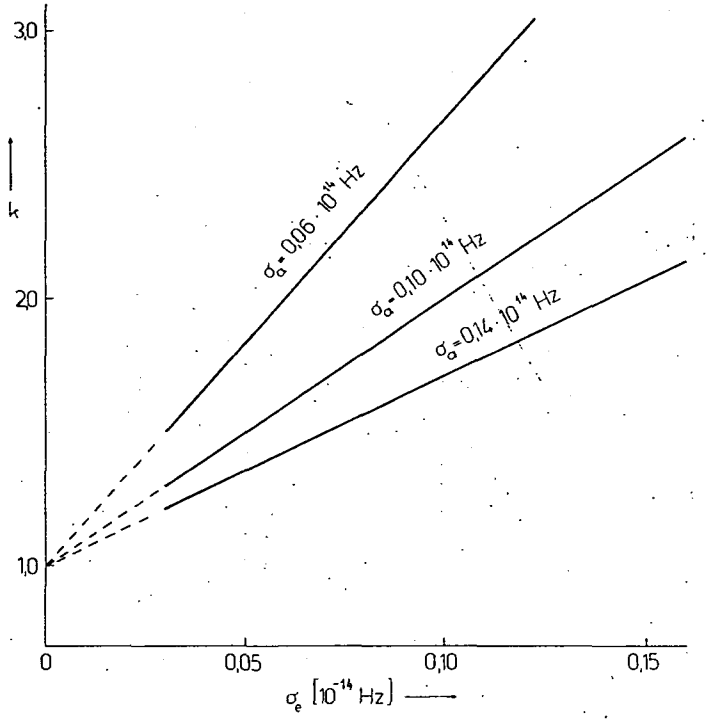

Fig. 6. Slope k of the mirror symmetry relation $v_a-v_0=k(v_0-v_e)$ as a function of the standard deviations of the fluorescence and absorption bands (σ_e and σ_a) of Gaussian distribution

$f_q(v)$ have Gaussian distributions with different standard deviations σ_a and σ_e, and v_0 is in the interval $n<v_0<m$, while further the condition

$$\exp[-(v_0-n)^2/2\sigma_e^2] = \exp[-(v_0-m)^2/2\sigma_a^2]$$

is fulfilled, the following relationship is valid:

$$\frac{\sigma_e}{\sigma_a} = \frac{v_0-n}{m-v_0}. \tag{13}$$

Introducing this into (12)

$$k = \frac{v_0-n}{m-v_0}+1 = \frac{m-n}{m-v_0} \tag{14}$$

This is another possibility for the determination of the slopes of the straight lines in Fig. 6.

References

[1] *Normann, I., G. Porter:* Proc. Roy. Soc. London **A 230**, 399 (1955).
[2] *Albrecht, A. C., W. T. Simpson:* J. Amer. Chem. Sec. **77**, 4454 (1955).
[3] *Albrecht, A. C. :* J. Chem. Phys. **27**, 1413 (1957).
[4] *Jablonski, A.:* Bull. Acad. Polon. **8**, 655 (1960).
Lisicki, E.: Bull. Acad. Polon. **11**, 665 (1963).
[5] *Albrecht, A. C.:* J. Mol. Spectr. **6**, 84 (1961).
[6] *Jabloński, A.:* Int. Conf. on Luminescence, Torun (1963).
[7] *Kozma, L., L. Szalay, J. Hevesi:* Acta Phys. et Chem. Szeged **10**, 67 (1964).
[8] *Hevesi, J. Kozma L., L. Szalay:* Acta Phys. Polon. **29**, 57 (1966).
[9] *Ketskeméty, I., L. Szalay, Z. Várkonyi:* Acty Phys, et Chem. Szeged. **11** 15 (1956).
[10] *Kennard, E. H.:* Phys. Rev. **11**. 29 (1918); **28**, 672 (1926).
[11] *Stepanov, B. I.:* Dokl. Akad. Nauk SSSR **112**, 839 (1957); Soviet Phys. **2**, 81 (1957);
Kazachenko, L. P., B. I. Stepanov: Opt. Spektr. **2**, 339 (1957).
[12] *Ketskeméty, I., J. Dombi, R. Horvai:* Ahn. Phys. **7**, 342 (1961); Acta Phys. Hung. **12**, 263 (1960); **14**, 165 (1962);
[13] *Alentsev, M. N.:* Opt. Spektr. **4**, 690 (1958);
Alentsev, M. N.: L. A. Pahomitcheva: Izv. Akad. Nauk SSSR Fiz. Ser. **22**, 1377 (1958); **24**, 734 (1960;
Kravtsov, L. A., A. N. Rubinov: Opt. Spektr. **12**, 636 (1962);
Hevesi, J., L. Kozma: Acta Phys. et Chem. Szeged **8**, 103 (1962);
Razhanova, E. F., M. S. Fadeeva, T. S. Pavlina: Izv. Akad. Nauk SSSR Fiz. Ser. **24**, 769 (1960);
Mazurenko, Yu. T., B. S. Neporent: Opt. Spektr. **12**, 317 (1962);
Klochkov, V. P., S. M. Korotkov: Opt. Spektr. **22**, 189 (1967);
Bálint, E., E. Lehoczki, J. Hevesi: Acta Phys. et Chem. Szeged **17**, 1 (1971);
Szalay L., J. Hevesi, L. Kozma: Magyar Fizikai Folyóirat **13**, 170 (1965).
[14] *Borisevich, N. A., V. V. Gruzinski:* Opt. Spektr. **14**, 39 and 457 (1963);
Hevesi, J., G. S. Singhal: Spectrochim. Acta **25 A**, 1751 (1969);
Borisevich, N. A.: Acta Phys. et Chem. Szeged. **10**, 9 (1964).
[15] *Levshin, V. L.:* Fotoluminescencia zhidkih i trovrduch veshtchestv, Moscow—Leningrád, 1951.
[16] *Blohintsev, D. I.:* J. Phys. SSSR **1**, 127 (1959).
[17] *Dombi, J., I. Ketskeméty, L. Kozma:* Acta Phys. et Chem. Szeged **10**, 15 (1964).
[18] *Kazachenko, L. P.:* Opt. Spektr. **18**, 703 (1965).

СВЯЗЬ КОЛЕБАТЕЛЬНОЙ ТЕМПЕРАТУРЫ ОРГАНИЧЕСКИХ МОЛЕКУЛ С АБСОРБЦИОННЫМИ И ЭМИСИОННЫМИ СПЕКТРАМИ РАСТВОРОВ

А. Ринглер, Л. Салаи

Определены колебательная температура в зависимости от ширины полосы и смещения Стокса для разных случаев зеркальной симметрии, и для несимметрического случая на основании сректров электронного возбуждения, обладающих распределением по Гауссу. Предложено приближенное уравнение для быстрого расчета вибрационной температуры на основе спектральных характеристик.

ABSORPTION SPECTRA OF PEROXIDASE SOLUTIONS

By

L. SZALAY and Z. VÁRKONYI

Institute of Biophysics, Attila József University, Szeged

(Received January 15, 1974)

In the absorption spectra of neutral tris-buffered solutions of $5 \cdot 10^{-8}$—$1 \cdot 10^{-5}$ M horseradish peroxidase, beside the known bands at 270—280 and 405 nm, a band at 190 nm is reported. The Beer—Lambert law of absorption is not valid, the molar extinction coefficients are concentration dependent even at the lowest concentrations investigated. The deviation from the Beer—Lambert law is explained by assuming the presence of aggregates. The extinction coefficient of the short wave band at 190 nm is $1.10 \cdot 10^6$ $l \cdot M^{-1} cm^{-1}$ in $2 \cdot 10^{-6}$ M solutions. Because of the invalidity of the Beer—Lambert law, the RZ-value (Reinheitszahl, extinction at 402 nm/extinction at 280 nm), generally used for characterizing the purity of peroxidase, is not unequivocal.

Introduction

Comparatively few data concerning absorption of peroxidase have been published until now. The earliest data are due to H. THEORELL and A. MAELY [1], who gave a relative absorption spectrum and proposed the ratio of the height of the band at 402 nm to the height of the band at 280 nm (the so-colled RZ-value) for characterizing the purity of peroxidase. K. G. PAUL [2] and L. M. SHANNON *at al.* [3] found significant changes in this ratio during purification of peroxidase. Also E. M. STRICKLAND [4] published absorption spectra, but without further explanation, as the emphasis in his investigations was on the study of circular dichroism spectra. The absorption spectra were measured in the wavelength range 250—450 nm, but the value of the molar extinction coefficient can be deduced only in some cases, for example at 401 nm, calculated from data of [3], it is $1.02 \cdot 10^5$ $l \cdot M^{-1}$ cm^{-1}.

As a criterion of purity was given on the basis of the absorption spectrum and this criterion, according to the investigations in [2] and [3] seems to be problematic, these spectra were redetermined and also the validity of the Beer—Lambert law for peroxidase solutions was studied. In addition, it seemed worth while to clear up the existence of an absorption band in the region below 250 nm, where an increase in absorption was found by earlier measurements.

Materials and methods

Lyophilized and 3× crystallized horseradish peroxidase of the Nutritional Biochemical Corporation (Cleveland) was used. The preparate was of 3170 units/mg activity and of RZ=3.0 purity. Tris-buffered solutions of pH=7.0 were prepared from the crystallized material by diluting a standard solution of $1 \cdot 10^{-5}$ M to the concentrations $5 \cdot 10^{-6}$, $2 \cdot 10^{-6}$, $1 \cdot 10^{-6}$, $5 \cdot 10^{-7}$, $2 \cdot 10^{-7}$, $1 \cdot 10^{-7}$ and $5 \cdot 10^{-8}$ M,

respectively. The solutions were stored at a temperature between 0 °C and 4 °C for about 24 hrs. before use.

Absorption spectra were measured partly with an Optica Milano (Type CF 4DR), partly with a Unicam (Type 1800) spectrophotometer. In a series of measurements made with $1 \cdot 10^{-5}$ M solutions the temperature dependence of the spectra in the temperature range 10—55 °C was also determined.

Results

The absorption spectra have three characteristic bands (Fig. 1—2). In the figures only curves of selected concentrations are presented. The maximum of the band in the ultraviolet is at 190 nm, that in the near ultraviolet between 270—280 nm and the third at about 405 nm. At 500 and 620 nm there are two shoulders (see [5]). The molar decadic extinction coefficients of the maxima in the region of shortest waves are about two orders of magnitude higher than in the two other regions ($110 \cdot 10^4$, $2.6 \cdot 10^4$ and $7.2 \cdot 10^4$ $l \cdot M^{-1}$ cm^{-1} in the order of increasing wavelengths of the locations of maxima in $2 \cdot 10^{-6}$ M solution). The absorption spectra are plotted with different scales according to the $\varepsilon(\lambda)$ values of the different spectral regions denoted by *A*, *B* (Fig. 1) and *A*, *B*, *C* (Fig. 2). The absorption spectra of the $2 \cdot 10^{-6}$ and $1 \cdot 10^{-5}$ M solution are, however, continued according to the scale of section *B* also in section *C*. The absorption is comparatively very low in the 250—450 nm

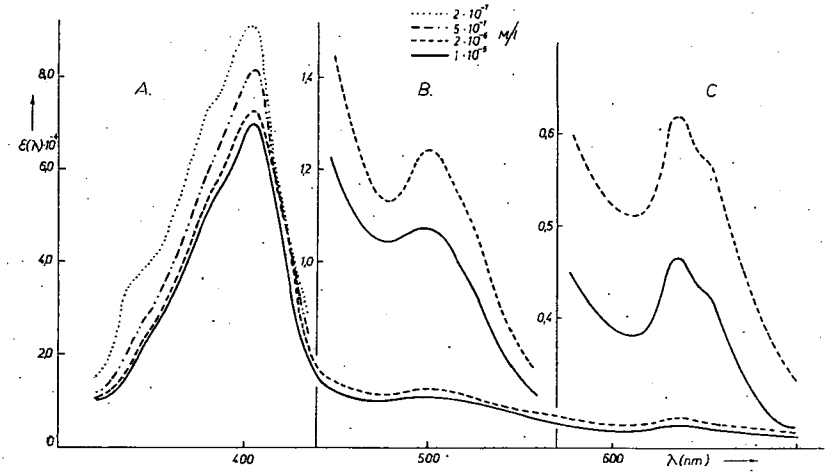

Fig. 1. Absorption spectra of neutral tris-buffered and water solutions of peroxidase as a function of concentration

spectral range. A similar technique was used in the 350—700 nm spectral region (Fig. 2).

Under 205 nm the absorption of the tris-buffered solution cannot be determined owing to the strong absorption of the buffer even in nitrogen atmosphere. Therefore, in this spectrum region the absorption of water solutions of peroxidase was measured and is shown in Fig. 1. *A*.

The molar decadic extinction coefficients are highly concentration dependent, revealing that the Beer-Lambert law of light absorption does not hold. This should be ascribed to physical or chemical interactions occuring between peroxidase molecules with increasing concentration.

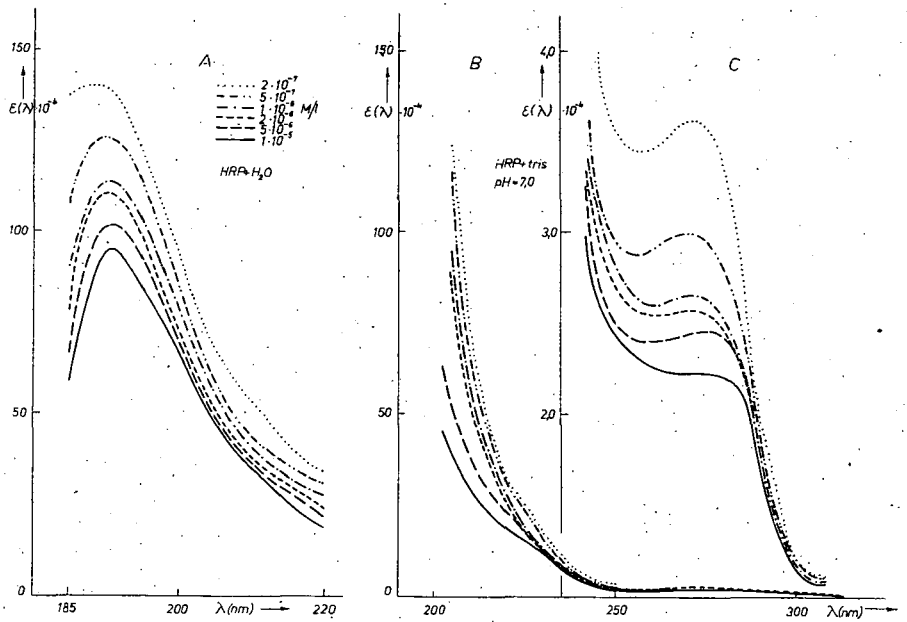

Fig. 2. Absorption spectra of neutral tris-buffered and water solutions of peroxidase as a function of concentration

Discussion

The absorption band at about 190 nm has not been published hitherto. This band of the spectrum corresponds partly to the absorption of the peptide bonds, partly to that of ring compounds [16]. The concentration dependence of the extinction coefficient was not described earlier. There are only few references to the Beer—Lambert law in treating the light absorption of proteins (see *e.g.* [1, 6]). According to our measurements the law is valid for the phosphate buffered (pH=7.0) solution of lysozyme in the $2 \cdot 10^{-4}$ M—$5 \cdot 10^{-7}$ M concentration range ($\varepsilon_{max}(\lambda)=3.5 \cdot 10^4$ $Ml^{-1}\,cm^{-1}$). Since the law is not valid for peroxidase, it seems questionable whether it is justified to define the purity of peroxidase on the basis of absorption spectra with the so-called RZ-value [1]. According to this definition, for pure peroxidase $RZ=\varepsilon(402)/\varepsilon(280)=3.04$. L. M. SHANNON and even H. THEORELL [1] found peroxidase preparations with RZ-values exceeding 3.04. Therefore, already L. M. SHANNON *et al.* [3] remarked that the use of the RZ-value is not satisfactory for characterizing the purity of the preparation. However, the critical remark was not

in connection with the Beer—Lambert law. In the case of our sample, RZ-values I. Since the absorption does not follow the Beer—Lambert law and the ratios of absorptions measured at different wavelengths changing with the concentration were found. These changes are presented in Table are concentration depe ndent, the RZ-value according to its original definition does not seem satisfactory for characterizing the purity of peroxidase.

Table I

Dependence of RZ-*values* $\left(\mathrm{RZ}=\frac{\varepsilon(402)}{\varepsilon(280)}\right)$ *on concentration*

C M/L	$\varepsilon(402)$ ($\mathrm{l \cdot M^{-1}\,cm^{-1}}$)	$\varepsilon(280)$ ($\mathrm{l \cdot M^{-1}\,cm^{-1}}$)	RZ
$2 \cdot 10^{-7}$	9.00	3.62	2.49
$5 \cdot 10^{-7}$	7.93	3.0	2.64
$1 \cdot 10^{-6}$	7.40	2.66	2.78
$2 \cdot 10^{-6}$	7.17	2.56	2.80
$5 \cdot 10^{-6}$	6.92	2.46	2.81
$1 \cdot 10^{-5}$	6.80	2.23	3.05

In some cases the deviation from the Beer—Lambert law can be explained by the appearence of associates. If, however, the molecules were spherical, an aggregation would be very difficult according to the following arguments. A spherical peroxidase molecule should have a radius $r=52$ Å, calculated from $r=1.67\ (M/d)^{1/3}$ with the molecular weight $\mathrm{M}=4 \cdot 10^4$ and density $d=1.3$ g $\mathrm{cm^{-3}}$. Supposing a random distribution of the spheres, from the formula $R^3=3(4\pi \cdot cN')^{-1}$ [8] (where c is the concentration in M/l, $N'=6 \cdot 10^{20}$ and R is the distance between two neighbouring molecules in Å), the average distance of neighbouring spheres in the $1 \cdot 10^{-5}$ M solution would be $R=326$ Å. If the distance between the centres of the spheres is 326 Å, the distance between the surfaces would exceed 200 Å; thus at this concentration no association could occur. Therefore, it should be supposed, that either the molecules can be better approached by ellipsoids, or some molecules are associated already during the dissolution of the crystalline material. Namely, with the axial ratio 12:1:1, neighbouring ellipsoids could come into contact in the solution mentioned above and the neighbouring molecules could form associates.

Approximate information concerning the form of the molecules can be obtained also by hydrodynamical methods. The constant β in the formula

$$M = \left[\frac{s \cdot N \cdot \eta_0}{\beta(1-\bar{v}d)}\right]^{3/2} \cdot [\eta_v]^{1/2}$$

is characteristic for the axial ratio [9]. M is the molecular weight of the protein, $\bar{v}$ the specific partial volume, η_0 the viscosity of the solvent, d the density of the solution, η_v the limiting viscosity, s the sedimentation constant, and $N=6\cdot10^{23}$. For tris-buffered solution of peroxidase, with $M=4\cdot10^4$, $\bar{v}=0.689\ \mathrm{cm^3\ g^{-1}}$, $s=3.5\cdot10^{-13}$ sec, $\eta_0=1$ cP, $\eta_v=1.087$ cP, $d=1.0012\ \mathrm{gcm^{-3}}$, $\beta=2.6\cdot10^6$ was obtained. The viscosities were determined at 25° C with a Höppler viscosimeter. The densities were measured, the other data were taken from [3] and [9]. According to H. A. SCHERAGA [10] the axial ratio of the ellipsoid for $\beta=2.6\cdot10^6$ is 15:1:1. With respect to the approximate character of the hydrodynamical methods, the accordance with our ratio (12:1:1) seems to corroborate the statement that the peroxidase molecule is rather well approximated by an ellipsoid.

As the Beer—Lambert law does not hold, the extinction coefficients obtained for different concentrations are only apparent. It can be supposed that in the $5\cdot10^{-8}$ M solution there are practically no aggregates. In this solution the extinction coefficients of the band maxima of the ring compounds are $\varepsilon(280)=3.6\cdot10^4$ and $\varepsilon(402)=8.5\cdot10^4\ \mathrm{l\cdot M^{-1}\ cm^{-1}}$, respectively. According to [12] $\varepsilon(280)=7\cdot10^4\ \mathrm{l\cdot M^{-1}\ cm^{-1}}$ and from [4] $\varepsilon(402)=10.8\cdot10^4\ \mathrm{l\cdot M^{-1}\ cm^{-1}}$. The deviations are due to differences in the preparations (in [4] A1 fraction was used).

The Beer—Lambert law is not valid even in 10^{-7} M solutions, in which the neighbouring molecules are in a distance of more than 1000 Å. Since the diluted solutions were prepared from a concentrated (in our case $1\cdot10^{-5}$ M) solution, if we assume that the aggregates formed in this solution are not completely disaggregated during dilution, this violation of the Beer—Lambert law can be understood. The validity of this explanation can be tested by studying the temperature dependence of the spectra. According to measurements in the temperature range 10—45° C the extinction coefficient at 280 nm increases only by a few percents. This means that the aggregates are not easily dissolved.

It seems unusual that the Beer—Lambert law is not valid for 10^{-7} M concentration; however, this case is not unique. It is known that in $1\cdot10^{-7}$ M dye solutions the Beer-Lambert law does not hold [13]. It was also concluded from fluorescence spectra that aggregates of pigment molecules may be present in similarly highly diluted solutions [15].

The deviation from the Beer—Lambert law may be in connection with the ratio of charged and neutral amino acids in peroxidase. Though the primary structure of peroxidase is not known in all details, the amino acid composition of the molecule is practically clarified [7, 14]; it consists of 60 charged and 250 neutral amino acids, the ratio of these numbers is 0.24. According to FISCHER [11] the minimum interaction energy originating from hydrophobic forces in water solutions is attained, if all charged amino acids are located on the surface of a sphere and the neutral ones in the interior. For a spherical particle a theoretical ratio $p=0.28$ is given. in [17] Since in our case the experimental p is smaller than the theoretical P_s, the surface is not completely covered by charged particles. Therefore, a decrease in the interaction energy of solute-solvent system association may occur and the molecular weight may depend on the concentration of the protein.

References

[1] *Theorell, H., A. Maehly:* Acta Chem. Scand. **4**, 422 (1950).
[2] *Paul, K. G.:* Acta Chem. Scand. **12**, 1312 (1958).
[3] *Shannon, L. M., E. Kay, F. Y. Lev:* J. Biol. Chem. **241**, 2166 (1966).
[4] *Strickland E. H.:* Biochim. Biophys. Acta **151**, 70 (1968).
[5] *Tamura, M.:* Biochim. Biophys. Acta **243**, 249 (1971).
[6] *Strickland, E. H., T. Horwitz, E. Kay, L. M. Shannon, M. Wilchek, C. Billups:* Biochemistry, **10**, 2631 (1971).
[7] *Welinder, K. G., L. B. Smillie, G. R. Schonbaum:* Can. J. Biochem. **50**, 44 (1972).
[8] *Förster, Th.:* Fluoreszenz organischer Verbindungen, Vandenhoeck und Ruprecht, Göttinge (1951). p. 177
[9] *Előd i P.:* Biológiai Tanulmányok (Biological Studies, in Hungarian) **2**, 33 Akadémiai Kiadó, Budapest (1966).
[10] *Scheraga, H. A., L. Mandelkern:* J. Amer. Chem. Soc. **75**, 179 (1953).
[11] *Fisher, B. F.:* Biochemistry **51**, 1285 (1964).
[12] *Flohe, L., E. Schaick, W. Voelter, A. Wendel* Hoppe-Seyler's Z. Physiol. Chem. **352**, 170 (1971).
[13] *Rabinowitch, E., L. F. Epstein:* J. Amer. Chem. Soc. **63**, 69 (1941).
[14] *Welinder, K. G., L. B. Smille:* Can. J. Biochem. **50**, 63 (1972).
[15] *Singhal, S., L. Szalay, E. Tombácz:* Acta Phys. et Chem. Szeged **19**, 11 (1973).
[16] *Preiss, J. W., R. Setlow:* J. Chem. Phys. **25**, 138 (1956).

АБСОРБЦИОННЫЙ СПЕКТР РАСТВОРА ПЕРОКСИДАЗЫ

Л. Салаи, З. Варкони

В нейтральных „трис"-буферных растворах пероксидазы, полученной из хрена пр концентрациях $5 \cdot 10^{-8} - 1 \cdot 10^{-5}$ моль/л в абсорбционных спектрах обнаружена, кроме известных 270—280 и 405 нм полос поглощения, новая полоса при 190 нм. Закон Ламберта—Бера не удовлетлетворяется ни в одном случае для этих полос, молярные экстинкционные коеффициенты показывают концентрационную зависимость даже при самых больших разбавлениях. Отклонение от закона Ламберта—Бера может объясняться образованием ассоциатов. Коеффициент экстинкции при поглощении на 190 нм составляет для раствора концентрации $2 \cdot 10^{-6}$ моля $1{,}1 \cdot 10^{6}$ л. м.$^{-1}$. см.$^{-1}$ Вследствие неприемлености закона Ламберта—Бера, обычно применяемое RZ-число (=экстинкция при 402 нм/экстинкция при 280 нм) не является однозначной характеристикой.

ОСОБЕННОСТИ ГЕНЕРАЦИОННЫХ СВОЙСТВ КРАСИТЕЛЕЙ В ПОЛЯРНЫХ РАСТВОРАХ

А. Н. РУБИНОВ, В. И. ТОМИН

Институт физики АН БССР, Минск

(Поступило в редакцию 11 января 1974 г.)

Рассмотрено влияние ориентационного уширения электронно-колебательных уровней, возникающего в результате влияния межмолекулярных взаимодействий на пороговые, энергетические и спектральные характеристики генерации полярных растворов красителей.

Установлено, что величина ориентационного уширения уровней существенно влияет на порог и мощность генерации красителей.

Выведена формула, позволяющая хорошо рассчитывать частоту генерации при различных температурах, накачках и потерях излучения в резонаторе.

Показано, что ориентационное уширение приводит к дополнительным зависимостям спектра генерации от температуры среды, интенсивности и частоты излучения накачки.

Спектрально-люминесцентные свойства молекул органических красителей при внесении их в раствор существенно изменяются. Эти изменения сзязаны с возникновением межмолекулярных взаимодействий (ММВ) молекулы красителя с молекулами растворителя [1—3].

К настоящему времени спектрально-люминесцентные свойства растворов красителей изучены неплохо. Особый интерес представляют полярные растворы красителей, т. к. как их спектральные свойства имеют ряд существенных особенностей [1, 2].

Строгое описание оптических свойств красителей в полярных растворах, как показано авторами данной работы [4—7] должно производитсья с обязательным учетом ориентационного уширения как спектров люминесценции, так и спектров поглощения с помощью соответствующих функций распределения. Их аналитический вид может быть получен если исходить из схемы уровней элементарной ячейки раствора (рис. 1), состоящей из рассматриваемой молекулы красителя и ближайших молекул растворителя (сольватная оболочка). Согласно данной концепции,

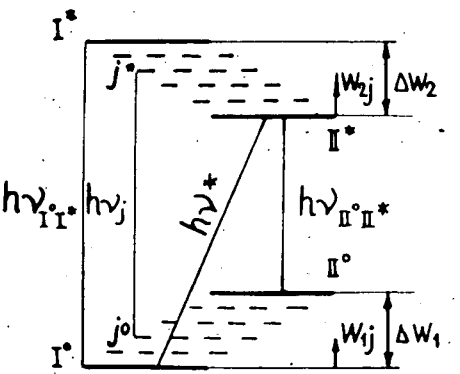

Рис. 1. Схема уровней элементарной ячейки полярного раство ра.

все электронные уровни полярных растворов красителей, характеризующиеся отличными от нуля постоянными дипольными моментами, уширяются, в основном, вследствие ориентационных взаимодействий молекул. Элементарные акты поглощения и испускания в таких растворах происходят с изменением не только электронной и колебательной, но и ориентационной энергии раствора, а спектры поглощения и испускания представляют собой интегралы по всем ориентационным подуровням исходного электронного состояния.

$$K_{12}(\nu) = \int\limits_{w_{1j}} K_{12}^{j}(\nu)\, dW_{1j} = \frac{n, h\nu}{v} B_{12}(\nu) \tag{1}$$

$$W_{21}(\nu) = \int\limits_{w_{2j}} W_{2j}^{j}(\nu)\, dW_{2j} = n_2 h\nu \frac{8\pi h\nu^3}{v^3} B_{21}(\nu), \tag{2}$$

где

$$B_{12}(\nu) = \int\limits_{w_{1j}} B_{12}^{j}(\nu)\, \varrho_1^j\, dW_{1j}, \tag{3}$$

$$B_{21}(\nu) = \int\limits_{w_{2j}} B_{21}^{j}(\nu)\, \varrho_2^j\, dW_{2j}. \tag{4}$$

В выражениях (1)—(4) ϱ_1^j и ϱ_2^j-функции распределения ячеек по ориентационным подуровням в основном и возбужденном электронных состояниях, $K_{12}^j(\nu)$ и $W_{2j}^j(\nu)$-коэффициент поглощения и мощность люминесценции, а $B_{12}^j(\nu)$ и $B_{21}^j(\nu)$-спектральные коэффициенты Эйнштейна поглощения и испускания для j-ой франк-кондоновской пары ориентационных состояний с энергиями ориентационного уширения W_{1j} и W_{2j}, n_1 и n_2-населенности основного и возбужденного электронных уровней.

Анализ [5] соотношения между интегральными спектрами люминесценции и поглощения показал, что оно принимает вид универсального соотношения Степанова (УСС) лишь в том случае, когда функции распределения элементарных ячеек по энергии взаимодействия всех молекул ячейки являются равновесными. Такие функции распределения элементарных ячеек реализуются в условиях термодинамического равновесия, необходимым условием которого является малая по сравнению со временем жизни τ^* электронного состояния постоянная τ_p межмолекулярной ориентационной релаксации среды

$$f = \frac{\tau_p}{\tau^*} \ll 1. \tag{5}$$

Это условие является также условием ориентационной спектральной однородности полярного раствора (спектры люминесценции в этом случае не зависят от частоты возбуждающего света). При малых интенсивностях возбуждения время жизни основного электронного состояния чрезвычайно велико и распределение по ориентационным подуровням этого состояния следует считать равновесным для всех видов растворов. В возбужденном электронном состоянии равновесие по ориентационным подуровням устанавливается или не устанавливается в зависимости от выполнимости (5) и легко может

быть нарушено. В этом случае распределение элементарных ячеек по энергии взаимодействия в возбужденном состоянии не будет равновесным и, следовательно, УСС не должно иметь место. Установленные с помощью модели элементарной ячейки границы выполнимости УСС соответствуют экспериментально наблюдаемым [1].

В условиях медленной переориентации, когда (5) не выполняется, существует неоднородное ориентационное уширение спектров. Экспериментально оно может проявляться в зависимости спектра люминесценции от частоты возбуждения.

Так как в выражении (5) величина f определяет характер ориентационной спектральной однородности, то будем её называть фактором ориентационной спектральной однородности.

Отличительной особенностью систем с ориентационным уширением уровней является сравнительно простая возможность перевода их от однородного к неоднородному состоянию и обратно. Необходимый характер спектральной однородности может быть реализован за счет изменения как времени ориентационной релаксации среды, так и времени жизни возбужденного состояния (см. (5)). На эксперименте изменение характера ориентационной однородности достигнуто четырьмя различными способами:

1) увеличением τ_p за счет понижения температуры раствора [1];

2) увеличением τ_p за счет использования твердых растворов [1];

3) сокращением τ^* при тушении возбужденного состояния красителя посторонними примесями [7];

4) уменьшением τ^* под действием поля мощной световой волны [7].

Первоначально теория расчета ОКГ исходила из спектрально-люминесцентных свойств отдельной молекулы, по существу не учитывая её взаимодействия с молекулами растворителя. Такое приближение вполне пригодно для описания неполярных растворов красителей, но довольно грубо для молекул, находящихся в полярных растворах, т. к. не учитывает специфических особенностей, возникающих в результате влияния ММВ. В то же время в большинстве случаев наиболее эффективными активными средами являются именно полярные растворы красителей (например, производные фталимида, ксантеновые и полиметиновые красители в спиртах и глицерине) [10—11].

Цель настоящей работы — анализ генерационных свойств полярных растворов красителей с учетом специфических особенностей их спектральных свойств.

В работе рассматривается влияние ориентационного уширения на

1) коэффициент усиления, порог и мощность генерации;

2) зависимость характеристик генерации от температуры среды;

3) зависимости генерационных свойств от интенсивности и частоты накачки.

При рассмотрении мы исходили из того, что процессы возбуждения, генерации и изменения температуры среды могут вызывать нарушение распределения элементарных ячеек в возбужденном электронном состоянии и, следовательно, приводить к изменению спектров люминесценции и нарушению универсального соотношения Степанова.

Влияние ориентационного уширения на коэффициент усиления, порог и мощность генерации растворов красителей

Переход от полярного раствора к неполярному, а также сильное охлаждение раствора приводит в большинстве случаев к существенному повышению порога и падению мощности генерации [12]. Правильная качественная трактовка вопроса предложена в работе [13]: явление повышения порога генерации красителей прежде всего связывается в ней с ориентационным уширением электронных состояний.

Как следует из [10], коэффициент усиления $K_{21}(\nu)$, пороговая плотность радиации накачки $U_{\text{н}}^{\text{пор}}(\nu)$ и удельная мощность квазистационарной генерации $W_{\text{ин}}$ связаны со спектрально-люминесцентными свойствами раствора красителя и параметрами резонатора следующими выражениями:

$$K_{21}(\nu) = \sigma_{21}(\upsilon)\left[n_2 - n_1 \exp\left\{-\frac{h\Delta\nu}{KT}\right\}\right], \tag{6}$$

$$\tau BU_H^{\text{пор}} = \frac{K_{\text{пот}}(\nu) + \sigma_{12}(\nu)\cdot n}{\sigma_{21}(\nu)\cdot n}, \tag{7}$$

$$W_{\text{ин}}(\nu) = nh\nu[BU_H - BU_H^{\text{пор}}], \tag{8}$$

где $BU_H = \int_0^\infty B_{12}(\nu)U_H(\nu)\,d\nu$-скорость накачки, $\sigma_{21}(\nu)$ и $\sigma_{12}(\nu)$-сечения вынужденного испускания и поглощения, n-концентрация активных молекул в растворе, n_1 и n_2-суммарные населенности основного и возбужденного электронных состояний.

При выводе (6)—(8) считалось, что молекулы раствора находятся только в основном и возбужденном состояниях, т. е. $n = n_1 + n_2$.

Из формулы (6) следует, что коэффициент усиления возрастает с уменьшением величины

$$n_1(\Delta\nu) = n_1 \exp\left\{-\frac{h\Delta\nu}{KT}\right\}, \tag{9}$$

пропорциональной населенности подуровня с энергией $h\Delta\nu$.

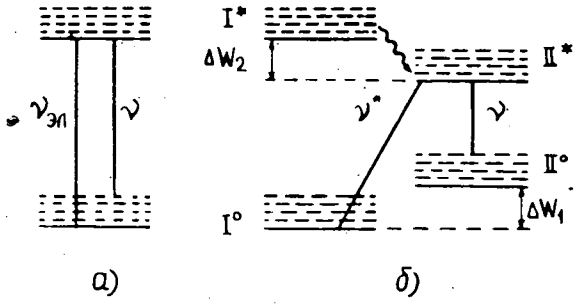

Рис. 2. Схема электронных уровней красителя в неполярном (а) и полярном (б) растворителях.

Следует иметь в виду, что, как показано в [9], в соотношениях, описывающих полярные растворы при условии (5), роль частоты чисто электронного перехода выполняет частота ν^*, определяемая энергетическим расстоянием между подуровнями I^0 и II^* (рис. 2б). Как видно из выражения (9), с увеличением зазора $h\Delta\nu$ значение $n_1(\Delta\nu)$ убывает по экспоненциальному закону.

Сравним величины зазоров $\Delta\nu$ в неполярных (рис. 2,а) и полярных (рис.2,б) растворах. Переход от одного типа раствора к другому связан с изменением схемы электронных уровней красителя в результате влияния ориентационных ММВ. В жидких полярных растворах при комнатной температуре (усл.(5)) конечным для испускания является ориентационный подуровень II^0, который расположен выше равновесного подуровня I^0 на величину ΔW_1. Для простоты можно предположить, что лазерный переход будет заканчиваться на одинаковых колебательных подуровнях основного состояния как в полярных, так и в неполярных растворах. В этом случае энергетический зазор $h\Delta\nu$ в полярном растворе, как это видно из рис. 2, больше на величину ориентационного уширения ΔW_1 основного электронного состояния. Для полярных растворов, как было показано в [9], величина ΔW_1 может достигать несколько тысяч обратных сантиметров. Следовательно, процессы межмолекулярной ориентационной релаксации, приводящие к значительному увеличению энергетического зазора $h\Delta\nu$, увеличивают инверсию лазерного перехода и поэтому могут вызывать существенный рост коэффициента усиления. Одновременно с увеличением коэффициента усиления в таких случаях, как это следует из формулы (7), должен заметно падать порог генерации из-за уменьшения поглощения $\sigma_{12}(\nu)$ в области генерации (для схемы 2б спектр люминесценции сильнее сдвинут в красную область по отношению к спектру поглощения, чем для схемы 2а).

Расчёт пороговых зависимостей накачки, выполненный для элементарных ячеек одного и того же красителя в неполярном и полярном растворителях, свидетельствует о существенном понижении порога при ориентационном уширении уровней. Особенно существенное снижение порога и, следовательно, увеличение мощности генерации полярных растворов достигается при малых коэффициентах потерь резонатора. Для коэффициентов потерь $\sim 0{,}01$ см$^{-1}$ величина порога в полярном растворителе почти в 2,5 раза ниже. При больших потерях ~ 1 см$^{-1}$ пороги практически совпадают.

С расчетами качественно согласуются экспериментальные измерения [12], в которых порог генерации 4-амино-*N*-метилфталимида при Kпот$\sim 0{,}01$ см$^{-1}$ возрастал в 3,7 раза при переходе от глицерина к диоксану (с учетом отличия квантовых выходов). К сожалению, более тщательное сопоставление экспериментальных данных с расчетными очень затруднено, так как на опыте характеристики генерации определяются не только ориентационным уширением, но и рядом других факторов (например, влиянием поглощения возбужденных молекул, для детального учета которых в большинстве случаев нет достоверных данных).

Понижение порога генерации раствора при возникновении ориентационного уширения уровней неизбежно и, как это следует из формулы (8), должно приводить к увеличению мощности генерируемого излучения. Наиболее существенное увеличение мощности генерации за счет ориентационного уширения уровней проявляется для накачек, не очень сильно превышающих пороговую.

Генерация растворов красителей при различных температурах

Для полярных растворов красителей, характеризующихся существенным ориентационным уширением уровней, экспериментально получены [12] сильные температурные зависимости частоты генерации. Так как эти зависимости представляют значительный практический интерес, то желательно было бы иметь математическое соотношение, которое позволяло бы рассчитывать их во всех необходимых случаях. Такое выражение для квазистационарной генерации выводится в данном разделе.

Частота генерации всегда удовлетворяет условию

$$\frac{\partial[K^0_{yc}(\nu)-K_{\text{пот}}(\nu)]}{\partial\nu}=0. \tag{10}$$

В общем случае, когда спектры поглощения и испускания могут не подчиняться УСС, выражение для коэффициента усиления может быть записано в виде:

$$K^0_{yc}(\nu)=n_2\sigma_{21}(\nu)-n_1\sigma_{12}(\nu). \tag{11}$$

Пусть потери в пределах спектральной области усиления одинаковы

$$\frac{\partial K_{\text{пот}}(\nu)}{\partial\nu}=0, \tag{12}$$

а длинноволновая часть контура $\sigma_{21}(\nu)$ описывается распределением Гаусса

$$\sigma_{21}(\nu)=\sigma_m\exp\left\{-\left(\frac{\nu_m-\nu}{\gamma_0}\right)^2\right\} \tag{13}$$

где σ_m-сечение предельного усиления в максимуме, γ_0-спектральная ширина $\sigma_{21}(\nu)$. Зависимость контура поглощения сложных молекул от температуры можно [14] описывать с помощью гиперболической функции

$$\sigma_{12}(\nu)=\sigma e^{b\nu}\operatorname{sech}\left[\frac{a}{T}(\nu-\nu_1)\right], \tag{14}$$

где σ, a, b и ν_1-постоянные, характеризующие данный сорт молекул (ν_1-величина, близкая к частоте электронного перехода). В области генерации, где $\frac{a}{T}(\nu-\nu_1)>2$, из (14) следует

$$\sigma_{12}(\nu)=\sigma\exp\left[\left(b-\frac{a}{T}\right)\nu\right]. \tag{15}$$

После подстановки (13) и (15) в (II) с учетом (12) получаем

$$\nu_{\text{г}}=\nu_m(f)-\frac{\left(b-\frac{a}{T}\right)\gamma_0^2}{2\left\{1+\dfrac{K_{\text{пот}}}{n_1\sigma\exp\left[\left(b-\frac{a}{T}\right)\nu\right]}\right\}}. \tag{16}$$

Уравнение (16) позволяет проанализировать зависимость частоты генерации $\nu_г$ от свойств активной среды и резонатора. Прежде всего, из (16) видно, что частота генерации $\nu_г$ меньше частоты максимума ν_m спектра предельного усиления и зависит от концентрации n_1 и коэффициента потерь $K_{пот}$ излучения в резонаторе во всех случаях, кроме одного, когда населенность основного состояния равна нулю. В этом случае второе слагаемое в формуле (16) обращается в нуль, и генерация идет только на частоте ν_m. На практике для получения генерации вблизи максимума сечения вынужденного испускания ν_m достаточно, чтобы второе слагаемое в правой части (16) было значительно меньше спектральной ширины контура люминесценции. Это условие может быть выполнено для веществ с большим стоксовым сдвигом спектров $\left(\sigma \exp\left[\left(b-\frac{a}{T}\right)\nu\right]\text{-мало}\right)$. Соответствующие закономерности наблюдаются экспериментально [10].

Частота излучения генерации, как правило, зависит от температуры раствора красителя (см. (16)).

Чувствительность частоты генерации к изменению температуры зависит от концентрации вещества и потерь резонатора. Если во всем интервале вариации температуры второе слагаемое в (16) очень мало по сравнению с шириной контура люминесценции, то независимо от температуры, генерация будет происходить вблизи максимума полосы люминесценции вещества. При увеличении концентрации красителя и уменьшении коэффициента потерь резонатора, второе слагаемое в (16) растет, что создает условие для проявления температурной зависимости спектра генерации.

В полярных растворах красителей при уменьшении температуры вследствие изменения времени ориентационной релаксации среды осуществляется переход от условия однородного уширения (5) к условиям неоднородного уширения ($f \gg 1$).

Как известно [1,2], такой переход сопровождается сильным смещением спектров люминесценции $\sigma_{21}(\nu)$ и следовательно, $\nu_m(f)$ в коротковолновую область вследствие изменения ориентационных взаимодействий. Спектры поглощения при этом практически не изменяются.

Из выражения (16) видно, что если уменьшение температуры приводит к коротковолновому смещению максимума спектра испускания $\nu_m(f)$, то смещение частоты генерации раствора будет всегда превышать его из-за влияния второго слагаемого. Температурная перестройка спектра генерации, основанная на ориентационных эффектах, особенно эффективна в растворах производных фталимида [12]. Температурное смещение спектра генерации такого типа наблюдалась нами экспериментально также на примере глицеринового раствора криптоцианина [15].

При расчете частоты генерации полярных растворов по формуле (16) необходимо знать функцию $\nu_m(f)$ и учесть еще зависимость фактора ориентационного уширения f от излучения, сокращающего время жизни возбужденного состояния. Если в качестве такого излучения служит генерируемая радиация, то в выражении для величины f вместо времени спонтанного распада возбужденного состояния следует рассматривать время жизни с учетом вынужденных переходов, вызванных генерируемым излучением. В этом случае расчёт

частоты генерируемого излучения в общем случае должен производиться по формуле (16), в которой под параметром ориентационной однородности f следует понимать выражение

$$f_x = \frac{\tau_p(T)[(1-p)+px]}{\tau^*}, \tag{17}$$

где

$$p = \frac{K_{\text{пот}}}{n_1\sigma_{21}(\nu)} + \frac{\sigma_{12}(\nu)}{\sigma_{21}(\nu)},$$

x-число порогов накачки.

Так как смещение частоты генерации может быть связано не только с температурой, но и с изменением накачки (формула (17)), то правильнее говорить о температурном смещении генерации при каком-то постоянном уровне накачки.

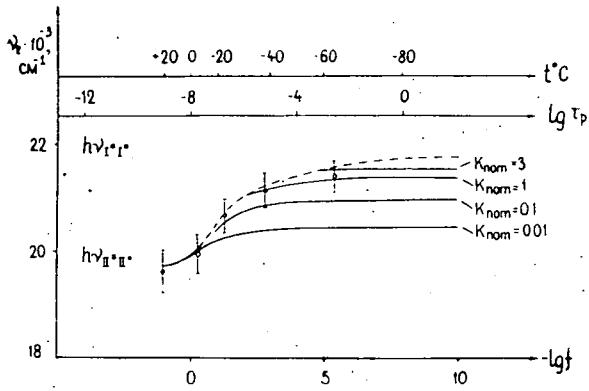

Рис. 3. Зависимость частоты генерации 3-аминофталимида в глицерине от фактора ориентационной спектральной однородности, рассчитанная по (16) для различных коэффициентов потерь резонатора $K_{\text{пот}}$. Вертикальными отрезками обозначены экспериментальные спектры генерации, полученные при вариации фактора f изменением температуры раствора. Пунктиром указана зависимость максимума люминесценции от фактора f.

На рис. 3 приведены рассчитанные по (16) частоты генерации 3-аминофталимида в глицерине в пороговом режиме $x \sim 1$ для различных температур (а, следовательно, и различных значений фактора ориентационной однородности f) и для разных величин коэффициента потерь излучения в резонаторе $K_{\text{пот}}$. Если значение коэффициента потерь невелики $K_r = 0{,}01$ см$^{-1}$, то зависимость ν_r от T слабая. Измеренная на опыте при коэффициенте потерь на зеркалах $K_r \sim 0{,}01$ см$^{-1}$ зависимость спектра генерации (вертикальные отрезки на рисунке 3) от температуры для 3-аминофталимида в глицерине ($\tau^* = 1{,}2 \cdot 10^{-8}$ сек) при небольших превышениях накачки над порогом $x \sim 1$ оказалась близкой к рассчитанной при коэффициенте потерь $K_{\text{пот}} = 1$ см$^{-1}$.

Из формулы (17) следует, что одно и то же смещение спектра генерации может быть получено как изменением накачки δx при фиксированной температуре, так и при изменении температуры δT раствора за счет изменения τ_p при постоянной накачке, если только при этом одинаково изменилось значение фактора ориентационного уширения f.

Связь между величинами δx и δT, необходимая для того, чтобы эти величины приводили к одинаковому смещению спектра генерации, имеет вид:

$$dx = \frac{1}{\tau_p}\frac{d\tau_p}{dT}\frac{(1-\gamma)+\gamma x}{\gamma}\delta T. \qquad (18)$$

Для глицериновых растворов красителей при комнатной температуре $\tau_p = 10^{-9}$ сек, $\frac{d\tau_p}{dT} = -3\cdot 10^{-10}$ сек град$^{-1}$. Подставляя эти значения в (18) получаем, что при $x=1$ понижение температуры ниже комнатной на 22° по своему действию эквивалентно увеличению мощности накачки в 15 раз. Эта оценка согласуется с результатами эксперимента: в глицериновом растворе 3-аминофталимида при комнатной температуре мы наблюдали смещение частот генерации на $\Delta\nu = 300$ см$^{-1}$ при увеличении накачки от $x=1$ до $x=15$. Такое же смещение, как видно из рис. 3, получается при охлаждении раствора на 27° С от 20 °С до −7 °С при фиксированной накачке красителя $x=1$. В неполярных растворах спектр генерации не зависит от накачки x.

Зависимости частоты и порога генерации от частоты возбуждения

Непосредственная связь спектров генерации со спектрами люминесценции в растворах красителей, выражаемая формулой (16), позволяет сделать вывод о том, что спектры генерации красителей должны зависеть от частоты возбуждения при тех же условиях в растворах, при которых наблюдается батохромная люминесценция [4—9], т. е. когда существует зависимость максимума люминесценции ν_m от частоты возбуждения $\nu_b (f \gg 1)$. Следует отметить, что подобная зависимость до сих пор не наблюдалась. Она может рассматриваться как аналог батохромной люминесценции в вынужденном испускании красителей. В неполярных растворах частота генерации не зависит от частоты возбуждения.

На рис. 4 приведены рассчитанные по (16) частоты генерации (кривые 1—6) полярного раствора типичного фталимида в зависимости от частоты возбуждения при различных потерях излучения в резонаторе $K_{\text{пот}}$, а также зависимость максимума батохромной люминесценции от частоты возбуждения (кривая 7). Из этого рисунка видно, что уменьшение частоты возбуждения раствора, не находящегося при условии (5), может приводить к существенному изменению частоты генерации. Интервал частот накачки, в котором происходит наиболее существенное смещение частоты генерации, примерно соответствует диапазону самого значительного изменения максимума батохромной люминесценции. При коэффициентах потерь $K_{\text{пот}} > 0{,}5\cdot 10^{-4}$ см$^{-1}$ частота генерации смещается в красную область с уменьшением частоты возбуждения. Для очень малых значений коэффициент потерь $K_{\text{пот}} < 0{,}5\cdot 10^{-4}$ см$^{-1}$

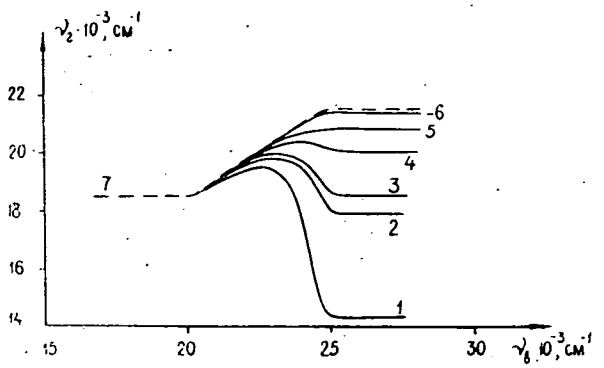

Рис. 4. Расчётные зависимости частоты генерации полярного раствора от частоты возбуждения при различных потерях в резонаторе (1—6) и зависимость максимума спектра коэффициента $B_{21}(\nu)$ от частоты возбуждения (7): 1: $K_{\text{пот}}=0{,}5\cdot10^{-5}$ см$^{-1}$; 2: $K_{\text{пот}}=10^{-5}$ см$^{-1}$; 3: $K_{\text{пот}}=1{,}25\cdot10^{-5}$ см$^{-1}$; 4: $K_{\text{пот}}=2{,}5\cdot10^{-5}$ см$^{-1}$; 5: $K_{\text{пот}}=0{,}6\cdot10^{-4}$ см$^{-1}$; 6: $K_{\text{пот}}=0{,}5\cdot10^{-3}$ см$^{-1}$.

частота генерации нетривиальным образом изменяет свое поведение и описывает крюк при изменении возбуждения в области 20 000—25 000 см$^{-1}$. В этом случае с уменьшением частоты возбуждения частота генерации сначала смещается в синюю сторону (несмотря на то, что спектр люминесценции при том же изменении возбуждения смещается в красную сторону), а затем, после достижения максимума, наблюдается смещение частоты генерации в красную сторону. Это происходит вследствие того, что в условиях неоднородного ориентационного уширения при изменении частоты возбуждения ν_B осуществляется переход к возбуждению элементарных ячеек, характеризующихся иными спектральными свойствами люминесценции. Для растворов с однородным ориентационным уширением спектров (усл. (5)) спектр коэффициента усиления (кр.2) при одинаковой скорости накачки $B_{12}(\nu_b)U_h(\nu_b)$ не зависит от частоты возбуждения, так как перед актом испускания успевает устанавливаться универсальное равновесное распределение возбужденных ячеек раствора.

Результаты, изложенные в данной работе показывают, что при описании свойств генерации полярных растворов красителей необходим учет влияния ММВ, приводящего к ориентационному уширению электронных состояний. Учет влияния ММВ необходимо производить при решении всех практически важных задач: при расчете порога и мощности генерации, зависимостей генерационных параметров от температуры и частоты возбуждения. Разумеется, что расчёт генерационных характеристик растворов красителей должен производиться с одновременным учетом как процессов, связанных с ориентационным уширением уровней, так и триплет-триплетного поглощения, свойств резонатора и накачки.

* * *

В заключение авторы считают своим приятным долгом выразить признательность академику **Б. И. Степанову** за постоянное внимание и поддержку.

ЛИТЕРАТУРА

[1] *Бахшиев, Н. Г.:* Спектроскопия ММВ, „Наука", Ленинград, 1972.
[2] *Мейстер, Т. Г.:* Электронные спектры многоатомных молекул, Ленинград, 1970.
[3] *Liptay V. V.* Modern Quantum Chemistry, 2, Acad Press, New York, 1965.
[4] *Томин, В. И.:* Материалы I респ. конфер. молодых ученых, 77, Минск, 1970.
[5] *Рубинов, А. Н., В. И. Томин:* Опт. и спектр. **29,** 1082 (1970); **32,** 424 (1972).
[6] *Рубинов, А. Н., В. И. Томин:* Опт. и спектр. **30,** 859 (1971).
[7] *Томин, В. И., А. Н. Рубинов, В. Ф. Воронин:* Опт. и спектр. **34,** 1108 (1973); Acta Phys. et Chem. Szeged **18,** 115 (1972).
[8] *Томин, В. И.:* Материалы II республ. конф. молодых ученых, **49,** Минск, 1972.
[9] *Томин, В. И.:* Автореферат канд. диссертации, Минск, 1973.
[10] *Степанов, Б. И., А. Н. Рубинов:* УФН **95,** 45 (1968).
[11] *Bass, M. T. F. Deutsch, M. I. Weber:* Lasers, 3, M. Dekker Ine, New York, 1971.
[12] *Пикулик, Л. Г., Л. Ф. Гладченко:* Сб. „Квантовая электроника" и лазерная спектроскопия", 120, Минск, 1971.
[13] *Бахшиев, Н. Г., В. И. Студенов:* Опт. и спектр. **33,** 115 (1972).
[14] *Домби, И., И. Кечкемети, Л. Козма:* Опт. и спектр. **18,** 710 (1965).
[15] *Рубинов, А. Н., В. И. Томин:* ЖПС **13,** 788 (1970).
[16] *Аристов, А. В., Н. Г. Бахшиев, В. А. Кузин, И. В. Питерская:* Опт. и спектр. **30,** 143 (1971).

CHARACTERISTICS OF STIMULATED EMISSION OF DYES IN POLAR SOLUTIONS

A. N. Rubinov and V. I. Tomin

The effect of orientational broadening of vibronic (electronic vibrational) levels due to molecular interactions, on the threshold and the spectral characteristics of stimulated emission in polar dye solutions has been investigated. It has been stated that the extent of the orientational broadening of the levels exerts a considerable influence on the threshold and the power of stimulated emission. A formula permitting to calculate the frequency of stimulated emission at different temperatures, pumping intensities, and loss coefficients of the resonator is deduced. It is shown that the orientational broadening leads to additional dependence of the spectrum of stimulated emission on temperature of the medium, on intensity and frequency of pumping.

THERMAL DECOMPOSITION OF ACETALDEHYDE IN THE PRESENCE OF NITRIC OXIDE

By

I. BÁRDI and F. MÁRTA

Gas Kinetics Research Group of the Hungarian Academy of Sciences, Szeged and Institute of General and Physical Chemistry, Attila József University, Szeged

(Received 10 December, 1973)

The pyrolysis of acetaldehyde in the presence of nitric oxide has been studied in the temperature range 495—550 °C at an initial acetaldehyde pressure of 25—200 torr and at 0—50 torr nitric oxide pressure. The decomposition was followed by pressure measurements and by GC analysis. The order of reaction with respect to CH_3CHO and NO was determined by different methods. From pressure measurement data "influencing curves" were deduced and on this basis, some properties of the catalytic and inhibition region are summarized. Arrhenius parameters are given for the overall decomposition in the catalytic region. The effect of nitric oxide on the formation of major and some of the minor products (*e.g.* H_2, C_2H_6, C_2H_4, acetone, HCN) was investigated in the catalytic and inhibited regions. The possible routes of product formation are shortly discussed and a simple mechanism is given for the NO influenced aldehyde decomposition.

Introduction

The influence on the acetaldehyde decomposition of different substances has been a frequently studied field of reaction kinetics. It was established that N_2O, H_2S, I_2, Br_2, O_2, HCl, HBr, propylene, nitric oxide, etc. have a strong catalytic effect on the decomposition of acetaldehyde, while in the case of nitric oxide and propylene, inhibition takes place, too [1, 31—34]. In consequence of this double effect, the NO aroused considerable interest.

Many articles have been published in this field, the earlier ones, based on pressure measurements, did not provide detailed information [2, 3—5]. More recent investigations were carried out by gas chromatography (GC) and mass spectroscopy (MS) [6, 7]. These latest publications, altogether with LAIDLER's recent investigations [8, 9] give us nowadays the best informations in this field, stating the following: the order of decomposition with respect to acetaldehyde is 3/2 in a wide pressure range of aldehyde and NO, and in the catalytic region the decomposition is proportional to the square root of NO concentration. SCHUCHMANN and LAIDLER [9] during the pyrolysis have indentified the products listed in Table I. Rates of formation of the most important products as a function of NO pressure are shown according to [9], in Fig. 1.

On the basis of the mentioned experimental results, LAIDLER assumes two chain carriers in the system, namely CH_3 and CH_2CHO radicals. The concentrations of these two chain carriers are independent of each other, and the NO influences

Table I

Products of pyrolysis in the presence of NO *according to* SCHUCHMANN *and* LAIDLER [9]

Major products	Minor products	N_2-containing products	Compounds, which were not obtained during pyrolysis
CO	H_2, CO_2, H_2O, C_2H_5CHO, C_2H_4	N_2, N_2O, HCN, CH_3NCO, C_2H_5NCO	CH_2O, CH_3ONO, CH_3NO_2, CH_3ONO_2, CH_3OH, CH_2CO, CH_3CN, C_2H_5OH, $CH_3OC_2H_3$, $(CH_3)_2CHOH$, $CH_3COCOCH_3$
CH_4	C_2H_6, C_3H_6 CH_3COCH_3 $CH_3COOCH=CH_2$ (crotonaldehyde)?		

their concentrations in different ways. In the case of methyl radicals, both generation and removal take place in a direct reaction with NO, while in the case of CH_2CHO radicals, the formation takes place in an indirect way

$$CH_3+CH_3CHO \rightarrow CH_4+CH_2CHO$$

and the consumption of this radical commences in a direct reaction with NO.

$$CH_2CHO+NO \rightarrow ONCH_2CHO \rightarrow HCN+CO+H_2O.$$

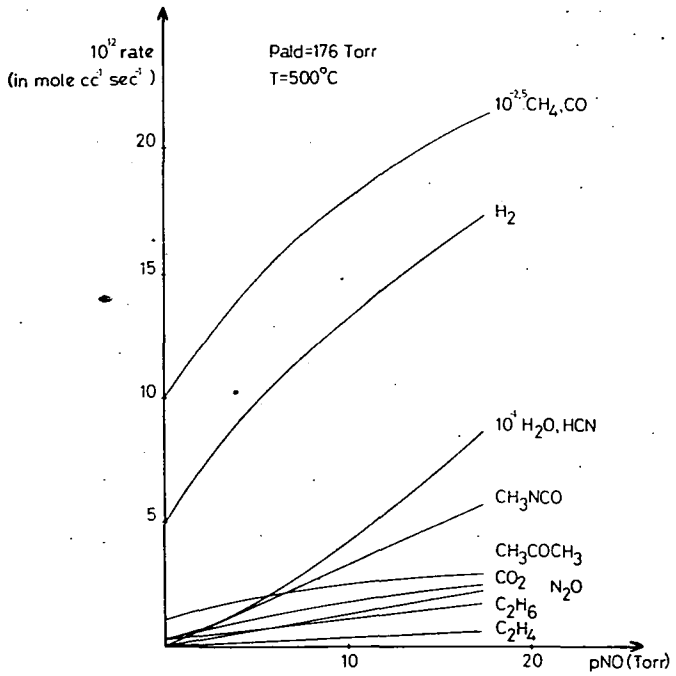

Fig. 1. Rate of formation of pyrolysis products as function of NO pressure, according to SCHUCHMANN and LAIDLER [9]. $p_{ald}=176$ torr, $t=500$ °C

LAIDLER assumes new initiation steps in the presence of NO, wich explain the increase in the amount of major products According to their very detailed analytical investigations SCHUCHMANN and LAIDLER proposed a more accurate mechanism consisting of 41 steps. The steady-state equations derived from this mechanism are in good agreement with the experimental rate—[NO] curves, which verifies the validity of the mechanism.

After finishing the investigation of the decomposition of the pure acetaldehyde [25], we wished to clear up the influence of NO on the kinetics of decomposition and the distribution of products. Detailed investigations had been carried out earlier in our Institute with the propionaldehyde—NO system [10, 11], which offered a good opportunity to compare these two systems.

Experimental

The apparatus and procedures were essentially the same as used previously [25]. The mixture of aldehyde and NO was left to stand half an hour, during which, to promote good mixing, we used thermodiffusional stirring. This time was enough to reach a good mixing, and the "cold reaction", mentioned by SCHUCHMANN and LAIDLER [9], (*i.e.* the reaction between aldehyde and NO at room temperature and in darkness) could not be observed. In most cases the reaction was followed by the measurement of pressure change and the products were analysed by GC. To facilitate the analysis, the products were separated into fractions condensable and non condensable at liquid air temperature. The GC apparatus used and the methods of analysis were similar to those used previously [25].

Materials. NO was produced by the method of WINKLER [12]. The frozen NO was subjected to low temperature bulb to bulb distillation and was stored in a storage vessel.

CH_3CHO. The purification and storage of acetaldehyde were the same as described earlier [25]. In the same paper we gave detailed methods of purification of the chemicals used to calibrate the GC.

Pressure—time measurements

The experiments were carried out at five temperatures (495.5, 512, 527.5, 539.5, 550.5 °C) and at four different aldehyde concentrations (25, 50, 100, 200 torr). The concentration of NO changed between 0 and 50 torr. The reproducibility of our experiments was satisfactory. The character of pressure—time curves, plotted from the experimental data, does not change in the presence of NO, as it can be seen in Fig. 2; only, depending on the effect of NO, a rate increase is observable.

The order of reaction

The order of reaction with respect to aldehyde has been found to be 3/2 in a wide pressure range [7]. From the initial rates (calculated from the pressure—time curves by computer), the order of reaction with respect of aldehyde was determined and agreement with literature was found, but only in the case when the aldehyde

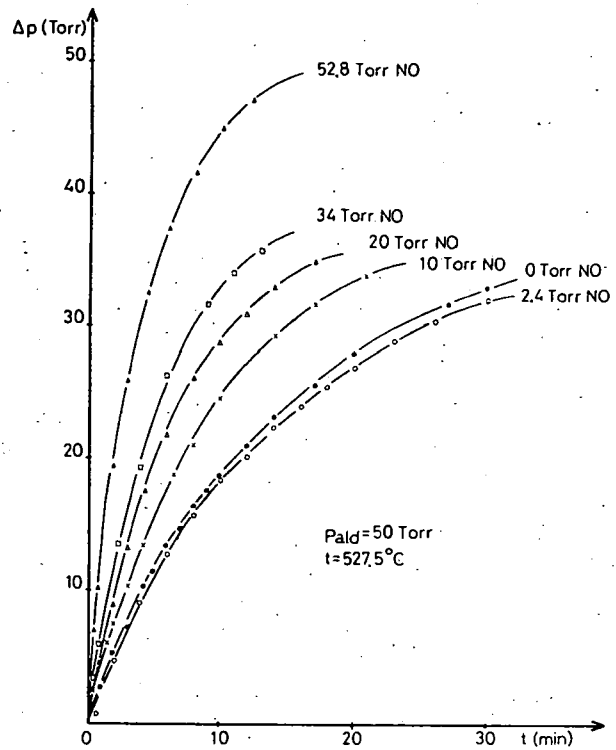

Fig. 2. Pressure—time curves at different NO concentrations. ● 0 torr; ○ 2.4 torr; × 10 torr; △ 20 torr; □ 34 torr; ▲ 52.8 torr NO. $p_{ald}=50$ torr, $t=527.5$ °C

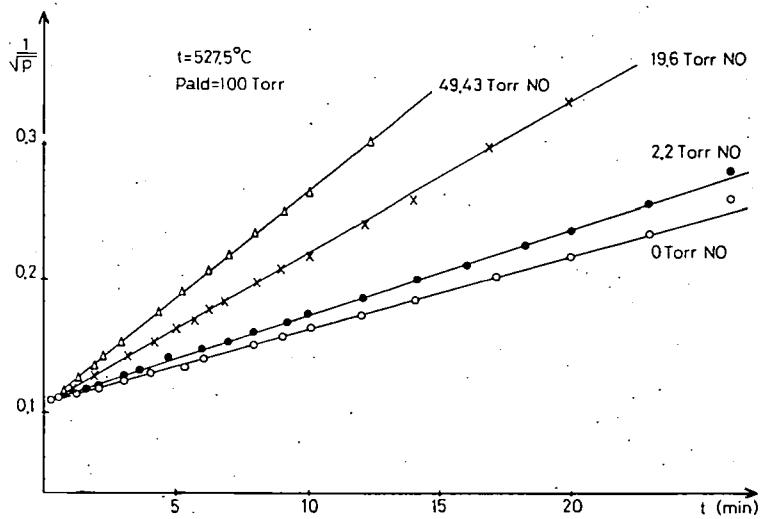

Fig. 3. $p^{-1/2}$—t curves at different NO concentrations. $t=527.5$ °C, $p_{ald}=100$ torr. ○ 0 torr; ● 2.2 torr; × 19.6 torr; △ 49.43 torr NO

concentration was above 50 torr and the NO concentration above 5 torr (*i.e.* in the so called catalytic region). This order did not show any significant change neither by the effect of temperature increase, nor due to the increase of NO concentration. This value and the same behaviour was found to be valid if the rate was calculated point by point from the pressure—time curves.

To check the validity of the above value of reaction order, the inverse square root of the actual pressure *vs.* time was plotted. This must give a straight line if the order of reaction is 3/2. As it can be seen from Fig. 3, this condition is fulfilled above 100 torr initial aldehyde concentration at any NO concentration, but at 50 and 25 torr aldehyde pressures a slight curvature can be observed.

Using the $\log w_0$—$\log p_0$ graphs the order of reaction was determined with respect of NO concentration.

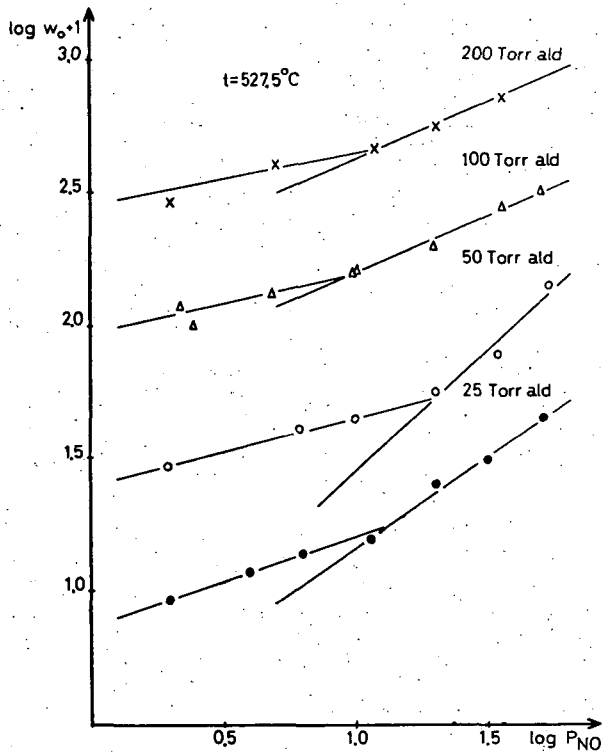

Fig. 4. $\log w_0$—$\log p_0^{NO}$ curves at different aldehyde concentrations. $t = 527.5$ °C. ● 25 torr; ○ 50 torr; △ 100 torr; × 200 torr aldehyde

As it can be seen from Fig. 4, where the results of a series of experiments are plotted, the experimental points under 5 torr NO always deviate consequently and a break appears in the line. Omitting these values, the order of decomposition with respect of NO will be very close to 0.5, which agrees quite well with the value found in literature.

As it was mentioned above, the order with respect to aldehyde in the presence of NO, under special circumstances ($p_{ald}>50$ torr and $p_{NO}>5$ torr) was found to be 3/2, similarly to the decomposition of pure acetaldehyde, and on the basis of these data obtained by pressure measurements, 3/2 order rate constants (k') were calculated. As the values of these rate constants showed no trend within one experiment; this means that the right order has been established. The mean values of the rate constants collected in Table II were used for the calculations. As it can be seen from the table, the rate constants change with increasing NO concentration.

On the basis of our experimental data the validity of the expression

$$x^{-1/2} = 1 + \frac{1}{2} k\tau$$

was checked.

Table II

3/2 Order rate constants, $k' \cdot 10^{-2}$ (in $l^{1/2}$ mole^{-1} sec^{-1}) calculated from pressure—time measurements at different temperatures and at different initial aldehyde and NO *pressures*

t °C	P_{NO} (torr) / P_{ald} (torr)	0.5	1	10	20	35	50
512 °C	25	2.0466	2.2842	3.3214	4.3910	6.2307	7.8356
	50	2.0061	2.0780	3.5765	4.9359	5.7482	6.4391
	100	2.2864	2.4938	3.3433	5.0071	6.1949	7.6908
	200	2.5683	2.8815	3.8727	—	6.4220	7.4857
527.5 °C	25	4.1725	3.0955	5.6788	7.9451	9.9824	13.0743
	50	4.0180	4.0552	5.7085	7.1422	9.4212	12.6311
	100	4.5319	4.5650	6.5204	8.1801	10.3819	12.0651
	200	—	—	7.0976	8.4977	10.4713	—
539.5 °C	25	5.6820	6.4810	7.9751	10.5422	17.9280	18.9714
	50	5.8059	6.0799	8.7783	10.9755	13.9311	17.4890
	100	6.4289	—	9.1310	11.9646	15.4762	18.2058
550.5 °C	25	8.7468	9.8916	13.3774	17.0703	22.3297	—
	50	9.0301	7.8097	12.2757	15.9104	19.9267	23.1799

This expression is obtained from

$$k = \frac{2}{t} [c^{-1/2} - c_0^{-1/2}]$$

by rearranging and introducing some symbols ($c/c_0 = x$ and $c_0^{1/2} t = \tau$).

In the case of reactions of 3/2 order, plotting $x^{-1/2}$ against τ, a straight line is obtained, the slope of which gives $k/2$. This expression was found to be valid only in the catalytic region, as Fig. 5 shows.

On the basis of this expression, 3/2 order rate constants were calculated from our experimental data.

Influencing curves

If k'_{NO} (the rate constant calculated from experiments in the presence of NO) is divided by k (rate constant in the absence of NO), and k'_{NO}/k $(F(I))$ is plotted as a function of the pressure of NO, the curves obtained very characteristically show the inhibition and catalysis phenomena and offer the possibility of a quick view of experimental data. Typical influencing curves are shown in Fig. 6.

In Fig. 6, the points of the curves below and above the value 1 indicate inhibition and catalysis, respectively.

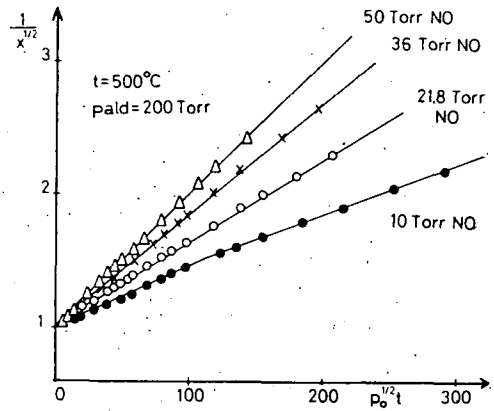

Fig. 5. $x^{-1/2}$—$p_0^{1/2}\,t$ (τ) relationship at different NO concentrations. $t=500$ °C $p_{ald}=200$ torr. ● 10 torr; ○ 21.8 torr; × 36 torr; △ 50 torr NO

It can be seen from Fig. 6 that above 100 torr aldehyde concentration the rate of reaction monotonously increases with NO concentration (catalytic region). As seen from Fig. 6, above 150 torr aldehyde concentrations the effect of NO practically does not depend on the initial aldehyde concentration. This is proved by the fact that the experimental points at 150 and 200 torr aldehyde concentrations coincide with each other. The aldehyde dependence of the NO effect below 50 torr aldehyde appears not only in the decrease of catalytic effect, but also in inhibition. With increasing NO concentration the inhibition changes into catalysis.

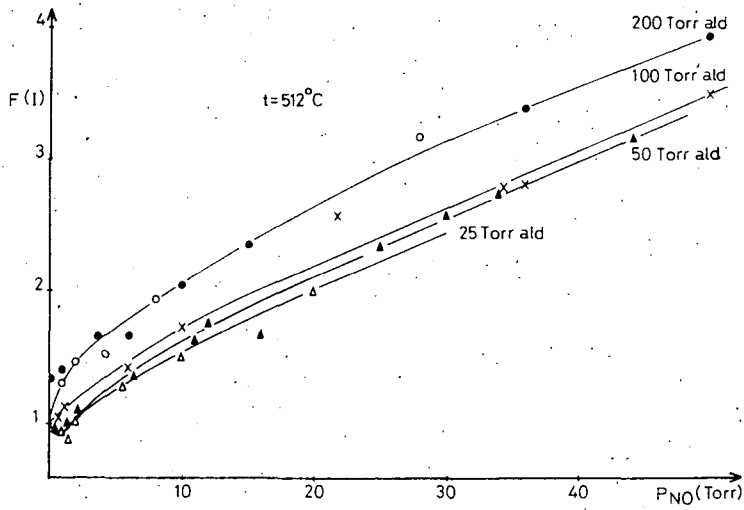

Fig. 6. Aldehyde dependence of influencing curves at 512 °C. △ 25 torr; ▲ 50 torr; × 100 torr; ○ 150 torr; ● 200 torr aldehyde

Similar behaviour was found by LAIDLER and EUSUF [13] in the case of propionaldehyde, where, independently from the initial aldehyde concentration, an inhibition period going over into catalysis was always found to appear. In the catalytic region the rate of reaction is independent of the pressure of aldehyde.

With increasing temperature, the degree of catalysis strongly decreases, as it can be seen from Fig. 7.

This decrease is very significant at higher concentrations of NO and aldehyde.

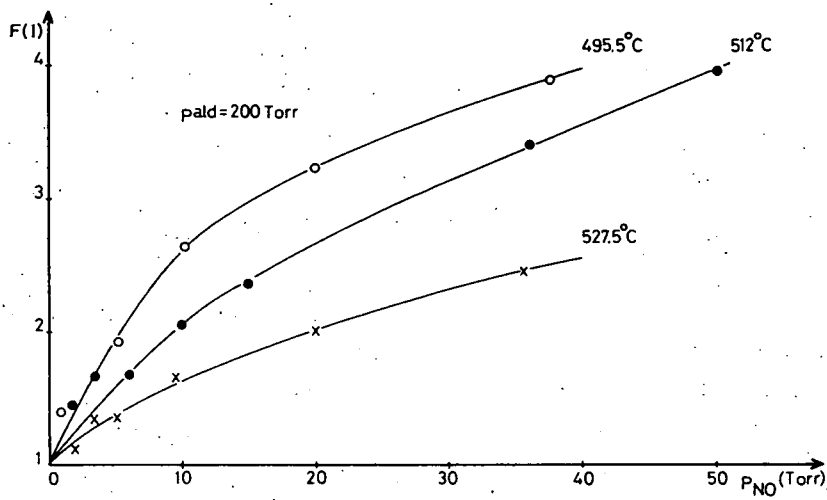

Fig. 7. Temperature dependence of influencing curves in the catalytic region. p_{ald}=200 torr. ○ 495.5 °C; ● 512 °C; × 527.5 °C

In contrary, by increasing the temperature, the inhibition markedly increases (Fig. 8).

It turns out from the influencing curves that the aldehyde decomposition in the presence of NO may be divided into two sections, *i.e.* the catalytic and inhibition sections. The characteristic features of these two stages can be summarized as follows.

Catalytic region

At above 100 torr aldehyde concentrations, only catalysis exists at any NO concentration. In this region, the rate of decomposition was found to be proportional to $p_{NO}^{1/2}$. If the 3/2 order rate constants k' (presented in Table II) are divided by the square root of p_{NO}, then the rate constant values tend to be independent of the NO and aldehyde concentrations (within the limits of experimental error), as it can be seen in Table III.

Using the mean values of these rate constants (Table IV), the overall activation energy of the NO influenced decomposition was determined from the temperature

Table III

$k'/p_{NO}^{1/2} \cdot 10^{-2}$ values at 512 °C at different NO and aldehyde pressures

P_{ald} (torr) \ P_{NO} (torr)	10	20	35	50
25	1.0226	0.9820	1.0531	1.0948
50	1.0318	0.9872	0.9857	0.9104
100	1.0573	1.0724	1.0447	1.0875
200	1.2247	—	1.0709	1.0587

dependence of $k'/p_{NO}^{1/2}$ for the catalytic region. These values are:

$$E_a = 41.38 \pm 0.79 \text{ kcal/mole}.$$

$$A = 3.618 \pm 0.214 \cdot 10^{12}$$

(at 25—200 torr aldehyde and 10—50 torr NO concentrations). The Arrhenius parameters obtained in this way are comparable with LAIDLER and EUSUF's values,

$$k = 2.2 \cdot 10^{12} \exp -43.5/RT \; l^{1/2} \text{ mole}^{-1} \text{ sec}^{-1}$$

(at 100 torr aldehyde and 50 torr NO concentration).

Table IV

Mean values of $k'/p_{NO}^{1/2} = \bar{k}$ at different temperatures ($k' \cdot 10^{-2}$ values in $l^{1/2}$ mole^{-1} sec^{-1}, p_{NO} in torr)

t °C	$\bar{k}$
512	1.0456[a]
527.5	1.8073[a]
539.5	2.5980[b]
550.5	3.6578[c]

Notes

(*a*) Average of 15 data
(*b*) Average of 12 data
(*c*) Average of 7 data

Inhibition region

On the basis of our experimental data, only qualitative remarks can be given for this region of reactions. The appearance of inhibition is the function of aldehyde and NO concentration. Above 100 torr initial aldehyde concentration, inhibition is practically impossible to be detected, since a small amount of NO (~0.5 torr) causes a significant catalysis. The inhibition region caused by NO is very narrow (it is observable up to max. 5—6 torr NO) and the inhibition is inversely proportional to the aldehyde concentration. The inhibition region significantly increases with the temperature (for example at 50 torrin itial aldehyde concentration, 50 °C temperature rise increased the inhibition region to the threefold). The degree of inhibition also increases, as can be seen from Fig. 8.

Fig. 8 shows that the value of the rate minimum (the maximally inhibited rate) shifts towards lower NO concentrations, due to the effect of temperature rise. This behaviour is in contradiction with that found by MÁRTA and SZABÓ [15] in the propionaldehyde—NO system, where the value of the rate minimum shifts towards higher NO concentrations. This fact is interpreted by the authors considering that, at higher temperatures, the primary steps take place much more often, thus the radical concentration is higher and to remove this higher radical concentration more NO is needed. A similar effect of temperature on the degree of inhibition was found in the investigation of RICE and VARNERIN [6]. In contrary to our observations, EUSUF and LAIDLER [8] found the degree of inhibition to decrease with temperature.

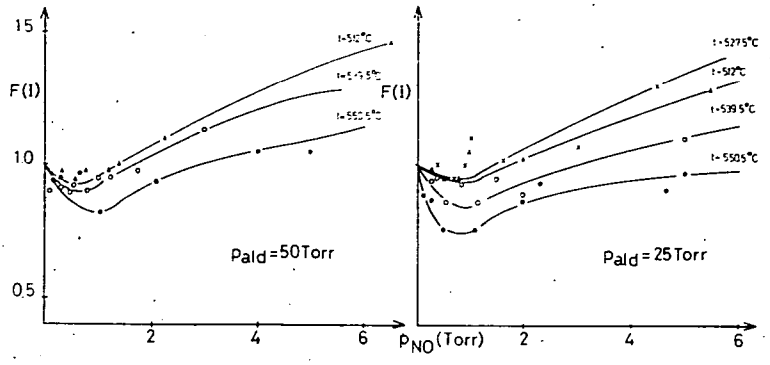

Fig. 8. Temperature dependence of influencing curves in the inhibited region. $p_{ald} = 50$ torr and 25 torr. $t = \times$ 527.5 °C; ▲ 512 °C; ○ 539.5 °C; ● 550.5 °C at 25 torr aldehyde. $t =$ ▲ 512 °C; ○ 539.5 °C; ● 550.5 °C at 50 torr aldehyde

As well known, oxygen in very small amounts ($\sim 10^{-3}$%) exerts a strong catalytic effect on the decomposition of aldehyde [14], and changes very significantly the rate of NO influenced decomposition. In the presence of trace amounts of oxygen, we observed significant inhibition at 200 torr initial aldehyde concentration, at which concentration under oxygen-free conditions, only catalysis could be observed.

Analytical survey of products

In some cases our experiments were connected with GC analysis. These measurements were made at 512 °C with two aldehyde concentrations (80 and 50 torr) and four NO concentrations (0.75, 10, 20, 40 torr), which cover both the catalytic and inhibition regions.

The effect of NO *on major products*

Some typical concentration—time plots for CH_4 and CO formation in the presence of NO are shown in Figs. 9 and 10, respectively, where the results of experiments at 512 °C, at 80 torr aldehyde pressure and at different NO concentration are plotted. This reaction mixture represents the catalytic region.

It can be seen from the Figs 9 and 10 that the shapes of the curves representing the formation of major products in the presence of NO do not change, however strongly the amount of major products increases with the increase in NO concentration. This increase is observable in the pressure—time curves, too (Fig. 2). In the maximally inhibited region, as it can be seen in Fig. 11, this increase is smaller but definitely exists.

This increase in the concentration of major products with increasing NO concentration can be interpreted by supposing that the NO reacts with the aldehyde molecule, abstracting hydrogen and producing R radicals, which can continue the chain

$$RH + NO \rightarrow HNO + R.$$

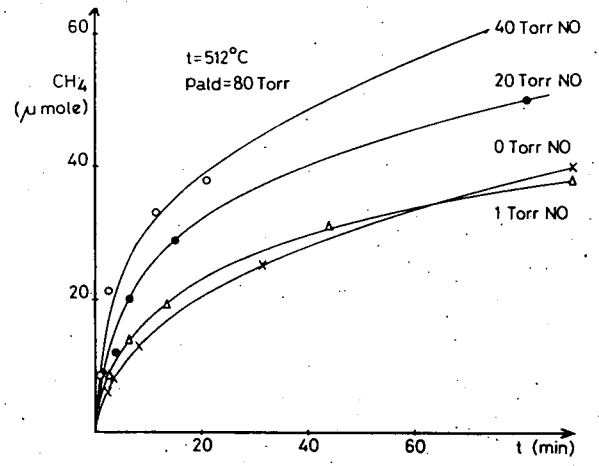

Fig. 9. Formation of CH_4 as function of time at different NO concentrations (catalytic region) $t=512$ °C, $p_{ald}=80$ torr; p_{NO}: △ 0 torr; × 1 torr; ● 20 torr; ○ 40 torr

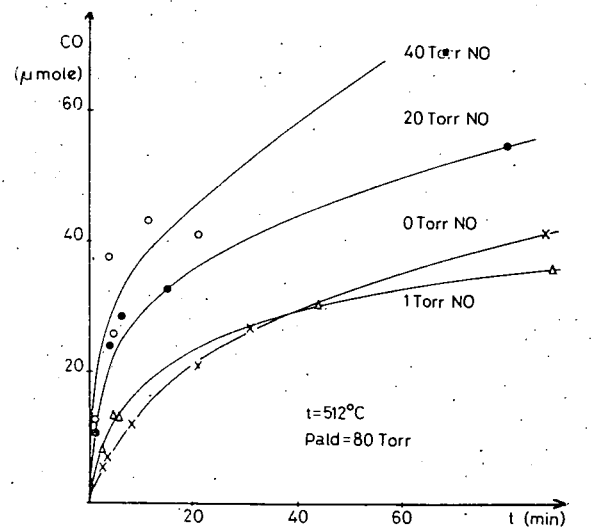

Fig. 10. Formation of CO as function of time at different NO concentrations (catalytic region) $t=512$ °C $p_{ald}=80$ torr; p_{NO}: × 0 torr; △ 1 torr; ● 20 torr; ○ 40 torr

From the Figs 9 and 10 it can also be seen that in absence of NO, the amounts of CH_4 and CO agree well, while in the presence of NO, the amount of CO exceeds that of CH_4, especially at higher conversions. This experimental fact has not been observed by other authors. It is to be explained by assuming that a greater part

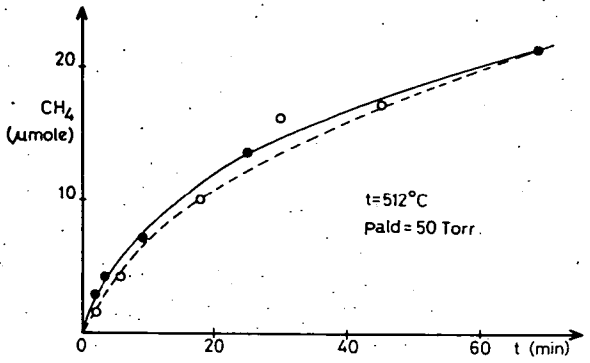

Fig. 11. Formation of CH_4 as function of time at 512 °C (inhibited region) $p_{ald}=50$ torr: p_{NO}: ○ ○ 0 torr; ● 0.75 torr

of methyl radicals, mainly at higher NO concentrations, are in the form of RNO and not in the form of free methyl radicals. The former does not produce CH_4 at all in the reaction.

From the initial rate values, calculated from the curves of the formation of major products, the partial order related to NO was found to be 0.61, in agreement with the value calculated from pressure—time measurements.

In the maximally inhibited region (50 torr acetaldehyde + 0.75 torr NO) there is no difference in the amount of major products within limits of experimental error.

The effect of NO *on minor products*

H_2. Among the minor products, hydrogen forms in the greatest amount. A typical H_2 yield—time curve is given in Fig. 12, showing the analysis data of a series of experiments carried out at 512 °C, at 80 torr aldehyde pressure and at different pressures of NO.

The shape of these curves does not change in the presence of NO, and remains similar to the curves of major products due to the effect of NO; however, the hydrogen yield increases markedly. The degree of this increase is higher than in the case of major products. As it can be seen, *e.g.* from Fig. 12, after an hour pyrolysis time, the increase of the amount of major products is twofold, while in the case of hydrogen is 6fold. This increase in hydrogen formation takes place in the maximally inhibited region too, but in a smaller extent (Fig. 13). This fact indicates that in both regions the formation of hydrogen takes place with the same mechanism.

Acetone, ethane, ethylene. In the presence of NO, the amount of acetone formed does not change significantly, while that of ethane and ethylene slightly

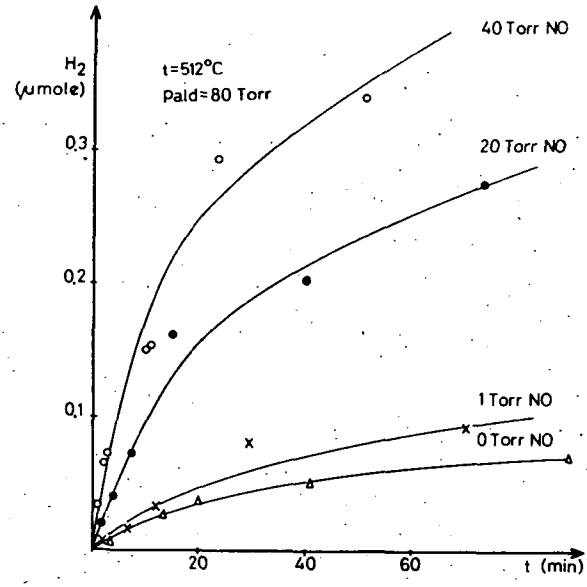

Fig. 12. Formation of H_2 as function of time at different NO concentrations (catalytic region) $t=512$ °C, $p_{ald}=80$ torr; p_{NO} △ 0 torr; × 1 torr; ● 20 torr; ○ 40 torr

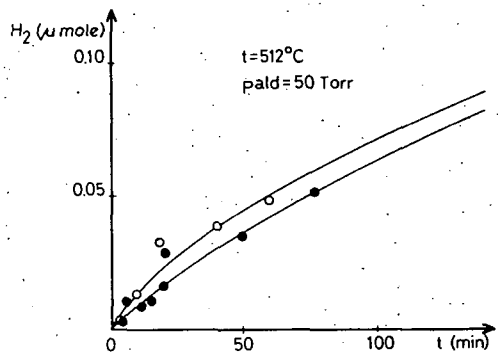

Fig. 13. Formation of H_2 as function of time at 512 °C. (inhibited region) $p_{ald}=50$ torr; p_{NO}: ● 0 torr; ○ 0.75 torr

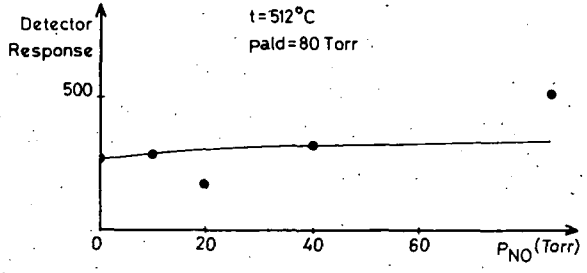

Fig. 14. Formation of acetone as function of NO concentrations at 512 °C, $p_{ald}=80$ torr. (The amount of acetone was measured at 50% conversion)

increases, as seen from Figs 14—16. These observations are in agreement with literature [9].

HCN. It is a general observation that in the pyrolysis of organic compounds in the presence of NO, HCN is always an easily detectable product. A typical HCN formation curve is shown in Fig. 17. It can be clearly seen that the formation of HCN takes place with an induction period, which indicates that HCN is a secondary

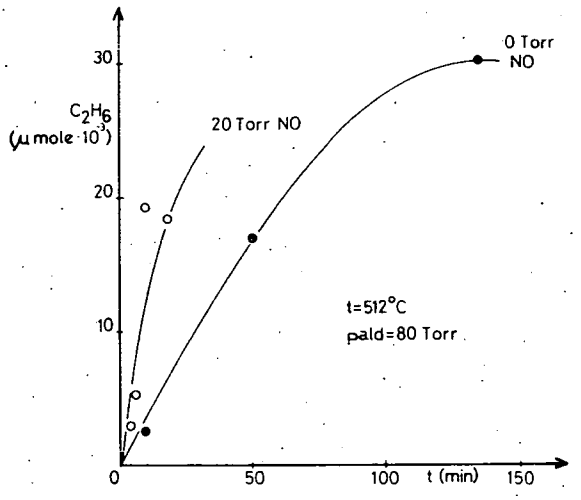

Fig. 15. Formation of ethane as function of time at 512 °C (catalytic region) $p_{ald}=80$ torr; p_{NO} ● 0 torr; ○ 20 torr

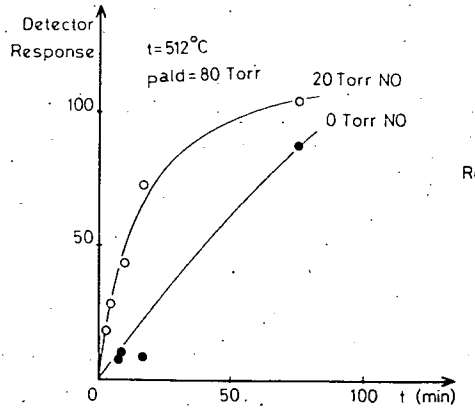

Fig. 16. Formation of ethylene as function of time at 512 °C. (catalytic region) $p_{ald}=$ 80 torr; p_{NO}: ● 0 torr; ○ 20 torr

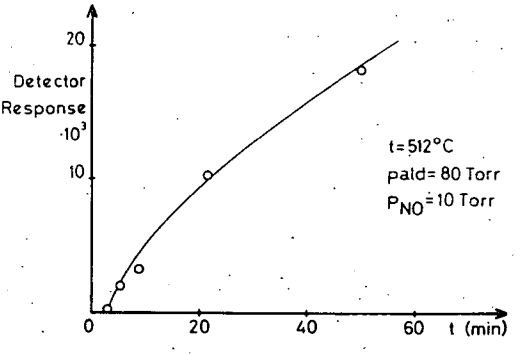

Fig. 17. Formation of HCN as function of time at 512°C (catalytic region) $p_{ald}=80$ torr, $p_{NO}=$ 10 torr

product. The shape of HCN formation curves is similar to that of major products, and the amount of HCN formed increases proportionally to NO concentration as seen from Fig. 18. where the amount of HCN, obtained in the pyrolysis of 80 torr aldehyde at 50% conversion, is plotted against NO concentration.

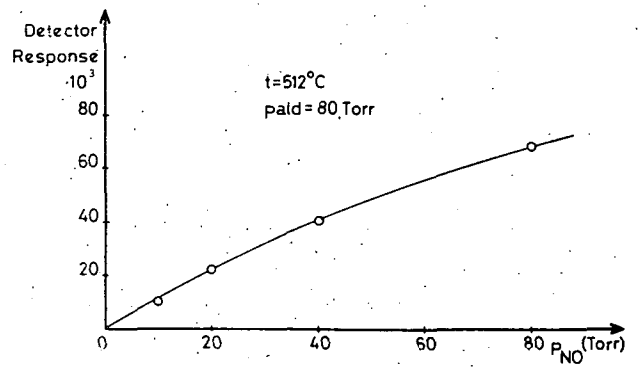

Fig. 18. Formation of HCN as function of p_{NO} at 512 °C $p_{ald}=80$ torr

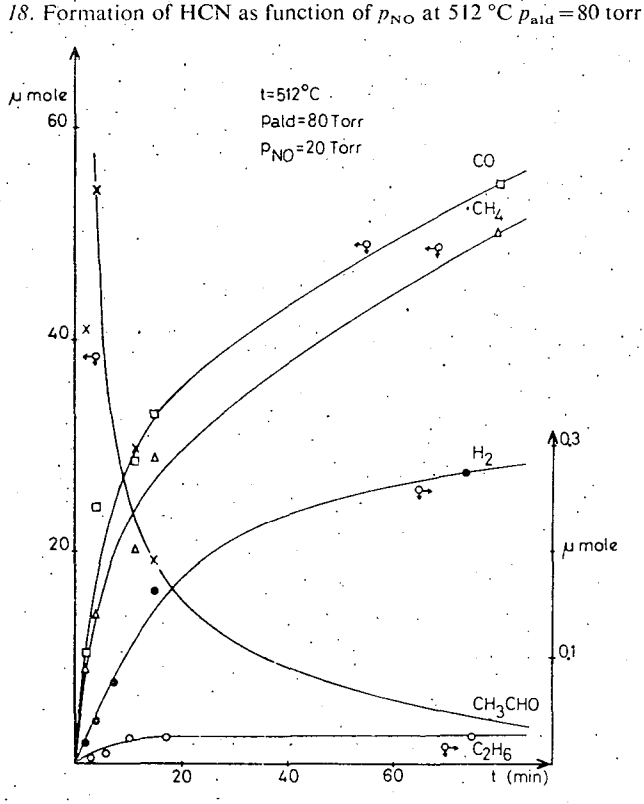

Fig. 19. Mass-balance curves at 512 °C (catalytic region) $p_{ald}=80$ torr. $p_{NO}=20$ torr. □ CO; △ CH_4; ● H_2: × CH_3CHO; ○ C_2H_6.

It is to be noted that, besides the products mentioned above, N_2, N_2O, H_2O, CO_2 could also be detected with the MS technique. A typical mass balance curve of the pyrolysis products at 512 °C of 80 torr aldehyde and 20 torr NO (catalysis region) is to be seen in Fig. 19.

Discussion

It can be seen from our experimental results that, in the presence of NO, in the catalytic region the amounts of major and minor products increase. This is in agreement with the findings of other authors [7, 9]. The increase in concentration of major products can be interpreted by the chain initiation role of NO. So besides the initiation process,

$$CH_3CHO \rightarrow CH_3 + \dot{C}HO, \quad (1)$$

we have to take into consideration the step

$$CH_3CHO + NO \rightarrow CH_3\dot{C}O + HNO, \quad (2)$$

too. This step was first suggested by WOJCIECHOWSKI and LAIDLER [16] as an initiation step in NO influenced pyrolyses of organic compounds. These steps are followed by the decompositions

$$CH_3\dot{C}O \rightarrow CH_3 + CO \quad (3)$$

$$\dot{C}HO \rightarrow CO + H \quad (4)$$

$$HNO \rightarrow H + NO, \quad (5)$$

which, at the temperature of pyrolysis (500 °C), take place instantly.

The further reactions of methyl radicals are the following:

$$CH_3 + CH_3CHO \rightarrow CH_4 + CH_3\dot{C}O \quad (6)$$

$$CH_3 + CH_3CHO \rightarrow CH_4 + \dot{C}H_2CHO. \quad (7)$$

The ratio of these two rate constants (k_6/k_7), on the basis of literature, is about 10 [22, 23].

Part of the methyl radicals reacts with NO in an equilibrium reaction, forming nitrosomethane [17, 18]

$$CH_3 + NO \rightleftharpoons CH_3NO. \quad (8)$$

The nitrosomethane, formed in step (8) could isomerize to formaldoxime [26]

$$CH_3NO \rightarrow CH_2NOH \quad (9)$$

which later decomposes

$$CH_2NOH \rightarrow HCN + H_2O \quad (10)$$

into water and HCN. In the direct decomposition of formaldoxime, TAYLOR and BENDER [27] has found, among others, NH_3 and CO as products, but these results were confirmed neither by other authors nor by our results. The steps (8), (9) and (10) show one route of NO consumption. Another route (*i.e.* further reactions

of nitrosomethane) was first described by BROWN [19]. According to BROWN the nitrosomethane reacts with NO at higher NO concentrations

$$RNO + 2\,NO \rightarrow R(NO)_3 \rightarrow RN_2NO_3 \rightarrow R + N_2 + NO_3$$

and gives N_2 and R radical, while the NO_3 in the $NO_3 + NO \rightarrow 2\,NO_2$ reaction gives a stable product.

On the basis of our experimental data, the existence of this type of NO consumption is confirmed. Similar reactions were established by CHRISTIE and EDWARDS [20] in the photolysis of acetaldehyde—NO system, and by EASTMOND and PRATT [28] in the pyrolysis of ethane and butane in the presence of NO.

The reaction

$$RNO + NO \rightarrow RO + N_2O$$

supposed by CHRISTIE [21] has to be rejected, because we could not detect any products originating from further reactions of methoxy radicals. N_2O, which was detected in our system, probably formed in an another way (maybe in the "cold reaction" mentioned by SCHUCHMANN and LAIDLER).

According to our analytical results, the amount of acetone does not change significantly in the presence of NO, so the consideration of a new acetone forming reaction, besides the

$$CH_3 + CH_3CHO \rightarrow CH_3COCH_3 + H \qquad (11)$$

step, is not necessary.

The great increase in the hydrogen formation in the presence of NO can be explained, besides the steps

$$H + CH_3CHO \rightarrow H_2 + CH_3CO \qquad (12)$$

$$H + CH_3CHO \rightarrow H_2 + CH_2CHO \qquad (13)$$

with (11), (4), and (5) as a new step.

The slight increase in formation of ethylene in the presence of NO can be interpreted on the basis of LAIDLER's mechanism, because, according to step

$$H + CH_2{=}CHOH \rightarrow C_2H_4 + OH \qquad (14)$$

with the increase of H atom concentration the rate of ethylene formation also increases.

The formation of CO_2 and N_2O, detected by MS method, can be described with the following reactions:

$$CH_3CO + NO \rightarrow CH_3CONO \qquad (15)$$

$$CH_3CONO + NO \rightarrow CH_3CO(NO)_2 \rightarrow CH_3 + CO_2 + N_2O. \qquad (16)$$

Step (15), which was supposed by several authors at room temperature photolyses [24, 29, 30] is only to be regarded as formal because its existence at higher temperatures is questionable.

Besides the termination steps described for the decomposition in the absence of NO

$$2\,CH_3 \rightarrow C_2H_6 \tag{17}$$

and

$$CH_3 + CH_2CHO \rightarrow C_2H_5CHO, \tag{18}$$

the following new termination steps take place:

$$CH_3 + CH_3NO \rightarrow C_2H_6 + NO \tag{19}$$

$$CH_2CHO + NO \rightarrow ONCH_2CHO \rightarrow OCHCHN{=}OH \rightarrow H_2O + HCNO + CO \tag{20}$$

The CO formed in step (20) could give a contribution to the experimentally found CO overproduction.

During our investigations, we were not able to detect CH_3NCO. So the existence of a new NO addition step, described by SCHUCHMANN and LAIDLER [9]

$$CH_3CHO + NO \rightleftharpoons CH_3\overset{\displaystyle O^-}{\underset{|}{C}}H{-}NO \rightarrow CH_3 + OCHCNO$$

was not confirmed by us. According to this step, numerous products containing CN (so CH_3NCO, too) should form.

The elementary steps summarized above are suitable for interpreting the main features of the influenced reaction both in the inhibited and catalytic regions.

This elementary steps account also for the change in the distribution of products found experimentally.

* * *

The authors are grateful to Prof. Z. G. SZABÓ for the inspiration of the investigation and for the helpful suggestions at the initial stages of this work, to Dr. T. BÉRCES for valuable discussions, Dr. I. SZILÁGYI for mass spectrometric analyses, Dr. L. ZALOTAI for computer calculations and Mrs. M. TÓTH for technical assistance.

References

[1] *Steacie, E. W. R.:* Atomic and free radical reactions, Reinhold Publ. Corp., New York, 1954.
[2] *Verhoek, F. H.:* Trans. Faraday Soc. **31**, 1533 (1935).
[3] *Staveley, L. A. K., C. N. Hinshelwood:* J. Am. Chem. Soc. **59**, 1568 (1937); *ibid.* **60**, 812 (1938).
[4] *Rice, F. O., O. L. Polly:* J. Chem. Phys. **6**, 273 (1938).
[5] *Smith, J. R. E., C. N. Hinshelwood:* Proc. Roy. Soc. **A180**, 247 (1942).
[6] *Rice, F. O., R. E. Varnerin:* J. Am. Chem. Soc. **76**, 2619 (1954).
[7] *Freeman, G. R., C. J. Danby, C. N. Hinshelwood:* Proc. Roy. Soc. **A245**, 456 (1958).
[8] *Eusuf, M., K. J. Laidler:* Can. J. Chem. **42**, 1861 (1964).
[9] *Schuchmann, H. P., K. J. Laidler:* J. Chem. Kinetics **II**, 349 (1970).
[10] *Szabó, Z. G., F. Márta:* J. Am. Chem. Soc. **83**, 768 (1961).
[11] *Márta, F., G. Ács, Z. G. Szabó:* Acta Chim. Hung. **50**, 263 (1968).
[12] *Winkler, L. W.:* Ber. **34**, 1908 (1901).
[13] *Laidler, K. J., M. Eusuf:* Can. J. Chem. **43**, 278 (1965).
[14] *Letort, M.:* J. Chim. Phys. **34**, 428 (1937).
[15] *Szabó, Z. G., F. Márta:* Magy. Kém. Folyóirat **62**, 333 (1961).

[16] *Wojciechowski, B. W., K. J. Laidler:* Can. J. Chem. **38**, 1027 (1960).
[17] *Szabó, Z. G.:* Nature **170**, 246 (1952).
[18] *Ree, T., K. Yang, H. Eyring:* Trans. Faraday Soc. **58**, 2375 (1962).
[19] *Brown, J. F. Jr.:* J. Am. Chem. Soc. **79**, 2480 (1957).
[20] *Christie, M. J., J. M. Edwards:* J. Chem. Soc. **1969**, 1134.
[21] *Christie, M. J.:* Proc. Roy. Soc. **A249**, 258 (1958).
[22] *Laidler, K. J., M. T. H. Liu:* Proc. Roy. Soc. **A297**, 365 (1967).
[23] *Liu, M. T. H., K. J. Laidler:* Can. J. Chem. **46**, 479 (1968).
[24] *Christie, M. J., J. M. Collins, M. A. Voisey:* Trans. Faraday Soc. **61**, 462 (1964).
[25] *Bárdi, I., F. Márta:* Acta Phys. et Chem. Szeged, **19**, 227 (1973).
[26] *Batt, L., G. Gowenlock:* Trans. Faraday Soc. **56**, 682 (1960).
[27] *Taylor, H. A., H. J. Bender:* J. Chem. Phys. **9**, 761 (1941).
[28] *Eastmond, G. B. M., G. L. Pratt:* J. Chem. Soc. **A 1970**, 2329; *ibid.* **A 1970**, 2333.
[29] *Avery, H. E., D. M. Hayes, L. Phillips:* J. Phys. Chem. **73**, 3498 (1969).
[30] *Allen, E. R., K. W. Bagley:* Ber. d. Bunsenges. **72**, 227 (1968).
[31] *Imai, N., Y. Yoshida, O. Toyama:* Bull. Chem. Soc. Japan **35**, 752 (1962).
[32] *Imai, N., T. Fujii, O. Toyama:* Bull. Chem. Soc. Japan **38**, 411 (1965).
[33] *Imai, N., O. Toyama:* Bull. Chem. Soc. Japan **40**, 81 (1967).
[34] *King, K. D., V. R. Stimson:* Austr. J. Chem. **21**, 2293 (1968).

ИЗУЧЕНИЕ ТЕРМИЧЕСКОГО РАЗЛОЖЕНИЯ АЦЕТАЛЬДЕГИДА В ПРИСУТСТВИИ ОКИСИ АЗОТА

И. Барди, Ф. Марта

Изучен пиролиз ацетальдегида при температурах 496—550 °C, при давлениях ацетальдегида 25—200 торр и окиси азота 0—50 торр. За кинетикой разложения следили по давлению смеси и газохроматографическим методом. Разными методами определены порядки реакции разложения относительно ацетальдегида и окиси азота. На основании данных по измеренным давлениям выведены „кривые влияния", на основании которых пришли к определенным выводам относительно областей индукции и катализа. В каталитической области были определены Аррениусовые параметры для общей реакции. Изучено влияние окиси азота на образование основного продукта и некоторых других продуктов разложения (H_2, C_2H_6, C_2H_4, HCN, и CH_3COCH_3) как в каталитической, так и ингибиционной областях реакции. Кратко рассмотрены механизмы образования продуктов и предлагается простой механизм разложения ацетальдегида в присутствии окиси азота.

NITRIC OXIDE INFLUENCED THERMAL DECOMPOSITION OF ISOBUTANE

By

M. GÖRGÉNYI, L. SERES and F. MÁRTA

Gas Kinetics Research Group of the Hungarian Academy of Sciences, Szeged, and Institute of General and Physical Chemistry, Attila József University, Szeged

(Received January 25, 1974)

Pyrolysis of isobutane has been studied in the presence of different amounts of nitric oxide in the temperature range of 773 to 823 K. Beside hydrogen and hydrocarbons, compounds containing oxygen and nitrogen were identified. The initial rate of formation of hydrogen and hydrocarbons decreased in the presence of small amounts (0—15%) of nitric oxide. The initial rate of formation of all products increased in the presence of greater amounts of nitric oxide.

The mechanism suggested includes the formation of "polymeric" radicals followed by isomerization and decomposition.

Introduction

The effect of nitric oxide on hydrocarbon pyrolytic processes has been extensively studied. The interpretations given in early studies were based on the principle of a molecular mechanism excluding the possibility of the contribution of chain processes in the "maximally inhibited region". This idea was accepted in the only paper published on nitric oxide influenced thermal decomposition of isobutane [1].

Nowadays the radical chain character of the pyrolysis of hydrocarbons in the presence of nitric oxide is generally recognized and the formation of compounds containing the oxygen and nitrogen atoms of the nitric oxide has been observed [2, 3].

Experimental

The reaction was studied in a conventional static system. Different quantities of nitric oxide (up to 200 torr) and 200 torr isobutane were mixed and admitted in a Supremax reaction vessel.

The isobutane used was of 99.5% purity, major impurities being propane, propene, isobutene and ethylene. Nitric oxide was prepared from potassium nitrite and potassium iodide. Both gases were further purified by trap to trap distillation in vacuum. The composition of the reaction mixture was determined by gas chromatography. Two columns were used: activated alumina (60—80 mesh) for the separation of ethane, nitrous oxide, ethylene, propane, propene, isobutane, isobutene; molecular sieve 5A for that of hydrogen, nitrogen and methane. Water and acetonitril were identified by mass spectrometry.

Results

The initial rates of formation of hydrogen and hydrocarbons decreased in the presence of small amounts (1—15%) of nitric oxide. Higher amounts of nitric oxide gave rise to an increase in the rate formation of most of the products.

The relative rate of hydrogen and methane production decreased considerably with increasing nitric oxide partial pressure (Fig. 1).

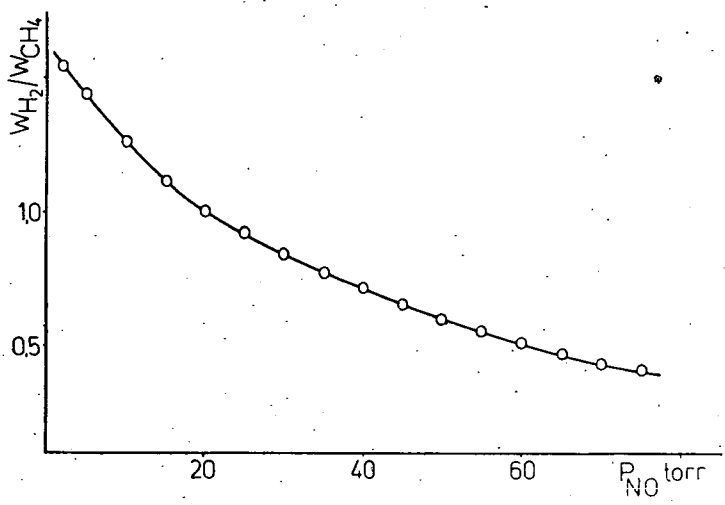

Fig. 1. Influence of nitric oxide on the ratio of initial rates of formation of hydrogen and methane (T=793 K).

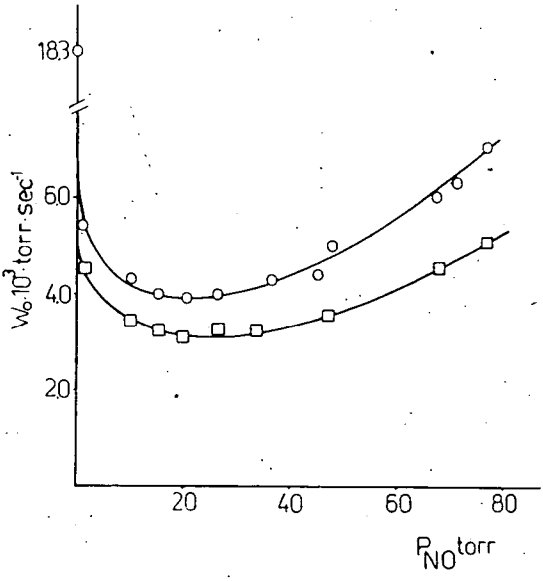

Fig. 2. Effect of nitric oxide on the initial rate of formation of methane and propylene (○ methane; □ propylene; T=793 K)

The increase in the rate of production of methane and propylene was remarkable at higher nitric oxide partial pressures (Fig. 2).

This effect is less pronounced in the case of hydrogen and isobutene (Fig. 3).

It is surprising that the rate of formation of propylene increases to a higher extent than that of isobutene.

An induction period can be observed in the ethane formation (Fig. 4). Its length shows a minimum at moderate nitric oxide pressures. The position of the minimum shifts to higher nitric oxide pressures with increasing temperature.

The same type of behaviour can be observed in propane and ethylene formation. A considerable increase can be observed in ethylene formation with increasing nitric oxide partial pressures (Fig. 5).

The plot of nitrogen partial pressures against time gives a good straight line (Fig. 6). An induction period can be observed at lower temperatures.

The order of nitrogen formation with respect to nitric oxide was found to be 1.05 ± 0.05 and did not exhibit any systematic change in the temperature range of 773—823 K. Similarly, an order of 1.10 ± 0.06 with respect to isobutane was obtained.

The production of nitrous oxide shows no induction period. Its rate of formation is considerably lower than that of nitrogen and decreases at relatively moderate conversions (Fig. 7).

Discussion

The mechanism of the reaction influenced by olefins was described earlier [4]. On the basis of the above

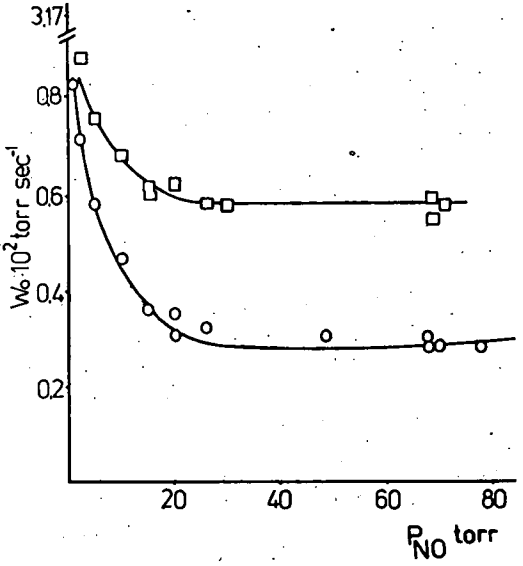

Fig. 3. Effect of nitric oxide on the initial rate of formation of hydrogen and isobutene (○ hydrogen; □ isobutene; T = 793 K)

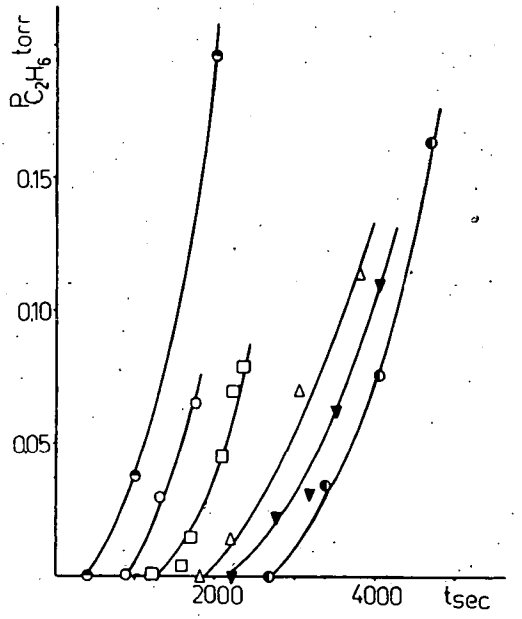

Fig. 4. Effect of nitric oxide on ethane formation (p_{NO}: ◓ 0; ◐ 10; ▾ 25; △ 50; □ 100; ○ 200 torr; T = 773 K)

experimental data, some features of the nitric oxide influenced reaction can be elucidated. The importance of the possible bimolecular initiation steps

$$NO + i\text{-}C_4H_{10} \rightarrow HNO + t\text{-}C_4H_9 \quad (1a)$$

$$\rightarrow HNO + i\text{-}C_4H_9 \quad (1b)$$

increases with the amount of nitric oxide present. There is no experimental evidence for the bimolecular initiation (1a, 1b), but this assumption can be supported by other experimental data [5].

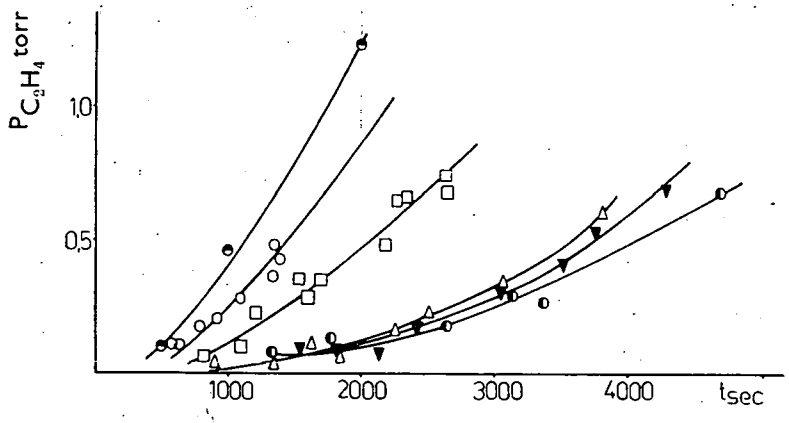

Fig. 5. Effect of nitric oxide on ethylene formation (p_{NO}: ◓ 0; ◐ 10; ▼ 25; △ 50; □ 100; ○ 200 torr; T = 773 K)

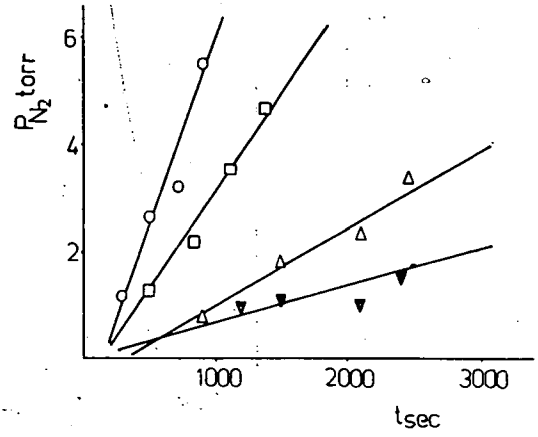

Fig. 6. Nitrogen formation in the nitric oxide influenced thermal decomposition of isobutane (p_{NO}: ○ 200; □ 100; △ 50; ▼ 25 torr; T = 773 K)

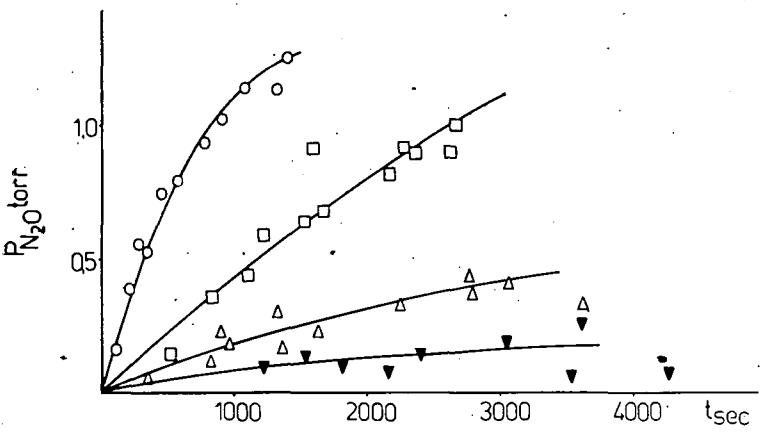

Fig. 7. Nitrous oxide formation in the nitric oxide influenced thermal decomposition of isobutane (p_{NO}: ○ 200; □ 100; △ 50; ▼ 25 torr; T=773 K)

	lg A	E	lg k_{800}	
$\dot{C}H_3+C_2H_6 \rightarrow CH_4+\dot{C}_2H_5$	11.3	10.4	8.46	(a)
$\dot{C}H_3+(CH_3)_2O \rightarrow CH_4+\dot{C}H_2OCH_3$	11.5	9.5	8.91	(b)
$NO+(CH_3)_2O \rightarrow HNO+\dot{C}H_2OCH_3$	14.0	43.4	2.15	(c)

Using the above kinetic parameters, the rate coefficient of the initiation step:

$$NO+C_2H_6 \rightarrow HNO+\dot{C}_2H_5 \qquad (d)$$

can be estimated by making the following assumptions:

(a) $k_b/k_c=k_a/k_d$

(b) the rate coefficients of primary H-atom abstractions from i-C_4H_{10} and C_2H_6 corresponds to the ratio of primary H atoms present in the molecules (9:6)

(c) the rate of tertiary H-atom abstraction exceeds that of primary atoms by a factor of two [6].

By using these assumptions the ratio of the rates of the unimolecular: i-$C_4H_{10} \rightarrow \dot{C}H_3+2$-$\dot{C}_3H_7$ (1) and the bimolecular reactions (1a) and (1b) can be calculated:

$$\frac{w_1}{w_2}=\frac{k_1[i\text{-}C_4H_{10}]}{k_2[i\text{-}C_4H_{10}][NO]}=\frac{10^{-4.7}}{10^{2.2}10^{-5.7}}=10^{-1.2}.$$

The error involved in the above calculation is probably large. All the same, it can be regarded as an evidence that H-atom abstraction by nitric oxide contributes to the initiation.

The concentration of methyl radicals drops less drastically than that of hydrogen

atoms in the presence of nitric oxide (Fig. 1). The decrease in hydrogen formation (Fig. 3) can be accounted for by the reactions

$$t\text{-}\dot{C}_4H_9 + NO \rightarrow i\text{-}C_4H_8 + HNO \quad (2)$$

$$H + NO + M \rightarrow HNO + M \quad (3)$$

as the hydrogen atoms are produced mainly from the t-C_4H_9 radicals. As a consequence, the rate of all reactions involving H-atoms decreases.

The decreases in the radical concentration in reactions (2), (3), (4) and (5)

$$i\text{-}\dot{C}_3H_7 + NO \rightarrow HNO + C_3H_6 \quad (4)$$

$$\dot{C}_2H_5 + NO \rightarrow HNO + C_2H_4 \quad (5)$$

results in the inhibition of the formation of secondary products (ethane and propane) (Fig. 4).

To account for the increase in the rate of the overall process and the pattern of rate increase in the formation of various products, other reactions involving nitric oxide must also be included in the mechanism.

The addition of nitric oxide to the double bond and H-atom abstraction from olefins by nitric oxide can yield radicals, too.

$$NO + C_3H_6 \rightarrow CH_3\text{—}\underset{\displaystyle NO}{\underset{|}{CH}}\text{—}\dot{C}H_2 \quad (6)$$

$$\rightarrow HNO + \dot{C}_3H_5 \quad (7)$$

$$NO + i\text{-}C_4H_8 \rightarrow (CH_3)_2C\text{—}\underset{\displaystyle NO}{\underset{|}{C}}\text{—}\dot{C}H_2 \quad (8)$$

$$\rightarrow HNO + i\text{-}\dot{C}_4H_7 \quad (9)$$

The observed increase in the rate of formation of ethane and propane in the presence of higher amounts of NO reflects a similar change in the concentration of ethyl and secondary propyl radicals. They are not formed in the addition steps.

$$H + C_2H_4 \rightarrow \dot{C}_2H_5$$

$$H + C_3H_6 \rightarrow i\text{-}\dot{C}_3H_7,$$

since the formation of hydrogen does not show any major increase. Ethane and propane are shown to be the products of propylene and isobutene pyrolysis and the above radicals are suggested to be formed from "polymeric" radicals undergoing internal H-atom transfer processes and dissociation [7, 8].

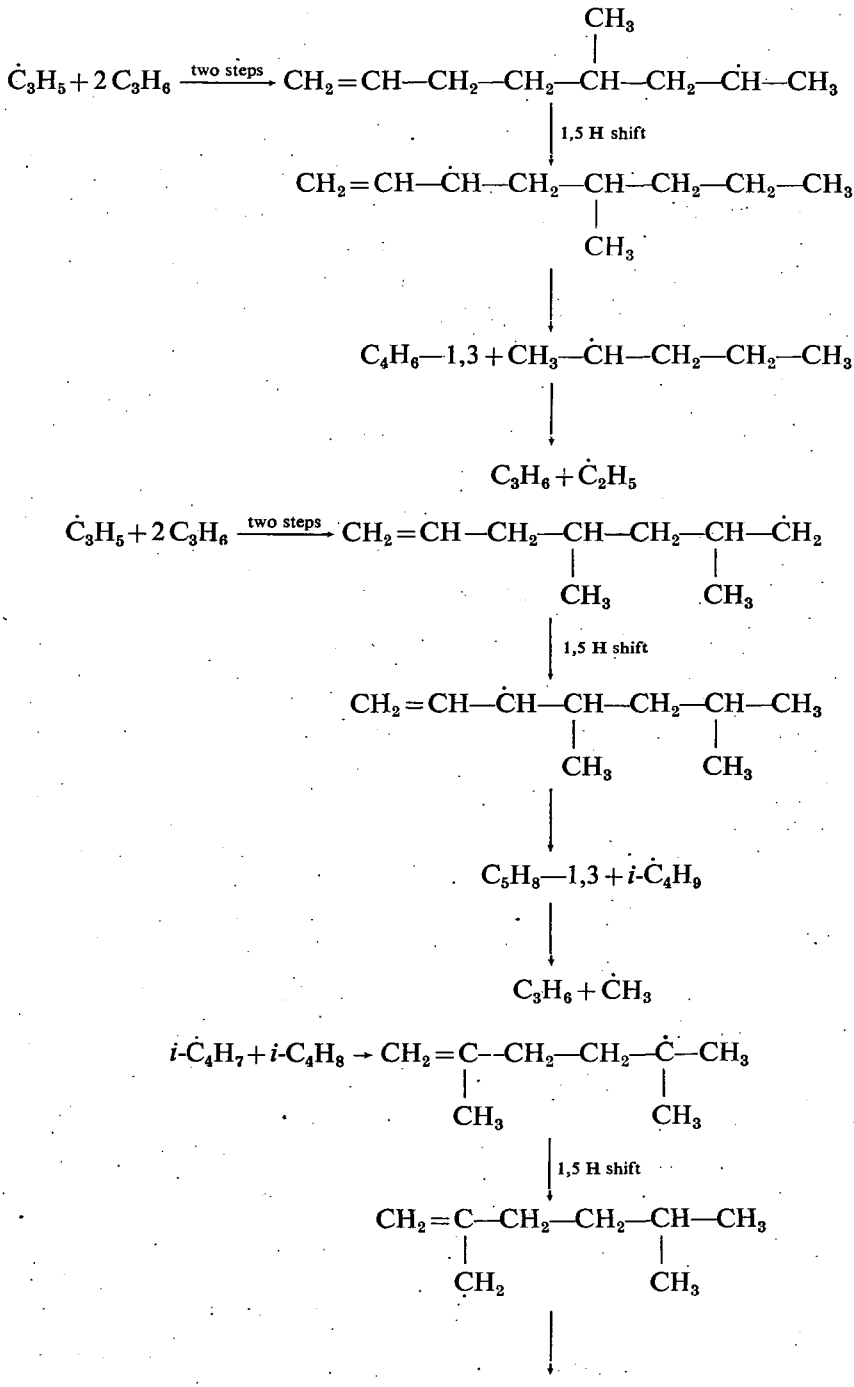
$\dot{C}_3H_5 + 2\,C_3H_6$
two steps
$CH_2=CH-CH_2-CH_2-CH(CH_3)-CH_2-CH(CH_3)-CH_3$
1,5 H shift
$CH_2=CH-\dot{C}H-CH_2-CH(CH_3)-CH_2-CH_2-CH_3$
$C_4H_6-1,3 + CH_3-\dot{C}H-CH_2-CH_2-CH_3$
$C_3H_6 + \dot{C}_2H_5$
(10)
$\dot{C}_3H_5 + 2\,C_3H_6$
two steps
$CH_2=CH-CH_2-CH(CH_3)-CH_2-CH(CH_3)-\dot{C}H_2$
1,5 H shift
$CH_2=CH-\dot{C}H-CH(CH_3)-CH_2-CH(CH_3)-CH_3$
$C_5H_8-1,3 + i\text{-}\dot{C}_4H_9$
$C_3H_6 + \dot{C}H_3$
(11)
$i\text{-}\dot{C}_4H_7 + i\text{-}C_4H_8 \rightarrow CH_2=C(CH_3)-CH_2-CH_2-\dot{C}(CH_3)-CH_3$
1,5 H shift
$CH_2=C(CH_2)-CH_2-CH_2-CH(CH_3)-CH_3$

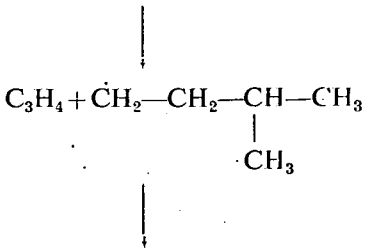

(12)

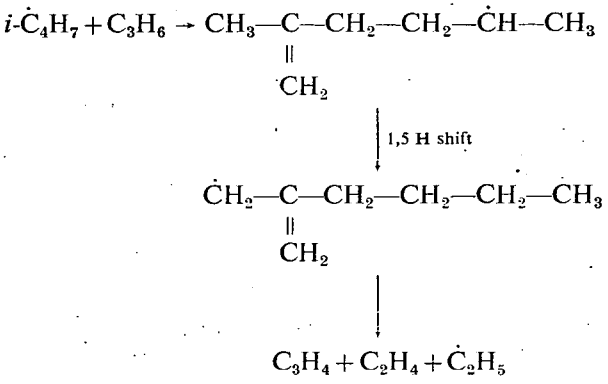

(13)

"Polymeric" radicals can be produced in the isobutane pyrolysis, too. Some of the possible reactions are shown above. They are intended only to demonstrate the possibility of interpreting the experimental facts using the basic idea outlined in [8].

The steps suggested above and other addition—isomerization—decomposition steps result in the formation of products with increased rates of formation in the presence of nitric oxide. Allene is an exeption. Under the condition of the reaction, this compound is converted into various products in fast reactions demonstrated in separate experiments.

The nitroso compounds formed from various R radicals present in the system are probably the source of nitrogen [3]:

$$RNO + 2\,NO \rightarrow R(NO)_3 \rightarrow RN_2NO_3 \rightarrow R + N_2 + NO_3 \qquad (14)$$

In agreement with this assumption, increased nitrogen formation was observed in a system of 200 torr i-C_4H_{10} + 100 torr NO + 25 torr C_3H_6, compared to that in the absence of the olefin.

The formation of N_2O is proposed to occur in reactions similar to those suggested by ESSER and LAIDLER [2] in the nitric oxide influenced ethane decomposition.

$$\begin{array}{l} \mathrm{R{-}\underset{\displaystyle R}{\underset{|}{CH}}{-}NO \rightarrow R{-}\underset{\displaystyle R}{\underset{|}{C}}{=}NOH \xrightarrow{+NO} R{-}\underset{\displaystyle R}{\underset{|}{C}}{=}\dot{N} + HNO_2} \\ \qquad\qquad\qquad\qquad\qquad\qquad\quad \Big\downarrow -OH \qquad\qquad\qquad\quad \Big\downarrow +NO \\ \qquad\qquad\qquad\qquad\qquad\quad \mathrm{R{-}\underset{\displaystyle R}{\underset{|}{C}}{=}\dot{N} \xrightarrow{+NO} N_2O + products} \end{array} \qquad (15)$$

With $R = CH_3$ and $R = H$, reaction (15) results in the formation of CH_3CN.

The OH radicals formed in reactions (15) and (16)

$$HNO_2 + M \rightarrow NO + OH + M \qquad (16)$$

give rise to water formation

$$OH + RH \rightarrow H_2O + R. \qquad (17)$$

HNO formed in various reactions is a source of N_2O

$$HNO + NO \rightarrow N_2O + OH. \qquad (18)$$

Termination is expected to occur between NO and the various radicals present.

$$R + NO \rightarrow products. \qquad (19)$$

However, no reliable information specifying these processes is available.

References

[1] *Peard, M. G., F. S. Stubbs, C. N. Hinshelwood: Proc. Roy. Soc.* **A214**, 330 (1952).
[2] *Esser, J., K. J. Laidler:* Int. J. Chem. Kinetics **2**, 37 (1970).
[3] *Eastmond, G. B. M., G. L. Pratt*: J. Chem Soc. **A1970**, 2329.
[4] *Seres, L., F. Márta, Á. Kiss:* Ber. Bunsenges. Phys. Chem. **73**, 571 (1969).
[5] *Trotman-Dickenson, A. F., G. S. Milne:* Tables of Bimolecular Gas Reactions, U.S. Government Printing Office, Washington, 1967, p. 122.
[6] *Konar, R. S., R. M. Marshall, J. H. Purnell:* Trans. Faraday Soc. **64**, 403 (1968).
[7] *Görgényi, M., et al.:* to be published.
[8] *Seres, L., P. Ausloos:* Symposium on the Mechanism of Hydrocarbon Reactions, Siófok (Hungary), 5—7 June, 1973.

ВЛИЯНИЕ ОКИСИ АЗОТА НА ТЕРМИЧЕСКОЕ РАЗЛОЖЕНИЕ ИЗОБУТАНА

М. Гергени, Л. Шереш, Ф. Марта

Изучен пиролиз изобутана в присутствии различных концентраций окиси азота в интервале температур от 773 до 823 К. Наряду с водородом и углеводородами были определены также соединения содержащие кислород и азот. Скорости образования водорода и углеводородов уменьшались в присутствии (0—15%) окиси азота. Начальная скорость образования всех продуктов возрастала с повышением концентрации окиси азота. Предложенный механизм реакции включает в себе образование „полимерных" радикалов, сопровождающееся изомеризацией и разложением.

MECHANISM OF ANODIC OXIDATION OF PRIMARY ALCOHOLS

By

M. NOVÁK and J. LANTOS

Institute of General and Physical Chemistry, Attila József University, Szeged

(Received September 27, 1973)

Previous investigations [1—3] have shown that the rate of oxidation of primary alcohols is controlled by a non-electrochemical step. Results of further study support the view that the rate-determining step is an adsorption process of non-electrochemical type.

Introduction

Earlier investigations concerning oxidation of primary alcohols on Pt electrode in acidic solution resulted in contradictory opinions regarding the kinetic characteristics of the reaction. Regarding the chemistry and the stoichiometry of oxidation, it was assumed [4] that the process goes to the formation of CO_2, whereas other results [5] and our gas-chromatographic analysis showed definitely that the alcohol—aldehyde transformation is the main current producing reaction in the overall process. Thus the experimentaly measured current corresponds to this reaction. The data concerning the change in rate of the reaction with the potential are in variance too. In the literature, attemps to characterize the rate by Tafel-slope [6], and the experience that the rate is not or only slightly changing with the potential can be found [7]. On the other side, experimental results regarding the role of adsorbed material in the current generating process were scarcely found in literature [8, 9]. During the course of our investigations of the mechanism of oxidation it was concluded that the adsorbed material cannot be considered to be the intermediate product of aldehyde formation [14, 2]. The material adsorbed on the surface gives rise to an inhibition effect and the decrease in the rate of the process with time is due to the increase in the amount of adsorbed material. Since the intermediate product of the alcohol—aldehyde reaction could not be detected, its amount must be very small ($\theta < 0.1$) and negligible in comparison with the amount of adsorbate causing the inhibition (similarly to the results of PODLOVCHENKO [10]). Therefore, in describing the characteristics of the process, the inhibition effect has to be taken into account with every kinetic parameter. In this way, the value of the rate of the process is proved to be independent of the potential, *i.e.* the rate-determining step is not an electrochemical process [3].

In the interpretation of the characteristics of the oxidation which considers the adsorbed material as an intermediate [4], the experimentally measured current at 400 mV is in direct connection with the adsorption. This is due to the premise that at this potential value only adsorption takes place and the current results

from the charge transfer which occurs during the adsorption. On this basis, the rate of change of the coverage and the experimentally detectable current are in close relationship. Assuming one electron transfer on each adsorption centre during the adsorption, the two rates were found to be equal [4, 11] in the case of methanol and higher primary alcohols. Although other relations were also obtained for methanol [12], it was accepted as a proof that the process of oxidation goes only to the first step *i.e.* to the adsorption at this potential.

Since in the oxidation of primary alcohols the adsorbed material shows an inhibiting effect, experiments have been carried out to obtain further data on the above relationship.

Experimental

The equipment and the method applied in the investigation have been described elsewhere [1]. The measurements were carried out at 25 °C in 1*N* H_2SO_4 solution prepared from triple distilled water, finally distilled in a closed system from charcoal. Sulphuric acid was Merck p.a. product. A hydrogen electrode in the same solution served as reference electrode, and special care was taken for its preparation, *i.e.* its potential value. During the measurements, the disc type working electrode was rotated with 1000 r.p.m.; its real surface area was 1.6 cm^2. Highly purified N_2 gas was used to deoxygenate the solution.

Results and discussion

Measurements were carried out in the case of ethanol, *n*-propanol, *n*-butanol and propionaldehyde. The progress of adsorption as well as the simultaneous current were measured, too. Each adsorption value was obtained with freshly cleaned surface and simultaneously the current passed during the adsorption was recorded each time to ensure reproducibility.

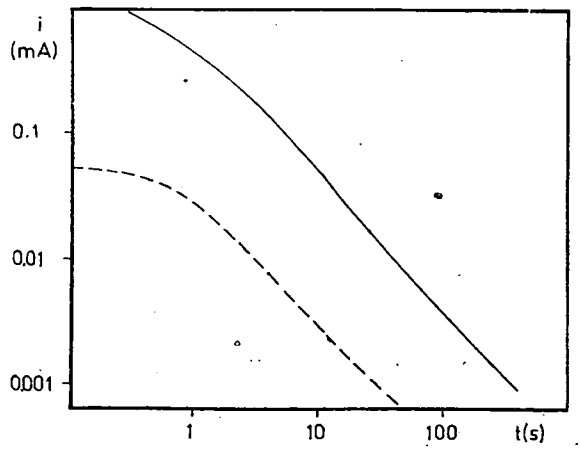

Fig. 1. Experimentally measured (—) and calculated (– – –) current for 0.1 mole·dm^{-3} *n*-propanol solution

With the assumption that one electron transfer occurs at each adsorption centre during the adsorption, the current corresponding to the rate of increase in coverage was calculated. This and the experimentally measured current are given in Figs. 1—3.

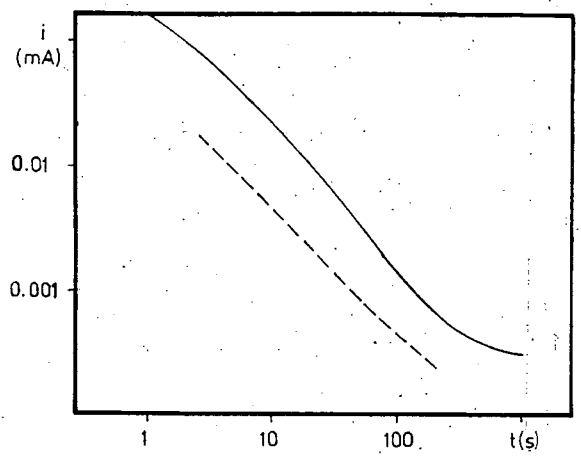

Fig. 2. Experimentally measured (—) and calculated (– – –) current for 0.1 mole·dm^{-3} *n*-butanol solution

for the alcohols. As can be seen, the experimentally measured current is higher with all materials. This deviation is contrary to the assumption that the adsorbed material is an intermediate product and supports the view that two processes are taking place on the surface. One is the alcohol—aldehyde reaction, and the other the adsorption process which results in strongly bounded species and inhibits the alcohol—aldehyde transfer.

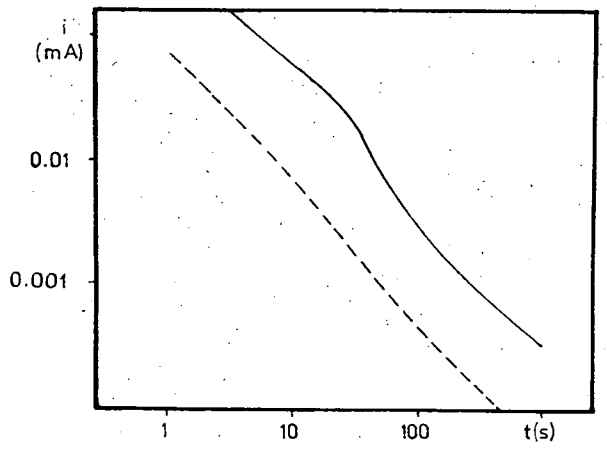

Fig. 3. Experimentally measured (—) and calculated (– – –) current for 0.1 mole·dm^{-3} ethanol solution

Since the investigations carried out on the oxidation of propionaldehyde have shown [15] that the organic material adsorbed at 400 mV is an intermediate of the aldehyde oxidation, it was expected, that in this case the two currents should be equal. The experimental results shown on Fig. 4 are in agreement with this assumption and the above conclusions.

As the rate of the oxidation of primary alcohols does not change with the potential if the currents belonging to the same coverage are compared [3], it may

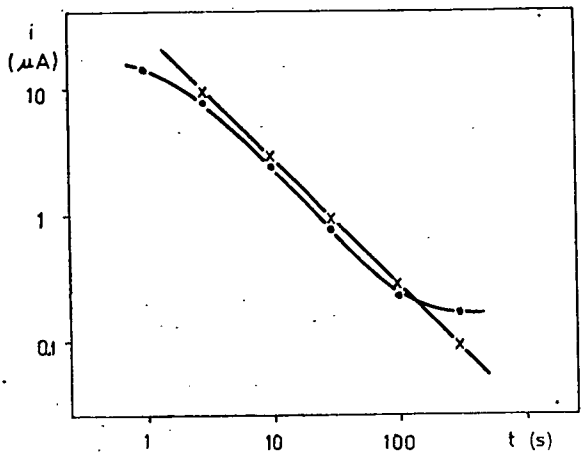

Fig. 4. Experimentally measured (·) and calculated (×) current for 0.1 mole·dm^{-3} propionaldehyde solution

be assumed that the non-electrochemical rate-determining step is connected with the adsorption of the reacting alcohol molecule or with some other chemical change of the adsorbed intermediate. The second possibility should give rise to an appreciable amount of intermediate product on the surface. This could not be detected, therefore the first assumption is to be considered as valid.

Further data might be obtained by investigating members of the homologue series of alcohols. It could be expected that the reaction rate would not change within the homologue series in the case of equal inhibition effect, *i.e.* coverage, because of the same reactivity of the functional group in each member. The experimentally observed currents given in Fig. 3 of [3] show that the reaction rate decreases in order of ethanol, *n*-propanol, *n*-butanol, which is apparently at variance with the equal reactivity of the functional groups. In order to explain the change in current, it seems to be obvious that it is connected with the change in molecular size. On this basis it can be assumed that the rate-determining step in the reaction depends on the size of the molecule. In this respect the diffusion of the organic reagent has to be disregarded, since its effect was eliminated by the experimental arrangement; furthermore the kinetical behaviour of the reaction excludes this possibility. Similarly, the desorption might be excluded, too, because of the inhibiting effect of the adsorbed material.

In order to explain the effect of the molecular size, one possibility remains, namely that the rate-determining step is the adsorption of the reagent molecule. Several cases might be taken into account:

(*i*) The alcohol molecule has to be oriented properly for the reaction, which is in favour of smaller molecule.

(*ii*) The larger molecule has to remove possibly more water molecules from the surface before the reaction [13].

(*iii*) The larger molecule which is already strongly attached to the surface, and therefore acts as an inhibitor, interferes to a larger extent with the incoming molecule than the smaller one.

Although we have to consider all these possibilities, it seems that with increasing coverage the second and third effect should be more important than the first one.

On the basis of the experimental results, the following processes might be suggested for the alcohol—aldehyde transformation:

$$ROH_{sol.} \rightleftharpoons ROH_{oriented}$$

$$ROH_{oriented} \xrightarrow{r.d.s.} ROH_{ads}$$

$$ROH_{ads} \xrightarrow{fast} ROH_{ads} + H^+ + e$$

$$ROH_{ads} \xrightarrow{fast} RO + H^+ + e$$

With the suggested steps we do not exclude the possibility that the adsorption step in the process might take place with dissociation followed by fast charge transfer and desorption. However, it seems unlikely that, in such cases, only the ionisation of the forming H atoms should be fast and the reaction of the forming organic radicals should be slow. This would be in contradiction with the inhibiting effect of the adsorbed material, since under such circumstances the intermediate product of aldehyde formation should accumulate.

References

[1] *Novák, M., J. Lantos, F. Márta:* Acta Phys. et Chem. **18**, 147 (1972).
[2] *Novák, M., J. Lantos, F. Márta:* Acta Phys. et Chem. **18**, 151 (1972).
[3] *Novák, M., J. Lantos, F. Márta:* Acta Phys. et Chem. **18**, 115 (1972).
[4] *Николов, И., Б. Янчук, С. С. Бескоровайная, Ю. Б. Васильев, В. С. Багоцкий:* Электрохимия **6**, 597 (1970).
[5] *Подловченко, Б. Й., Р. П. Петухова:* Электрохимия **8**, 899 (1972).
[6] *Rightmire, R. A., R. L. Ronland, D. L. Boos, D. L. Beals:* J. Elctrochem. Soc. **111**, 242 (1964).
[7] *Bagotzky, V. S., Yu. B. Vasilyev:* Electrochim. Acta **12**, 1323 (1967).
[8] *Taylor, A. H., R. D. Pearce, S. B. Brummer:* Trans. Farad. Soc. **67**, 801 (1971).
[9] *Breiter, M. W.:* Electrochemical Processes in Fuel Cells, Springer-Verlag, Berlin, 1969.
[10] *Подловченко, Б. Й., Р. П. Петухова:* Электрохимия **9**, 273 (1973).

[11] *Бескоровайная, С. С., Ю. Б. Васильев, В. С. Багоцкий:* Электрохимия **2**, 167 (1966).
[12] *Biegler, T.:* J. Phys. Chem. **72**, 1571 (1968).
[13] *Kirowa-Eisner, E., E. Gileadi:* J. Electroanal. Chem. **42**, 111 (1973).
[14] *Horányi, Gy., M. Novák:* Magy. Kém. Folyóirat **78**, 169 (1972).
[15] *Novák, M. J. Lantos:* To be published.

МЕХАНИЗМ АНОДНОГО ОКИСЛЕНИЯ ПЕРВИЧНЫХ СПИРТОВ

М. Новак, Й. Лантош

На основании предыдущих исследований [1—3] пришли к выводу, что скорость окисления определяется стадией не электрохимического характера. Полученные экспериментальные данные подтверждают представление, что процесс, определяющий скорость окисления не электрохимической природы, носит адсорбционный характер.

MECHANISM OF THE CATALYTIC DECOMPOSITION OF AMMONIUM PERCHLORATE

By

F. SOLYMOSI

Gas Kinetics Research Group of the Hungarian Academy of Sciences, Szeged

(Received January 10, 1974)

A critical survey on the various interpretations suggested for the effect of different additives on the thermal decomposition and ignition of ammonium perchlorate is given. On the basis of all the data and observations, a mechanism for the catalytic decomposition of ammonium perchlorate is proposed.

In the previous paper we summarized the main results of kinetic and thermal analytical measurements concerning the effect of oxides and different salts on the slow and fast decomposition of ammonium perchlorate (AP) [1]. In the present review we examine first the influence of catalysts on the gas-phase decomposition of AP, and collect all the data regarding the interaction between catalysts and AP, and then give a critical survey on the various interpretations proposed for the effect of additives on the stability of AP.

Finally, on the basis of all the data and informations we attempt to derive the most probable mechanism for the catalytic decomposition of AP.

Catalysis of the gas phase decomposition of AP

The first experiments on the catalysis of the gas phase decomposition of AP were reported by HERMONI and SALMON [2]. According to the brief conference abstract, chromic oxide and copper oxide are able to catalyse the gas phase reaction of AP.

In the more detailed experiments of BOLDYREV *et al.* [3] the AP was separated from oxides by glass wool. It was found that the rate of the gas phase decomposition of AP is increased by many oxides, but data were reported only for the effect of NiO (Fig. 1).

In the presence of nickel oxide the pressure of permanent gases increased, the effect being the greater, the larger the surface of the oxide. Since the decomposition of AP occurred under the reaction conditions used also in the absence of the catalyst, it could not be excluded that the oxides affected the secondary reactions between the products in such a way that the pressure of the permanent gases increased.

Experiments convincing with regard to the catalysis of the gas phase reaction were those made with 30% decomposed AP, the oxides being placed on sintered glass above the AP residue after the reaction [4, 5]. As can be seen from the few measurements in Fig. 2, decomposition of the pure AP was extremely small or

negligible in this case, and the observed pressure increase was due exclusively to the catalytic decomposition of vaporized AP.

In general, transition metal oxides catalysing also the low temperature decomposition of AP proved to be effective. ZnO, however, exhibited a strikingly high catalytic activity; even at 260°C it accelerated the gas phase decomposition of AP to a large extent. For comparison, the effects of some oxides on both the slow decomposition of AP and the lowest temperature of ignition were studied.

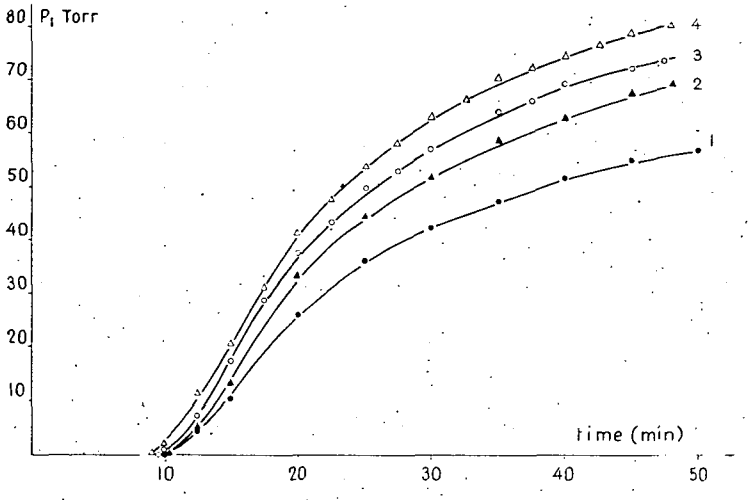

Fig. 1. Gas-phase decomposition of AP on nickel oxide of different surface area. 1: pure AP; 2: NiO 2 m²/g; 3: NiO 5,4 m²/g; 4: NiO 36 m²/g

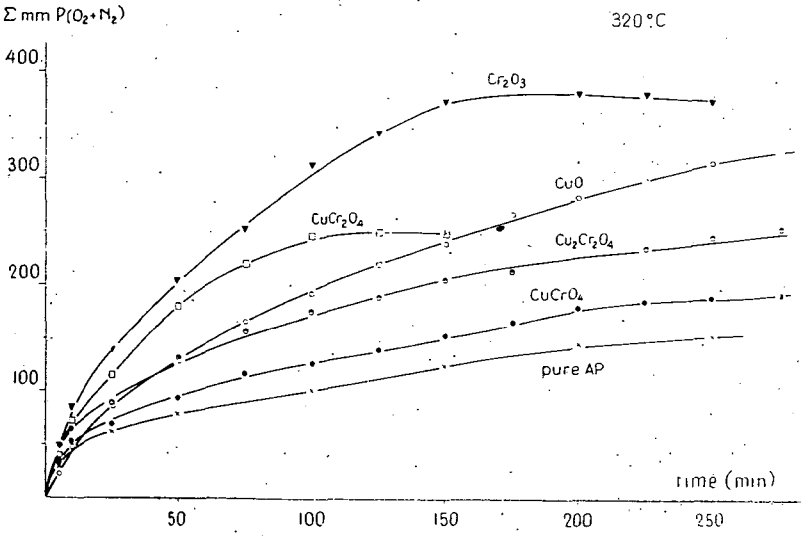

Fig. 2. Gas-phase decomposition of AP on different oxides

According to the typical data in Table I, the series of effectiveness of the oxides is fairly different in the low temperature decomposition from that in the high temperature decomposition; this permits conclusions on the change of importance of the individual reaction steps. Nor was there a close connection between the effects of the oxides exerted on the decompositions of perchloric acid and of AP (Tables I and IV).

Table I

Effect of oxides on the slow decomposition, the ignition, and the gas-phase decomposition of AP; mole ratio of the AP:oxide mixture 10:1

Catalyst	Slope of p—t curves, 225°C	Minimum ignition temp., °C	t_0, at 320°C
ZnO	1.71	252	6.1
MgO	1.04	280	42.0
Cu_2O	0.795	256	—
CdO	0.692	268	—
NiO	0.650	263	18.0
CoO	0.592	261	20.5
CuO	0.487	264	16.0
Fe_2O_3	0.319	307	28.5
TiO_2	0.303	385	43.5
Cr_2O_3	0.300	293	13.3
SnO_2	0.287	390	53.0
$CrO_{1.97}$	0.262	270	—
Al_2O_3	0.257	385	35.0
CaO	0.190	360	—
Without catalyst	0.250	420	57.0

t_0 = time (in minutes) for 50% decomposition

BOLDYREV *et al.* [6] recently investigated the gas phase decomposition of AP on manganese dioxide, copper chromite, iron(III) oxide and silica. The activities of the oxides decrease according to the following sequence:

$$MnO_2 > CuCr_2O_4 > Fe_2O_3 > SiO_2.$$

It was shown that in the presence of ammonia the decomposition of perchloric acid increased to about the 10-fold; this was explained by the re-establishment of the original state of the catalyst oxidized by the perchloric acid.

In their view, the order of effectiveness of the oxides is the same in the decompositions of both AP and perchloric acid; from this, conclusions were drawn on the importance of the catalytic decomposition of perchloric acid in the decomposition of AP. Since their studies covered only four oxides, their comparison was not sufficiently founded.

Effect of additives on the products of decomposition of AP

Rather few investigations have been reported on the effects of additives on the products of decomposition of AP.

HERMONI and SALMON [7] found that the quantity of oxygen decreased in the presence of nickel, cobalt, manganese and chromic oxides. An increase in the chlorine

dioxide content was reported, but this result was not confirmed by later studies; the increase of the ClO_2 content was attributed to the use of a wrong analytical method [8].

The studies of SHMAGIN and SHIDLOVSKII [9] showed that transition metal oxides decreased the extent of chlorine and dinitrogen oxide formation. The nitrogen was found primarily in the form of NO. These oxides barely affected the formation of HCl. An extremely large decrease of the HCl content was observed only in the presence of zinc oxide.

INAMI, ROSSER and WISE [8] studied the decomposition products of AP in the presence of copper chromite, as well as of cobalt and iron oxides. The products of the catalytic reaction were determined by subtracting the values measured in the decomposition of pure AP from the data found.

The most substantial difference between the products of the two reactions was that N_2O and HCl are not formed in the catalysed reaction. The results of the chemical analyses are reported in Table II.

Table II

Products of decomposition of ammonium perchlorate in the presence of *Harshaw* $CuCr_2O_4$

Temp. (°C)	Conc. (Wt %)	Yield							Recovery		
		O_2	N_2	N_2O	Cl_2	HNO_3	HCl	NO	N (atom%)	Cl (atom%)	Wt % decomp.
250	0	0.61	0.055	0.37	0.39	0.14	0.15	0.006	98.7	93.4	19.8
250	1.79	0.54	0.064	0.32	0.45	0.15	0.091	0.019	93.8	100.2	29.4
250	3.99	0.54	0.078	0.30	0.43	0.15	0.11	0.026	93.6	100.0	31.0
275	0	0.55	0.051	0.36	0.39	0.15	0.17	0.011	97.8	96.0	26.8
275	0	0.50	0.047	0.35	0.39	0.19	0.16	0.019	99.1	94.9	26.5
275	1.03	0.56	0.073	0.29	0.41	0.17	0.12	0.014	91.7	94.7	35.3
275	1.79	0.47	0.080	0.28	0.44	0.20	0.095	0.023	94.9	99.4	36.5
275	2.73	0.47	0.090	0.26	0.44	0.20	0.10	0.026	92.9	100.9	36.2
275	3.90	0.53	0.12	0.25	0.42	0.22	0.10	0.024	97.6	96.8	38.7

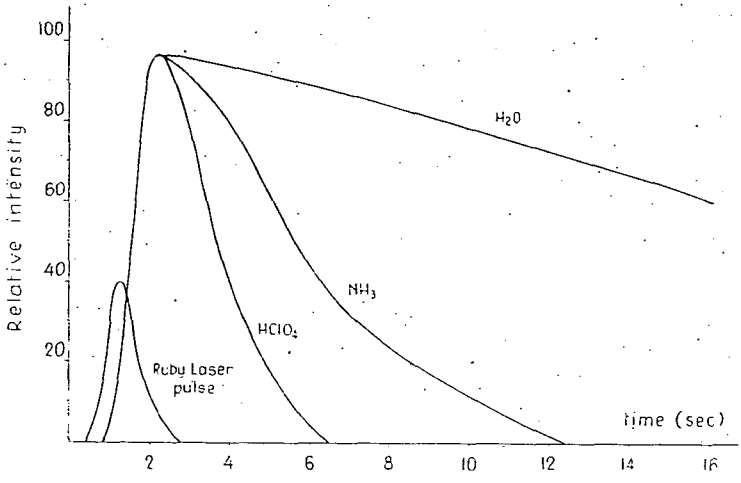

Fig. 3. Evolution history of the products in laser pyrolysis of a mixture of AP: Fe_2O_3 (5 w%)

PELLETT and SAUNDERS [10] studied the effects of iron oxide, copper chromite and manganese dioxide on the decomposition products of AP with a time-of-flight mass-spectrometer. The AP was heated up rapidly with a diamond laser. It was assumed that the decomposition products were formed in the heterogeneous phase reaction at high temperature (500—600°C). The first step was the dissociation of AP to ammonia and perchloric acid. The latter decomposes rapidly on the surface of the solid, the main products being chlorine dioxide and hydrogen chloride. A fairly slight decomposition of the chlorine dioxide was also observed; in high vacuum, under the experimental conditions, its stability exceeded that of perchloric acid. NO also occurred as a main product. The sequence for the amounts of nitrogen compounds formed was:

$$NO \gg N_2 > N_2O > NO_2.$$

Fig. 3 shows the time dependence of the primary products in the presence of iron oxide.

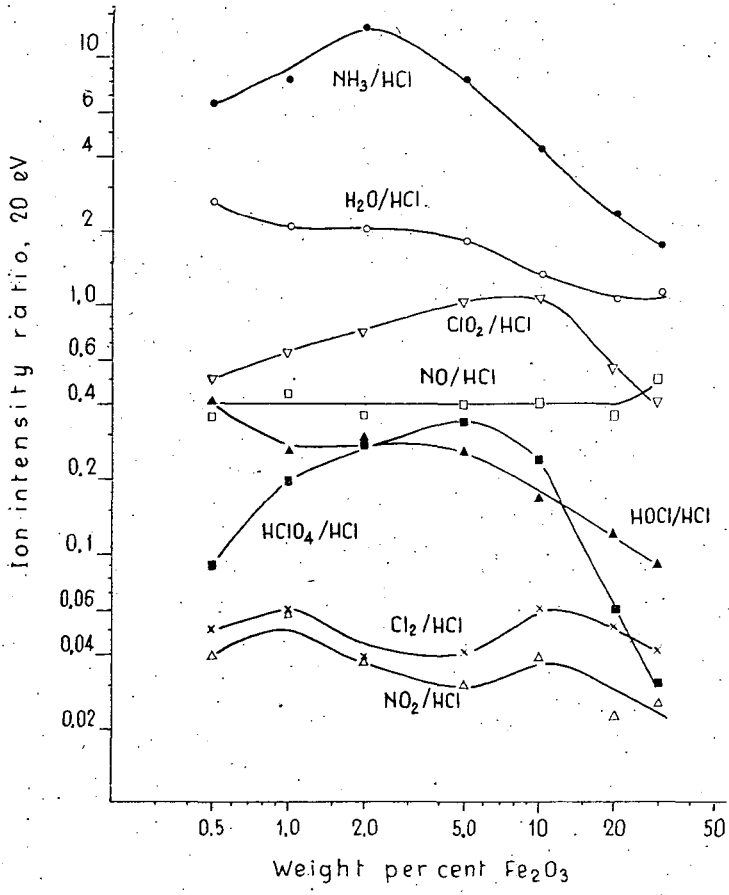

Fig. 4. Laser pyrolysis of AP: Harshaw copper chromite and Fe_2O_3

In Fig. 4 the product distributions in the presence of copper chromite and iron oxide is presented.

In order to distinguish nitrogen and nitrogen dioxide from carbon monoxide and carbon dioxide, ^{15}N-containing AP was used in some experiments. The relative amounts of products in the presence of various oxides are given in Table III.

Table III

20 eV product distributions obtained from Laser pyrolyses of $^{15}NH_4ClO_4$/metal oxide mixtures

	Harshaw Cu 0202	Fe_2O_3	MnO_2
Wt % (estimated)	50	50	70
HCl	1.00	1.00	1.00
N_2	0.20	0.14	0.31
CO	0.2	0.19	0.2
N_2O	0.11	0.04	0.13
CO_2	0.75	0.57	0.45
NO	0.88	0.67	0.40
NO_2	0.08	0.03	0.06
ClO_2	0.72	0.31	1.65
NOCl	0.30	0.09	0.38
NH_3+H_2O	15	3.3	12.3

An important difference in the effects of the oxides appeared in the case of iron oxide, where the amounts of N_2O, ClO_2 and HOCl were significantly smaller than in the other two cases.

The effects of various oxides on the products of the gas phase decomposition of AP were studied by BOLDYREV *et al.* [6] by mass-spectrophotometric analysis. Some measurements were also made with perchloric acid. The data are given in Table IV.

According to their analyses, there is a temperature range in which the perchloric acid decomposes to chlorine dioxide without the formation of chlorine. This is described by the following reactions:

$$HClO_4 \rightarrow HO_2+ClO_2$$

$$HClO_4 \rightarrow ClO_3+OH$$

$$ClO_3 \rightarrow ClO_2+O.$$

It is clear from the reported data that if ammonia is present in the system, then there is no molecular oxygen among the secondary products of the catalytic decomposition of perchloric acid. In the low temperature decomposition of AP, however, it was found earlier that oxygen is formed; this was explained by a different decomposition of the perchloric acid.

Table IV

Mass-spectrometric analysis of the gas-phase decomposition of AP *in the presence of catalysts* [6]

Catalysts (m^2/g)	28 N_2^+ CO^+	30 NO^+	32 O_2^+	36 HCl^+	44 N_2O^+ CO_2^+	46 NO_2^+	51 ClO^+	67 ClO_2^+	70 $^{35}Cl_2^+$	72 $^{37,35}Cl_2^+$	83 ClO_3^+	100 $HClO_4^+$	T, °C
MnO_2 (25)	15	540	54	61	69	108	—	—	230	155	—	—	200
	68	415	83	108	177	77	15	—	346	223	—	—	150
	50	208	50	82	98	46	25	46	216	140	—	—	100
CuO (0.2)	8	100	33	47	55	—	38	63	56	—	1	—	275
	5	16	34	20	25	—	68	78	—	—	27	11	200
Bauxit (30)	13	252	118	59	173	—	36	82	227	—	—	—	330
	39	131	23	46	31	—	62	92	100	—	—	—	300
	40	50	23	46	67	—	70	111	—	—	—	—	260
	19	5	15	19	24	—	56	85	—	—	40	16	210
SiO_2 (10^{-3})	7	7	10	20	17	—	60	113	—	—	43	17	300
	8	6	26	20	20	—	60	109	—	—	51	20	260
	15	—	11	20	14	—	48	111	—	—	72	29	210
Fe_2O_3 (3)	69	120	82	45	71	38	69	106	138	106	10	—	210
$CuCr_2O_4$ (20)	15	19	71	31	71	13	50	96	79	44	60	27	165

Interaction between AP *and the catalyst*

As has been seen above, the admixture of oxides to AP essentially changes the direction and products of the decomposition of AP in many cases. As has already been shown in numerous instances in contact catalytic reactions, the products of the catalytic reaction modify the surface composition and physical and chemical properties of the catalyst. It was mentioned above that in the case of copper(I) oxide the catalyst is oxidized to copper(II) oxide [11]. A number of authors have observed a similar oxidation with chromic oxide and copper chromite catalysts [7, 12]. HERMONI and SALMON [2] found the formation of CrO_2Cl_2 at 200—240°C.

It was observed by ROSSER, INAMI and WISE [8, 13] that the copper chromite catalyst was oxidized at 275°C; even at the beginning of the decomposition of AP its colour changed from black to brown, and this was accompanied by the cessation of the catalytic effect. (Under the decomposition conditions cobalt oxide was also oxidized but its catalytic effect did not cease.) An aqueous solution of the catalyst contained chromate ions. The authors assumed that the oxidation of the catalyst is caused by a strongly oxidizing intermediate (chlorine dioxide) formed in the catalytic reaction. It was considered less probable that the oxidation was caused by $HClO_4$ formed in the dissociation of AP.

However, the first results reported on the oxide-catalysed decomposition of perchloric acid showed that even below 200°C perchloric acid is capable of oxidizing

chromic oxide [14, 15]. Accordingly, it is not necessary to assume the formation of a strong oxidant in the catalytic reaction. Similar observations were published by PEARSON and SUTTON [16] in connection with the copper chromite catalyst. The oxidation by perchloric acid is supported by recent measurements of INAMI and WISE [17] in which the oxidation of the catalyst was also observed when it was not directly in contact with the AP.

Other authors found that chromic oxide is not oxidized in the decomposition of AP at 310°C, and in fact, in the presence of AP the oxidation of Cr_2O_3 by air is inhibited [18]. Oxidation was observed only if the mixture also contained potassium chloride.

A substantially greater change than the above occurs when the catalyst reacts with the AP, and the perchlorate salt formed in the reaction exerts a very large promoting effect. With the oxides, such reactions were observed in the presence of ZnO, CdO, MgO, PbO and CaO [19—24].

The formation of perchlorate salts was also observed in the presence of $BaCO_3$ and $CaCO_3$ [25, 26].

Unquestionably, the most probable way of formation of the perchlorate salts is that the perchloric formed in the dissociation of the AP reacts with the additive. However, since the above additives also react with other perchlorate salts when no perchloric acid is present, it cannot be excluded that in the case of AP the process occurs *via* an exchange reaction in the solid phase.

Other studies

In spite of the great number of kinetic investigations, rather few attempts have been made to elucidate the effects of mixing and of different reaction conditions. These data, however, can supply very useful information on the mechanism of the effects exerted by the additives and also on the nature of the solid phase catalytic reactions. The extent of the catalytic effect of an additive oxide, and the question whether the catalytic effect need be considered after the termination of good contact between the AP and the oxide, appeared fundamental.

From the analysis of the decomposition curve of an AP—MnO_2 mixture under high pressure, it appeared that the effect of the MnO_2 extends only up to 4% decomposition owing to the termination of the contact between AP and the oxide. Using a powder mixture, HERMONI and SALMON [7] observed almost 100% decomposition, even at low temperature; in this case the continuous renewal of the contact between the AP and the oxide powders was possible, in contrast with the situation in the tablet.

In the case of AP—CuO, the effect of the compression of the powder mixture on the rate of decomposition was studied in more detail [27]. The experiments were carried out in air. Although the effect of the pressure is fairly complex, it is evident from the measurements that the better contact between the substances, brought about by high pressure, favourably affects the commencement of the decomposition of the AP, the initial reaction, and hence, the explosion of the AP. However, high pressure is disadvantageous in the later stage of decomposition and for the extent of the reaction.

Concerning the effect of the gas pressure (air, oxygen, nitrogen), some measure-

ments were made with regard to the rate of the catalysed reaction and the occurrence of the explosion [28]. The increase in pressure of all three gases increased the catalytic reaction rate and, at a sufficiently high temperature, brought about the explosion of the AP. The hindrance to vaporization of the AP and restriction of the reaction to the solid phase clearly play a role in the gas pressure effect.

In this respect it would seem worth-while to study in detail how the course of the catalysed reaction varies with the partial pressure of ammonia. WISE [8] found that, in contrast to the decomposition of pure AP, the introduction of 2 torr ammonia does not inhibit the catalytic reaction at all.

The significance of the contact in the AP—oxide mixture was established by studying various pre-treatments and interruptions [28]. The pre-treatment at 215°C in air, up to the commencement of decomposition, of an AP—CuO tablet (16:1 molar ratio), compressed at 2700 atm, decreased the induction period of the explosion of the mixture at 270°C by about 50%. A similar effect was also observed in the case of the substance decomposed to 25%. Identical behaviour was found in 1:1 molar mixtures, too.

If the pre-treatment and the subsequent measurements were carried out in vacuum, the decomposition began sooner (16:1 molar ratio), here too. However, the pre-treatment even up to 2% decomposition decreased the rate of decomposition considerably.

The pre-treatment exerted substantially greater effects on AP—ZnO [28] and AP—CdO [22] mixtures. The time up to the explosion of a mixture at 270°C decreased with the increase of the pre-treatment time at 200—220°C. The results concerning cadmium oxide are given in Fig. 5.

If the interruption occurred at the temperature of the explosion, on renewed heating the AP—ZnO or AP—CdO mixture exploded after a time which was shorter by the time of previous heating at this temperature ("memory effect"). The duration of the interruption (5 min—24 hours) was an unimportant factor in this behaviour.

A possible explanation for the phenomenon is that, even at a low temperature during the pre-treatment, reaction between the AP and the oxide begins, resulting in zinc or cadmium perchlorate, which are extremely effective in the decomposition of AP [28, 22]. As a result, at higher temperature, the AP explodes after a substantially shorter time.

It is surprising, however, that this effect also occurred with the AP—CuO mixture, though to a smaller extent [28]. This mixture exploded in air at 270°C after 310 seconds. If the material was taken out of the reaction vessel in different stages of the decomposition preceding the explosion, and replaced after standing for about 15 minutes, then the explosion occurred substantially sooner than in the non-pre-treated tablet. The total time up to the explosion, however, was longer here. On the other hand, if the interruption was made at the end of the acceleration stage of the decomposition preceding the explosion (1:1 molar ratio), then the material did not explode any longer on renewed heating.

This means that in the presence of a larger quantity of copper oxide the decomposition could not accelerate to such an extent and could not produce so much heat that the tablet containing this amount of copper oxide should attain a temperature necessary for explosion.

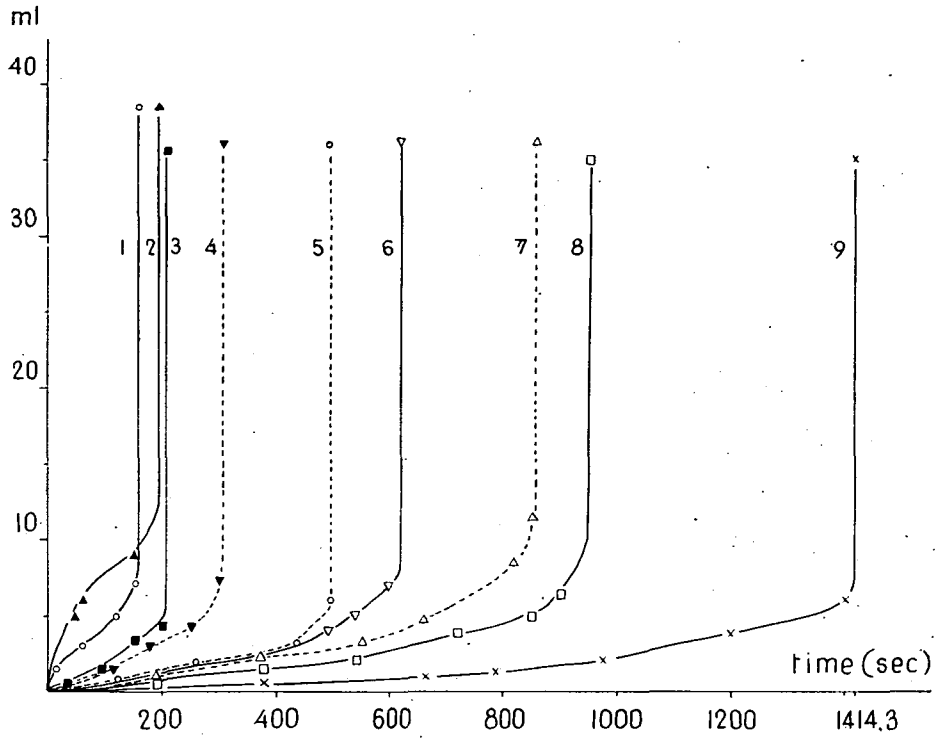

Fig. 5. Effect of low-temperature decomposition on the induction period for ignition of an AP—CdO mixture (mole ratio 10:1) at 285°C. Volume of gases formed *vs.* time. Pre-treatment temperature and time: 1. 200°C, 390 min; 2. 220°C, 240 min; 3. 220°C, 120 min; 4. 200°C, 260 min; 5. 200°C, 160 min; 6. 220°C, 60 min; 7. 200°C, 70 min; 8. 220°C, 20 min; 9. without pre-treatment

Mechanism of the catalytic decomposition of AP

In spite of the large number of studies reported, a generally valid theory of the role of the additives and of the mechanism of the catalytic decomposition of AP has not yet emerged. In the following a detailed account of the different views, their development, applicability and limitations is given.

1. *Mechanism of action of oxides*

In the derivation of the mechanism of the catalytic reaction, research workers in the overwhelming majority of cases relied on kinetic data, and primarily on the activation energy values. BIRCUMSHAW *et al.* [29, 30] and GALWEY and JACOBS [31, 32] found various activation energy values for the decomposition of pure AP, depending on the temperature region, and ascribed this to different reaction mechanisms. Kinetic studies with pure AP carried out from 1954 to 1962 showed clearly that the low temperature decomposition of AP, below 300°C, occurs by an electron-transfer

reaction. GALWEY and JACOBS [31] presumed that radicals produced in the electron-transfer process form molecular complexes. The decomposition of these complexes takes place in the further reaction steps; the separate, independent decomposition of perchlorate and ammonium radicals was considered less probable. Since the activation energy of the decomposition catalysed by manganese dioxide well approximated the activation energy value ascribed to the electron-transfer mechanism for the decomposition of AP, the action of the oxide was interpreted as the promotion of the electron-transfer process [35]. It was assumed that the AP complex formed after the electron-transfer is stabilized by manganese(IV) ions ($Mn^{3+}ClO_4.NH_4^+$), and the rate of re-formation of the perchlorate ion decreases. The fact that the catalysed and uncatalysed reactions have the same activation energies was explained by the electron-transfer to the catalyst taking place *via* the conductance band of the AP. The effect of iron oxide in the decomposition at 240—300°C was also explained later by the acceleration of the electron-transfer process [34].

From the point of view of elucidating the mechanism of the catalytic reaction and the role of the catalyst, it seemed of fundamental importance to determine which properties of the catalysts are responsible for the catalysis of the decomposition of AP.

According to the view generally accepted earlier, the low temperature decomposition of AP occurs by the electron-transfer process, and the first kinetic studies on the catalytic reaction supported the validity of this reaction [33, 19, 34], therefore, it was rightly assumed [27] that the electrical properties of the oxides may play a decisive part in the coming about of the catalytic action. From this it was expected that the modification of the electrical conductivities of the catalyst oxides should influence their catalytic actions [19, 27, 35]. The systematic investigations carried out from this point of view confirmed this working hypothesis and, on the basis of the available results, led to the conclusion that *p*-type semiconductors are the most effective substances, while *n*-conductors and insulators are substantially less effective or completely inactive [27, 36, 35].

From this it was concluded that the rate-determining process in the catalytic reaction is the first of the following two elementary steps:

$$\oplus MeO\ominus + ClO_4^- = ClO_4 + \ominus MeO\pm$$

$$\ominus MeO\pm + NH_4^+ = NH_4 + \ominus MeO\oplus,$$

i.e. the formation of the perchlorate radical [27, 35]. Clearly, *p*-type oxides can accelerate only the first reaction. The fact that *n*-conducting oxides (titanium(IV), tin(IV), aluminium(III), molybdenum(VI), tungsten(VI) oxides) are practically ineffective on the decomposition of AP, is in agreement with the proposed reaction mechanism since these oxides of high electron density cannot (or only to a small extent) promote the formation of perchlorate radicals.

Results obtained on doping the semiconductor oxides supported the above picture [27, 35, 37, 38]. From the properties of semiconductor oxides it is known that their conductivities and, therefore, electron and defect-electron concentrations can be increased or decreased by the incorporation of ions of different valency. In the case of *p*-type oxides, the defect-conductance of an oxide is increased by the incorporation of ions of lower valency, while ions of higher valency bring about a decrease of the defect-conductance. The reaction rate of the catalytic decomposition

of AP changed with varying the defect-electron densities of the *p*-type copper(II) oxide [27], nickel(II) oxide [37] and chromium(III) oxide [35]. Increase of the defect-electron density increased the catalytic effect of an oxide, and *vice versa*. It is an important result that the catalytic activity of an oxide was modified by doping only if its electrical properties also changed. It could be seen from Fig. 3 of the previous paper [1] that the induction period preceding the explosion of AP was increased by doping the Cr_2O_3 with TiO_2, while neither ZnO nor NiO additives caused any change. In contrast with TiO_2, the latter practically did not affect the electrical conductivity of Cr_2O_3.

In the case of *n*-conducting oxides (TiO_2 or SnO_2), changes in the electron concentration did not bring any essential change; from this it was concluded that, even with the decrease of the electron concentrations (the Fermi potentials of the electrons), the oxides were not capable of promoting the formation of perchlorate radicals. The only exceptions were titanium dioxide [35] or tin dioxide [38] doped with a small amount of chromic oxide.

A detailed study of the chromic oxide—titanium dioxide system led to the result that, due to of the oxidation of chromium (valence inductivity) accompanying the incorporation of the chromic oxide,

$$Cr_2O_3 + 1/2\,O_2 \rightleftharpoons 2\,Cr\bullet^{X}(Ti) + 2\,TiO_2$$

and further oxygen chemisorption

$$1/2\,O_2 + Cr\bullet^{X}(Ti) \rightleftharpoons 1/2\,O_2^{-} + \dot{C}r\bullet\cdot(Ti),$$

some of the chromium is converted to valency states four and five [39]. The substitution defects of the $Cr\bullet^{X}(Ti)$ and $Cr\bullet\cdot(Ti)$ readily dissociate according to the following two equations

$$Cr\bullet^{X}(Ti) \rightleftharpoons Cr\bullet'(Ti) + \oplus$$

and

$$Cr\bullet\cdot(Ti) \rightleftharpoons Cr\bullet^{X}(Ti) + \oplus$$

and so defect electrons are formed in a considerable amount. This process occurs primarily in the surface layer of the titanium dioxide where, as a result, an extremely good defect-conductor layer exists. With the assumption of *n*-type → *p*-type conversion on the surface, the large catalytic effect of titanium dioxide doped with chromic oxide was explained in an exactly similar way as above [35]. Accordingly, the practically inactive titanium dioxide as a carrier promotes only the formation of a component which is extremely active in the decomposition and explosion of AP. Since the titanium dioxide—chromic oxide mixture has a surplus oxygen content and a surface defect-electron density which considerably exceed those of the same amount of pure chromic oxide, it can be understood on the basis of the above reaction scheme why the effectiveness of the titanium dioxide + chromic oxide surpasses the effect of pure chromic oxide.

Similar processes take place on the incorporation of chromic oxide into the surface layer of *n*-type tin dioxide (formation and stabilization of higher valency chromium ions) [38], and the increased catalytic effect of the tin dioxide doped

with chromic oxide was explained, here too, by the formation of higher valency chromium ions with their large electron affinity.

However, the fact that a significant catalytic effect was observed in the presence of the *n*-conductor zinc oxide [19, 20, 36], cadmium oxide [22], and the insulator magnesium oxide [7, 24] is contradictory to the above assumption. The activation energies of the catalytic reactions agreed again with the value ascribed to the electron-transfer process.

Detailed investigations showed, however, that the role of the oxides in these cases fundamentally differred from those above. It was an essential difference that all three oxides reacted with the AP according to the following reaction:

$$2\,NH_4ClO_4 + MO = 2\,MClO_4 + 2\,NH_3 + H_2O.$$

The fact that the perchlorate salts formed exerted similar effects on the above oxides permitted the conclusion that not the oxides but the perchlorate salts formed in the above reaction were responsible for the observed acceleration of the reaction [20, 22, 24]. This is supported by the finding that, when a small amount of additive is used, the rate of decomposition is the same in the presence of the perchlorate or of the oxide; the time lag, however, is longer in the presence of the oxide. This difference is clearly caused by the fact that, in the case of the oxides, the formation of the catalyst must precede the catalytic reaction, *i.e.* the oxide must react with the AP. As regards the decomposition of AP, this reaction is primarily disadvantegeous; the reaction between the two substances presumably occurs with the participation of the most active surface centres which are also of primary importance for the decomposition. (The decomposition of AP begins on the surface.) On using small amounts of oxide this effect appears either not at all or only to a small extent; in the presence of a larger amount, however, at higher temperature it can assume such an extent that the decomposition of AP commences later than in the absence of the oxide. The interpretation of the effects of metal perchlorates is dealt with below.

From the kinetic data given in the previous paper [1] it is clear that, in many cases, the raising of the temperature region is accompanied by the increase of the activation energy of the catalytic reaction. Disregarding a few abnormal values, it is found that the values of the higher activation energy fall in the range 40—45 kcal.

This increase of the activation energy can be interpreted as due to the change in the mechanism of the catalytic decomposition and of the rate-determining step. It was assumed earlier that in this case the primary reaction is the decomposition of the perchlorate ion, where the slowest process is the rupture of the Cl-O bond. Since the dissociation energy of this bond (63.3 kcal) is substantially higher than the activation energy values obtained from kinetic measurements, HERMONI and SALMON [7] assumed that both the electron-transfer process (32 kcal) and the decomposition of the perchlorate ion (63 kcal) play a part in the decomposition of AP. The 40—45 kcal is derived from the above two values. However, it cannot be excluded that, in the presence of oxides, the decomposition of the perchlorate ion proceeds with a smaller activation energy. This is supported by experiments with alkali chlorates and perchlorates. The activation energies of the uncatalysed reaction well approximate the value of the dissociation energy of the Cl-O bond [40—43]. In the presence of the effective transition metal oxides, however, the value of the activation energy was signigicantly smaller [40, 44].

After the development of these mechanisms for the catalytic decomposition of AP, more recent kinetic and other investigations with pure AP brought about a fundamental change [45]. This work is summarized as follows.

(*a*) Repeated kinetic measurements on both the low and the high temperature decomposition and the sublimation of AP led to identical activation energies of 30 kcal.

(*b*) Mass-spectrographic studies did not confirm the existence of the molecular complex and definitely showed that the primary step in the decomposition of AP is the dissociation to ammonia and perchloric acid.

(*c*) Calculations, using the most reliable physical data, of the thermal activation energy value necessary for the electron-transfer in AP gave substantially larger values than the above (33—35 kcal).

From all this it was assumed that, regardless of the temperature range, AP decomposes by a proton-transfer process. Although a number of authors consider the generalized proton-transfer model [46] as over-simplified and maintain the view that the decomposition mechanism of AP varies with the temperature region [47, 48], it is certain that many facts reported in detail in the previous paper [49] prove the general importance of the proton-transfer process.

On the basis of the proton-transfer model, the interpretation given by JACOBS and RUSSEL-JONES [12] for the decomposition of AP catalysed by copper chromite was that the perchloric acid formed during the dissociation of the AP migrates to the surface of the oxide and there decomposes in a heterogeneous phase reaction. The following steps comprise the oxidation of ammonia by the decomposition products of the perchloric acid. A proof of this route for the catalysis is provided by the fact that the oxides also exhibited catalytic effects when they were physically separeted from the AP [2, 3]. Another result which may be regarded as important in this respect was that the effect of nickel oxide mixed with AP, regardless of the quantity, depended on the extent of the BET surface [3].

Since the activation energy of the catalysed decomposition (45 kcal) agreed with the activation energy of the homogeneous phase decomposition of perchloric acid, the authors assumed that the rate-determining process was the decomposition of perchloric acid on the surface of the oxide.

This latter conclusion is, however, subject to criticism, since it is difficult to imagine that the catalysed and non-catalysed decompositions should take place with the same activation energy values [14, 15, 50]. Study of the decomposition of $HClO_4$ catalysed by chromic oxide confirmes this doubt [15].

Since the dissociative vaporization of AP becomes more important at higher temperature (300°C), this reaction path seems very plausible at least at higher temperatures, and with high probability, such an effect on the high temperature decomposition of AP is exerted by the other oxides, too.

It is questionable, however, whether at low temperature (below 240 or 200°C), where the dissociative vaporization of AP is extremely small, the catalytic decomposition of AP proceeds in this way. The fact that the activity series of the oxides differ somewhat in the low and the high temperature region may be an indication of different reaction mechanisms.

From a consideration of the products of the catalysed and non-catalysed reactions and of the oxidation of the $CuO.Cr_2O_3$ catalyst, WISE [8] came to the

conclusion that in contrast with the decomposition of pure AP the catalysed reaction proceeds according to the electron-transfer mechanism given above.

Knowledge of the catalytic decomposition of perchloric acid appeared fundamentally important for the elucidation of the mechanism of the catalytic decomposition of AP, since the literature did not contain any data in this respect. The main results of investigations carried out recently in this field by the author of this paper and his colleagues are given in Table V [4, 14, 15, 51].

Table V

Kinetic data of the catalytic decomposition of perchloric acid [49]

Catalyst	Temperature range of the reaction, °C	k_{spec} ($sec^{-1} m^{-2}$) at 300°C	Activation energy, kcal/mole	% conversion at 300°C m^{-2}
Cr_2O_3	150—180		31.0	39.8*
MiO	210—250	3.9585	27.1	9.7**
CuO	270—300	1.4350	42.8	38.3
CO_2O_3—CO_3O_4	210—260	(1.4)	—	20.5
Fe_2O_3	250—285	0.5831	42.6	20.2
Al_2O_3	240—290	0.2942	26.5	10.6
SnO_2	295—340	0.2220	20.7	5.8
TiO_2	305—330	0.0350	33.0	0.86
ZnO	330—335	0.0154	45.6	0.40
CdO	400	—	—	—
MgO	400	—	—	N.D.***
SiO_2	400	—	—	N.D.***
CaO	400	—	—	N.D.***

* At 180°C ** At 250°C *** No decomposition

To characterize the effectiveness of the oxides, the temperature ranges of the decomposition were given together with the first order rate constants measured at or extrapolated to 300°C. On this basis, the catalysts were divided into three groups.

(*a*) Particularly effective oxides which display considerable catalytic action even at 130°C (chromic oxide) or 240—290°C (cobalt, nickel, copper, iron and aluminium oxides).

(*b*) Less effective oxides (tin dioxide, titanium dioxide, zinc oxide) which catalyse the decomposition of perchloric acid at 300—360°C.

(*c*) Inactive oxides (cadmium, magnesium and calcium oxides) in the presence of which catalytic reaction was not observed.

The apparent activation energies of the catalytic reaction fall in the range 20—45 kcal.

From a comparison of the data of Tables I and V it is quite clear that the activity series for the oxides are significantly different in the two decomposition reactions. Chromic oxide, which proved the most effective substance as regards the decomposition of perchloric acid, affected the slow decomposition of AP only to a small extent. Aluminium oxide, titanium dioxide and tin dioxide, which exerted only a very slight effect on the decomposition and explosion of AP, catalysed the decomposition of perchloric acid fairly well. Nickel, cobalt and copper oxides are

effective catalysts of the slow decomposition of AP [7, 27], but catalyse the decomposition of perchloric acid at a considerably higher temperature than does the less active chromic oxide.

On the basis of all these facts, the mechanism proposed by JACOBS for the catalysed reaction seems to be an over-simplification, or at least cannot be generally applied. The experiment referred to in JACOBS' review [45] that NH_3 streaming over the potassium perchlorate catalyst system did not ignite even above the ignition temperature of AP cannot be considered as a proof of his theory. This was interpreted by JACOBS to mean that the catalysts act on the $HClO_4$ and not on the ClO_4^- anion. The oxides effective in the decomposition of AP are also very good catalysts in the decompositions of potassium perchlorate and other alkali metal perchlorates. There are many possible reasons for the failure to ignite: a different decomposition mechanism; the substantially higher stability than that of AP (the pure salt decomposes above 560°C); etc.

The fact that the series of effectiveness of the oxides in the low temperature decomposition of AP essentially agrees with the series found in the oxidation of ammonia permits the conclusion that the oxidation of ammonia plays a substantially greater part in the catalytic process than was assumed. Since the electrical properties of the catalysts are decisive in the oxidation of ammonia with molecular oxygen, and the rate of oxidation increases with increasing *p*-character of the catalyst, it cannot be excluded that the essential role of the electrical properties of the oxides is to be ascribed to their role in oxidizing ammonia in the decomposition of AP.

It is highly probable that the effectiveness of the oxides is due to two factors: the catalysis of the heterogeneous phase decomposition of perchloric acid, and the catalysis of the oxidation of ammonia. Oxides able to catalyse both reactions can be considered as most effective. This also means that the decisive step in each reaction occurs on the surface of the catalyst, presumably in such a way that the adsorbed ammonia is oxidized by the radicals formed in the decomposition of the adsorbed perchloric acid (O, ClO, ClO_2). If the temperature and reaction conditions are altered, then, depending on the properties of the oxide, the adsorption of $HClO_4$ and NH_3, and the decomposition of adsorbed $HClO_4$ change, and this may lead to the modification of the series of effectiveness of the oxides with the temperature region.

It is not possible to decide on the basis of the data available at present whether the direct reaction between the ammonia and the perchloric acid does proceed on the surfaces of the oxides. According to unpublished measurements, the above reaction occurs in the homogeneous phase [45].

The fact that the gas phase decomposition of AP (NH_3+HClO_4) on ZnO proceeds with a well-measurable rate at temperatures where neither the ZnO-catalysed decomposition of $HClO_4$ nor the oxidation of NH_3 takes place, permits conclusions on the promotion of the direct reaction between the two substances [5, 51]. The optimum adsorption of the substances appears necessary for the catalysis of the reaction; according to the above, this is available on ZnO in spite of the fact that ZnO is not an outstanding catalyst for either the decomposition of $HClO_4$ nor the oxidation of NH_3.

2. *Mechanism of action of salts*

A further question remains concerning the interpretation of the accelerating action of various salts, primarily of metal ions introduced in the form of perchlorates.

In the first works the effects of the ions were similarly explained on the basis of the electron-transfer mechanism. Silver, copper and iron perchlorates proved to be particularly effective substances [52, 53]. Since these metal ions are effective electron acceptors, it was assumed that, like the *p*-type oxides, they promote the formation of the perchlorate radical, and increase its lifetime and the probability of its decomposition [52, 53]. The effects of bromide and iodide ions were also explained by the electron-transfer reaction [52]. The role of chlorate ions in decreasing the stability of AP to a large extent was likewise explained by the electron-transfer mechanism, the chlorate radical formed acting both as an electron acceptor and also as a radical producer, promoting thereby the reaction [54—56].

However, it cannot be expected that the zinc, cadmium and magnesium ions participate directly in the electron-transfer reaction between the ammonium and perchlorate ions, accelerating by this means the electron-transfer. It appears much more probable that the increased tendency to decompose of the AP is the result of its partial melting [19, 20, 22, 24, 57, 58], though the melting point of pure AP is not known since the substance explodes before the melting point is reached. However, in the presence of the perchlorate salts in question (and also of the corresponding oxides) AP was observed to melt at the temperature of the experiments. This can be conceived in the present case as due to the formation of an eutectic of lower melting point between the AP and the perchlorate added.

In addition, the polarizing effects of the metal ions should also play a part in the action of the additives; the greater the polarizing power (effective electric field strength) of the cations, the greater their accelerating action on the reaction [22, 57, 58]. The series of effectiveness of the substances:

$$Mg^{2+} < Cd^{2+} < Zn^{2+}$$

corresponds to the series of effective electric field strengths of the cations:

$$Mg^{2+}\ 5.444;\quad Cd^{2+}\ 5.750;\quad Zn^{2+}\ 6.654.$$

It should be remembered that the effective electric field strengths of the cations play an important part in determining the thermal stabilities of metal perchlorates: the higher the value, the lower the stability of the substance [41—43, 59]. The significance of the polarizing power of the cations is shown by the fact that, although lithium perchlorate causes the melting of AP, it does not exhibit the large acceleration of the reaction observed for magnesium, cadmium and zinc ions [60]. Similarly, the other alkali metal perchlorates and calcium perchlorate did not possess a catalysing action. It is well known that the polarizing power of the alkali metal ions is the lowest, their effective electric field strengths increasing from caesium to lithium from 1.3 to 2.9. At all events, however, the melting of the mixtures seems necessary for the polarizing action of the cations to be exerted. This can be seen from the fact that, when magnesium, cadmium and zinc ions were added in the form of their sulphates to the AP, no acceleration occurred and the AP did not explode even at 400°C [22, 57, 58]. The melting points of magnesium, cadmium and zinc sulphates are extremely high, and their mixtures with AP did not melt, even partially below 400°C.

It was, however, an open question up to now, by what mechanism AP decomposes in the presence of the above metal ions and how these ions are involve in this mechanism. Leaving out of consideration the above findings, RUSSEL—JONE and JACOBS [61] explained the actions of these metal ions and of silver by ammin formation and hence the promotion of the proton-transfer process. This explanatio is, however, not very probable because almost the same effects were exerted b $Zn(NH_3)_2(ClO_4)_2$ and $Zn(ClO_4)_2$ [57]. In addition, at the temperature of the decomposition of AP the reaction

$$Zn(NH_3)_2(ClO_4)_2 + 2\ NH_3 \rightleftharpoons Zn(NH_3)_4(ClO_4)_2$$

proceeds almost completely towards the left, and thus, at this temperature, the abov process can be excluded. The situation is completely similar in the case of the cadmium salt, too [62]. Irrespective of this fact, it would be difficult to imagine that th tremendous acceleration effect of a very small amount of the perchlorate sal ($AP:Zn(ClO_4)_2$, molar ratio 1000:1) would result merely from the displacemen of the dissociation of the AP. In the view of JACOBS and ACHESON [63], in the presenc of magnesium perchlorate, oxide ions are formed from the decomposition of th perchlorate ion in the molten phase

$$2\ ClO_4^- = Cl_2 + O^{2-} + 7/2\ O_2$$

and these, as effective proton acceptors, promote the formation of ammonia

$$2\ NH_4^+ + O^{2-} = H_2O + 2\ NH_3.$$

In our opinion, this reaction path is not probable either, since in the decomposition of zinc perchlorate, which is more effective than magnesium perchlorate, predominantly chloride ions are formed, and the decomposition of the likewise effectiv cadmium perchlorate does not lead to the formation of oxide ions at all.

We consider that in interpreting the actions of perchlorate salts it is essential to rely on the findings reported above, according to which the partial melting of the mixture and the high polarizing power of the cations are necessary for the emergence of the accelerating effect. In studying the thermal decomposition of variou perchlorate salts it was observed [41—43] that the melting of the mixtures is accompanied by the substantial increase by (1—2 orders of magnitude) of the rate of decomposition. This is probably caused by the increased mobility of the ions and the ceasing of the restriction of the reaction to the surface (external and internal) of the crystals. In the present case the following ions can be considered in the molten phase: M^{2+}, ClO_4^- and NH_4^+. If the latter dissociates partially, then H^+ and NH_3 are also formed.

The decomposition of the perchlorate ion in the melt begins depending on the polarizing power of the metal ion. This means that in the presence of the metal ions, in a molten phase a new reaction path is available for the decomposition o the perchlorate ion, a path which played essentially no role in the absence of the metal ions, in other words in solid AP. Earlier investigations showed clearly that

he perchlorate salts of both alkali metals and bivalent metals decompose stepwise with the transitional formation of chlorate and chlorite:

$$ClO_4^- = ClO_2^- + O$$

$$ClO_3^- = ClO_2^- + O$$

$$ClO_2^- = ClO^- + O$$

$$ClO^- = Cl^- + O.$$

The disproportionation of the oxy anions of chlorine takes place parallel to the decomposition. The slowest step in the decomposition of perchlorates is the first reaction. If only the first step is considered, it is evident that both the chlorate ion, which is extremely effective as regards the decomposition of AP, and the oxygen atom necessary for the oxidation of ammonia are formed. Both products can bring about the increase of the rate of decomposition.

Considering the presence of NH_4^+ and NH_3, it is very unlikely that the decomposition of the chlorate ion proceeds in the above way. Ammonium chlorate is an extremely unstable substance, slowly decomposing even at 40—50 °C, and exploding above 70°C [64]. Its decomposition is assumed to occur in a proton-transfer process; the unstable $HClO_3$ formed decomposing, the radicals proceed oxidizing the ammonia.

Accordingly the most probable reaction path seems to be the formation of $HClO_3$ by reaction of ClO_3^- ions with free H^+ or with protons from NH_4^+; the $HClO_3$ rapidly decomposing with the formation of the radicals necessary for the oxidation of ammonia.

This reaction path is in agreement with experimental observations. The decomposition of the perchlorate ion in the molten phase occurs only in the presence of cations of high polarizing power. When lithium perchlorate was used, although the mixture melted, the extremely powerful catalytic effect observed in the presence of zinc, cadmium and magnesium ions did not occur, since the polarizing power of the lithium ion is substantially lower than that of these other metal ions [60]. For similar reasons, no acceleration of the reaction occurred with barium [65] and calcium perchlorates [62], although both substances caused partial melting of the AP. In the case of zinc, cadmium and magnesium sulphates, no catalytic effect was observed, because the mixture remained in the solid phase [22, 58].

References

[1] *Solymosi, F.:* Acta Phys. et Chem. Szeged **19**, 255 (1973).
[2] *Hermoni, A., A. Salmon:* Abstract of Proceedings of the 33rd. Meeting of the Israel Chemical Society **1**, 313 (1963).
[3] *Болдырева, А.В., Безруков, Б. Н., Болдырев, В. В.:* Кин. и кат. **8**, 29 (1957).
[4] *Solymosi, F., L. Gera, S. Börcsök:* 13th Symposium (International) on Combustion, The Combustion Institute, Pittsburgh, 1971, p. 697.
[5] *Solymosi, F., L. Gera:* J. Phys. Chem. **75**, 491 (1971).
[6] *Коробейничев, О. П., Карпенко, Ю. Я. Болдырев, В. В.:* Изв. акад. наук, **7**, 1663 (1970); **7**, 1663 (1970).
[7] *Hermoni, A., A. Salmon:* Eighth Symposium (International) on Combustion, The Williams and Wilkins Co., Baltimore, p. 656, 1962.

[8] *Rosser, W. A., S. H. Inami, H. Wise;* Combustion and Flame, **12**, 427 (1968).
[9] *Шмагин, Л. Ф., Шидловский, А. А.:* Иссл. в обл. хим. и технол. минер. солей и окислов, АН СССР, Сб. Статей 112—114 (1965).
[10] *Pellett, G. L., A. R. Saunders:* AIAA Sixth Aerospace Sciences Meeting, New York, N. Y., AIAA Preprint 68—149 (1968).
[11] *Jacobs, P. W. M., A. R. T. Kureishy:* Eighth Symposium (International) on Combustion, The Williams and Wilkins Co., Baltimore, Md., 1962, pp. 672—677.
[12] *Jacobs, P. W. M., A. Russel-Jones:* Eleventh Symposium (International) on Combustion, The Combustion Institute, Pittsburgh, Pa., 1967, pp. 457—462.
[13] *Rosser, W. A., N. Fishman, H. Wise:* AIAA. J. **4**, 1615 (1966).
[14] *Solymosi, F., S. Bőrcsök, E. Lázár:* Combust. Flame **12**, 398 (1968).
[15] *Solymosi, F., S. Bőrcsök:* J. Chem. Soc. **A1970**, 601.
[16] *Pearson, G. S., D. Sutton:* Combust. Flame **13**, 330 (1969).
[17] *Inami, S. H., H. Wise:* Combust. Flame, **13**, 556 (1969).
[18] *Burcat, A., B. Carmon, J. Pelly, M. Steinberg:* Israel J. Chem. **6**, 859 (1968).
[19] *Solymosi, F., L. Révész:* Nature, **192**, 64 (1961).
[20] *Solymosi, F., L. Révész:* Z. anorg. Chem. **322**, 86 (1963).
[21] *Болдырева, А. В., Мозхова, В. Н.:* Кин. и кат. **7**, 734 (1966).
[22] *Solymosi, F., K. Fónagy:* Eleventh Symposium (International) on Combustion, The Combustion Institute, Pittsburgh, Pa., 1967, pp. 429—437.
[23] *Hermoni, A., A. Salmon:* Bull. Res. Counc. of Israel **9**, 206 (1960).
[24] *Solymosi, F.:* Magy. Kém. Foly. **73**, 358 (1967).
[25] *Simchen, A. E., L. Inbar-Rosem:* Israel J. Chem. **6**, 937 (1968).
[26] *Osada, H., E. Sakamoto:* Kogyo Kayaku Kyokaishi **24**, 236 (1963).
[27] *Solymosi, F., E. Krix:* J. Catalysis **1**, 468 (1962).
[28] *Solymosi, F.:* Paper Presented at IUPAC Congress in 1963, London.
[29] *Bircumshaw, L. L., B. H. Newman:* Proc. Roy. Soc. **A227**, 228 (1955).
[30] *Bircumshaw, L. L., T. R. Phillips:* J. Chem. Soc. **1957**, 4741.
[31] *Galwey, A. K., P. W. M. Jacobs:* Proc. Roy. Soc. **A254**, 454 (1960).
[32] *Galwey, A. K., P. W. M. Jacobs:* J. Chem. Soc. **1959**, 837.
[33] *Galwey, A. K., P. W. M. Jacobs:* Trans. Faraday Soc. **55**, 1165 (1959).
[34] *Шоймоши, Ф., Л. Ревес:* Кин. и кат. **4**, 88 (1963).
[35] *Solymosi, F.:* Combustion and Flame **9**, 141 (1965).
[36] *Kuratani, K.:* Rept. Aeronaut. Res. Inst. No. 372, 79 (1962).
[37] *Krix, E.:* Thesis, Szeged, 1961.
[38] *Solymosi, F. T. Bánsági:* Proceedings of the 2nd International Conference on Space Engineering, D. Reidel Publ., Dordrecht 1970, p. 145.
[39] *Szabó, Z. G., F. Solymosi:* Acta Chim. Hung. **25**, 145 (1960).
[40] *Solymosi, F. E. Krix:* Acta Chim. Hung. **34**, 241 (1962).
[41] *Solymosi, F.:* Acta Chim. Hung. **57**, 11 (1968).
[42] *Solymosi, F.:* Kémiai Közlemények (Budapest) **35**, 171 (1971).
[43] *Glasner, A. L. Weidenfeld:* J. Am. Chem. Soc. **74**, 2467 (1952).
[44] *Solymosi, F.:* Unpublished results.
[45] *Jacobs, P. W. M., H. M. Whitehead:* Chem. Revs. **69**, 551 (1969).
[46] *Davies, J. V., P. W. M. Jacobs, A. Russel-Jones:* Trans. Faraday Soc. **63**, 1737 (1967).
[47] *Maycock, J. N., V. R. Pai Verneker:* Proc. Roy. Soc. **A307**, 303 (1968).
[48] *Pai Verneker, V. R., J. N. Maycock:* J. Inorg. Nucl. Chem. **29**, 2723 (1967).
[49] *Solymosi, F.:* Acta Phys. et Chem. Szeged **19**, 67 (1973).
[50] *Pearson, G. S.:* Oxidation and Combustion Revs. **4**, 1 (1969).
[51] *Solymosi, F.:* Third International Conference of Space Technology, Rome, 1971. Nr. 26.
[52] *Solymosi, F., K. Dobó:* Fifth International Symposium on the Reactivity of Solids, Elsevier Publishing Co., Amsterdam, 1965.
[53] *Freeman, E. S., D. S. Anderson, J. J. Campisi:* J. Phys. Chem. **64**, 1727 (1960).
[54] *Petricciani, J. C., S. E. Wiberley, W. H. Bauer, T. W. Clapper:* J. Phys. Chem. **64**, 1309 (1960).
[55] *Freeman, E. S., D. A. Anderson:* J. Phys. Chem. **65**, 1662 (1961).
[56] *Freeman, E. S., D. A. Anderson:* Symposium on Physical and Chemical Effect of High Energy Radiation, American Society for Testing and Materials, 1964, p. 58.
[57] *Solymosi, F., J. Rask:* Z. phys. Chem. N. F. **67**, 76 (1969).
[58] *Solymosi, F.:* Magy. Kém. Foly. **73**, 366 (1967).
[59] *Solymosi, F.:* Acta Chim. Hung. **57**, 35 (1968).

[60] *Solymosi, F., M. Ránics:* Combust. Flame **10**, 398 (1960).
[61] *Jacobs, P. W. M., A. Russel-Jones:* AIAAJ. **5**, 829 (1967).
[62] *Raskó, J.:* Thesis, Szeged, 1969.
[63] *Acheson, R. J., P. W. M. Jacobs:* J. Phys. Chem. **74**, 281 (1970).
[64] *Solymosi, F., T. Bánsági:* Combust. Flame **13**, 262 (1969).
[65] *Acheson, R. J., P. W. M. Jacobs:* Can. J. Chem. **47**, 3031 (1969).

МЕХАНИЗМ КАТАЛИТИЧЕСКОГО РАЗЛОЖЕНИЯ ПЕРХЛОРАТА АММОНИЯ

Ф. Шоймоши

В работе дан критический обзор разных взглядов, связанных с влиянием различных добавок на термическое разложение и горение перхлората аммония. На основании всех данных и наблюдений нами предлагается механизм каталитического разложения перхлората аммония.

PREPARATION OF SOME DI- AND TRIPEPTIDES CONTAINING OPTICALLY ACTIVE PIPECOLIC ACID AS FRAGMENTS OF PIPECOLIC ACID-BRADYKININ ANALOGUES

By

L. BALÁSPIRI, GY. PAPP, P. PALLAI and K. KOVÁCS

Institute of Organic Chemistry, Attila József University, Szeged

(Received January 17, 1974)

Some di- and tripeptides of L- and D-pipecolic acid, fragments of the corresponding pipecolic acid-bradykinin analogues, are described.

Changes in the structure of known peptide hormones by substituting amino acids of similar character for the constituting amino acids are very important for the investigation of the connections between hormone structure and biological activity [1]. Among the amino acids substituted several "non-proteinogenic" amino acids [2] are found, mainly as corresponding homologues of "proteinogenic" amino acids.

Proline is an important constituent of several biologically active peptide hormones. Three of the nine amino acids contained in the well-known tissue hormone Bradykinin (I) are prolines:

Arg-Pro-Pro-Gly-Phe-Ser-Pro-Phe-Arg
(I)

Thus it is easy to see that the use of proline homologues in peptide chemistry may yield much valuable information. The most important homologues to be considered in their optically active form are pipecolic acid*, azetidine-2-carboxylic acid, oxazolidine-4-carboxylic acid, thiazolidine-4-carboxylic acid and α-homoproline.

According to literature, oxazolidine-4-carboxylic acid has not been used in peptide chemistry owing to various circumstances, and only in three instances [3, 4, 17c] the use of azetidine-2-carboxylic acid is found; three papers [3—5] were published on the substitution of thiazolidine-4-carboxylic acid, while α-homoproline was applied only most recently, after a suitable way of synthesis had been elaborated [6].

* The abbrevations are those accepted by IUPAC—IUB for peptide chemistry: Pip = pipecolic acid (piperidine-2-carboxylic acid); Aze = azetidine-2-carboxylic acid; Thz = thiazolidine-4-carboxylic acid; Oxz = oxazolidine-4-carboxylic acid; HPro = α-homoprolin (pyrrolidine-2-acetic acid). Z = benzyloxycarbonyl; Boc = *t*-butyloxycarbonyl; ONb = *p*-nitrobenzyl.

Pipecolic acid was applied more frequently than the above amino acids, mainly in connection with the preparation of the corresponding analogues. The first papers on this topic were concerned with collagen models [7] and 3-L-pipecolic acid-bradykinin [8]. Then the synthesis of 7-L-pipecolic acid-oxytocin [9] followed. All these publications give very little information on the synthetic work, therefore it seemed justified to elaborate a suitable resolution method for preparing optically active pipecolic acids and derivatives suitable for peptide chemical purposes [10]. At the same time with our paper [10a] the first use of pipecolic acid in solid phase peptide synthesis for preparing 7-L-pipecolic acid-angiotensine II was described [11]. In the last years, several papers concerning the use of pipecolic acid for preparing sequence-polypeptides [3] as well as pipecolic acid-bradykinin analogues, both with solid-phase and conventional peptide synthesis [12, 13], are found in literature. In the total synthesis of an analogue of the antibiotic Penicillin-Cephalosporin, too [14], an optically active pipecolic acid derivative was used. Most recently, isolation and structure determination of Actinomycin [15] and Amphomycin [16] also points to the presence of optically active pipecolic acids. The structure supporting syntheses are to be expected in the next future.

During the synthetic work aiming at the preparation of pipecolic acid-bradykinin analogues, numerous di- and tripeptides containing pipecolic acids were prepared in our research group. The present paper wishes to review the latter and to compare them with the results other authors of, published after our work had been finished [17a—c].

The dipeptides containing L- and D-pipecolic acids were prepared (Table I) with the mixed anhydride method [18] to obtain protected dipeptide esters (**1**—**4**), or by acylating the salt of the amino component with the N-hydroxysuccinimid esters of the protected acyl component [19] to form protected dipeptides (**5**—**7**). For comparison, in the case of two protected dipeptide esters (**1** and **2**) the corresponding protected dipeptides were prepared by alkaline hydrolysis (**6** and **7**), too. From the corresponding dipeptide derivatives the C-terminal (**8**—**11**) and N-terminal (**12**—**13**) protected tripeptide esters or protected tripeptides (Table II) used for the synthesis of the pipecolic acid-bradykinin analogues were also prepared with the mixed anhydride method. The preparation of greater fragments obtained from the latter or with other methods will be described in a subsequent paper [20]

Experimental

Melting points were determined with a Kofler block, optical rotations with a Zeiss polarimeter. The values given are uncorrected. TLC on Kiesel G (Merck) was used for purity control with the following systems:

1. *n*-butanol—acetic acid—water 4:1:1
2. ethyl acetate—pyridine—acetic acid—water 60:20:6:11
3. chloroform—methanol 8:2
4. chloroform—methanol—acetic acid 85:10:5.

Methyl benzyloxycarbonyl-L-pipecolyl-L-pipecolate (**1**). 14.48 g (55 mmole) benzyloxycarbonyl-L-pipecolic acid, solved in 75 ml chloroform, was cooled to −15°C. 6.05 ml (55 mmole) N-methylmorpholine and 5.28 ml (55 mmole) ethyl chloroformate was added dropwise to the cooled solution. After three minutes stirring 9.98 g (50 mmole) methyl L-pipecolinate hydrochloride and 5.55 ml (50 mmole)

N-methylmorpholine, both solved in 75 ml chloroform and cooled, were added to the reaction mixture and the stirring continued at −5°C for 3 hrs, then at room temperature for 2 hrs. After standing in a refrigerator overnight, the small amount of precipitated N-methylmorpholine hydrochloride was filtered off, the solution evaporated and the rest solved in ethyl acetate. The solution was washed with diluted sodium hydrocarbonate, diluted hydrochloric acid, then with water. After drying, the ethyl acetate solution was evaporated to obtain an oil, which was crystallized.

Benzyloxycarbonyl-L-pipecolyl-D-pipecolic acid (**7**). 7.2 g (20 mmole) N-hydroxysuccinimide benzyloxycarbonyl-L-pipecolate and 3.25 g (25 mmole) D-pipecolic acid were solved in a mixture of 15 ml water and 15 ml pyridine. The reaction mixture was brought to pH 8.8 by adding 4*N* sodium hydroxide under continuous stirring and held at the same pH for 3 hrs. Then the solution was adjusted to pH 8.0 by adding 4*N* hydrochloric acid, saturated with solid sodium hydrocarbonate and extracted with ethyl acetate. The aqueous solution was acidified to pH 2.0 with 4*N* hydrochloric acid and the precipitate solved in ethyl acetate, washed with water and dried, the ethyl acetate evaporated in vacuum and the oil obtained was crystallized.

p-Nitrobenzyl t-butyloxycarbonyl-D-pipecolyl-L-phenylalanyl-L-nitroargininate (**10**). Trifluoroacetate of *p*-nitrobenzyl-L-phenylalanyl-L-nitroargininate, obtained from the protected compound with trifluoroacetic acid, was solved in 30 ml dimethylformamide and 1.33 ml (12 mmole) N-methylmorpholine was added to the solution. Then, after 1 minute, 3.26 g (10 mmole) N-hydroxysuccinimide *t*-butyloxycarbonyl-D-pipecolinate was added under stirring. After 24 hrs stirring at room temperature the reaction mixture was poured in water and the suspension obtained solved in ethyl acetate, the cooled ethyl acetate solution rapidly washed with diluted hydrochloric acid, diluted sodium hydrocarbonate and water. After drying and evaporating, an oil was obtained, which was crystallized.

Benzyloxycarbonyl-L-nitroarginyl-L-pipecolyl-L-pipecolic acid (**13**). 4.2 g (12 mmole) benzyloxycarbonyl-L-nitroarginine was solved in 15 ml dimethylformamide, the solution cooled under −15°C, then 1.33 ml (12 mmole) N-methylmorpholine and 1.15 ml ethyl chloroformate were added dropwise. After 3 minutes, the cooled solution of dipeptide hydrochloride ($R_f(1)=0.5$, $R_f(3)=0.35$) was added to the reaction mixture. The dipeptide hydrochloride solution was prepared in advance from 3.74 g (10 mmole) benzyloxycarbonyl-L-pipecolyl-L-pipecolic acid (**6**), solved in hydrochloric acid—metanol, by hydrogenation in the presence of Pd-C catalyst, then solving in 15 ml dimethylformamide and adding 1.11 ml (10 mmole) N-methylmorpholine. The reaction mixture was stirred at a temperature lower than −5°C for 3 hrs and held in a refrigerator overnight. The solution was evaporated in vacuum and the remaining oil digerated with diluted sodium hydrocarbonate and 0.1*N* hydrochloric acid, filtered, washed several times with diluted sodium hydrocarbonate solution, diluted hydrochloric acid, water and finally with ether, then crystallized.

* * *

The authors are indebted to thanks to Mrs. G. BARTÓK-BOZÓKI and Mrs. É. GÁCS-GERGELY for elemental analysis and to Miss I. BAGI for technical assistance.

Table I

*Physical properties of dipeptides**

Peptide		Method	Crystallized from	Yield %	M. p. °C	$[\alpha]_D^{25}$ c=1, DMF	Analysis (%) Calculated / Found C	H	N
Z-L-Pip-L-Pip-OMe	(1)	MA	EtOH—petroleum ether	69	67—70	−62	64.9 64.9	7.3 7.3	7.2 7.1
Z-L-Pip-D-Pip-OMe**	(2)	MA	EtOH—petroleum ether	78	56—59	+16	64.9 64.8	7.3 7.3	7.2 7.0
Z-D-Pip-L-Pip-OMe	(3)	MA	EtOH—petroleum ether	75	66—68	+18	64.9 64.8	7.3 7.3	7.2 7.1
Z-D-Pip-D-Pip-OMe***	(4)	MA	EtOH—petroleum ether	81	64—66	+64	64.9 64.8	7.3 7.3	7.2 7.0
Z-L-Pip-L-Pro-OH	(5)	SuOH	MeOH	68	170—173	−72	63.3 63.1	6.7 6.7	7.8 7.6
Z-L-Pip-L-Pip-OH	(6)	SuOH hydrolysis	MeOH MeOH	60 93	172—174 171—174	−58 −57	64.1 64.0 63.8	7.0 6.9 6.9	7.5 7.5 7.4
Z-L-Pip-D-Pip-OH	(7)	SuOH hydrolysis	MeOH MeOH	65 95	170—173 170—173	+16 +16	64.1 64.0 64.1	7.0 6.9 6.9	7.5 7.3 7.4

* EtOH = ethanol; MeOH = methanol; SuOH = N-hydroxysuccinimide activated ester; MA = mixed anhydride; hydrolysis-ester hydrolysis

** [17] DCCl method, oil, $[\alpha]_D^{25} = +22.6°$C (c=0.15, in methanol). Found: C: 64.70 H: 6.82, N: 7.47%

*** [17] DCCl method, m.p. 61—62.5°C, $[\alpha]_D^{25} = +76.6°$ (c=0.4, in methanol). Found: C: 64.8, N: 7.34, N: 7.02%

Table II

*Physical properties of tripeptides**

Peptide		Method	Crystallized from	Yield %	M. p. °C	$[\alpha]_D^{25}$ c=1, DMF	Analysis (%) Calculated / Found C	H	N
Boc-L-Pip-Phe-Arg(NO_2)-OMe	**(8)**	SuOH	EtOAc—petroleum ether	83	77—83	−23	54.9 55.2	6.9 6.9	16.5 16.3
Boc-D-Pip-Phe-Arg(NO_2)-ONb	**(9)**	SuOH	EtOAc—petroleum ether	82	76—84	−5	55.9 55.6	6.2 6.1	15.7 15.5
Z-L-Pip-Phe-Arg(NO_2)-OMe	**(10)**	SuOH	EtOH—petroleum ether	78	130—137	−26	57.6 57.5	6.3 6.2	15.7 15.4
Z-L-Pip-Phe-Arg(NO_2)-ONb	**(11)**	SuOH MA	EtOAc—ether EtOAc—ether	70 72	114—117 113—117	−14 −14	58.0 58.0 57.8	5.7 5.7 5.6	15.1 15.0 15.0
Z-Arg(NO_2)-L-Pip-Pro-OH	**(12)**	MA	MeOH—ether	61	72—77	−20			16.6 16.5
Z-Arg(NO_2)-L-Pip-L-Pip-OH	**(13)**	MA	MeOH—ether	55	74—86	−16			16.2 16.0

*EtOAc=ethyl acetate

References

[1] *Schröder, E., K. Lübke:* The Peptides, Vol. II, Acad. Press, New-York, London, 1966.
[2] *Rudinger, J.:* 6th European Peptide Symposium, Athens, 1963.
[3] *Fairweather, R., J. H. Jones:* J.C.S. Perkin I **1972**, 2475.
[4] *McGee, J., M. H. Jimenez, A. M. Felix, G. J. Cardinale, S. Udenfriend:* Arch. Biochem. Biophys. **154**, 483 (1973).
[5] *Goodman, M., K. C. Su, G. C. C. Niu:* J. Amer. Chem. Soc. **92**, 5220 (1970).
[6] *Balászpiri, L., B. Penke, Gy. Papp, K. Kovács:* in preparation.
[7] *Katchalski, E., A. Berger, J. Kurtz:* Internat. Symposium on Protein Structure and Crystallography, Madras, 1963.
[8] *Nicolaides, E. D., H. A. DeWald, M. K. Craft:* Ann. N. Y. Acad. Sci. **104**, 15 (1963).
[9] *Bespalova, Z. D., O. A. Kairov, U. F. Martinov, V. U. Natosky, M. I. Titov, E. I. Sachmatova:* Vest. Leningrad. Univ. Ser. Fiz. Chim. **21**, 157 (1966).
[10] *Balászpiri, L., B. Penke, J. Petres, K. Kovács:* Monatshefte **101**, 1177 (1970);
Balászpiri, L., Gy. Papp, K. Kovács: Monatshefte **103**, 581 (1972);
Kovács, K., B. Penke, J. Czombos, J. Petres, L. Balászpiri: Acta Phys. et Chem. Szeged **17**, 61 (1971).
[11] *Chaturvedi, N. C., W. K. Park, R. R. Smeby, F. M. Bumpus:* J. Med. Chem. **13**, 177 (1970).
[12] *Neubert, K., L. Balászpiri, G. Losse:* Monatshefte **103**, 1575 (1972).
[13] *Balászpiri L., Gy. Papp, B. Penke, K. Kovács:* Annual Meeting of the Hungarian Chemical Society, Debrecen 1971.
[14] *Brunwin, D. M., G. Lowe, J. Parker:* Chem. Commun. **1971**, 865;
Brunwin, D. M., G. Lowe, J. Parker: J. Chem. Soc. (C) I. **1971**, 3756.
[15] *Formica, J. V., E. Katz:* J. Biol. Chem. **248**, 2066 (1973).
[16] *Bodanszky, M., G. F. Sigler, A. Bodanszky:* J. Amer. Chem. Soc. **95**, 2352 (1973).
[17] *Vičar, J., J. Smolikova, K. Bláha:* Coll. Czechoslov. Chem. Commun. **37**, 4060 (1972);
Vičar, J., J. Smolikova, K. Bláha: ibid. **38**, 1940 (1973);
Vičar, J., J. Smolikova, K. Bláha: ibid. **38**, 1957 (1973).
[18] *Anderson, G. W., J. E. Zimmerman, F. M. Callahan:* J. Amer. Chem. Soc. **89**, 5012 (1967).
[19] *Anderson, G. W., J. E. Zimmerman, F. M. Callahan:* J. Amer. Chem. Soc. **86**, 1839 (1964).
[20] *Balászpiri, L., Gy. Papp, B. Penke, K. Kovács:* Acta Phys. et Chem. Szeged, to be pullished.

СИНТЕЗ ДИ- И ТРИПЕПТИДОВ В СОСТАВЕ НЕСКОЛЬКИХ МОЛЕКУЛ ОПТИЧЕСКИ АКТИВНОЙ ПИПЕКОЛИНОВОЙ КИСЛОТЫ, КОТОРЫЕ СООТВЕТСТВУЮТ ФРАГМЕНТАМ АНАЛОГОВ БРАДИКИНИНА С ПИПЕКОЛИНОВОЙ КИСЛОТОЙ

Л. Балашпири, Дь. Папп, П. Паллаи, К. Ковач

Авторы сообщают синтез и физические константы ди- и трипептидов, в составе нескольких молекул пипеколиновой кислоты „L" и „D", которые соответствуют фрагментам аналогов брадикинина с пипеколиновой кислотой.

KONFORMATIONSANALYSE DES PHENANTHRO-CHINOLIZIDINS

Von

S. FÖLDEÁK und P. HEGYES

(Institut für Organische Chemie der Attila-József-Universität, Szeged)

(Eingegangen am 27. Februar 1974)

Mittels NMR-Daten wurde die Konformation des Phenanthro-chinolizidins und zum Vergleich die des Dehydrophenanthro-chinolizidins untersucht und aus den Ergebnissen Folgerungen auf die Struktur des *trans*-Chinolizidins abgeleitet.

In einer früheren Mitteilung über die Synthese von Kryptopleurin-Analogen [1] stellten wir fest, daß die untersuchten Phenanthro-chinolizidine im Gleichgewicht aufgrund der BOHLMANNschen Banden hauptsächlich in der *trans*-Chinolizidin-Konformation vorkommen. Nach der Ergänzung dieses Befundes mit NMR-Untersuchungen teilen wir unsere Ergebnisse im folgenden mit.

Bei Benzo-chinolizidinen zeigte sich, daß in $CHCl_3$ im Gleichgewicht 75% *trans*- und 25% *cis*-Chinolizidin vorkommen [2]. Andere Autoren [3] berichten über stabile *cis*- und *trans*-Dibenzochinolizidine, was sie wegen der geringen Energieunterschiede der beiden Konformationen in Frage stellen [4]. Die Phenanthro-chinolizidine können prinzipiell drei Konformationen, nämlich eine *trans* ($\mathbf{I}_A$) und zwei *cis*-Koformationenn ($\mathbf{I}_B$, $\mathbf{I}_C$) annehmen.

Von diesen ist die Konformation $\mathbf{I}_C$ weniger wahrscheinlich. Die Protonen 9, 12 und 14, und in flexibler Form die Protonen 9 und 13, treten innerhalb des van der Waalsschen Radius miteinander in Wechselwirkung.

Zur Ergänzung der Konformationsanalyse haben wir die chemische Verschiebung der Methylen-Protonen in Ar-CH_2-N-Bindung untersucht. Die chemische Verschiebung solcher Protonen wird nämlich von ihrer Stellung im Verhältnis zu dem Elektronenpaar des Stickstoffs bestimmt [5, 6]. Aus dem äquivalenten oder

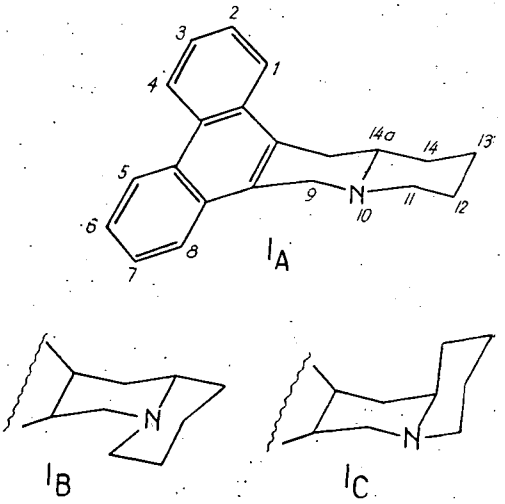

Abb. 1

nicht-äquivalenten Charakter der Methylengruppe läßt sich auf die Konformation schließen. Die für die Protonen in 9-Stellung erhaltenen chemischen Verschiebungen und die Kupplungs-Konstante $J_{9\,\ddot{a}qu-9\,ax}=16$ Hz (Tab. I) zeigen, daß die beiden Protonen nicht äquivalent und nicht symmetrisch zum Orbital des freien Elektronenpaares des Stickstoffs lokalisiert sind. Ähnliche Werte wurden auch bei Kryptopleurin gemessen [7]. Nach Untersuchung der Konformationsmöglichkeiten am Dreiding-Modell kann sich diese Situation nur ergeben, wenn das Chinolizidin in *trans*-

Tabelle I

Chemische Verschiebung und Kupplungskonstante von Ar-CH_2-N *Protonen in δ-Werten* ($CDCl_3$, TMS, 60 MHz)

Verbindung	$\delta_{9\,\ddot{a}qu}$	$\delta_{9\,ax}$	$J_{\ddot{a}qu\text{-}ax}$
Phenanthro-chinolizidin (I)	4,45	3,56	16
Dehydro-phenanthro--chinolizidin	4,63	4,63	–

Konformation ($\mathbf{I}_A$) vorkommt. Im Falle der *cis*-Konformation ($\mathbf{I}_B$) ist nämlich die Lage der beiden Protonen symmetrisch zur Orientation des freien Elektronenpaares des Stickstoffs und dann wäre ihre chemische Verschiebung äquivalent. Das Gesagte wird durch die Newmansche Projektion in Abb. 2 verdeutlicht, in der die Lage der Substituenten der C_9-N-Paare in beiden Konformationen dargestellt ist.

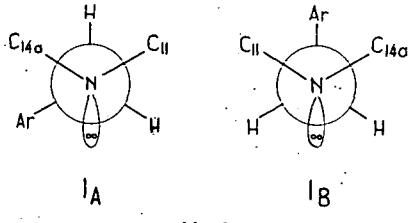

$\mathbf{I}_A$ $\mathbf{I}_B$

Abb. 2

Unsere Hypothese wird praktisch dadurch unterstützt, daß die $\mathbf{I}_B$-Konformation sich durch Einführung von Doppelbindungen beim Phenanthro-chinolizidin in $\Delta^{14a(15)}$ Stellung (**II**) erzwingen läßt, wobei das Signal der Ar-CH_2-N-Protonen bei $\delta=4{,}63$ (Tab. I) als Singlett erscheint.

Die Äquivalenz der Protonen in Stellung 9 ist aber nur dann möglich, wenn sie sich in einer zum den freien Elektronenpaaren des Stickstoffs symmetrischen Lage befinden. Es ist zu bemerken, daß in dieser Konformation die beiden Protonen auch quasi-symmetrisch zur Phenanthren-Ebene liegen.

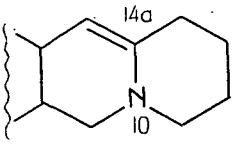

II

Experimenteller Teil

Die Schmelzpunkte sind nicht korrigiert. Die IR-Spektren wurden mit einem Spektrophotometer Unicam-SP 200 in KBr gemessen. Die NMR-Spektren wurden mit einem Kernresonanzspektrometer JEOL-60 aufgenommen mit TMS als innerem Standard.

$\Delta^{10(14)a}$-Dehydro-phenanthro(9,10b)*-chinolizidinum-perchlorat* [1]

1,0 g Phenanthro-chinolizidin-15-ol werden in 200 ml Eisessig in Gegenwart von 1,5 ml 70%iger Perchlorsäure $1^1/_2$ Stunden lang am Rückfluß erwärmt, nach dem Erkalten das kristalline Produkt filtriert und in Äthanol gewaschen. Die gewonnenen 1,1 g gräulichen Kristalle nehmen von 280°C an unter Zersetsung eine braune Farbe an. ν^*_{max}=1702 (C=N$^+$). Ber.: C 65,36; H 5,22; N 3,63. Gef.: C 65,20; H 5,31; N 3,70%.

$\Delta^{14}a^{(15)}$-Phenanthro(9,10b)*-chinolizidin*

Von dem vorerwähnten Immonium-perchlorat werden 0,5 g in 10 ml Aceton suspendiert und 1—2 Minuten mit 1 ml 50%igem KOH gründlich gerührt, dann 5 ml Wasser zugesetzt, der Niederschlag rasch filtriert und mit Wasser neutral gewaschen, in 10 ml Aceton gelöst und durch Zugabe von Wasser auskristallisiert. Nach Trocknen im Vakuum in Stickstoffatmosphäre über P_2O_5: gelbe Nadeln, Schmp. 139—142°C. Ber.: C 88,38; H 6,71; N 4,90. Gef.: C 88,07; H 6,91; N 4,78%. ν^*_{max}=1575 (C=C).

Phenanthro(9,10b)*-chinolizidin*

0,5 g Immonium-perchlorat werden in 15 ml Äthanol mit 0,2 g $NaBH_4$ 20 Min. reduziert, mit Wasser verdünnt, mit Chloroform extrahiert, das Chloroform im Vakuum bei 40°C abdestilliert und die kristalline Masse aus Benzol umkristalliziert. Farblose Kristalle, Schmp. 174—175°C. Identisch mit den Literaturangaben [1].

Literatur

[1] *Földeák, S.:* Tetrahedron **27**, 3465 (1971).
[2] *Van Binst, G., J. C. Ails:* J. Chem. Soc. (C) **1970**, 150.
[3] *Takemoto, T., J. Kondo, K. Kondo:* J. Pharm. Soc. Japan **83**, 162 (1963).
[4] *Aaron, H. S.:* Chem. and Ind. (London) **1965**, 1338.
[5] *Fitzgerald, J. S., S. R. Johns, J. A. Lamberton, A. H. Redcliffe:* Aust. J. Chem. **19**, 151 (1966).
[6] *Hamlow, H. P., S. Okuda, N. Nakagawa:* Tetrahedron Letters **1964**, 2553.
[7] *Johns, S. R., J. A. Lamberton, A. A. Sioumis, R. I. Willing:* Aust. J. Chem. **23**, 353 (1970).

КОНФОРМАЦИОННЫЙ АНАЛИЗ ФЕНАНТРОКИНОЛИЗИДИНА

Ш. Фелдеак, Р. Хедьеш

Изучена конформация фенантро-кинолизидина, и дегидро-фенантро-кинолизидина. На основании наших ранних ИК-спектроскопических и полученных ПМР данных, сделаны выводы о структуре анелляции кольца кинолизидина.

SYNTHESIS OF HOMOVANILLIC ACID DERIVATIVES OF CAPSAICIN-LIKE EFFECT

By

P. HEGYES and S. FÖLDEÁK

Institute of Organic Chemistry, Attila József University, Szeged

(Received December 28, 1973)

Capsaicin analogues containing inverse acid-amide bonds, alkyl-amides of homovanillic acid, were prepared and their pungent and desenzitizing effect, as well as the relation of the latter to the structure of the compounds were investigated.

New homovanillic acid derivatives of capsaicin-like effect (esters and carboxamides) were prepared, in order to study the connections beetween pungent effect and chemical structure. The present paper deals with preparation and effects of the amides of homovanillic acid.

Pungency of natural and synthetic products, and chiefly investigation of their structural elements responsible for this effect, attracted the interest of a number of investigators. Among them, NELSON [1], NEWMANN [2], OFF and ZIMMERMAN [3], SZÉKI [4], and JANCSÓ [5] are to be mentioned, who performed pioneer work in this field. On the basis of their work, the above connections can be summarized as follows.

For producing pungency, the fellowing structural elements are necessary:

(*a*) *p*- or *o*-hydroxybenzylamine or their ring-substituted derivatives, in alkyl--acid amide bonding

(*b*) *p*-hydroxy group is more effective than *o*-hydroxy group

(*c*) substitution of the hydroxy group results in ceasing of the pungent effect

(*d*) vanillin-amide derivatives are the most pungent, but guaiacol and ethanolamine derivatives are also effective

(*e*) only aliphatic carboxamide analogues have a pungent effect

(*f*) C_9—C_{11} straight-chain carboxamides are the most pungent.

On the basis of these connections, it is chiefly vanillyl alkyl amides which (**I**) produce the pungent effect.

Continuing the research of these connections, we made use of the principle of interchangeability of the prosthetic groups (HN—CO—), and synthesized alkyl--amides of homovanillic acid (**II**) in order to study their pungency. Suprisingly, we found not only pungent species among these compounds, but also some of stronger desenzitizing effect than capsaicin.

An obvious explanation of this circumstance is the structural similarity of **I** and **II**. The change in the bonding of the acid amide in inverse position, as one of the prosthetic groups responsible for the effect, did not diminish, but rather

increased the effect. Concerning other effects, we had found earlier that inversion in the acid amide function did not cause loss of the effect [8].

The changes in pungency of the compounds of type **II** on changing the alkyl chain R, compared also with the capsaicin homologues, are shown by the hatched

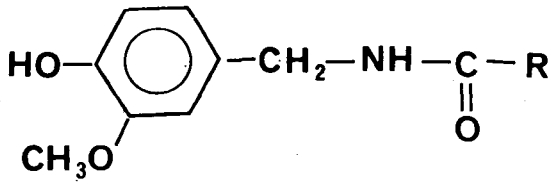

I a-c

Fig. 1

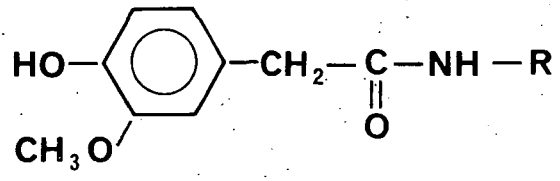

II a-g

Fig. 2

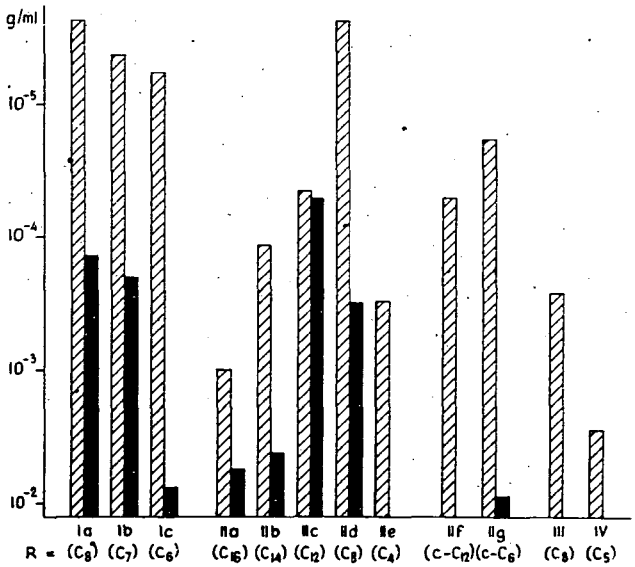

Fig. 3

columns of Fig. 3. It can be seen that the pungency first increases, then decreases with the number of C-atoms, with a maximum in the case of the C_8 amide. The connection with the desenzitizing effect (black columns) is interesting, as it does not go parallel to the pungency but reaches its maximum at C_{12}. Among the compounds of type **II** investigated, we did not find any having only desensizitizing effect (without pungency), so it is to be inferred that the structure is responsible for both effects. From the fact that cycloalkyl derivatives are only pungent and have no desensizitizing effect, it seems probable that the latter is to be attributed to the NH-groups.

Experimental

The course of the reactions was followed by thin layer chromatography; the purity of the products was controlled by m.p. measurement, elementar analysis and IR spectroscopy.

All melting points were measured on a Kofler-block; the m.p. values given are uncorrected. IR measurements were made generally in KBr pellets (in some cases in nujol) with a Unicam SP 200 IR spectrophotometer.

Homovanillic acid [6]

To 150 ml 21% sodium bisulfite solution (technical grade) 30.4 g vanillin was added (three-necked flask, mixer, reflux cooler, dropping funnel) and mixed at room temperature until the vanillin totally dissolved; then the solution was cooled to −5—10°C, and 26 g (0.4 mole) sodium cyanide dissolved in 40 ml water was slowly dropped to the cooled solution. The reaction mixture was stirred for 30 minutes after the KCN addition; during this time it transformed to a crystalline masse, which, after adding 60 ml 5*N* H_2SO_4 dropwise in an hour and continuing the stirring for another hour, was filtered.

The substance remaining on the filter was washed with ether three times. The ethereal phase was acidified with 1—2 ml glacial acetic acid and the ether destilled off. The residue is a yellowish oil, 4-hydroxy-3-methoxyamigdalic acid nitrile, wich can be used without further purification.

35 g (0.195 mole) of the acid nitrile obtained was measured into a round bottomed flask and 66 g (0.29 mole) $SnCl_2.2H_2O$ dissolved in 58.5 ml 37% HCl was added, shaken throroughly and heated on 110°C oil-bath for 3.5 hours. After the reaction had come to an end, the mixture was diluted with 25 ml water, left standing for 12 hours and filtered. The air-dried substance was recrystallized from 50 ml boiling water. M.p. 142°C, yield: 14.0 g (38.4%).

Acetylhomovanillic acid [7]

25 g homovanillic acid dissolved in 150 ml acetic anhydride was refluxed for 6 hours, then diluted with 1600 ml water. The diluted solution was stirred at room temperature for two hours, possible solid substances filtered off, and the filtrate evaporated to dryness. The midly yellowish, crystalline residue was recrystallized from boiling water (white plates). M.p. 115—137°C. Analysis: Calc.: C 58,64; H 5.30. Found: C 59.19; H 5,40%.

Acetylhomovanillic acid chloride [7]

20 g acetylhomovanillic acid was suspended in 25 ml thionyl chloride and heated on water bath for an hour. The greenish-yellow solution was evaporated to dryness, taken up in 25 ml abs. benzene and evaporated to dryness again. The latter process was repeated three times. The remaining light-yellow oil crystallizes after standing overnight and can be used with further purification.

Preparation of acetylhomovanillincarboxamides

0.01 mole acetylhomovanillic acid chloride was dissolved in 15 ml abs. benzene with ice-cooling and stirring. To the solution cooled to about 8—10°C, 0.02 mole amine dissolved in 15 ml abs. ether was added dropwise. The reaction mixture was stirred with ice-cooling for 3 hrs., then at room temperature for 1 hr. The hydrochloride precipitated was filtered, washed with 2×10 ml ether. The filtrate was extracted with water (until the water became neutral) and dried over Na_2SO_4. After removing the solvent, the remaining carboxamide was recrystallized from ethanol.

Table I

Acetylhomovanillincarboxamides

Formula	Amines used	M.w.	Calculated / Found % C	H	N	M.p. °C	Yield %	νC=O Carboxamide	νC=O Acetyl
$C_{19}H_{25}O_4N$	3-azabicyclo-(3.2.2)nonane	331.41	68.85 68.33	7.60 7.20	4.25 4.51	97—101	78	1642	1758
$C_{23}H_{37}O_4N$	dodecylamine	391.54	70.55 69.78	9.52 9.74	3.57 3.33	81—82	85	1650	1755
$C_{17}H_{23}O_4N$	homo-piperidine	305.38	66.86 66.53	7.59 8.02	4.58 4.43	oil	83	1648	1750
$C_{19}H_{29}O_4N$	dibutylamine	335.45	68.03 68.78	8.71 8.96	4.17 4.00	oil	85	1640	1755
$C_{19}H_{27}O_4N$	cyclooctyl-amine	333.43	68.44 69.11	8.76 9.02	4.20 3.96	oil	85	1652	1756
$C_{18}H_{27}NO_4$	heptylamine	321.42	67.26 66.73	8.15 8.28	4.35 4.04	oil	75	1645	1752
$C_{19}H_{19}O_6N$	piperonylamine	357.36	63.58 64.02	5.36 5.50	3.91 3.60	oil	70	1644	1755
$C_{25}H_{41}O_4N$	tetradecyl-amine	419.61	71.56 70.80	9.84 9.78	3.33 3.40	86—89	95	1650	1758
$C_{16}H_{21}O_4N$	piperidine	291.35	66.00 65.78	7.27 7.53	4.81 4.60	55—57	76	1645	1755

Preparation of homovanillincarboxamides

(*a*) 0.01 mole $KHCO_3$ was suspended in 30 ml abs. ethanol and the solution of 0.01 mole acetylhomovanillincarboxamide in 10 ml ethanol was added. The reaction mixture was stirred at room temperature for 4—10 hours, then mildly acidified with HCl. 50 ml water was added to the mixture and the precipitate extracted with 3×30 ml benzene, the benzene phase washed with water to neutrality and dried over Na_2SO_4, the benzene evaporated in vacuum and the oily residue crystallized from ethanol.

(*b*) If the amine component is used in at least threefold excess in the preparation of the acetylhomovanillincarboxamide and the acetylcarboxamide is not isolated but stirred at room temperature for 10—12 hours, quantitative hydrolysis of the acetyl groups occurs. After the stirring, isolation is performed as described under (*a*).

The physical constants of the acetylhomovanillincarboxamides and homovanillincarboxamides prepared are presented in Tables I and II.

* * *

We wish to exspress our thanks to Dr. A. GÁBOR-JANCSÓ and Dr, J. SZOLCSÁNYI for kindly performing the pharmacological investigations and to L. FÖLDHÁZI for preparing the starting materials.

Table II

Homovanillic carboxamides

Formula	Amines used	M.w.	Calculated / Found % C	H	N	M.p. °C	Yield %	ν C=O Carboxamide	ν OH Hydroxy
$C_{17}H_{23}O_3N$	3-azabicyclo-(3.2.2)	289.38	70.56 70.51	8.01 8.31	4.84 4.91	153—154	95	1600	3200
$C_{21}H_{35}O_3N$	dodecylamine	349.52	72.27 71.81	10.10 10.10	4.00 4.04	70.5—71	98	1650	3600
$C_{15}H_{21}O_3N$	homopiperidine	263.34	68.41 68.62	8.03 8.21	5.31 5.16	110—111.5	90	1610	3200
$C_{17}H_{27}O_3N$	dibutylamine	293.41	69.59 68.62	9.27 9.38	4.77 4.78	56.5—57.5	90	1630	3350
$C_{16}H_{25}O_3N$	cyclooctylamine	291.40	70.07 69.94	8.64 8.73	4.80 5.05	48—50	96	1642	3400
$C_{17}H_{25}O_3N$	heptylamine	279.38	68.78 67.78	9.01 9.58	5.01 5.70	oil	91	1650	3400
$C_{17}H_{17}O_5N$	piperonylamine	315.33	64.75 64.15	5.43 5.17	4.44 4.37	119—120.5	90	1628	3440
$C_{23}H_{38}O_3N$	tetradecylamine	378.56	72.97 73.36	10.11 10.48	3.70 3.95	75.5—76	96	1650	3600
$C_{14}H_{19}O_3N$	piperidine	249.31	67.44 67.45	7.68 7.39	5.61 5.02	oil	93	1630	3800

References

[1] *Nelson, E. K.:* J. Am. Chem. Soc. **41**, 1115 (1919); **42**, 597 (1920); **45**, 2179 (1923).
[2] *Newmann, A. A.:* Chem. Prod. London **27**, 343, 379, 413, 467 (1953); **28**, 14, 102 (1954).
[3] *Ott, E., K. Zimmermann:* Ann. **425**, 314 (1921).
[4] *Széki, T.:* Archiv der Pharm. und Ber. Dtsch. Pharmazeutische Ges. **268**, 1 (1930).
[5] *Jancsó, N.:* Pharmacology of Pain, Vol. 9, Pergamon Press, Oxford (1968).
[6] *Grewe, R., H. Fischer:* Chem. Ber. **96**, 1520 (1963).
[7] *Fischer, A. E., H. Hibbert:* J. Am. Chem. Soc. **69**, 1210 (1947).
[8] *Porszász, J., P. K. Gibiszer, T. Barankai, S. Földeák, B. Matkovics:* Separatum of II. Conferentia Hungarica pro Therapia et Investigatione in Pharmacologia (1964).

СИНТЕЗ ПРОИЗВОДНЫХ ГОМОВАНИЛИНОВОЙ КИСЛОТЫ С АНАЛОГИЧНЫМИ ПО ВЛИЯНИЮ СВОЙСТВАМИ КАПСАИЦИНА

П. Хедьеш, Ш. Фелдеак

Были синтетизированы алкиламиды гомованилиновой кислоты — аналоги капсаицина, со структурными элементами обратной связи амида карбоновой кислоты, изучены их горькие свойства и эффект десенсибилизации. Коротко излагаются выводы относительно данной химической структуры и ее влияния.

SYNTHESIS OF CARBOXYL-^{14}C-LABELLED 1-O-(3'-INDOLYLACETYL)-β-D-GLUCOPYRANOSE

By

F. SIROKMÁN

Biological Research Center of the Hungarian Academy of Sciences

and

E. KÖVES

Department of Plant Physiology, Attila József University, Szeged

(Received February 11, 1974)

For studying indole derivatives with hormonal activity occurring in plants, it is necessary to synthesize ^{14}C-labelled compounds. The paper describes the syntheses of carboxy-^{14}C-labelled 2,3,4,6-tetra-O-benzyl-1-O-(3'-indolylacetyl)-β-D-glucopyranose, 2,3,4,6-tetra-O-benzyl-1-O-(3'-indolylacetyl)-β-D-glucopyranose and 1-O-(3'-indolylacetyl)-β-D-glucopyranose.

In recent years a great number of papers dealing with the metabolism of 3-indolylacetic acid in plants were published. At the same time various 3-indolylacetic acid conjugates, drawing attention to the different sugar conjugates of 3-indolylacetic acid [7, 11, 12] and its amino acid conjugates [1, 6] were also detected. Studies on 3-indolylacetic acid conjugates have also demonstrated that, besides the amino acid or sugar components, phosphoric acid, too, may be linked to 3-indolylacetic acid [8], while the existence of complexes in which 3-indolylacetic acid is bound to nucleic acids [3] permits the conclusion that the 3-indolylacetic acid—nucleotide conjugates are also of importance in the metabolism of 3-indolylacetic acid.

The β-D-glucopyranoside of 3-indolylacetic acid was detected in 1961, on the basis of its qualitative reactions [7, 12]. Similar types of conjugates are formed by various groups of plant materials possessing hormonal activity, *e.g.* gibberellins, cytokinines and abscisic acid. Investigation of the physiological importance of the individual conjugates demands the preparation of the chemically pure compounds both in inactive and radioactive forms. In a great number of cases research workers failed to prepare the authentic conjugate desired and, therefore, experiments concerning their effects and mechanisms of action are virtually still lacking. In the absence of such experiments, numerous authors assume that the various conjugates have no physiological importance [7, 12], and are formed only as detoxification products. The simplest means of deciding wether the 3-indolylacetic acid in the conjugates appears under *in vivo* conditions in the free 3-indolylacetic acid, in a metabolite, or in the other conjugates, is investigation with isotope technique. For this purpose the synthesis of conjugates labelled in the 3-indolylacetic acid seems justified. The *in vivo* formation of 3-indolylacetic acid-β-D-glucopyranose cannot be utilized for the isolation of greater amounts of the compound, nor is it possible to ensure

the specific activity necessary for the biological experiments. On the basis of analogous reactions, carboxy-^{14}C-1-O-(3-indolylacetyl)-β-D-glucopyranose was prepared by synthesis of 2,3,4,6-tetra-O-acetyl-β-D-glucopyranosyl chloride, followed by its coupling with the silver salt of carboxy-^{14}C-3-indolylacetic acid.

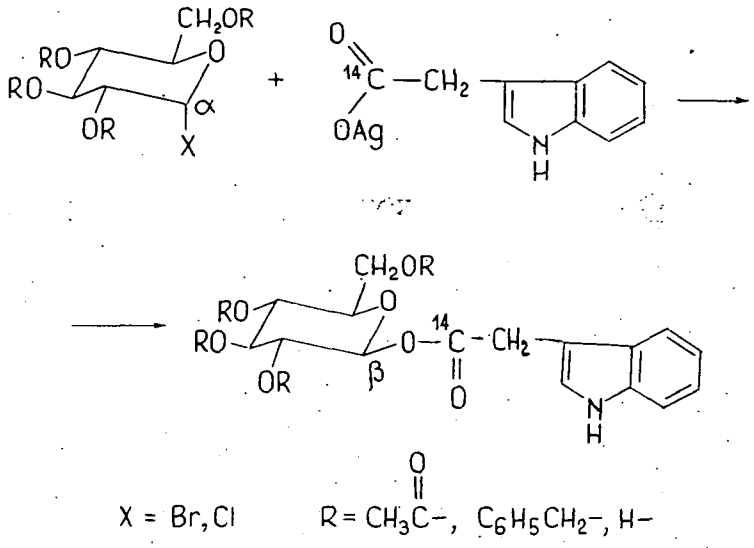

Because of the sensitivity of the molecule, the deacetylation may be questionable, therefore, 2,3,4,6-tetra-O-benzyl-β-D-glucopyranosyl chloride was used for the preparation of the free glycoside, and, after the separation of the anomers, the benzyl groups could be succesfully removed by reduction on 10% palladium on charcoal, on the analogy of the methods applied in the chemical synthesis of 1-O-(3-indolylacetyl)-β-D-glucopyranose [5].

Chromatographic comparison of the synthetized product indicated that it is not identical with the compound isolated from pea roots, the properties of which have been described [9].

Experimental

Carboxy-^{14}C-3-indolylacetic acid

was prepared from 10.5 mmole gramine and 40 mmole 20 mCi K^{14}CN by the method of GORDON *et al.* [4], by the reaction path indole, gramine, 3-indolylacetonitrile-^{14}C, 3-indolylacetic acid-^{14}C. Yield: 70%, 1225 mg, molar activity: 500 μCi/mmole. The radioactive purity was checked chromatographically and autoradiographically.

2,3,4,6-*Tetra*-O-*acetyl*-α-D-*glucopyranosyl chloride*

was synthetized by the method of REDMANN and NIEMANN [10]. Yield: 5%; m.p.: 70—71°C (decomp).

2,3,4,6-*Tetra*-O-*acetyl*-1-O-*indolylacetyl-carboxy*-^{14}C-β-D-*glucopyranose*

2,3,4,6-tetra-O-acetyl-β-D-glucopyranosyl chloride (1.12 g, 3.0 mmole) was dissolved in 25 ml abs. benzene and the freshly prepared silver salt of 3-indolylacetyl-carboxy-^{14}C (843 mg, 3 mmole, 750 μCi) was added. The reaction mixture was shaken in the dark at room temperature for 36 hours. The precipitate was separated by centrifugation, and washed once with 5 ml benzene. The combined supernatants were evaporated to dryness. The residue was fractionated on a silica gel column (1 cm in diameter, 40 cm high, containing 8 g silica gel), the solvent being a 1:1 mixture of benzene:ethyl acetate. Dried above concentrated sulfuric acid in vacuum, the chromatographically homogeneous syrup solidified within 24 hours. The 2,3,4,6-tetra-O-acetyl-1-O--(3-indolylacetyl)-carboxy-^{14}C-β-D-glucopyranose was recrystallized from abs. ether—pentane. Yield: 0.64 g, 42%. M.p.: 119—121°C (uncorrected) (lit.: 121—122°C [5]), $[\alpha]_D = -27°$C, c=1, in chloroform (lit. $[\alpha]_D = -26° \pm 0.2°$). Activity: 250 μCi/mmole.

2,3,4,6-*Tetra*-O-*benzyl*-α-D-*glucopyranosyl chloride*

was synthesized from 2,3,4,6--tetra-O-benzyl-α-D-glucopyranose with thionyl chloride by the method of AUSTIN, HARDY *et al.* [2]. The product was purified by chromatography on a silica gel column, 2:1 petroleum ether—ether mixture being used for elution. The product was a pale-yellow oil. Yield: 55%. The purity was checked by thin-layer chromatography.

2,3,4,6-*Tetra*-O-*benzyl*-1-O-*(3-indolylacetyl)-carboxy*-^{14}C-β-D-*glucopyranose*

A mixture of the halogen sugar (2.57 g, 4.61 mmole), Ag salt of 3-indolylacetic acid-carboxy-^{14}C (1.3 g, 4.6 mmole) and 1 g anhydrous $CaSO_4$ protected by aluminium foil was refluxed in 100 ml absolute benzene for 8 hours, with magnetic stirring, under exclusion of moisture. The reaction was checked by thin-layer chromatography in a 3:2 mixture of ether—petroleum ether. The precipitate was separated by centrifugation and washed with 2×5 ml benzene. The combined supernatant was evaporated in vacuum, and the residue chromatographed on a silica gel column, with 3:2 ether—petroleum ether as eluent; 4 ml fractions were collected. The unchanged chloride was eluted first, then the desired ester product (2.26 g) with a little colouring matter, and finally, by chloroform elution, the substituted tetrabenzyl-glucose. The anomer composition can be checked by thin-layer chromatography in a 3:2 ether—petroleum ether mixture. A violet double spot was obtained with 10% sulfuric acid. The reaction mixture was separated in layers, and the more slowly moving β-anomer fractions were collected, dissolved in abs. benzene, and evaporated to dryness. The residual oil was dissolved in abs. benzene, petroleum ether was added, and after 8 hours at 0°C the β-anomer had crystallized (0.8 g); m.p.: 98—100°C; $[\alpha]_D = -1.7°$, c=1.0, in chloroform. The physical constants agree with those found in literature [5]. The α-isomer could not be isolated as crystals. Activity: 0.25 mCi/mmole. Chromatographically homogeneous.

1-O-*(3-indolylacetyl)-carboxy*-^{14}C-β-D-*glucopyranose*

400 mg 2,3,4,6-tetra-O-benzyl-1-O-3-indolylacetyl-carboxy-^{14}C-glucopyranose was dissolved in 15 ml 2-methoxyethanol, and reduced for 30 hours at room temper-

ature with 500 mg 10% palladium on charcoal in the presence of 0.4 ml acetic acid. The reaction mixture was checked chromatographycally in a 6:2:1 mixture of ether—petroleum ether—methanol, with 10% sulfuric acid as developer. The debenzylated glycoside had an R_f-value of ca. 0.1 and was reddish-violet. The catalyst was removed by centrifugation and washed with 2-methoxyethanol, and the solution was evaporated in vacuum at 35°C. The remaining 200 mg light-violet oil was dissolved in a 55:30:11 mixture of isopropanol—petroleum ether—water, and chromatographed with this solvent on a column containing 25 g cellulose. The individual fractions were checked by layer chromatography, and the eluates containing the glycoside were collected and evaporated in vacuum. The oily residue was extracted with 3×10 ml ethyl acetate. The extract was evaporated to 1/3 volume and petroleum ether was added until the first signs of turbidity. The glass-like material at 0°C, after 24 hours, solidified over concentrated sulfuric acid, and was pulverized to a pink powder (80 mg). This was extracted with a 20:1 mixture of ethyl acetate—isopropanol, a few drops of petroleum ether were added, and the filtered solution was left to stand at 0°C to separate the remaining coloured material. The practically colourless supernatant was put in a centrifuge tube and precipitation was promoted with petroleum ether. The 1-O-(3-indolylacetyl)-carboxy-^{14}C-β-D-glucopyranose crystallized in the form of very pale pinkish-white needles. Yield: 40 mg. M.p.: 168—172°C (lit. m.p.: 172—173°C [5]). Paper-chromatographic R_f-value in 12:3:5 butanol—acetic acid—water: 0.7. Chromatographycally homogeneous. Activity: 0.25 mCi/mmole.

References

[1] *Andreae, W. A., N. E. Good:* Plant Physiol. **30**, 380 (1955).
[2] *Austin, P. W., F. E. Hardy, J. G. Buchanan, J. Baddiley:* J. Am. Chem. Soc. **86**, 2128 (1964).
[3] *Galston, A. W., P. Jackson, R. Kaur-Sawhney, N. P. Kefford, W. J. Meudt:* Colloq. int. Cent. nat. Rech. sci., p. 251, Paris, (1963).
[4] *Gordon, S. A., R. P. Weber:* Plant Physiol. **26**, 192 (1951).
[5] *Keglević, D., M. Pokorny:* Biochem. J. **114**, 827 (1969).
[6] *Klämbt, H. D.:* Naturwiss. **17**, 398 (1960).
[7] *Klämbt, H. D.:* Planta **56**, 618 (1961).
[8] *Köves, E., F. Sirokmán:* Nature **200**, 910 (1963).
[9] *Köves, E., F. Sirokmán:* Biochem. Physiol. Pflanzen **164**, 276 (1973).
[10] *Redemann, C. E., C. Niemann:* Org. Synth. Coll. Vol. **3**, p. 11. Ed.: E. C. Horning, John Wiley and Sons. Inc., New York, (1955).
[11] *Schantz, E. M., F. C. Steward:* Plant Physiol. **32**, suppl. VIII, (1957).
[12] *Zenk, M. H.:* Nature **191**, 493 (1961).

СИНТЕЗ 1-О-(ИНДОЛ-3'-ИЛАЦЕТИЛ)-β-D-ГЛЮКОПИРАНОЗЫ МЕЧЕНОЙ ПО КАРБОКСИ-^{14}С

Ф. Широкман, Е. Кёвеш

Синтез ^{14}С меченных соединений, необходим к изучению индолных веществ растений, имеющих гормональное действие. В работе описан синтез 2,3,4,6-тетра-О-ацетил-1-О-(индол-3'-илацетил)-β-D-глюкопиранозы, 2,3,4,6-тетра-О-бензил-10-(индол-3'-илацетил)-β-D-глюкопиранозы и 1-О-(индол-3'-илацетил)-β-D-глюкопиранозы, меченых по карбоксил-^{14}С.

SYNTHESIS OF ^{14}C- AND ^{3}H-LABELLED 3-INDOLYLACETYL-ASPARTIC ACID

By

F. SIROKMÁN

Biological Research Center of the Hungarian Academy of Sciences, Szeged

E. KÖVES

Department of Plant Physiology, Attila József University, Szeged

and

L. BALÁSPIRI

Institute of Organic Chemistry, Attila József University, Szeged

(Received February 12, 1974)

The paper describes the syntheses of 3-indolylacetyl-carboxy-^{14}C-aspartic acid, 3-indolylacetyl-aspartic acid-^{3}H and the doubly labelled 3-indolylacetyl-carboxy-^{14}C-aspartic acid-^{3}H.

The literature dealing with the physiological effects and metabolism of 3-indolylacetic acid describes the occurrence of 3-indolylacetyl amino acid conjugates in plants [1, 3]. The details of the physiological roles of the individual conjugates have not been clarified. The problem of whether the bound 3-indolylacetic acid becomes free again can be investigated by means of an isotope technique. Labelling of the 3-indolylacetil amino acid conjugates on the amino acid permits study of the connection of the amino acid and protein metabolisms, while labelling on the 3-indolylacetic acid permits study of the turnover of 3-indolylacetic acid. Some labelled combinations of 3-indolylacetylaspartic acid were prepared, utilizing carboxy-^{14}C--3-indolylacetic acid and ^{3}H- and inactive aspartic acid.

Syntheses of a number of inactive 3-indolylacetyl amino acids have been dealt with by HUTZINGER *et al.* [2], who applied the methods for carboxyl activation of the amino acids, and made use of 3-indolylacetic acid active esters with N-hydroxysuccinimide.

MOLLAN *et al.* [4] describe the preparation of the compound in accordance with the known synthesis steps, by using 3-indolylacetic acid *p*-nitrophenyl ester. On the basis of inactive experiments we found that the latter method gives a substantially better yield in the active syntheses, and achieved the synthesis of 3-indolylacetyl-aspartic acid by coupling the *p*-nitrophenyl ester of 3-indolylacetic acid with L-aspartic acid.

The purity of the compounds formed were checked, among others, by radiochromatography; these compounds could be used to identify radiochromatographycally natural 3-indolylacetylaspartic acid.

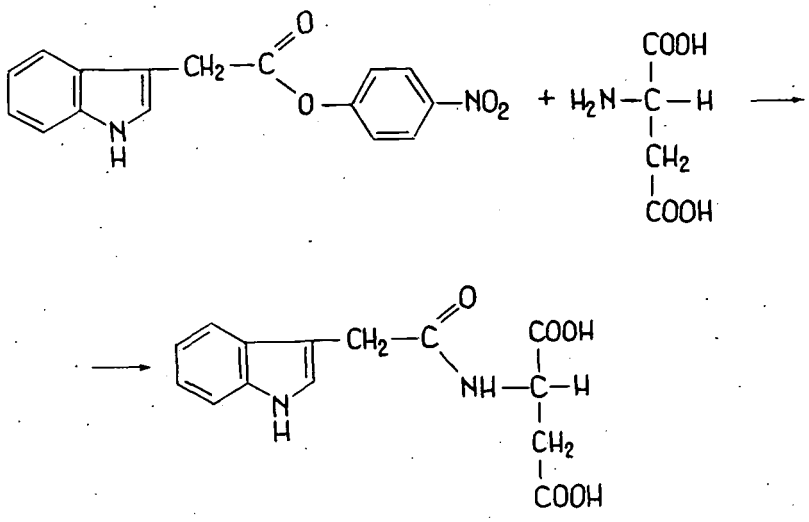

Experimental

Carboxy-^{14}C-3-*indolylacetic acid* was synthesized by the method of STUTZ *et al.* [5] from 10.5 mmole gramine and 40 mmole 20 mCi K^{14}CN, *via* the reaction path indole, gramine, 3-indolylacetonitrile-^{14}C, 3-indolylacetic acid-1-^{14}C. Yield: 1225 mg, 70%. Molar activity: 0.5 mCi/mmole. Radioactive purity checked by chromatography and autoradiography. M.p.: 164—166°C.

Carboxy-^{14}C-L-*aspartic acid* was a New-England Nuclear preparation. Specific activity: 250 μCi/mmole.

^{3}H-L-*aspartic acid* was also a New-England Nuclear preparation. Specific activity: 1 mCi/mmole.

Inactive 3-*indolylacetic acid p-nitrophenyl ester.* 0.40 g (2.2 mmole) 3-indolylacetic acid and 0.32 g (2.2 mmole) *p*-nitrophenol were dissolved in 8.5 ml ethyl acetate and the mixture was cooled to 0—5°C. A solution of 0.46 g (2.2 mmole) N,N′-dicyclohexylcarbodiimide in 1.6 ml ethyl acetate was added at 0°C, and the mixture stirred for one hour at room temperature. The N,N′-dicyclohexylcarbamide was filtered off, and the solution concentrated to 1.6 ml, cooled and filtered again. Crystalline *p*-nitrophenyl ester was obtained by removing the residual solution. M.p.: 100—103°C. Recrystallization from an ethyl acetate—petroleum ether mixture gave pale-yellow needles. Yield: 0.85 g, 72%. M.p. 106—107°C.

3-*Indolylacetyl-carboxy-*^{14}C-*p-nitrophenyl ester* was prepared from 0.7 g 3-indolylacetyl-carboxy-^{14}C, 0.556 g (4 mmole) 3-*p*-nitrophenol and 0.832 g (4 mmole) N,N′-dicyclohexylcarbodiimide. Yield: 0.88 g, 75%. M.p. 106—107 °C.

3-*Indolylacetyl-*L-*aspartic acid.* 0.92 g (1.66 mmole) L-aspartic acid was dissolved in 25% aqueous tetramethylammoniumhydroxide solution (1.22 g, 3.33 mmole), and the mixture lyophilized. The salt was suspended in 8.3 ml dimethylsulfoxide. Dissolution was achieved after addition of 0.49 g (1.66 mmole) 3-indolylacetyl-*p*-nitrophenyl ester and stirring the mixture overnight. The dimethylsulfoxide was removed in vacuum, and the product taken up in 17 ml 5% $NaHCO_3$ solution and in 17 ml ether. The aqueous phase was extracted with 2×20 ml ether,

acidified with concentrated hydrochloric acid, and extracted with ether again. The aqueous phase was further acidified to pH 1, and extracted with 2×8.5 ml butanol. The butanol phase was washed with 8.5 ml 0.1*N* hydrochloric acid and with 10 ml water. Removal of the butanol in vacuum led to a pink glass, and recrystallization from water to colourless crystals. Yield: 0.31 g, 66%. M.p.: 189—190°C.

3-*Indolylacetyl-carboxy*-^{14}C-L-*aspartic acid.* The method used in the preparation of inactive 3-indolylacetyl-L-aspartic acid was used. A 25% aqueous solution of 0.365 g tetramethylammoniumhydroxide and 0.133 g (1 mmole) L-aspartic acid was lyophilized. The residue was dissolved in 6 ml dimethylsulfoxide and 0.296 g (1 mmole) 3-indolylacetyl-*p*-nitrophenyl ester was added. Yield after working up: 0.159 g, 60%. Activity: 1 mCi/mmole. M.p.: 188—190°C. Autoradiographically: one spot.

3-*Indolylacetyl*-L-*aspartic acid*-^{3}H. 1 mCi L-aspartic acid-^{3}H was diluted to an activity of 1 mCi/mmole with inactive L-aspartic acid. The synthesis was performed with mmole amounts. Yield: 0.145 g, 50%. Total activity: 450 μCi. Specific activity: about 1 mCi/mmole.

3-*Indolylacetyl-carboxy*-^{14}C-L-*aspartic acid*-^{3}H. 0.13 g (45%) 3-indolylacetyl--carboxy-^{14}C-L-aspartic acid-^{3}H was formed from 1 mmole L-aspartic acid, activity 1 mCi/mmole, and 1 mmole 3-indolylacetyl-*p*-nitrophenyl ester, activity 250 μCi/ /mmole. Total activity ^{14}C: 112 μCi; ^{3}H: 440 μCi. The activities were measured with a Nuclear Chicago liquid scintillation spectrometer.

References

[1] *Andreae, W. S., N. E. Good:* Plant Physiol. **30**, 380 (1955).
[2] *Hutzinger, O., J. C. Hart, E. M. Matheson:* Can. J. Chem. **48**, 177 (1970).
[3] *Klāmbt, H. D.:* Naturwissenschaften **17**, 398 (1960).
[4] *Mollan, R. C., D. M. X. Donnelly, M. A. Harmey:* Phytochemistry **11**, 1485 (1971).
[5] *Stutz, R. E., D. E. Atkinson, S. A. Gordon:* Atomic Energy Comission Report ANL, 4710, Nuclear Sci. Abstr. **6**, 164 (1952).

СИНТЕЗ ^{14}C И ^{3}H МЕЧЕННОЙ ИНДОЛ-3'-ИЛАЦЕТИЛ-АСПАРАГИНОВОЙ КИСЛОТЫ

Ф. Широкман, Е. Кёвеш, Л. Балашпири

В работе описан синтез индол-3'-илацетил-карбоксил-^{14}C-аспарагиновой кислоты, индол-3'-илацетил-аспарагиновой-^{3}H кислоты и вдвойне меченной индол-3'-илацетил-карбоксил-^{14}C-аспарагиновой-^{3}H кислоты.

STEREOCHEMICAL STUDIES, XX*
Studies on Cyclic 2-Hydroxycarboxylic Acids, III**
Molecular Structure and Dipole Moment Relationships of Ethyl *cis*- and *trans*-2-Hydroxycarboxylates

By

ÉVA TÓMORI

Research Institute for Pharmaceutical Chemistry, Budapest

S. FERENCZI-GRESZ

Institute of Inorganic Chemistry, Technical University, Budapest

and

G. BERNÁTH

Institute of Organic Chemistry, Attila József University, Szeged

(Received February 5, 1974)

The dipole moments of alicyclic ethyl *cis*- and *trans*-2-hydroxycarboxylates were studied. On the basis of the dipole moment values it proved possible to investigate the validity of the conformation rule in the case of these compounds. The fairly good agreement between measured and calculated dipole moments permitted to assume the presence of intramolecular hydrogen-bonds in the *cis*-isomers and of intermolecular hydrogen bonds in *trans*-isomers.

Introduction

Alicyclic ethyl *cis*- and *trans*-2-hydroxycarboxylates may serve as starting materials for the synthesis of stereochemically homogeneous bifunctional alicyclic derivatives. Several papers describe the synthesis and spectroscopic studies [5, 6] of *cis*- and *trans*-2-hydroxycyclopentanecarboxylic acid (**1**), *cis*- and *trans*-2-hydroxycyclohexanecarboxylic acid (**2**), *cis*- and *trans*-2-hydroxycycloheptanecarboxylic acid, and of the respective esters [3, 4]. IR and NMR spectroscopy reveals primarily the intramolecular and intermolecular hydrogen bonds of the isomers as well as the preferential conformation of the individual substituents. IR spectroscopy and viscosity measurements led CASTELLS and PALAU [5] to the conclusion that in the molecules of ethyl *cis*- and *trans*-2-hydroxycyclopentanecarboxylate and ethyl *cis*- and *trans*-2-hydroxycycloheptanecarboxylate the *cis*-isomer is less prone to associate than the *trans*-isomer.

BAUMANN and MÖHRLE [7, 8] studied the conformation of isomers and determined their equilibrium constants [9]. Equatorial hydroxy groups promote a more pronounced association than axial ones. Based on NMR spectra of BAUMANN and

* Part XIX: Zs. Vajna-Méhesfalvy, G. Bernáth, P. Sohár: Acta Chim. Acad. Sci. Hung. in press.

** Part II: G. Bernáth, Gy. Göndös, P. Márai, L. Gera: Acta Chim. Acad. Sci. Hung. 74, 471 (1972).

MÖHRLE [8] as well as our own IR and NMR spectroscopic data, and measurement of dissociation constants and reaction rate of chromic acid oxidation, the preferential conformation of compounds **Ia** and **Ib** was established in agreement with literature data [10]. NMR spectra suggest that in *cis*-2-hydroxycyclohexanecarboxylic acid equatorial position may be assigned to the carboxy group and axial to the hydroxy group [6].

It seemed justified to investigate the interrelationship between physical constants of isomers and their configuration with regard to dipole moment studies, too. Determination of the dipole moments may enable us to examine the validity of the "conformation rule" in the specific case of these molecules.

Determination of the dipole moment

The dipole moments of ethyl *cis*- and *trans*-2-hydroxycyclopentanecarboxylate (**Ia,b**), ethyl *cis*- and *trans*-2-hydroxycyclohexanecarboxylate (**IIa,b**), and ethyl *cis*- and *trans*-2-hydroxycycloheptanecarboxylate (**IIIa,b**) (Fig. 1) were determined. The synthesis of the model compounds was published in former communications [4, 11]. The samples used for dipole moment measurements did not contain impurities [4, 11].

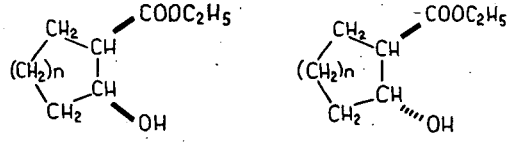

Ia : n = 1 Ib : n = 1
IIa : n = 2 IIb : n = 2
IIIa : n = 3 IIIb : n = 3

Fig. 1

The determinations were made at 25±0.1°C, the density d of the solutions was measured with a scaled dilatometer; n_D was assayed with Abbe's refractometer. The dielectric constant was recorded on a WTW Type DM 01 instrument at a frequency of 2 MHz, with a DFL 1 condenser. The cyclohexane used as solvent was dried on molecular sieve Klinosorb 4. The dipole moment was calculated according to HEDESTRAND [12] and GUGGENHEIM [13] from the following equation:

$$P_\infty = \frac{\varepsilon_1 - 1}{\varepsilon_1 - 1}\left[\frac{M_2}{d_1} + \frac{M_1}{d_1^2}\beta\right] + \frac{3M_1 \cdot \alpha}{(\varepsilon_1 + 2)^2 \cdot d_1}$$

with the following symbols:

- B — slope of the density *vs.* mole fraction straight line
- ε_1 — value of the dielectric constant *vs.* mole fraction straight line extrapolated to infinite dilution
- α — slope of the dielectric constant *vs.* mole fraction straight line
- d_1 — value of the density *vs.* molar fraction straight line extrapolated to infinite dilution
- M_1 — molecular weight of the solvent
- M_2 — molecular weight of the solute.

The dipole moment at known K_∞ value is

$$\mu = 0.221\,23\sqrt{P_\infty - R},$$

where R is the sum of atomic and electronic polarization. The approximate value of R may be calculated from the molecular refraction (by multiplying with +1.05):

$$R = MR_D \cdot 1.05.$$

The measured data are listed in Table I.

Table I

*Dipole moments of alicyclic ethyl cis- and trans-2-hydroxycarboxylates (***Ia,b—IIIa,b***) measured and calculated with* HEDESTRAND'S *method*

Compound	X_2	$\varepsilon_{1,2}^{25}$	$d_{1,2}^{25}$		$\mu_{1,2}$ (D)
Ia	0.005 0.010 0.015 0.020	2.0586 2.0967 2.1353 2.1741	0.7805 0.7824 0.7840 0.7863	$\alpha = 7.700$ $\beta = 0.358$ $\varepsilon_1 = 2.019$ $d_1 = 0.7788$	2.75
Ib	0.005 0.010 0.015 0.020	2.0461 2.0746 2.0984 2.1281	0.7784 0.7806 0.7824 0.7847	$\alpha = 5.223$ $\beta = 0.395$ $\varepsilon_1 = 2.018$ $d_1 = 0.7765$	2.221
IIa	0.005 0.010 0.015 0.020	2.0500 2.0968 2.1298 2.1745	0.7782 0.7812 0.7832 0.7859	$\alpha = 7.730$ $\beta = 0.401$ $\varepsilon_1 = 2.010$ $d_1 = 0.7770$	2.740
IIb	0.005 0.010 0.015 0.020	2.0560 2.0867 2.1140 2.1460	0.7776 0.7805 0.7816 0.7839	$\alpha = 5.866$ $\beta = 0.4266$ $\varepsilon_1 = 2.027$ $d_1 = 0.7752$	2.359
IIIa	0.005 0.010 0.010 0.020	2.0603 2.1035 2.1360 2.1742	0.7794 0.7815 0.7834 0.7854	$\alpha = 7.710$ $\beta = 0.435$ $\varepsilon_1 = 2.022$ $d_1 = 0.776$	2.703
IIIb	0.005 0.010 0.015 0.020	2.0546 2.0835 2.1115 2.1400	0.7785 0.7810 0.7826 0.7846	$\alpha = 5.750$ $\beta = 0.407$ $\varepsilon_1 = 2.025$ $d_1 = 0.7779$	2.324

The dipole moments of the molecules were calculated by GUGGENHEIM'S method [13]:

$$\mu^2 = \frac{27kT}{4\pi N} \cdot \frac{1}{d_1(\varepsilon_1 + 2)^2} \cdot (a_e - a_n) \cdot M_2,$$

too, where

k — $1.381 \cdot 10^{-16}$ (Boltzmann constant)
N — $6.023 \cdot 10^{-23}$ (Avogadro number)
d_1^{25} — density of cyclohexane (0.77389 g/ml)
n_D^{25} — refraction index of cyclohexane (1.4233)
ε_1 — dielectric constant of cyclohexane (2.0199)
M_2 — molecular weight of the solute
a_ε — $\varepsilon_{1,2} - \varepsilon_1 = f(w_2)$
a_n — $n_{D1,2}^2 - n_{D1}^2 = f(w_2)$,

Plotting the data measured in 5 or 6 dilute solutions (of 1—7 mole percent) the above calculations were performed and the results obtained are listed in Table II.

Table III contains the comparative figures obtained by both methods. The dipole moment of the *cis*-isomers is always higher.

Based on the measured dipole moments displayed in Table III, it may be concluded that the dipole moment values are not substantially influenced by ring sizes.

Vectorial additive method for the calculation of dipole moments

The dipole moments of molecules are determined by their conformation. Knowing the approximate geometry of a given substance, its dipole moment may be calculated theoretically on the basis of its bond angles and bond moments, respectively. Using the unit vectors of the substituents of the cyclopentane and cyclohexane skeleton [14, 15], calculations based on the assumed conformation of the compounds could be performed. According to our vector analysis, and in agreement with BAUMANN's studies [8], the envelope form was chosen. BAUMANN's studies revealed that, though the substituents had no direct influence on the conformation of the ring itself, the interaction between functional groups may promote a preferential orientation. In the case of 1,2-disubstituted cyclopentanes the *trans*-isomer tends to adopt envelope conformation, consequently both substituents are in pseudoequatorial position. In the *cis*-isomer, having envelope conformation, only one of the substituents is pseudoequatorial, thus the energy content of the *cis*-isomer is higher than that of the *trans*-isomer.

In the case of *cis*- and *trans*-cyclohexane derivatives equatorial—axial and diequatorial orientation may be assigned to the substituents. The unit vectors of these conformers were used in the calculations.

The dipole moment of compounds containing freely rotating or rigidly fixed substituents, respectively, may be calculated on the basis of GILMAN's method [27] as follows:

$$\mu^2 = \mu_0^2 + \sum_{i=1}^{n} \mu_1^2 + 2 \sum_{i=1}^{n} \mu_i (\mu_0 a_{ix} + \mu_{0y} \cdot a_{iy} + \mu_{0z} \cdot a_{iz}) \times \cos Q_i +$$

$$+ 2 \sum_{i \neq j}^{n} u_i u_j (a_{ix} a_{jx} + a_{iy} a_{jy} + a_{iz} a_{jz}) \cos Q_1 Q_2,$$

wherefrom the simplified equation

$$\mu^2 = \mu_1^2 + \mu_2^2 + 2\mu_1 \mu_2 (a_{1x} a_{2x} + a_{1y} a_{2y} + a_{1z} a_{2z}) \cos Q_1 Q_2$$

Table II

*Dipole moments of alicyclic ethyl cis- and trans-2-hydroxycarboxylates (***Ia,b**–**IIIa,b***) determined by* GUGGENHEIM*'s method* [13]

Compound	W_2	$n^2_{D1,2}-n^2_{D1,2}$	$n^{25}_{1,2}$	$\varepsilon_{1,2}-\varepsilon_1$		μ(D)
Ia	0.011 0.020 0.030 0.040	0.0010 0.0021 0.0031 0.0041	1.42339 1.42372 1.42431 1.42445	0.0430 0.0850 0.1280 0.1710	$a_n=0.101$ $a_\varepsilon=4.22$	2.772
Ib	0.010 0.020 0.030 0.040	0.0009 0.0018 0.0027 0.0036	1.42335 1.42365 1.42400 1.42430	0.0320 0.0640 0.0960 0.1230	$a_n=0.09$ $a_\varepsilon=3.07$	2.375
IIa	0.010 0.020 0.030 0.040	0.0011 0.0021 0.0031 0.0041	1.42341 1.42372 1.42431 1.42445	0.0380 0.7700 0.1140 0.0540	$a_n=0.101$ $a_\varepsilon=3.80$	2.760
IIb	0.010 0.020 0.030 0.040	0.0010 0.0020 0.0030 0.0039	1.42339 1.42370 1.42405 1.42440	0.0300 0.0610 0.0930 0.1220	$a_n=0.099$ $a_\varepsilon=3.080$	2.479
IIIa	0.011 0.022 0.032 0.043	0.0014 0.0028 0.0041 0.0055	1.42350 1.42410 1.42450 1.42500	0.0404 0.0836 0.1175 0.1549	$a_n=0.135$ $a_\varepsilon=3.61$	2.784
IIIb	0.011 0.022 0.032 0.043	0.0013 0.0026 0.0040 0.0053	1.42320 1.42400 1.42449 1.42490	0.0341 0.0636 0.0916 0.1220	$a_n=0.135$ $a_\varepsilon=2.85$	2.462

Note. $\varepsilon^{25}_{1,2}$ data are to be found in Table I.

Table III

Dipole moments of alicyclic ethyl cis- and trans-2-hydroxycarboxylates calculated with GUGGENHEIM*'s and* HEDESTRAND*'s methods*

Compound	μ_G	μ_H	$\mu_\Delta=\mu_{cis}-\mu_{trans}$	
			G	H
Ia **Ib**	2.772 2.375	2.750 2.220	0.397	0.530
IIa **IIb**	2.760 2.479	2.740 2.359	0.281	0.381
IIIa **IIIb**	2.784 2.462	2.703 2.324	0.322	0.379

can be obtained, where

μ_0 — dipole moment of the rigidly fixed polar groups
$\mu_{0x}\mu_{0y}\mu_{0z}$ — projection in the direction of the coordinate axes of the dipole moment μ_0 of the groups
$\mu_i\mu_j$ — moments of the n rotating groups
Q_iQ_j — angles formed by group-moment-vectors with rotation axes a_ia_j
$a_{ix}a_{ij}a_{iz}$ — unit vectors of the rotation axis i in the chosen coordinate system.

Bond moments and bond angles according to literature, used for the calculation of the dipole moment of ethyl *cis*- and *trans*-2-hydroxycyclopentanecarboxylate (**Ia,b**), are presented in Fig. 2.

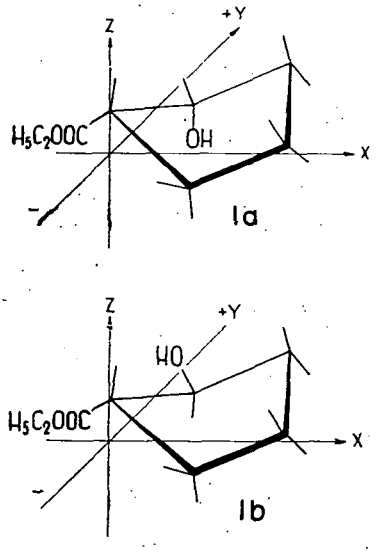

Fig. 2

$\vec{m}_{C_5H_{10}} = 0$ D [16]
$\vec{m}_{OH} = 1.6$ D [18]
$\vec{m}_{COOC_2H_5} = 1.8$ D [17]

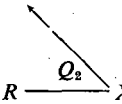

$X = 89°$ rotation angle of the carbethoxy group around axis a_1 [17]

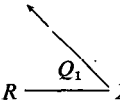

$X = 63°$ rotation angle of the hydroxy group around axis a_2 [18]

Table IV lists the unit vectors of cyclopentane substituents [14] in the chosen coordinate system.

Table IV

Unit vectors of cyclopentane substituents [14] *in the chosen coordinate system*

Position	Orientation	Unit vectors of substituents		
		x	y	z
1	equatorial	0.169	0.000	0.986
2	axial	−0.280	0.900	0.332
3	equatorial	−0.114	−0.039	−0.992

Bond moments and bond angles according to literature, used for the calculation of the dipole moment of ethyl *cis*- and *trans*-2-hydroxycyclohexanecarboxylate, are presented in Fig. 3.

$m_{C_6H_1}$ = 0 D [16]
m_{OH} = 1.6 D [18]
m_{COOC_2H} = 1.8 D [17]

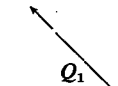

$X = 63°$ rotation angle of hydroxy group around axis a_2 [16]

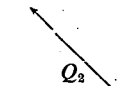

$X = 89°$ rotation angle of carbethoxy group around axis a_1 [17]

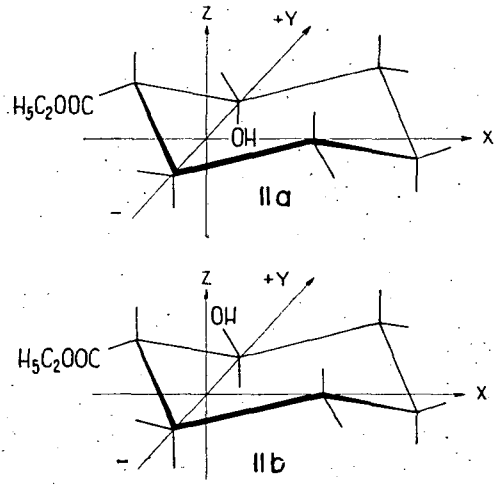

Fig. 3

Table V lists the unit vectors of cyclohexane substituents [15] in the chosen coordinate system.

Table V

Unit vectors of cyclohexane substituents [15] *in the chosen coordinate system*

Position	Orientation	Unit vectors of substituents		
		x	*y*	*z*
1	equatorial	−0.997	0.000	0.077
2	axial	−0.333	−0.067	0.940
2	equatorial	−0.333	−0.804	−0.492

Pertinent literature data of ethyl *cis*- and *trans*-2-hydroxycycloheptanecarboxylate were not available, consequently no vectorial calculations could be performed.

Using the above values of the substituent unit vectors, bond moments and bond angles, the dipole moments summarized in Table VI were obtained.

Table VI demonstrates the good agreement between the dipole moments calculated according to the supposed conformation and the measured values. This agreement is especially striking in the case of the *trans*-isomers. The discrepancies experienced in the *cis*-isomers will be dealt with later.

Table VI

*Calculated and measured dipole moments of alicyclic ethyl cis- and trans-2-hydroxycarboxylates (***Ia,b, IIa,b***)*

Compound	μ_{calc}	$\mu_{measured}$		$\mu_{\Delta}=\mu_{measured}-\mu_{calc}$	
		G	H	G	H
Ia	2.390	2.772	2.750	+0.372	+0.350
Ib	2.390	2.375	2.220	−0.015	+0.170
IIa	2.40	2.760	2.740	+0.360	+0.340
IIb	2.40	2.479	2.359	+0.079	−0.041

Discussion

Comparing the measured dipole moments of alicyclic ethyl *cis*- and *trans*-2-hydroxycarboxylates, it is apparent that the dipole moments of the *cis*-isomers are higher. Spectroscopic [5, 6] as well as other studies [9] revealed the presence of an intramolecular hydrogen bond in the *cis*-isomers.

The dipole moment of the *cis*-isomers should be lower due to the polarity-lowering effect of the intramolecular hydrogen bond. Other investigations [19], however, draw the attention to the circumstance that an intramolecular hydrogen bond enhances the rigidity of the skeleton, and thus increases the dipole moment. The increase in dipole moment of the *cis*-isomers may be attributed to the fact, that, due to the relative position of the functional groups in the *cis*-isomers, the skeleton of the molecule is less coplanar than in the *trans*-isomers with diequatorial substituents. Regarding the comparatively good agreement between measured and calculated dipole moments, it may be assumed that, under the applied conditions of measurement, the intermolecular hydrogen bond of the *cis*-isomers may be omitted, consequently, in the case of the *cis*-isomers of cyclopentane, cyclohexane, and cycloheptane derivatives, the presence of the intramolecular hydrogen bond may be considered the determining factor.

Knowing the dipole moments, the respective molecules may be studied according to the conformation rule. On the basis of AUWERS's equation [20, 21], in the case of *cis*—*trans*-isomers, it is the *cis*-isomer which has higher density, refraction index and lower molar refraction. This rule, or its modified form [26] can be used for comparing stereoisomers, though only interpretations on the basis of the conformation rule may lead to correct results [22]. ELIEL assumes that the less stable conformation may be assigned to the isomer of higher boiling point, refraction index, and density; *i.e.* it is the isomer of smaller molecular volume which has higher enthalpy. Isomers with conformations in which all substituents are equatorial, have lower boiling points, density and refraction index than those containing axial substituents as well.

Originally, the conformation rule was set up for cyclohexane derivatives; nevertheless it could be successfully applied to some cyclopropane, cyclopentane, cycloheptane and cyclooctane derivatives, too [23]. Its interpretation is the most clearcut in the case of hydrocarbons. Strong dipole—dipole interactions promote stronger association of the respective molecules through the increased dipole

moment; *i.e.* as a rule, in the case of dipole moments showing marked difference, the isomer having a higher dipole moment has a higher boiling point as well. The conformation rule, however, is not valid for isomers having highly different dipole moments. In this case ARKEL's dipole rule [24] should be applied, which is valid for broader ranges of dipole moment values (0.2 D).

ELIEL [25] demonstrated that in the case of polar substituents (OH, NH_2) boiling points do not follow the conformation rule, and the diequatorial *trans*-isomer has the higher boiling point. On the basis of his results obtained with 2-, 3-, and 4-methylcyclohexanols, he interpreted this fact with the circumstance that the intermolacular hydrogen bonds with the equatorial hydroxyl are more pronounced than in the case of axial conformers.

As a conclusion, van ALKEL's rule can be applied in the case of our model compounds. Components having higher physical constants (except boiling point and viscosity) have higher dipole moments as well. The higher boiling points of the *trans*-isomers may be due to intermolecular hydrogen bonds, which promote association. The intermolecular association of *trans*-isomers is confirmed both by spectroscopic studies and gas chromatographic data [4]. Dipole moment measurements were in agreement with LUTSKII's former observations [19] that in this type of molecules, beyond dipole—dipole interactions, intramolecular hydrogen bonds, enhancing the rigidity of the skeleton, may play a decisive role.

* * *

Thanks are due to Professor J. NAGY, Director of the Institute of Inorganic Chemistry, Technical University, Budapest, for useful discussions and to Dr. J. SZÁVA, Head of the Analytical Department of the Research Institute for Pharmaceutical Chemistry, Budapest, for supporting this work.

References

[1] *Pascual, J., J. Sistaré, J. Regás:* J. Chem. Soc. **1949**, 1943.
[2] *Pascual, J., J. Castells:* J. Am. Chem. Soc. **74**, 2899 (1952).
[3] *Pascual, J., J. Castells:* Annales Real. Soc. Espan. Fis. Quim. (Madrid). Ser. B. **63**, 455 (1967).
[4] *Bernáth, G., Gy. Göndös, P. Márai, L. Gera:* Acta Chim. Acad. Sci. Hung. **74**, 471 (1972).
[5] *Castells, J., J. Palau:* J. Chem. Soc. **1964**, 4938.
[6] *Bernáth, G., P. Sohár, K. L. Láng, I. Tornyai, Ö. K. J. Kovács:* Acta Chim. Acad. Sci. Hung. **64**, 81 (1970).
[7] *Baumann, H., H. Möhrle:* Tetrahedron **25**, 135 (1969).
[8] *Baumann, H., H. Möhrle:* Tetrahedron **23**, 4331 (1967).
[9] *Möhrle, H., H. Baumann:* Annalen **716**, 61 (1968).
[10] *Buys, H. R.:* Conformational Investigations on Five-Membered Ring Compounds. Thesis. Rijks University, Leiden. Bronder-Offset, Rotterdam, 1968, and references cited therein.
[11] *Bernáth, G., K. Kovács, K. L. Láng:* Acta Chim. Acad. Sci. Hung. **64**, 183 (1970).
[12] *Hedestrand, G.:* Z. Physik. Chem. **2B**, 428 (1929).
[13] *Guggenheim, E. A.:* Trans. Faraday Soc. **45**, 714 (1949).
[14] *Brutcher, F. V., Jr.:* J. Am. Chem. Soc. **81**, 4915 (1959).
[15] *Eliel, E. L., N. L. Allinger, S. J. Angyal, G. A. Morrison:* Conformational Analysis, Interscience Publishers, New York, 1965, p. 454.
[16] *Smyth, C. Ph.:* Dielectric Behavior and Structure, McGraw—Hill Book Co., Toronto, 1955, p. 262.
[17] See: [16] p. 301.
[18] *Minkin, V., O. A. Osipov:* Dipole Moments in Organic Chemistry, Plenum Press, New York, London, 1970.

[19] *Lutskii, A. E.:* Zhur. Obsh. Khim. **29**, 2073 (1959).
[20] *Auwers, K.:* Annalen **420**, 81 (1920).
[21] *Skita, A.:* Ber. **53**, 1792 (1920).
[22] *Allinger, N. L.:* J. Am. Chem. Soc. **79**, 3443 (1957).
[23] See: [18] p. 176.
[24] *van Arkel, A. E.:* Rec. Trav. Chim. **51**, 1081 (1931); ibid. **53**, 246 (1934).
[25] *Eliel, E. L.:* J. Org. Chem. **23**, 2041 (1958).
[26] *van Bekkum, H., A. van Veen, P. E. Verkade, B. M. Wepster:* Rec. Trav. Chim. **80**, 1310 (1961).
[27] *Gilman, T. S.:* J. Am. Chem. Soc. **88**, 1861 (1966).

СТЕРЕОХИМИЧЕСКИЕ ИССЛЕДОВАНИЯ, XX
ИЗУЧЕНИЕ ЦИКЛИЧЕСКИХ 2-ОКСИКАРБОНОВЫХ КИСЛОТ, III
СВЯЗЬ МЕЖДУ МОЛЕКУЛЯРНОЙ СТРУКТУРОЙ И ДИПОЛЬНЫМИ МОМЕНТАМИ ЭТИЛОВЫХ ЭФИРОВ *ЦИС-* И *ТРАНС*-2-ОКСИКАРБОНОВОЙ КИСЛОТЫ

Е. Томори, Ш. Ференци-Грес, Г. Бернат

Изучены дипольные моменты этиловых эфиров *цис-* и *транс*-2-оксикарбоновой кислоты. При известных величинах дипольных моментов представляется возможность проверки применимости конформационного правила. Хорошее совпадение между измеренными и рассчитанными величинами дипольных моментов указывает на вероятность наличия внутримолекулярных водородных связей у *цис*-изомеров и межмолекулярных — у *транс*-изомеров.

STEREOCHEMICAL STUDIES, XXI*

Studies on Cyclic 2-Hydroxycarboxylic Acids, IV*

Synthesis of *cis*- and *trans*-2-Hydroxycyclooctanecarboxylic Acid. Data on the Reduction of Cyclic Ethyl 2-Ketocarboxylates**

By

G. BERNÁTH, GY. GÖNDÖS and L. GERA

Institute of Organic Chemistry, Attila József University, Szeged

(Received September 4, 1973)

The preparation of *cis*- and *trans*-2-hydroxycyclooctanecarboxylic acid (**13, 14**) is described. It is shown that *cis*-2-hydroxycyclooctanecarboxylic acid, considered as stereohomogeneous in a recent paper [14], is actually a mixture of the *cis*- and *trans*-isomers. The isomer ratio of the catalytic and sodium borohydride reduction of homologous alicyclic 2-ketocarboxylates (**1—4**) has been studied.

Introduction

In the course of our investigations on the reaction mechanism and conformational analysis of alicyclic 1,3-disubstituted compounds [1—6], it proved necessary to elaborate methods suitable for preparing larger quantities of alicyclic *cis*- and *trans*-2-hydroxycarboxylic acids. We reported earlier [7] on our methods of synthesizing *cis*- and *trans*-2-hydroxycyclopentanecarboxylic acid as well as *cis*- and *trans*-2-hydroxycycloheptanecarboxylic acid.

Stereohomogeneous cyclic 2-hydroxycarboxylic acids can be obtained by reduction of the corresponding 2-ketocarboxylates and subsequent fractionation of the resulting *cis—trans* mixture. However, no suitable methods for the separation of greater quantities of *cis—trans* mixtures were available. The separation of ethyl *cis*- and *trans*-2-hydroxycyclopentanecarboxylates (**5, 6**) was elaborated by PASCUAL and CASTELLS [8], who separated the corresponding dinitrobenzoates by tedious fractional crystallization. Later on MÖHRLE and BAUMANN [9] separated the ethyl *cis*- and *trans*-2-hydroxycyclopentanecarboxylates (**5, 6**) by countercurrent distribution, and recently CAPON and PAGE [10] by preparative gas chromatography.

As we reported [7], a very efficient separation of these compounds, as well as of the corresponding cyclohexane and cycloheptane homologues can be achieved by fractional distillation on a column of about thirty theoretical plates. With this method we succeded in separating the ethyl *cis*- and *trans*-2-hydroxycyclooctanecarboxylate (**11, 12**).

* Part XX(III): É. Tomori, S. Ferenczi-Gresz, G. Bernáth: Acta Phys. et Chem. Szeged **20**, 129 (1974).

** Presented in part in a lecture delivered at the Congress of the Hungarian Chemical Society, Debrecen, August 31, 1971.

As the efficiency of the distillation depends highly on the isomer ratio of the starting mixture used, it seemed justified to study the isomer ratio of the catalytic and of sodium borohydride reduction.

In the present paper we report on the preparation of *cis*- and *trans*-2-hydroxycyclooctanecarboxylic acid (**13**, **14**) and on our investigations concerning the isomer ratio of the reduction of homologous cyclic ethyl 2-ketocarboxylates.

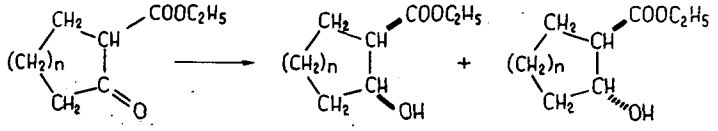

1 : n = 1 5 : n = 1 6 : n = 1
2 : n = 2 7 : n = 2 8 : n = 2
3 : n = 3 9 : n = 3 10 : n = 3
4 : n = 4 11 : n = 4 12 : n = 4

Fig. 1

Results and discussion

In the reduction of cyclic ethyl 2-ketocarboxylates, the isomer ratio of the reduction products was investigated only in the case of lower homologues [11], though the accuracy of the methods used for determining the isomer ratio, *e.g.* fractional crystallization, or m.p. determination of the 3,5-dinitrobenzoate of the product cannot be considered as sufficient. The reduction of ethyl 2-ketocycloheptanecarboxylate with Adams' PtO_2 catalyst and with sodium borohydride was also performed by PASCUAL *et al.* [12], without giving, however, the isomer ratio.

BHARGAVA, MATUR and SAHARIA, reporting [13] on the synthesis of *cis*- and *trans*-2-hydroxycycloheptanecarboxylic acid, assumed that under the experimental conditions used (sodium borohydride—ethanol, or W-7 Raney nickel catalyst—hydrogen—ethanol), only ethyl *cis*-2-hydroxycycloheptanecarboxylate (**9**) formed, without proving the homogeneity of the product. As we subsequently reported [7], both the catalytic and sodium borohydride reductions, under various experimental conditions, always leads to both isomers, though the *cis* isomer is predominant.

In 1968, SAHARIA and TYAGI supposed [15] the product obtained by sodium borohydride reduction of ethyl 2-ketocyclooctanecarboxylate (**4**) to be stereohomogeneous ethyl *cis*-2-hydroxycyclooctanecarboxylate (**11**).

With respect to the above, it seemed reasonable to study the catalytic and sodium borohydride reductions of the homologous ethyl 2-ketocarboxylates (**1**—**4**) using the less expensive Raney nickel catalyst. As we found earlier [7, 15, 16] that at lower temperatures the reduction of analogous ethyl 2-ketocarboxylates with sodium borohydride yielded a higher *trans* isomer ratio, we studied also the influence of temperature on the reaction under comparable experimental conditions. For determining the *cis*—*trans* isomer ratio we used gas chromatography. Results are summarized in Table I.

It can be seen that the catalytic reduction of all four homologues always yields about 90% *cis* isomer, the same beeing true for the sodium borohydride reduc-

*Table I**

Isomer ratio of the reduction of cyclic ethyl 2-ketocarboxylates (**1**—**4**)

Reaction	Isomer ratio, %					
	$NaBH_4$		Raney nickel/H_2			
	0°C		25°C		60°C	
	cis	*trans*	*cis*	*trans*	*cis*	*trans*
1 → **5**+**6**	31.2	68.8	40.6	60.4	87.3	12.7
2 → **7**+**8**	62.0	38.0	51.7	48.3	88.2	11.8
3 → **9**+**10**	94.1	5.9	91.8	8.2	89.7	10.3
4 → **11**+**12**	92.7	7.3	88.4	11.6	91.2	8.8

Note. * Reaction conditions see: Experimental part.

tion of ethyl 2-ketocycloheptanecarboxylate (**3**) and ethyl 2-ketocyclooctanecarboxylate (**4**), while in the case of the lower homologue the sodium borohydride reduction yields considerably more *trans* isomer than the catalytic process.

13 **14**

Fig. 2

SAHARIA and TYAGI, hydrolysing the product of sodium borohydride reduction of ethyl 2-ketocyclooctanecarboxylate, and assuming it to be homogeneous ethyl *cis*-2-hydroxycyclooctanecarboxylate (**11**), reported a m.p. of 70°C for the *cis*-2-hydroxycyclooctanecarboxylic acid (**13**) [14]. In contrary, by hydrolysis of the gas chromatographically homogeneous ethyl *cis*-2-hydroxycyclooctanecarboxylate, we obtained a m.p. of 97°C for the *cis*-2-hydroxycyclooctanecarboxylic acid (**13**), and 109°C for the *trans* isomer, similarly prepared from gas chromatographically homogeneous ethyl *trans*-2-hydroxycyclooctanecarboxylate (**12**). Stereohomogeneity of the *cis*- and *trans*-2-hydroxycyclooctanecarboxylic acid (**13**, **14**) is unequivocally supported by IR and NMR data (see: Table II and Figs 3 and 4). It follows from the above, that the reduction product of the Indian authors could not be homogeneous, consequently the hydroxy acid they obtained must also have been a mixture of the *cis* and *trans* isomers.

Experimental

M.ps were determined on a Kofler-block and are uncorrected. IR spectra were obtained in KBr pellets, with a Perkin—Elmer infrared spectrophotometer. NMR measurements were made with a 60 Mc/s J-NM-C-60 (JEOL) spectrometer, $CDCl_3$ was used as solvent and TMS as internal standard.

Table II

IR and NMR data of the cis- and trans-2-hydroxycyclooctanecarboxylic acid (**13, 14**)

Compound	IR data[a]			NMR data[b]		
	νOH (alcohol)	νOH (acid)	νC=O	CH_2 (12)	δ CH(COOH)	δ CH(OH)
13	3320	3500—3200	1698 (sharp)	70—130 Hz	2.75 (12 Hz)	4.25 (10 Hz)
14	3250	3500—2300	1695 (broad)	70—130 Hz	2.65 (20 Hz)	4.10 (20 Hz)

Note. [a] Measurements of IR spectra were made in KBr pellets with a Perkin-Elmer IR spectrophotometer. Spectra see Figs 3 and 4.
[b] Chemical shifts in δ ppm, coupling constants in Hz units. Solvent: $CDCl_3$.

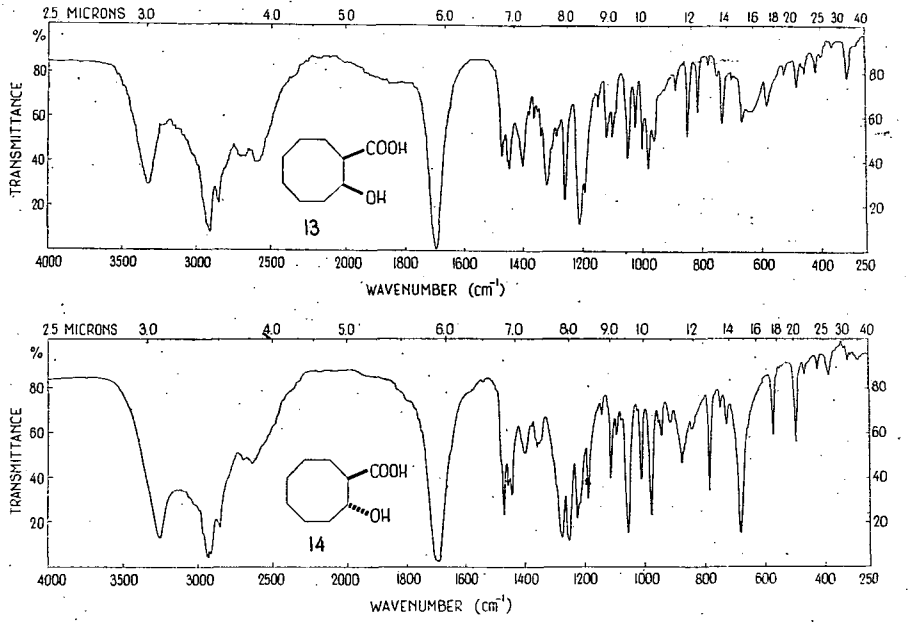

Figs 3 and 4

Reduction of cyclic ethyl 2-ketocarboxylates (**1—4**)

a) The catalytic reductions were performed in abs. ethanol with 0.2 mole ethyl 2-ketocarboxylate using 10.0 g Raney nickel catalyst previously washed with water and ethanol several times, and applying 120 atm starting hydrogen pressure. After the reduction had been completed, the catalyst was filtered off, the solvent removed in vacuum and the isomer ratio of the remaining crude product was deter-

mined by gas chromatography, using a Gazofract 400 C apparatus: column height 2 m; stationary phase: polyethyleneglycol adipate 20%; support: superthermolit 30—40 mesh; temperature 160°C; carrier gas: hydrogen.

b) 200 ml abs. ethanol was placed in a 750 ml three-necked round-bottomed flask equipped with stirrer and reflux condenser, then 0.15 mole sodium borohydride was added in portions under stirring. After the reagent dissolved, 0.1 mole of the corresponding ethyl 2-ketocarboxylate (**1-4**) dissolved in 50 ml abs. ethanol was added dropwise, maintaining the flask at 0°C or 25°C, respectively. The reaction mixture was stirred for 6 hrs, a mixture of 16 ml glacial acetic acid and 150 ml water was added dropwise under stirring. The ethanol was distilled off at reduced pressure (25—30 torr). The remaining mixture separated into two layers and was extracted 4 or 5 times with 100 ml ether and, after drying over Na_2SO_4, the ether was distilled off. The isomer ratio of the remaining cyclic ethyl 2-hydroxycarboxylate was determined as above.

Cis-2-hydroxycyclooctanecarboxylic acid (**13**)

20.0 g (0.10 mole) gas-chromatographically homogeneous ethyl *cis*-2-hydroxycyclooctanecarboxylate (**11**) was shaken with 150 ml 15% NaOH solution at room temperature for 12 hrs. To remove contaminations, the alkaline solution was extracted with 2×100 ml ether and acidified to pH 2 by adding conc. HCl, then extracted with 5×100 ml ether. The combined ethereal solution was dried over Na_2SO_4 and after eveporation gave 12.9 g (74.8%) *cis*-2-hydroxycyclooctanecarboxylic acid (**13**), which was crystallized from benzene, m.p. 95—96°C. After three recrystallizations from benzene the m.p. was 97°C, which remained constant on further recrystallization (Lit. [14] m.p.: 70°C). IR spectrum: Fig. 3, NMR spectrum: Table II.

$C_9H_{16}O_3$ (172.23). Calcd. C 62.77; H 9.36. Found C 62.50; H 8.96%.

Trans-2-hydroxycyclooctanecarboxylic acid (**14**)

2.0 g (0.01 mole gas-chromatographically homogeneous ethyl *trans*-2-hydroxycyclooctanecarboxylate (**12**) was hydrolysed as above to yield 1.55 g (89.9%) *trans*-2-hydroxycyclooctanecarboxylic acid (**14**). This was crystallized from benzene, m.p. 105—106°C, recrystallized two times from benzene and three times from ether. M.p. 109°C, which remained constant on further recrystallization. IR spectrum: Fig. 4, NMR spectrum: Table II.

$C_9H_{16}O_3$ (172.23). Calcd. C 62.77; H 9.36. Found C 62.79; H 9.59%.

* * *

The authors' thanks are due to Chemical Works CHINOIN Ltd., Budapest and to REANAL Factory of Laboratory Chemicals, Budapest for financial support of this work. We are indebted to Mrs. É. TOMORI (Research Institute for Pharmaceutical Chemistry, Budapest) for the gas chromatographic analyses, to Mrs. K. LOVASS for taking part in some experiments, to Dr. K. L. LÁNG and Mrs. G. BARTÓK—BOZÓKI for the microanalyses and to Miss A. VÍGH for valuable technical assistance.

References

[1] *Bernáth, G., Gy. Göndös, K. Kovács, P. Sohár:* Tetrahedron **29**, 981 (1973).
[2] *Bernáth, G., K. L. Láng, Gy. Göndös, P. Márai, K. Kovács:* Acta Chim. Acad. Sci. Hung. **74**, 479 (1972).
[3] *Bernáth, G., K. Kovács, K. L. Láng:* Acta Chim. Acad. Sci. Hung. **64**, 183 (1970).
[4] *Bernáth, G., K. L. Láng, K. Kovács, L. Radics:* Acta Chim. Acad. Sci. Hung. **73**, 81 (1972).
[5] *Sohár, P., G. Bernáth:* Org. Magnetic Resonance **5**, 159 (1973).
[6] *Bernáth, G., K. L. Láng, Gy. Göndös, P. Márai, K. Kovács,* Acta Phys. et Chem. Szeged **17**, 161 (1971).
[7] *Bernáth, G., Gy. Göndös, P. Márai, L. Gera:* Acta Chim. Acad. Sci. Hung. **74**, 471 (1972).
[8] *Pascual, J., J. Castells:* J. Amer. Chem. Soc. **74**, 2899 (1952).
[9] *Möhrle, H., H. Baumann:* Annalen **716**, 61 (1968).
[10] *Capon, B., M. I. Page:* J. Chem. Soc. (B) **1971**, 471.
[11] *Pascual, J., J. Vinas:* Bull. soc. chim. France **1960**, 1430.
[12] *Palau, J., J. Pascual, J. M.Ráfols:* Bull. soc. chim. France **1964**, 269.
[13] *Bhargava, S. S., K. C. Mathur, G. S. Saharia:* Indian J. Chem. **8**, 714 (1970).
[14] *Saharia, G. S., M. P. Tyagi*: Indian J. Chem. **6**, 69 (1968).
[15] *Bernáth, G., P. Sohár, K. L. Láng, I. Tornyai, Ö. K. J. Kovács:* Acta Chim. Acad. Sci. Hung. **64**, 81 (1970).
[16] *Bernáth, G., M. Svoboda:* Tetrahedron **28**, 3475 (1972).

СТЕРЕОХИМИЧЕСКИЕ ИССЛЕДОВАНИЯ, XXI ИЗУЧЕНИЕ ЦИКЛИЧЕСКИХ 2-ОКСИКАРБОНОВЫХ КИСЛОТ, IV СИНТЕЗ *ЦИС*- И *ТРАНС*-2-ОКСИЦИКЛООКТАНОВОЙ КИСЛОТЫ. ДАННЫЕ О ВОССТАНОВЛЕНИИ ЦИКЛИЧЕСКИХ СЛОЖНЫХ ЭФИРОВ 2-КЕТОКАРБОНОВОЙ КИСЛОТЫ

Г. Бернат, Дь. Гёндёш, Л. Гера

Описан синтез *цис*- и *транс*-2-оксициклооктановой (**13, 14**) кислоты. Показано, что описанная недавно в работе [14] *цис*-2-оксициклооктановая кислота является смесью *цис*- и *транс*-изомеров. Изучено распределение изомеров гомологического ряда сложных эфиров алициклической 2-кетокарбоновой кислоты (**1—4**) при каталитическом и натрий-боргидридном восстановлении.

SEDIMENTATION OF STRUCTURED SUSPENSIONS, I

Introduction and some General Statements

By

M. GILDE, F. SZÁNTÓ

Institute of Colloid Chemistry, Attila József University, Szeged

K. VARGA

Institute of Technological Chemistry, Attila József University, Szeged

and

F. J. GILDE

Institute of Theoretical Physics, Attila József University, Szeged

(Received February 27, 1974)

The first paper of our series on sedimentation of structured suspensions begins with summarizing the most important results available in literature. The principal types are presented by describing some characteristic processes. Then, based on the results, a model consisting of three sections, namely sedimentation, filtering and shrinking is drawn up. Finally the objectives of further investigations are outlined.

Introduction

Investigations on sedimentation of structured suspensions performed at the Institute of Colloid Chemistry during the last ten years made it necessary to review the results obtained from a uniform point of view. It seemed also justified to deal with the results to be expected in the series of articles beginning with this paper.

Preliminaries. Review of literature

The problem of sedimentation of extremely dilute suspensions seems to be practically resolved on the basis of Stokes' and Navier's conception and its further development. The question concerning more concentrated suspensions seems more problematical, even if dynamically independent spherical particles, settling individually, are considered. The most widely used approximations for this case were elaborated by STEINOUR as well as by RICHARDSON and ZAKI. These authors, like others, taking into account the upward streaming of the displaced medium and the effect on the settling process of the density and viscosity of the suspension, generally gave relations for determining the sedimentation rate of rigid monodisperse spheres as a function of the "free" volume (relative volume of the medium, *i.e.* porosity ε) and the classical parameters (radius or diameter of the sphere, difference in density, and viscosity of the medium). These relations are generally complicated functions

of ε, because the influence of hydrodynamical interactions, as well as the density and viscosity of the suspension also depend on ε. According to STEINOUR [1], for non-flocculated spherical suspensions in the range $0.5<\varepsilon<0.7$, the relation

$$Q = v_S \frac{\varepsilon^3}{1-\varepsilon} \tag{1}$$

is valid, where Q is the settling rate of a suspension of porosity ε, *i.e.* of volumetric density $(1-\varepsilon)$, consisting of spherical particles, and v_S the settling rate of the particles in a corresponding, infinitely dilute suspension according to Stokes. RICHARDSON and ZAKI [2] calculated with the following relation:

$$Q = v_S \varepsilon^{4.65}. \tag{2}$$

In comparetively more dilute, monodisperse suspensions, as long as ε can be considered as constant in the upper zone, the settling velocity of the interface between the slurry and the supernatant is constant, the beginning of the settling curve can be considered as linear (see later). In intermediate concentrations, technically in the shrinking zone, ε changes with the height of the zone during sedimentation. In this case, some authors [3, 4] assume as an empirical approximative solution that the sedimentation rate dV/dt is a linear function of the difference between the instantaneous volume V and the ultimate volume V_∞

$$-\frac{dV}{dt} = k(V - V_\infty), \tag{3}$$

where k is the velocity sonstant. Integrating with the initial condition that at $t=0$ $V(0)=V_0$, the following exponential formula

$$V(t) = V_\infty + (V_0 - V_\infty)e^{-kt} \tag{4}$$

is obtained.

In heterodisperse suspensions of rather low concentration, if interactions between the particles can be neglected, the particles of different sizes will fall individually with different velocities, according to Stokes' law. The settling suspension does not give a sharp interface and the weight of the sediment increases with time according to the classical analyses. In suspensions occurring in practice, the interactions (adhesive forces) between the particles cannot be neglected. In this case the formation of larger or smaller aggregates (orthokinetic coagulation) is to be expected, by which the sedimentation process becomes much more complex. Kinetics and mechanism of this process has been first dealt with in detail by TUORILA [5] and MÜLLER [6]; subsequently ANDERSSON [7] elaborated a theory, taking into account the hydrodynamical effects between the settling particles. The probability of collision and adhesion of the particles depends on the sign and the value of the resultant of the attractive and repulsive forces between the particles. These can be calculated on the base of Deryaghin—Landau—Verwey—Overbeek's (DLVO) theory. This was taken into account by JOVANOVIČ [8] in his recent calculations concerning more dilute suspensions containing individually settling aggregates.

The most complex cases — occurring most frequently in industrial practice — are those of comparatively more concentrated suspensions, in which the interactions

between the particles have also to be taken into account. Despite their heterogeneity, these suspensions mostly settle with a sharp interface; their particles are in more or less aggregated state. (The respective literature is not quite uniform and consequent in using the terms "coagulation" and "flocculation"; therefore we use the most general term*). This type of sedimentation was studied first in the case of kaolin suspensions by COE and CLEVENGER [9], who dealt with the concentration zones formed in the settling suspension, and pointed to the fact that the upward streaming of the displaced liquid in the sediment is actually a case of streaming through pores. Taking into account the results of POWERS [10] concerning concentrated, flocculated cement suspensions, STEINOUR [11, 12] gave the following relation:

$$Q = \frac{0.123 v_S}{(1-W_i)^2} \frac{(\varepsilon - W_i)^3}{1-\varepsilon} \tag{5}$$

where W_i is the volume of the so called "immobilized" liquid, which does not take part in the streaming through the pores. According to STEINOUR, in heterodisperse systems

$$v_S = \frac{2g(\varrho_s - \varrho_f)}{\eta \sigma^2} \tag{6}$$

where g is the gravity acceleration, ϱ_s the density of the suspended material, ϱ_f that of the liquid, η the viscosity of the medium and σ is the specific surface of the particles relative to their volume. For spherical particles of radius r, $\sigma = 3/r$, and v_S is in accordance with Stokes' relation. Equation (5) is very similar to the sedimentation formula of POWERS [10]:

$$Q = \frac{0.2}{\sigma^2} \frac{g(\varrho_s - \varrho_f)}{\eta} \frac{(\varepsilon - W_i)}{1-\varepsilon}. \tag{7}$$

It has to be mentioned that, in POWERS' formula, the specific surface is determined from gas permeability instead of the definition used by STEINOUR. The quantity of the immobilized water was taken into account in some cases, namely in filter-beds containing clay, by KOZENY [13] and CARMAN [14].

A partly different model was used by MICHAELS and BOLGER [17] in their investigations on sedimentation of flocculated kaolin suspensions. These authors, starting from the types of settling curves described already by SMELLIE and LA MER [16] (see Fig. 1), treated more dilute and more concentrated suspensions separately. They assumed a more complex structure to exist in more dilute suspensions too; the units of sedimentation are aggregates consisting of flocs formed by the primary kaolin particles. In dilute suspensions the aggregates, considered as spherical, settle individually, and produce a sharp interface. The settling curve begins with a linear part (Fig. 1, curve *a*). The model of MICHAELS and BOLGER is thoroughly connected with earlier X-ray absorption investigations of GAUDIN and FUERSTENAU [17], by which they

* To distinguish this case of sedimentation from other types, it is designed as "subsidence" in English literature. The expression "collective sedimentation" is also used.

verified the existence of a sedimentation zone of constant density. The sedimentation rate Q_0 can be characterized by the slope of the linear part of the settling curve; it is a function of Φ_A (volume concentration of the aggregates). MICHAELS and BOLGER applied the relation of RICHARDSON and ZAKI

$$Q_0 = v_{SA}\varepsilon_A^{4.65} \tag{8}$$

where v_{SA} is the settling rate of the aggregates according to Stokes, $\varepsilon_A = 1-\Phi_A$. With respect to the material balance,

$$Q_0 = \frac{g(\varrho_s-\varrho_f)d_A^2}{18\eta C_A}(1-C_A\Phi)^{4.65} \tag{9}$$

where d_A is the mean diameter of the aggregates, $\Phi = 1-\varepsilon$ the volume ratio of the solid component and $C_A = \Phi_A/\Phi$, *i.e.* the quotient characterizing the "looseness" of the aggregate (the ratio of the immobilized liquid). The above relation permits to determine d_A and C_A by a graphic method, which can be applied in the range of Φ in which v_{SA} and C_A are independent of Φ.

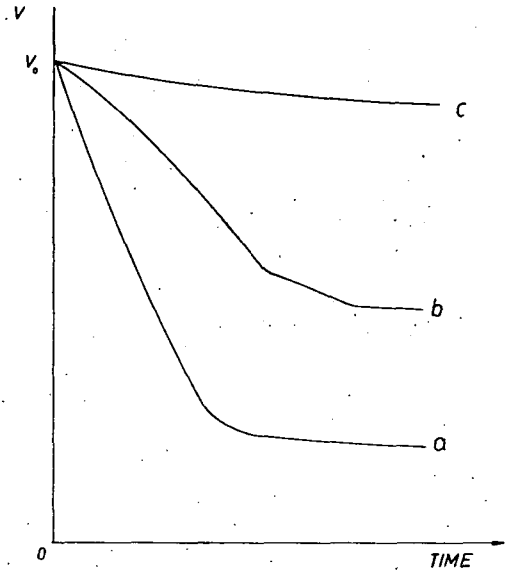

Fig. 1. Three general types of settling curves according to MICHAELS and BOLGER [15]

The behaviour of suspensions of intermediate concentration, the settling curves of which were of type *b*, was interpreted by MICHAELS and BOLGER using a network model of the aggregates. They found the central part of the curve to be linear; the corrected maximum settling rate, characterized by the slope of the straight, independent of the dimensions of the settling system, is

$$Q_1' = \frac{g(\varrho_s-\varrho_f)\Phi d_P^2}{32\eta}(1-C_{AF}\Phi_F). \tag{10}$$

In this equation d_P is the mean pore diameter in the network, $C_{AF} = \Phi_A/\Phi_F$, and Φ_F is the volume ratio of the flocs forming the aggregates relative to the volume of the suspension. The characteristics of the flocs can be determined by studying the sediment volume in detail. The corrections suggested in [15] can be obtained by studying the sedimentation of suspensions starting from different levels and in vessels of different size.

The above investigations on flocculated suspensions were, withouth exception, performed with aqueous suspensions. Simultaneously with the results of MICHAELS and BOLGER, as well as somewhat later, one of the present authors published results on the sedimentation rate of structured suspensions in organic media [18, 19] and described analogous sedimentation curves. Later on, we extended the evaluation method of MICHAELS and BOLGER to systematically coagulated aqueous kaolin

suspensions [20]. In a recent publication on suspensions of organophilic bentonite [21] the curves of type *b* were formally approximated by a hyperbolic tangent function with four parameters

$$V(t) = P\tanh(Nt+R)+S \tag{11}$$

where P, N, R and S are parameters of the function. In the same paper we presented a better fitting approximation by the function

$$V(t) = \frac{V_0+V_\infty\left(\frac{t}{t'}\right)^n}{1+\left(\frac{t}{t'}\right)^n} \tag{12}$$

where V_0 means the volume at $t=0$, $V(t)$ the actual settling volume, V_∞ the ultimate volume at $t=\infty$, and t' is given by the relation $V(t')=1/2\,(V_0+V_\infty)$. The meaning of n will not be considered here.

General description of the phenomenon of structured sedimentation

Suspensions settling with sharp interface may result from homodisperse systems containing particles of the same size, as well as from heterodisperse suspensions of semi-coherent structure. From a practical point of view, the latter are more important, because homodisperse suspensions are far more rarely found. A semi-coherent system can be formed *e.g.* from an aqueous suspension, if the adhesion between the particles is increased by an electrolyte. Namely, the ζ-potential of the electric double layer ensuring the stability of the suspension will decrease by the electrolyte, and thus coagulation may occur. The extent of coagulation can be controlled best by changing the concentration and valency of the ions. Polyelectrolytes can be also used as coagulants. In this case, besides the narrowing down of the double layer, it is very important that bounds of physical or chemical nature between the linear macromolecules and the solid particles may arise and so the particles become connected by the macromolecules. In this way, aggregates of very loose structure are formed.

In the case of suspensions in organic media, it is the lyophility of the particles which has the most important influence on stability. Between particles poorly wetted by the medium, adhesion will manifest itself and the particles become connected. The character of sedimentation both of aqueous and organic suspensions under given conditions will depend on the concentration of the suspension, a certain minimum of concentration being necessary for the forming of semi-coherent structure. At lower concentration a well observable interface will not develope. The concentration minimum necessary for obtaining a sharp interface crucially depends on the dispersity, the shape and interaction of the particles.

As an example, settling curves of aqueous sodium kaolinite suspensions of volume concentrations Φ, containing primary particles of diameter $d<2$ μm, are presented in Fig. 2. The coagulation occurs at a given electrolyte concentration. The aggregates easily disintegrate by mild shaking. In suspensions of different concentrations the following observations can be made during sedimentation.

At low concentrations, for a short time (some minutes) after shaking, practically no change can be observed in the system. Then the flocs appear simultaneously with the sharp interface which begins to sink rather quickly. Besides the settling, an upward streaming of the medium, carrying part of the flocs with the stream, can

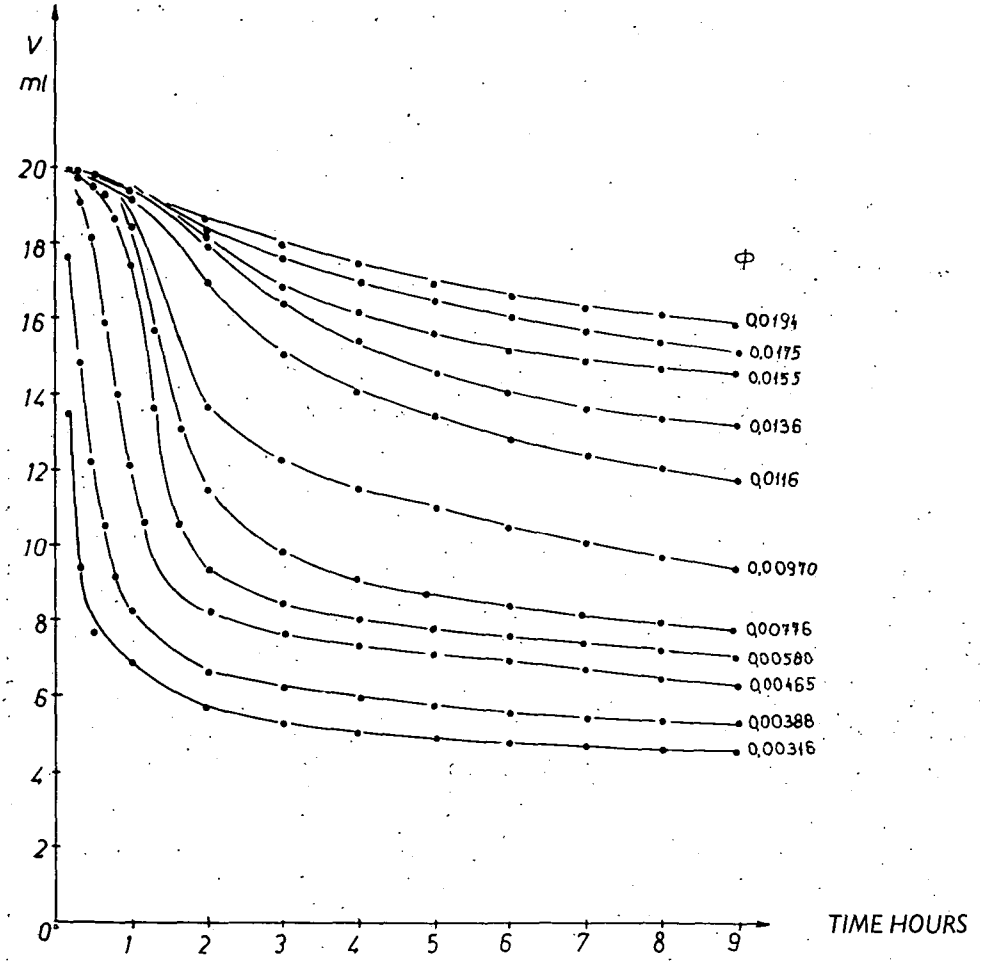

Fig. 2. Settling curves of sodium kaolinite suspensoins of different volume concentrations Φ, containing 19 mmole $CaCl_2$/l

be observed and the interface becomes diffuse. The perceptible upward streaming of the liquid ceases when the suspension becomes more concentrated due to the settling, and the sedimentation itself turns slower. Then the interface becomes sharper, more distinguished. In suspensions of intermediate concentration there is also a short time during which no change can be observed, then the sharp interface appears, but its sinking is slower. Meanwhile, visible inhomogenities (gaps and gross flocs) appear in the originaly homogeneous suspension. When this formation of

gaps can be observed in the whole suspension, fast sedimentation begins (Fig. 3). At the same time, the upward streaming of the medium can be observed and the interface becomes somewhat diffuse. The settling of the suspension progressing, the sediment formed becomes more compact and the process slows down. The visible upward streaming of the medium ceases, the interface between the sediment and the supernatant becomes sharper.

If the initial concentration of the suspension is further increased, then no period of fast sedimentation can be observed.

The picture of sedimentation in organic media is qualitatively similar if the particles are poorly wetted by the liquid, *e.g.* in the case of kaolin suspended in acetone (see Fig. 4).

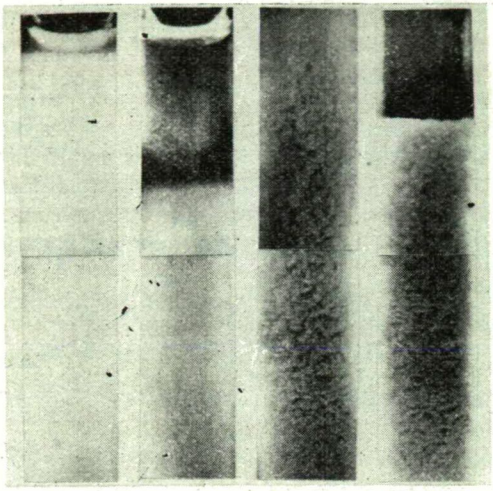

Fig. 3. Sodium kaolinite suspension in different phases of sedimentation. $\Phi=0.00388$, electrolyte concentration 50 mmole NaCl/l. *a* and *b*: upper part of the tube, *a:* at $t=5$ min; *b:* at $t=15$ min; *c* and *d*: lower part of the tube, *c:* at $t=22$ min; *d:* at $t=30$ min.

Three-section model

If the purpose is only numerical fitting of the settling curves, then several empirical formulas (*e.g.* the hyperbolic tangent function mentioned above) are available. In certain cases the different parameters calculated by this fitting may be used for characterizing the suspensions; it is, however, evidently difficult to find connections between these parameters and the structure of the suspensions.

In the following a model for describing the process is given. Though this model permits the evaluation of the curve only by sections, we hope that later we shall be able to obtain a unified equation by improving this model.

Let a suspension of volume V_0 and mass M, susceptible to sedimentation, be prepared in a test-tube of cross-section F. Let the shape of the settling curves measured at different concentrations $\Phi=M/V_0\varrho_s$ be corresponding to those of Fig. 1. Let $h(0)=h_0=V_0/F$ be the height of the interface at the time $t=0$, $Q=-dh/dt$ the sinking velocity of the interface plane, and $\varepsilon=1-\Phi$ the proportion of the free liquid.

In the case of comparatively low concentrations, the settling curve is similar to curve *a* in Fig. 1. At higher concentrations the sigmoid curve, characteristic for the sedimentation of structured suspensions, can be observed (see Fig. 1, curve *b*). For very high concentrations, the curve *c* shown in Fig. 1 is characteristic. It is important to observe that the values $h_\infty=h(\infty)$, pertaining to a series of increasing concentrations $\Phi_1<\Phi_2<\Phi_3$, often increase proportionally to M.

The particles may form aggregates already in dilute suspensions and, as this process involves "inclusion" of some liquid, a porosity $\varepsilon_A(<\varepsilon)$ will be characteristic for this system.

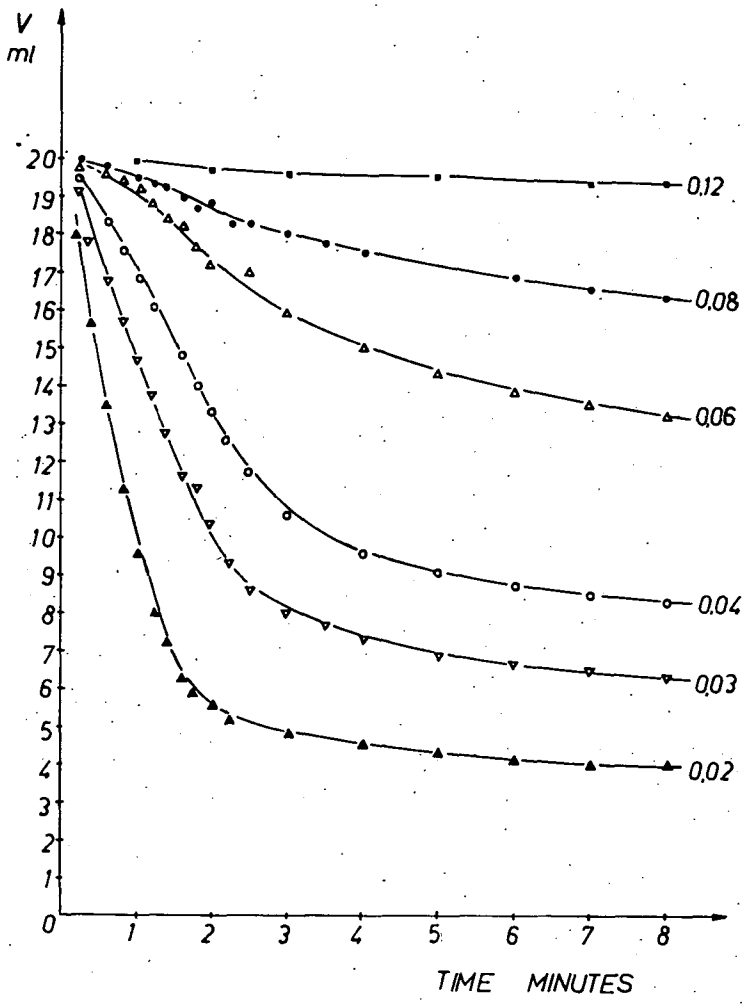

Fig. 4. Settling curves of non-fractionated kaolin suspensions of different volume concentrations Φ in acetone

Let us suppose that, in a certain concentration range (Φ_1, Φ_2) of the suspension, the aggregates form a semi-coherent structure. This condition can be characterized by a porosity $\varepsilon_s(<\varepsilon_A)$. The structure is not rigid; it "shrinks" under the influence of its own weight and, after a certain time, it "breaks down".

In the case of a given system, there is always a critical concentration Φ_2 above which coherent structures are formed. The sedimentation of such suspensions should be designed as "compression".

Based on this model, the types of settling curves shown in Fig. 1 can be interpreted as follows:

a) If $\Phi < \Phi_1$, then a state characterized by the porosity ε_A is formed. The settling rate is constant and proportional to the Stokes settling rate v_S of solid particles. The proportionality factor ε_A is a function of the porosity

$$Q = v_S f_1(\varepsilon_A). \tag{13}$$

In the settling phase, Φ is practically constant. The volume of the sediment settled at the bottom of the test-tube increases until the "quick" period of sedimentation is finished. The sediment volume is first proportional to $(1-\varepsilon_A)$, but it does not remain constant, because the sediment shrinks. For the shrinking a formula analogous to Eq. (3), or other similar relations can be applied:

$$Q = k(h - h_\infty). \tag{14}$$

b) If $\Phi_1 < \Phi < \Phi_2$, then a structure characterized by ε_s is formed. According to our assumption, this structure is similar to a coherent, soft filter bed and for the settling rate the equation

$$Q = v_S f_2(\varepsilon_s) \tag{15}$$

will be valid.

At the end of the "filtering" characterized above, the structure "breaks down", and the sedimentation of the aggregates proceeds according to Eq. (13); then the shrinking described by Eq. (14) can be observed.

c) If $\Phi > \Phi_2$, then only "compression" is to be observed; this can probably be described by Eq. (14).

From the above three cases, the curve of type *b*, shown separately in Fig. 5 is the most common. The ordinates delimiting the different parts of the curves (separating the sections of filtering, settling and compression) are h_1, h_2 and the corresponding abscissas are t_1, t_2. Under otherwise identical conditions it is always possible to find a concentration Φ for which t_1, is maximum. At this concentration the semi-coherent structure will be the most stable.

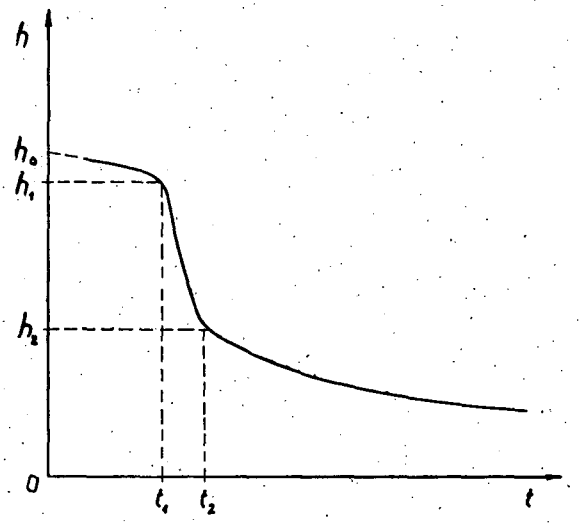

Fig. 5. Characteristic sections of a settling curve of type *b*

As a conclusion, this model indicates two critical points on the settling curve. Experimental investigation of the environment of these points is very important from a theoretical point of view. It is to be expected that by an exact description of these environments and of the deviations from the sections supposed to be linear in the model, it will be possible to find a formula permitting uniform characterization of the general settling curve. It seems that "fitting" of the values Q given by Eq. (13)—(15) might lead to such a formula if it were possible to express the respective variables as functions of the porosity. It seems favourable that an analogy between f_1 and f_2 can be found.

Some further conceptions

In our opinion, for the description of sedimentation, and of course also of the shrinking of more or less structured systems, a uniform method of description should be used. This follows chiefly from the conviction that the state of the system studied changes under the influence of external and internal forces, and the sedimentation in a given system can be considered as a motion due to gravitation. Of course, it cannot be sufficient to take into account only the external gravitational forces, as the formation of any structure points to the presence of considerable internal forces, too. Therefore it seems that a detailed investigation of the nature of these internal forces would lead to the desired result. In principale, the internal forces involved in the formation and preservation of the structure can be described with the means of modern physics. The units forming the system are, however, so different and their interactions so complex that this way does not seem practicable.

Up to now the efforts to give a complete description of the process do not seem to have been succesful. The above conception suggests, however, that a uniform way of description must exist. It is possible that the phenomenological aspect of the problem will become clear only after dividing the problem into parts and investigating these parts separately. But also in this case, a subsequent step, coordinating the description of the different parts, must exist. Namely, if a phenomenon can be approximated by dividing it into three partial processes, each of which is characterized by a parameter, then it can be tried to give a uniform description containing three parameters. Taking into account the necessary initial condition, four characteristic data will be needed. Similar efforts led to the formula given in Eq. (12), which satisfies the requirements mentioned above.

Comparing Eqs. (3) or (4), describing the shrinking phase, with Eq. (12) and approaching the latter for high values of t, the relation

$$V = V_\infty + (V_0 - V_\infty) \frac{1}{1 + \left(\frac{t}{t'}\right)^n} \tag{16}$$

can be obtained. The term e^{-kt} in Eq. (4) also tends to zero, though not in the same way, but similarly to $\left[1 + \left(\frac{t}{t'}\right)^n\right]^{-1}$. To decide the question as to in which way the factor of $(V_0 - V_\infty)$ approaches zero, further and more exact measurements will be necessary.

If our purpose is to give a complete phenomenological description of the process, a more general method has to be applied, because the movement in a complex system cannot be described by a single rate value. Therefore, it has to be supposed that the sinking velocity in the bulk of the settling system changes from point to point. Our objective should therefore be to find the equation of motion describing the field of velocity with the initial and boundary conditions determined by the experiment. The objective outlined earlier in this paper is only a part of this more general program, as its aim is only to describe the motion of the interface between the pure medium and the suspension.

Besides carrying out the total phenomenological program drawn up in the above, it will be necessary to raise the question of the microscopical interpretation of the phenomenon. This does not exclude the possibility of trying to find methods (see the three-section model), which describe directly the events occuring in the suspension. It will be certainly necessary to follow both ways.

References

[1] *Steinour, H. H.:* Ind. Eng. Chem. **36**, 618 (1944).
[2] *Richardson, J. F., W. N. Zaki:* Trans. Inst. Chem. Engrs. **32**, 35 (1954).
[3] *Garner, F. H., M. F. Mohtadi, C. W. Nutt:* Nature **172**, 259 (1953).
[4] *Bischoff, E.:* Kolloid-Z. **168**, 8 (1960).
[5] *Tuorila, P.:* Kolloid-Beih. **24**, 1 (1927).
[6] *Müller, H.:* Kolloid-Beih. **26**, 257 (1928).
[7] *Andersson, O.:* Svensk Paperstidn. **64**, 248 (1961).
[8] *Jovanovič, D. S.:* Kolloid-Z. **203**, 42, 48, 145 (1965).
[9] *Coe, H. S., G. H. Clevenger:* Trans. Am. Inst. Mining Engrs. **55**, 356 (1916).
[10] *Powers, T. C.:* Research Lab. Portland Cement Assoc., *Bull.* **2**, (1939).
[11] *Steinour, H. H.:* Ind. Eng. Chem. **36**, 840 (1944).
[12] *Steinour, H. H.:* Ind. Eng. Chem. **36**, 901 (1944).
[13] *Kozeny, J.:* Kulturtechniker **35**, 478 (1932).
[14] *Carman, P. C.:* J. Agr. Sci. **29**, 262 (1939).
[15] *Michaels, A. S., J. C. Bolger:* Ind. Eng. Chem. **1**, 24 (1962).
[16] *Smellie, R. H., V. K. La Mer:* J. Colloid Sci. **11**, 704 (1956); **12**, 230 (1957).
[17] *Gaudin, A. M., M. C. Fuerstenau:* Eng. Mining J. **159**, 110 (1958); Preprint. Intern. Mining. Proc. Congr. London, April 1960; Mining Eng. **11**, 613 (1959).
[18] *Szántó, F., S. Veres:* Acta Phys. et Chem. Szeged **8**, 151 (1962); **9**, 157 (1963).
[19] *Szántó F., F. Horkai, J. Czakó-Nagy:* Kolloid-Z. **201**, 136 (1965).
[20] *Gildéné Farkas M., F. Szántó:* Földtani Közlöny **99**, 60 (1969).
[21] *Szántó F., F. Gilde, E. Sipos:* Koll.-Z. u. Z. Polymere **250**, 683 (1972).

СЕДИМЕНТАЦИЯ СТРУКТУРИРОВАННЫХ СУСПЕНЗИЙ, I

Введение и некоторые общие положения

М. Гилде, Ф. Санто, К. Варга, Ф. Й. Гилде

В серии работ, посвященных исследованию седиментации структурированных суспензий, в данной статье рассматриваются основные положения по литературным данным. Представлены основные типы происходящих явлений. На основании литературных данных, создана модель из трех составляющих: оседания, фильтрации и уплотнения. Намечены пути дальнейших исследований.

ИССЛЕДОВАНИЕ СТРУКТУРЫ И РЕОЛОГИЧЕСКИХ СВОЙСТВ МНОГОКОМПОНЕНТНЫХ ЭМУЛЬСИОННЫХ СИСТЕМ, II

Реология и стабильность систем гомологического ряда кальциевых мыл предельных кислот—ксилол—вода

И. АНДОР,
Институт общей и физической химии университета им. Аттилы Йожефа, Сегед

Я. БАЛАЖ,
Кафедра коллоидной химии университета им. Аттилы Йожефа, Сегед

С. В. ФЕЛЬДМАН
Кафедра физико-химии полимеров университета им. И. И. Мечникова, Одесса

(Поступило в редакцию 16 января 1974 г.)

Исследованы структурно-механические свойства и стабильность систем мыло — ксилол — вода для кальциевых солей предельных монокарбоновых кислот с четным числом углеродных атомов от капроновой до стеариновой кислоты. Показана необходимость учета молярных, а не весовых концентраций мыл при рассмотрении реологических и других свойств исследуемых систем. Предложена и экспериментально показана целесообразность применения величины весового соотношения гидрофильных и липофильных частей молекул (СГЛ), представляющей возможность количественной оценки структурообразующих свойств мыл гомологического ряда в углеводородах. Проведено отнесение реологических параметров и показателей стабильности к молекулярным свойствам компонентов системы.

Несмотря на многочисленные исследования мылных смазок, теоретические основы подбора загустителя, оптимального для конкретного применения, до сих пор не созданы [1—4]. Между тем развитие техники требует как создания многофункциональных смазок, пригодных для широкого интервала температур, при высоких градиентах скорости сдвига и больших контактных напряжениях, так и смазок, обладающих оптимальными свойствами в определенных специфических условиях. Опыт применения мыльных смазок в процессах обработки металлов давлением и в ряде других случаев, свидетельствует о том, что наибольший интерес представляют именно эти смазки [5]. В последнее время при изготовлении смазок широко применяют индивидуальные жирные кислоты и их композиции. Это позволяет получать смазки с более воспроизводимыми свойствами, чем при использовании жирового сырья, состав которого сложнее. Производство и применение пластичных смазок, все же еще основываются главным образом на эмпирических результатах [6]. В литературе имеется много данных о характере структур мыльно-масляных

систем, однако, еще нет сведений о том, каким образом можно создать определенную требуемую структуру [7].

Чрезвычайно велика, хотя до сих пор мало изучена роль воды в смазках. Вода содержится в любых смазках и даже в небольших количествах нередко оказывает решающее влияние на их структуру и свойства [8, 9].

В предыдущем сообщении [10] нами было рассмотрено влияние интенсивности диспергирующего воздействия и времени созревания геля кальциевой соли лауриновой кислоты на его структурно-механические свойства и стабильность в эмульсионной системе мыло — ксилол — вода. Изучение свойств представителей гомологического ряда предоставляет особо благоприятные условия для изучения механизма возникновения структур и их течения в дисперсных системах и для интерпретации полученных результатов на молекулярном уровне.

Задача данной работы заключалась в определении влияния длины углеводородного радикала монокарбоновых предельных кислотных остатков кальциевых мыл на структурно-механические свойства и стабильность системы мыло — ксилол — вода.

Зкспериментальные результаты

Методика проведения опытов подробно описана нами ранее в работе [10]. В данной работе применялись жирные кислоты производства „Флука" марки „ч.д.а." Диспергирование систем производили в течение 5 минут при 4250 об/мин мешалки гомогенизатора. Реологические измерения с помощью ротационного вискозиметра проводили 10 минут спустя после приготовления системы. Во всех процессах и измерениях было осуществлено термостатирование с точностью до $\pm 0{,}2$ °С при температуре 25 °С.

В литературе нами не были найдены данные по систематическому исследованию реологических свойств мыльных систем гомологического ряда. В работах подобного характера авторы ограничивались рассмотрением разрозненных представителей рядов [8,11]. В тройных системах мыло — масло — вода, в которых вода находится в виде дисперсной фазы, на наш взгляд, особенно важно проведение исследования в широком интервале молекулярных весов для определения возможного влияния гидрофильно-липофильного баланса молекул мыла на структурообразование, реологические свойства и стабильность таких систем. Исходя из этого, нами было проведено изучение систем с кальциевыми солями предельных монокарбоновых кислот с четным числом атомов углерода от 6 до 18 углеродных атомов.

На рис. 1 представлены кривые течения систем с фазовым составом $\Phi_B = 0{,}14$ и $\Phi_K = 0{,}84$, приготовленных с равными весовыми концентрациями кальциевых мыл в системе 7,56 г/100 мл. Кривые течения представлены только нисходящей ветвью, поскольку не обнаружены отклонения от найденной ранее зависимости [10]. Как видно из данных рис. 1, для всех систем характерно течение обобщенных бингамовских тел. Все полученные нами кривые течения имели аналогичный характер, поэтому первичные данные в дальнейшем не приводятся.

На рис. 2 представлены величины предельных напряжений сдвига (τ_B)

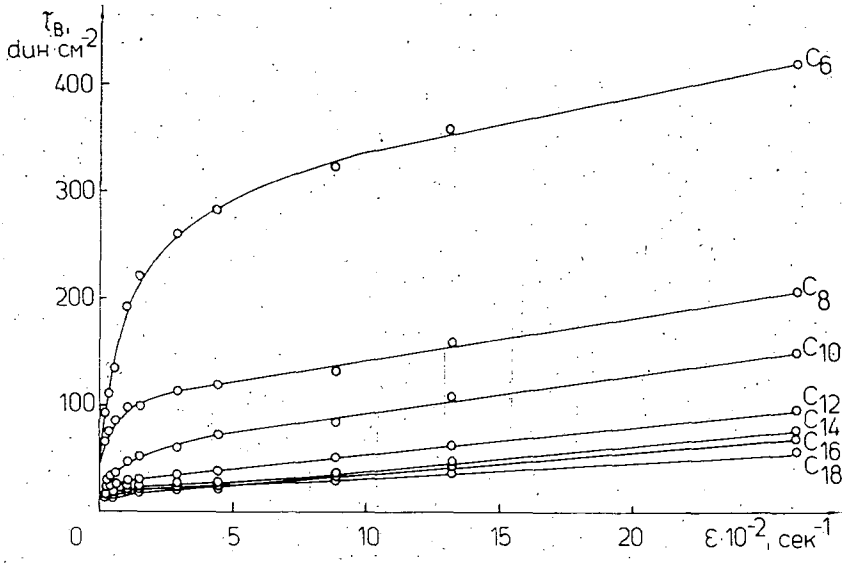

Рис. 1. Кривые течения систем мыло — ксилол — вода для кальциевых солей кислот гомологического ряда (C_n — число атомов углерода в кислоте)

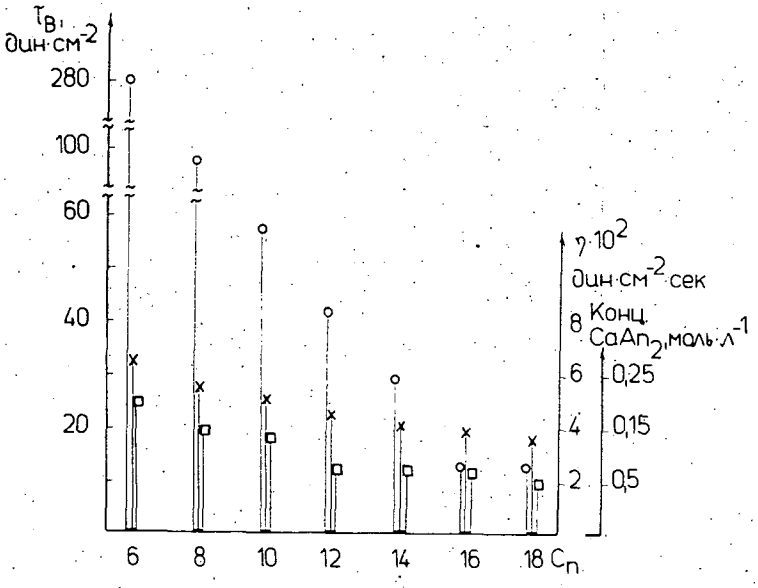

Рис. 2. Диаграмма предельного напряжения сдвига (τ_B) — ○ и пластической вязкости (η) — □ систем с кальциевыми мылами, при их концентрации 7,56 г/100 мл, для гомологического ряда кислот (C_n). Молярные концентрации мыл — ×

и пластических вязкостей (η) для систем с кальциевыми мылами с разным числом углеродных атомов в углеводородной цепи. Хорошо заметно, что при равной весовой концентрации мыл наблюдается резкое снижение бингамовского предельного напряжения сдига с увеличением длины углеводородной

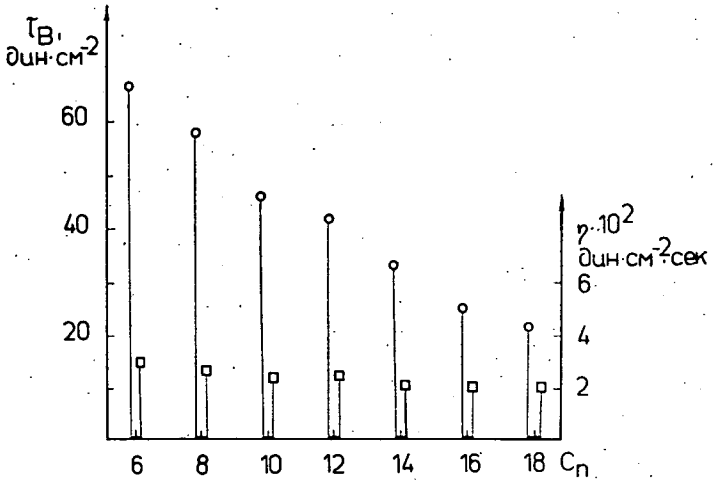

Рис. 3. Диаграмма предельного напряжения сдвига (τ_B) —○ и пластической вязкости (η) — □ систем с кальциевыми мылами, при их концентрации 0,17 моль/л, для гомологического ряда кислот (C_n)

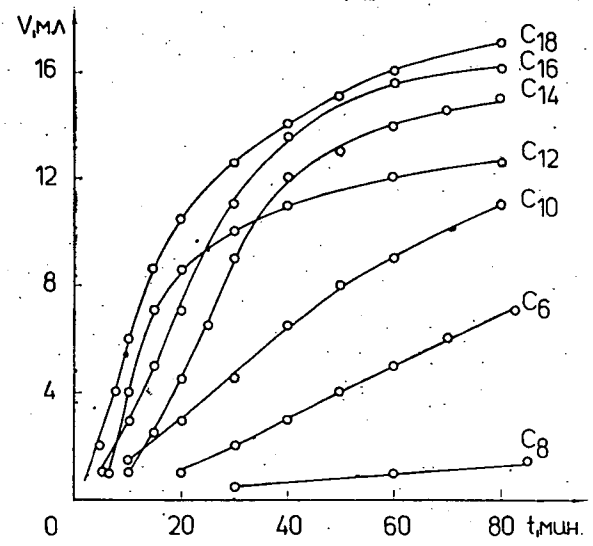

Рис. 4. Кинетика выделения ксилола из систем мыло — ксилол — вода для кальциевых солей кислот гомологического ряда при концентрации 1.75 г/100 мл, Φ_B=0,2, Φ_K=0,8 и $V_{общ}$=40 мл (C_n — число атомов углерода в кислоте)

цепи кислотного остатка. Значения величин пластической вязкости весьма малы — порядка нескольких сантипуазов —, но для первых членов изучаемого ряда достаточно явно выражена тенденция снижения η с увеличением длины углеводородного радикала мыла. Подобные зависимости наблюдаются в тех случаях, когда функциональные группы молекул играют основную роль в структурообразовании. При равной весовой концентрации мыл, количество функциональных групп в исследуемом интервале возрастает более чем в 2 раза с уменьшением молекулярного веса.

На рис. 3 представлены данные по предельным напряжениям сдвига и пластическим вязкостям для систем мыло — ксилол — вода, при равных молярных концентрациях кальциевых мыл. Из полученных данных следует, что пластическая вязкость, по-существу, незначительно меняется в изученных системах. В то же время бингамовское предельное напряжение сдвига снижается с удлинением углеводородной цепи в исследуемом ряду, примерно, в 3 раза. Эти данные показывают, что между реологическими и молекулярными

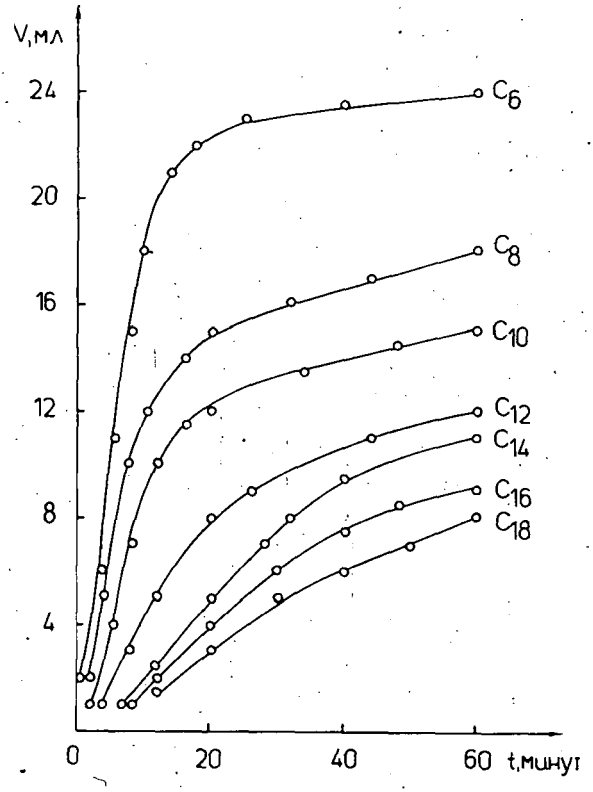

Рис. 5. Кинетика выделения ксилола из систем мыло — ксилол — вода для кальциевых солей кислот гомологического ряда при концентрации 0,04 моль/л, $\Phi_в=0{,}2$, $\Phi_к=0{,}8$ и $V_{общ}=40$ мл (C_n — число атомов углерода в кислоте)

свойствами изучаемой тройной системы нет столь простой зависимости как в тех случаях, когда какое-нибудь свойство системы определяется только числом функциональных групп.

Для выяснения характера взаимодействия между компонентами системы и установления закономерностей возникновения элементов структуры, ценные данные можно получить при изучении характера и кинетики процесса разделения фаз, т. е. стабильности системы. С этой целью нами были изучены системы, полученные аналогичным предыдущим методом, однако, для получения данных о возникновении структур необходимо было применение концентраций мыла, при которых не образуются сплошные структурные каркасы в системах ни с одним из изучаемых мыл. На рис. 4 и 5 представлены кинетики отделения масляной фазы в системах при равных весовых и молярных концентрациях мыл, соответственно. Весьма примечательно, что гомологический ряд дает противоположную зависимость в этих двух случаях. Исключение представляет только система с капронатом кальция при равных весовых концентрациях (рис. 4).

Изученные системы с точки зрения устойчивости представляют еще одну особенность: вода, кроме гидратирующей входящей в структуру мыла, как вторая жидкая фаза системы, во всех случаях (за исключением с капронатом кальция) отделялась сразу после прекращения перемешивания. Таким образом, для сравнения стабильности систем в отношении выделения водной фазы мы могли воспользоваться только полными объемами отделившейся воды. Для

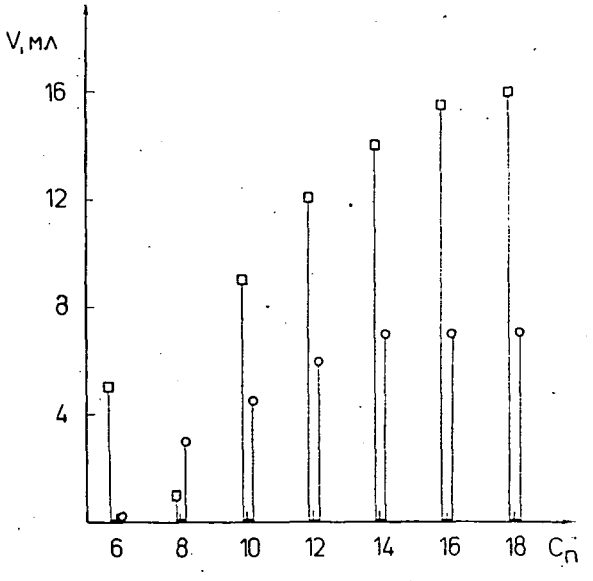

Рис. 6. Диаграмма неустойчивости (V мл выделившейся фазы) систем с кальциевыми мылами (конц. =1,75 г/100 мл) для гомологического ряда кислот (C_n): ксилол — □, вода — ○

количественного сравнения устойчивости систем в отношении выделения масляной фазы, мы пользовались объемами отделившегося ксилола за 1 час. Полученные экспериментальные данные представлены на рис. 6 и 7.

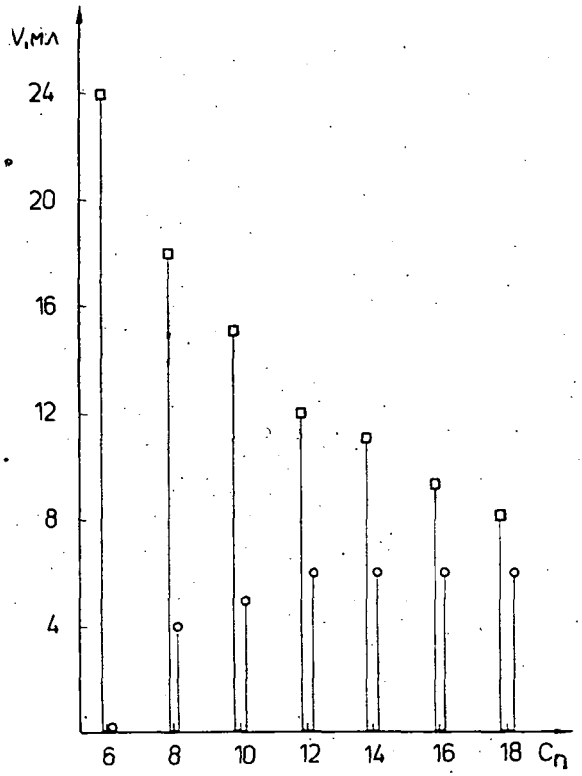

Рис. 7. Диаграмма неустойчивости (V мл выделившейся фазы) систем с кальциевыми мылами (конц. = 0,04 моль/л) для гомологического ряда кислот (C_n): ксилол — □, вода — ○

Обсуждение результатов

Установление механизма возникновения структур и их разрушения при течении на молекулярном уровне является одной из наиболее важных и интересных проблем реологии дисперсных систем. Как известно, структурно-механические свойства характеризуют возникновение в системе структур различного вида. В некоторых ранних работах [12] указывалось, что для построения молекулярной теории течения структурированных систем необходимо пользоваться эффективной вязкостью, как величиной, отражающей всю сложность процесса течения с той или иной степенью разрушения структуры, в равновесных условиях стационарного потока. За бингамовскими параметрами приз-

навалось их большое феноменологическое значение в расчетном аппарате теории пластичности и пластично-вязкого потока. Однако, со все более широким развитием исследований в области физико-химической механики дисперсных систем большинство авторов [13] стало пользоваться бингамовскими параметрами, как имеющими определяющее значение для характеристики реологического поведения вязко-пластичных тел. Так, например, в работах [8,14] отмечается, что сопротивление системы течению слагается из составляющих: сопротивления разрушению струрного каркаса и разрыву отдельных частиц дисперсной фазы (прочность структуры — τ_B); вязкого сопротивления течению дисперсионной среды и сопротивления создаваемого потоком частиц дисперсной фазы и обломками структурного каркаса (вязкость системы — η_B).

В работе [10] нами было показано, что в исследованной системе лаурат кальция — ксилол — вода предельное напряжение сдвига (τ_B), при прочих равных условиях, определяется дисперсностью структурообразующих элементов, а пластическая вязкость (η) в основном природой и силами взаимодействия, составляющих систему компонентов. Таким образом очевидно, что для систем, подчиняющихся закономерностям течения обобщенных вязко-пластичных тел, анализ экспериментальных данных по бингамовским параметрам представляет возможность получения наиболее достоверных сведений о характере имеющихся структур.

При изучении мыльно-масляных систем большую трудность составляет то обстоятельство, что при их изготовлении обычно образуются связи как кристаллизационного, так и коагуляционного характера. Последние имеют значительно меньшую прочность, примерно в 20 раз [15], чем кристаллизационные. При реологических испытаниях вязко-пластичных систем пространственная сетка в объеме, занятым стационарным потоком, оказывается разрушенной во все большей и большей степени, однако, такое разрушение никогда не доходит до конца [12]. Вследствие этого, получение достаточно достоверных количественных данных, позволяющих произвести отнесение реологических параметров к определенным элементам структуры, весьма затруднено. Принятая нами методика получения структурированной тройной системы, способом образования мыла на границе раздела фаз эмульсии в изотермических условиях, позволяет рассматривать структуры в отсутствие кристаллизационных связей, возникающих при обычных методах приготовления, когда структурный каркас образуется при охлаждении истинно растворенного в масляной фазе мыла, т. е. при кристаллизации. Наличие одних только коагуляционных контактов в наших системах обеспечивает получение более простых экспериментальных зависимостей и значительно облегчает их интерпретацию. Вследствие этого появляется возможность наметить вероятный механизм возникновения и течения структур в таких тройных системах мыло — масло — вода.

Из данных рис. 1 видно, что тройная система мыло — ксилол — вода, при изученной концентрации кальциевых мыл (7,56 г/100 мл) исследуемых кислот, имеет кривые течения характерные для обобщенных бингамовских тел в интервале градиентов скорости от 16,2 до 2620 сек$^{-1}$. Это показывает, что и следовало ожидать, что в гомологическом ряду мыл одного металла, возникающие структуры имеют одинаковую природу и, следовательно, аналогичный

характер течения. Однако, обращает на себя внимание непропорционально высокое значение τ_B в системе с капронатом кальция.

При равной весовой концентрации мыл предельное напряжение сдвига с увеличением молекулярного веса мыла снижается (рис. 2). Это свидетельствует о том, что основным структурообразующим элементом в этих системах являются полярные группы мыл. К такому же выводу приходили авторы в работах [16,17] на основании изучения влияния добавок солей на структурообразование в мыльных псевдогелях и по данным теплот адсорбции углеводородов на мылах. Все же прямой корреляции между прочностью структуры и количеством полярных групп нет, как это видно также из данных рис. 2, на котором приведены рассчитанные молярные концентрации соответствующих мыл. Непосредственную экспериментальную проверку роли полярных групп в структурах можно провести при реологическом изучении систем с равными молярными концентрациями мыл. В таком случае, если связи структуры строились бы по всем наличным полярным группам, следовало бы получить независимость прочности структуры от молекулярного веса. Данные рис. 3 показывают, что τ_B в случае равных молярных концентраций мыл снижается при удлинении цепи углеводородного радикала мыла, хотя в значительно меньшей мере, чем это наблюдалось при равных весовых концентрациях.

Из общей теории структуры мыльно-масляных псевдогелей известно [9, 18, 19], что мыльные кристаллиты (фибриллы) составляют основу структурного каркаса. Ввиду того, что углеводородные цепи обладают значительным сродством к ароматическим углеводородам [20, 21], коагуляционные связи могут возникнуть в наших системах в основном только за счет полярных групп, находящихся на гранях кристаллитов мыла. Из этого следует, что только определенная доля полярных групп может участвовать в создании структурной сетки системы. При этом само собой разумеется, что дисперсность и анизодиаметричность частиц мыльной фазы приобретает большое значение [22]. В работе [23] было показано, что в гомологическом ряду металлического мыла в ароматическом углеводороде число агрегаций при образовании мицелл уменьшается незначительно с увеличением длины цепи. Если к этому учесть структуру кристаллитов мыл [9,24], то становится очевидным, что дисперсность и анизодиаметричность частиц должна быть тем большей, чем меньше длина углеводородной цепи мыла. Естественно, с увеличением дисперсности и анизодиаметричности частиц возрастает вероятность образования коагуляционных контактов и возрастает прочность возникающих структур [8].

Рассматривая пластическую вязкость систем, данные рис. 2 указывают на непосредственную связь между молярной концентрацией мыла и пластической вязкостью в серии опытов с равными весовыми концентрациями мыл. В таком случае, при равных молярных концентрациях должно наблюдаться постоянство пластической вязкости в гомологическом ряду мыл. Данные рис. 3 показывают хорошее совпадение этих представлений с полученными экспериментальными данными, т. е. наличие постоянства пластической вязкости. Небольшие отклонения результатов объясняются экспериментальными ошибками, возникающими прежде всего вследствие того, что при высоких прочностях структур в условиях наших опытов (область измерений для экстрапо-

Таблица I

Сводные данные систем, изученных в реологических испытаниях

1	2	3	4	5		6		7	8	9	10	11	12
Тривиальное название мыла	C_n кисл.	Мол. вес кислоты	Мол. вес мыла	Концентр. весов. сер.		Концентр. моляр. сер.		СГЛ	τ_B дин/см² мол. сер.	τ_B дин/см² вес. сер.	$\eta \cdot 10^2$ из мол. сер.	$\eta \cdot 10^2$ из вес. сер	$\frac{\tau_B}{\text{СГЛ}} \cdot 10^{-2}$
				моль/л	г/100мл	моль/л	г/100мл						
Ca-капронат	6	116.16	270.40	0.28	7.56	0.17	4.66	0.66	65.6	283	2.9	4.9	1.0
Ca-каприлат	8	144.22	326.42	0.23	7.56	0.17	5.64	0.50	57.4	98.0	2.5	3.8	1.1
Ca-капринат	10	172.27	382.62	0.20	7.56	0.17	6.60	0.39	45.1	57.4	2.3	3.6	1.2
Ca-лаурат	12	200.32	438.72	0.17	7.56	0.17	7.56	0.33	41.0	41.0	2.3	2.3	1.2
Ca-миристат	14	228.32	494.72	0.15	7.56	0.17	8.55	0.28	32.8	28.7	1.9	2.3	1.2
Ca-пальмитат	16	256.43	550.86	0.14	7.56	0.17	9.50	0.24	24.6	12.3	1.9	2.3	1.0
Ca-стеарат	18	284.48	607.04	0.12	7.56	0.17	10.5	0.22	20.5	12.3	1.9	1.8	0.9

ляции от 880 до 2620 сек$^{-1}$) не достигается еще необходимое разрушение структуры. В результате этого экспериментально получаются несколько заниженные значения τ_B и завышенные η, в тем большей мере, чем выше прочность изучаемой структуры. Наличие количественной связи между платической вязкостью и молярной концентрацией мыл свидетельствует о том, что при течении этих систем основное влияние на величину вязкости имеют сильно взаимодействующие полярные группы мыл. Из этого следует, что после разрушения сплошного структурного каркаса вязкость системы определяется природой компонентов системы: вязкостью жидких фаз, количеством и характером мест твердой дисперсной фазы, способных образовать коагуляционные контакты. Влияние размера и формы первичных частиц в установившемся стационарном потоке, по-видимому, имеет второстепенное значение.

Нам представлялось весьма заманчивым попытатсья найти подобную количественную связь между полученными экспериментальными данными по предельным напряжениям сдвига структур и параметрами, которыми могут характеризоваться исследуемые мыла. В таблице I представлены основные данные по изученным мыльным системам. По данным табл. I можно сделать ряд заключений, кроме обсужденных уже выше вопросов. Весьма примечательно, что в опытах при равных молярных концентрациях мыл (столбец 6) их весовая концентрация, и соответственно объемное заполнение, по исследуемому интервалу возрастает более чем в 2 раза, но, несмотря на это, как τ_B, так и η уменьшаются (стб. 8 и 10). Для количественной характеристики наблюдаемой зависимости предельного напряжения сдвига при равных молярных концентрациях мыл, на наш взгляд, можно предложить величину (стб. 7), получаемую при расчете весового соотношения гидрофильной группы мыла (4 атома кислорода + атом кальция) к липофильной части (углеводородные цепи) молекул (СГЛ). Величина СГЛ представляет собой своеобразный гидрофильно-липофильный баланс мыльных молекул. То обстоятельство, что величины τ_B (стб. 8), отнесенные к величине СГЛ дают значения, по-существу, постоянные $(1 \pm 0{,}2) \cdot 10^2$ (стб. 12), показывает, что СГЛ можно рассматривать как коэффициент, соответствующий доле полярных групп, способных участвовать в образовании коагуляционных контактов структуры. Как уже указывалось выше, эта доля полярных групп, в результате строения молекул и кристаллитов мыл, должна уменьшаться в гомологическом ряду с увеличением молекулярного веса. По-видимому, в соотвествии с этим наблюдается уменьшение предельных напряжений сдвига в системах мыло — ксилол — вода (стб. 8).

К описанным реологическим испытаниям нами были подобраны ранее [25] такие соотношения компонентов, которые позволили получение достаточно устойчивых систем при проведении реологических испытаний для всех изучаемых мыл. Мы стремились при этом применить невысокие концентрации мыла, поскольку в менее концентрированных системах более явно проявляются и легче обнаруживаются основные закономерности образования и течения структур в дисперсных системах [26].

Весьма значительным в теоретическом и практическом отношениях является вопрос так называемой „коллоидной стабильности" мыльных систем, т. е. устойчивости системы во времени против процесса макроскопического разделения фаз. При изучении этого явления можно получить весьма

ценные сведения о свойствах системы и о взаимодействии ее компонентов, особенно при отсутствии сплошной пространственной структуры, наличие которой значительно усложняет происходящие процессы. Аналогично предыдущим реологическим опытам, изучение стабильности было проведено по двум сериям: при равных весовых (1,75 г/100 мл) и молярных (0,04 моль/л) концентрациях мыл в системах (табл. II). Такие системы в сильной мере агрегативно и седиментационно неустойчивы и удобно следить за происходящими в них процессами самопроизвольного разделения фаз.

Кинетика выделения ксилола во всех случаях (рис. 4 и 5) показывает обычный ход интегральных кривых накопления при седиментации. Однако, весьма примечателен факт противоположного изменения скорости выделения ксилола в гомологическом ряду кальциевых мыл в сериях при равных молярных и равных весовых концентрациях. Возрастание устойчивости системы с удлинением углеводородной цепи в молярной серии (рис. 7), легко объясняется влиянием изменений лиофильности [20, 21] и повышением весовой концентрации дисперсной фазы (табл. II, стб. 4).

Таблица II

Сводные данные систем, изученных в испытаниях по устойчивости

1	2	3		4		5	6	7
Тривиальное название мыла	C_n кисл.	Концентрации весовой сер.		Концентрации молярн. сер.		СГЛ	V ксил. мл	V/СГЛ
		моль/л	г/100мл	моль/л	г/100мл			
Ca-капронат	6	0.065	1.75	0.04	1.08	0.66	24	36.4
Ca-каприлат	8	0.054	1.75	0.04	1.30	0.50	18	36.0
Ca-капринат	10	0.045	1.75	0.04	1.53	0.39	15	38.5
Ca-лаурат	12	0.040	1.75	0.04	1.75	0.33	12	36.4
Ca-миристат	14	0.035	1.75	0.04	1.98	0.28	11	39.4
Ca-пальмитат	16	0.032	1.75	0.04	2.20	0.24	9	37.5
Ca-стеарат	18	0.029	1.75	0.04	2.43	0.22	8	36.3

Найденную экспериментально звисимость выделения ксилола в гомологическом ряду при равных весовых концентрациях (рис. 6), на наш взгяд, можно объяснить изменениями структурообразующих свойств, мыл. При самопроизвольном отделении фаз друг от друга происходит седиментация крупных структурированных агрегатов мыла. Размеры этих агрегатов и их разветвленность (рыхлость) тем больше, чем больше склонность к структурообразованию у соответствующих мыл и, наборот, тем меньше скорость разделения фаз. Как уже указывалось нами, количество коагуляционных контактов зависит от молярной концентрации, следовательно, с уменьшением молекулярного веса мыла, при равных весовых концентрациях, возрастает структурообразование и стабильность в системах.

Ценные сведения о структуре изученных систем дали наблюдения за выделением водной фазы при отсутствии сплошного структурного каркаса мыла. Проследить кинетику выделения воды не было возможности ввиду немедлен-

ного появления почти всего количества воды на дне сосуда, в котором производилось диспергирование системы. Как известно [9], часть воды входит в структуру мыльных кристаллитов, остальная же часть находится в диспергированном состоянии в виде эмульсии в масле. Факт немедленного выделения диспергированной доли воды и данные рис. 7 могут объясняться тем, что в системах с мылами, имеющими 24 углеродных атома и более, не образуется защитного адсорбционного слоя на капельках воды. В этих случаях вода остается в виде эмульсии только в том случае, если сплошное структурообразование в системе удерживает ее механическими силами в таком виде. Устойчивая обратная эмульсия воды в ксилоле в обычном смысле образовалась только в присутствии капроната кальция. В этом случае, за время наблюдения (48 часов) не обнаруживалось выделение воды в сплошную фазу, но ксилол выделялся несколько быстрее ожидаемого, вследствие седиментации не коалесцирующих капелек воды (рис. 4 и 6). Каприлат и капринат кальция образуют весьма слабый защитный адсорбционный слой (рис. 6 и 7). Таким образом, особенности реологического поведения системы с капронатом кальция становятся понятными: образование эмульсии воды в ксилоле, защищенной достаточно прочным адсорбционным слоем мыла, изменяет условия структурообразования в системе, что наиболее ярко проявилось при равных весовых концентрациях мыл (рис. 2).

Выделение ксилола в серии опытов при равных молярных концентрациях (табл. II, стб. 6) отнесенное к рассчитанным величинам СГЛ (стб. 5) дает аналогичную закономерность постоянства соотношения 38 ± 2 (стб. 7), как это наблюдалось нами для предельных напряжений сдвига (табл. I, стб. 12). Эти данные свидетельствуют о тесной связи структурообразования и стабильности мылно — масляных систем. Наши данные находятся в хорошем согласии с литературными [27], согласно которым в присутствии стеарата лития в масле, увеличение дисперсности и анизодиаметричности частиц приводит к возрастанию предела прочности и коллоидной стабильности системы.

Таким образом, можно прийти к заключению, что в системах кальциевых мыл — ксилол — вода, полученных в изотермических условиях, основным структурообразующим элементом, обусловливающим реологическое поведение и стабильность систем, являются коагуляционные связи полярных групп. Их общее количество и доля способная к образованию коагуляционных контактов изменяются в гомологическом ряду мыла при равном весовом содержании его в системах. В соответствии с этим при реологических и других испытаниях необходимо учитывать прежде всего молярную концентрацию мыл. Весьма пригодной величиной характеристики структурообразующих свойств мыл в углеводородах является, предложенная и проверенная экспериментально, величина СГЛ.

Низшие гомологи кальциевых мыл способны образовать защитный адсорбционный слой на каплях эмульсии воды в масле, что резко отражается на коллоидной стабильности и структурно-механических свойствах тройных систем мыло — масло — вода. Полученные закономерности изменений реологических параметров в гомологическом ряду кальциевых мыл в значительной мере определяются взаимодействием масляной фазы и мыл, следовательно, в углеводородных средах другой природы будут отличаться от найденных для ксилола.

Литература

[1] Сборн.: Трение и граничная смазка, Изд. ИЛ. Москва. 1953.
[2] *Braithwaite, E. R,* Editor: Lubrication and Lubricants, Elsevier Publ. Comp., Amsterdam--London-New York, 1967.
[3] *Синицын В. В.:* Подбор и применение пластичных смазок, Изд. Химия, Москва. 1969.
[4] *Кокрофт М. Г.:* Смазка и смазочные материалы, Изд. Металлургия, Москва. 1970.
[5] *Курчик Н. Н., В. В. Вайншток, Ю. Н. Шехтер:* Смазочные материалы для обработки металлов резанием, Изд. Химия, Москва, 1972, стр. 172.
[6] *Горенштейн М. М.:* Трение и технологические смазки при прокатке, Изд. Техника, Киев. 1972.
[7] *Vámos E., X. Liebl:* Magy. Kém. Lapja **23,** 694 (1968).
[8] *Фукс И. Г.:* Пластичные смазки, Изд. Химия, Москва. 1972.
[9] *Трапезников А. А., Е. М. Шлосберг:* Коллоидн. ж. **8,** 421 (1946).
[10] *Андор И., Я. Балаж:* Acta Phys. et Chem. Szeged **19,** 103 (1973).
[11] *Трапезников А. А., Г. В. Белугина, Ф. М. Ржавская:* Коллоидн. ж. **20,** 254 (1958).
[12] *Михайлов Н. В., П. А. Ребиндер:* Коллоидн. ж. **17,** 107 (1955)
[13] *Vámos E., Mózes Gy., Fehérvri A.:* Magy. Kém. Lapja **22,** 445 (1967).
[14] *Овчаренко Ф. Д., С. П. Ничипоренко, Н. Н. Круглицкий, В.Ю. Третинник:* Исследования в области физико-химической механики дисперсий глинистых минералов, Изд. Наукова думка, Киев. 1965, стр. 35.
[15] *Сегалова Е. Е., П. А. Ребиндер:* Коллоидн. ж. **10,** 223 (1948).
[16] *Трапезников А. А., Г. В. Белугина:* Докл. АН СССР **94,** 97 (1954).
[17] *Groszek A. J.:* Magy. Kém. Lapja **23,** 302 (1968).
[18] *Lawrence, A. C.:* Trans. Faraday Soc. **34,** 660 (1938).
[19] *Freund M., Helzler L., Pallay I., Vámos E.;* Ásványolajipar IV. (Нефтяная промышленность IV.) Kenőanyagok, parafin, bitumen, Nehézipari Könyvkiadó, Budapest, 1953.
[20] *Демченко П. А., А. В. Думанский, Л. Г. Демченко:* Коллоидн. ж. **14,** 164 (1952).
[21] *Шинода К., Т. Накагава, Б. Тамамуси, Т. Исемура:* Коллоидные поверхностно-активные вещества, Изд. Мир, Москва, 1966, стр. 109.
[22] *Синицын В. В., Ю. Л. Ищук, Б. Н. Картинин:* Коллоидн. ж. **27,** 264 (1965).
[23] *Nelson, S. M., R. C. Pink;* J. Chem. Soc. **1952,** 1744.
[24] *Солнышкин В. И.:* Коллоидн. ж. **19,** 736 (1957).
[25] *Andor J., V. Feldman, A. Balassiné-Benyus;* 10th Symposium on Colouristics, Eger. 1973, p. 87.
[26] *Мирза-Абдуллаева О., Г. В. Белугина, С. Х. Закиева,* П. А. Ребиндер: Коллоидн. ж. **31,** 97 (1969).
[27] *Синицын В. В., К. И. Климов, Е. В. Алеева:* Коллоидн. ж. **22,** 469 (1960).

INVESTIGATION OF THE STUCTURE AND RHEOLOGICAL CHARACTERISTICS OF MULTICOMPONENT EMULSION SYSTEMS

Rheological and Stability Studies in Systems of Calcium Soaps of the Homologous Series of Saturated Monocarboxylic Acids, Xylene and Water

J. Andor, J. Balázs and *S. V. Feldman*

Rheological properties and stability of soap—xylene—water systems of calcium salts of saturated carboxylic acids with even carbon numbers from caproic acid to stearic acid were studied. The necessity of using molar concentrations instead of weight concentrations for the characterization of systems in rheological and other studies is demonstrated. The usage of the weight ratio of the hydrophilic and lypophilic parts (RHL) is justified and recommended for quantitative characterization of the structure forming power of soaps of the homologous series in hydrocarbons. The rheological parameters and the characteristics of stability are interpreted in terms of molecular properties.

NITRIERUNGSVERSUCHE AM BANDREAKTOR

Von

M. SZABÓ, L. MÉSZÁROS und Z. URBANICS

Institut für Angewandte Chemie der Attila-József-Universität Szeged

(Eingegangen am 20. November 1973)

Von unseren im Laufe der letzten Jahre ausgearbeiteten Reaktortypen kann der Bandreaktor durch Vergößerung aus dem Fadenreaktor entwickelt werden. Während der Fadenreaktor für mikropräparative Zwecke im Laboratoriumsmaßstab brauchbar ist, sind die Band- und Gardinenreaktoren für präparative Laboratoriums- und Betriebszwecke geeignet. Betrieblich finden sie derzeit bei der Erzeugung organischer Phosphorsäureester und Kohlensäureester Verwendung.

In dem vorliegenden Artikel wird die Verwendbarkeit des Bandreaktors bei der Nitrierungsreaktion im Falle von Benzol und Toluol beschrieben.

Band- bzw. Gardinenreaktor

Aus dem Fadenreaktor [1] können nach dem einfachsten Vergrößerungsprinzip, mittels Planparallelisierung [2], Band- bzw. Gardinenreaktoren entwickelt werden [3].

Durch Vergrößerung der Breite des Bandes nimmt die produzierbare Materialmenge fast proportional der Oberflächenvergrößerung zu, während in Längsrichtung die lineare Vergrößerung natürlich nicht anwendbar ist.

Das Hauptelement unseres Bandreaktors (Abb. 1) ist das 120 cm lange, 5 cm weite, doppelwandige Glasrohr, in dessen Achse das über eine große Oberfläche verfügende Band aufgehängt ist. Das Material des Bandes kann den Ansprüchen bzw. Forderungen gemäß gewählt werden; in Betracht kommen Glas, Quarz, Keramik, Metall, Baumwolle oder zwischen Glasplatten gepreßte Glaswolle. Dem Reaktorkörper schließen sich oben die Dosierer an. Das Auftragen der Reaktionskomponenten auf das Band ist durch einfaches Auftropfen oder durch Zerstäubung möglich [4].

Durch Verbreiterung das Bandes gelangen wir zum Gardinenreaktor. Die Vergrößerung des Gardinenreaktors kann durch parallele Aneinanderkoppelung der einzelnen Elemente geschehen (Abb. 2). Die Wärmeableitung wird durch die zwischen den in Abständen von einigen cm angebrachten Gardinen zirkulierende Quer- oder Gegenstromluft gesichert. Die Reaktionskomponenten werden am zweckmäßigsten durch Zerstäubung auf den oberen Gardinenanteil auftragen. Der Bandreaktor gehört zur Familie der Filmreaktoren und ist so außer für chemische Reaktionen für alle Zwecke verwendbar, für die Benutzung von Filmreaktoren in Betracht kommen kann.

Nitrierung von Benzol und Toluol am Bandreaktor

Die Nitrierung ist eine Reaktion, zu deren Durchführung der Filmreaktor besonders geeignet ist. Die Reaktion wurde früher in Riesel- wie auch in Rotations-Filmreaktoren studiert [5, 6]. Der große Vorteil unseres Bandreaktors gegenüber den früheren Riesel-Reaktoren liegt in seiner einfachen Konstruktion.

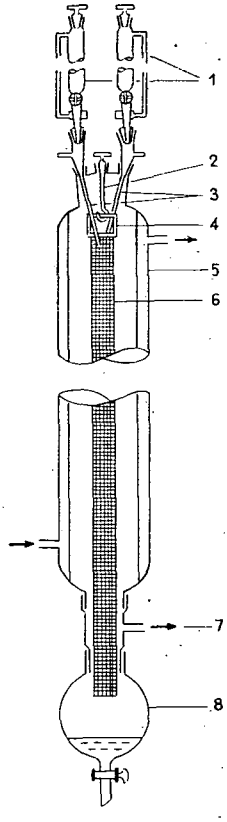

Abb. 1. Bandreaktor: 1: Dosierer; 2: Glashaken zum Aufhängen des Bandes; 3: Glasstümpfe zur Beschickung des Bandes mit Reaktionskomponenten; 4: Glasrahmen zum Aufhängen des Bandes; 5: Doppelwandiger Reaktorkörper aus Glas; 6: Glasband; 7: Öffnung zumAbführen der freiwerdenden Gase; 8: Sammelkolben mit Ablaßhahn

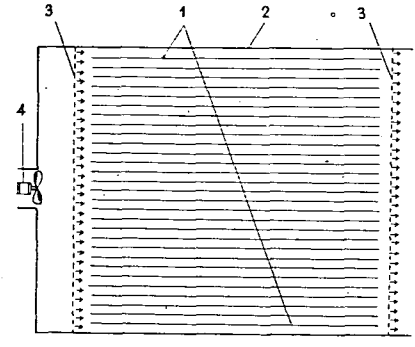

Abb. 2. Gardinenreaktor: 1: Gardinen aus Glasgewebe; 2: Reaktor; 3: Öffnungen für Luftzirkulation; 4: Ventillator

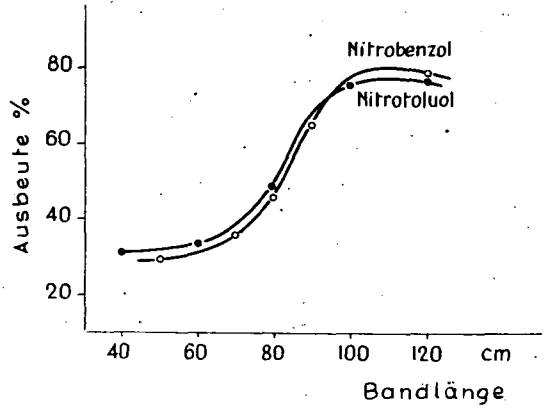

Abb. 3. Abhängigkeit der Produktion von der Bandlänge bei Benzol- und Toluolnitrierung

In unseren Versuchen haben wir die Wirkung der die Produktion beeinflussenden Parameter: der Bandlänge und der Dosierungsgeschwindigkeit, am Beispiel der Benzol- und Toluolnitrierung studiert.

Das im Reaktor verwendete Glasgewebe war 4,5 cm breit und enthielt pro Quadratzentimeter 6 Längs- und 8 Querfäden. Die Reaktionen wurden bei Raumtemperatur durchgeführt. Mit den Messungen wurde in jedem Falle erst begonnen, wenn der stationäre Zustand im Reaktor und am Band erreicht war, d.h. aus dem Reaktor ein dem thermodynamischen Gleichgewicht entsprechend zusammengesetztes Gemisch abging (nach 15—20 Minuten).

Der schnelle Abbruch der Reaktion wurde durch Auffangen des nitrierten Produkts in Eiswasser gelöst. Bei der Benzolnitrierung untersuchten wir den Mono- und Dinitrogehalt des erhaltenen Produkts und bei der Toluolnitrierung die Menge der *ortho*- und *para*-Isomeren. Die Berrechnung der Ausbeute geschah stets mit Bezug auf das zu nitrierende Material.

In der ersten Meßserie prüften wir — bei konstanter Benzol- und Nitriersäure- bzw. Toluol- und Nitriersäure-geschwindigkeit — den Einfluß der Bandlänge auf die Produktion. Die Meßergebnisse veranschaulicht Tabl. I. Die Abhängigkeit der Ausbeute von der Bandlänge hatten wir schon in früheren Arbeiten anläßlich der Sulfonierung von Dodecylbenzol bestimmt [7].

Die graphische Darstellung der Resultate zeigt den Zusammenhang zwischen Bandlänge und Produktion (Abb. 3). Es zeigt sich, daß von 100 cm Bandlänge an der Produktionswert praktisch unverändert bleibt. Zu jeder Dosierungsgeschwindigkeit gehört eine optimale Länge, über die sich die Steigerung der Länge als unzweckmäßig erweist. Bei der von uns benutzten Benzol- und Toluoldosierungsgeschwindigkeit von 50 g/Stunde betrug die optimale Bandlänge 100 cm. Beim Nitrieren von Benzol im Filmreaktor, wie auch im Bandreaktor, entsteht neben dem Nitrobenzol auch Dinitrobenzol, aber in niedrigerem Prozentsatz als bei der fraktionierten, klassischen Nitrierung. Wie aus Tab. I und II ersichtlich, ist der Dinitrobenzolgehalt zwischen 1,2 und 2,8%. Die Änderung des Dinitrophenolgehaltes in Verbindung mit der Bandlänge zeigt Abb. 4. Der Charakter der Kurve

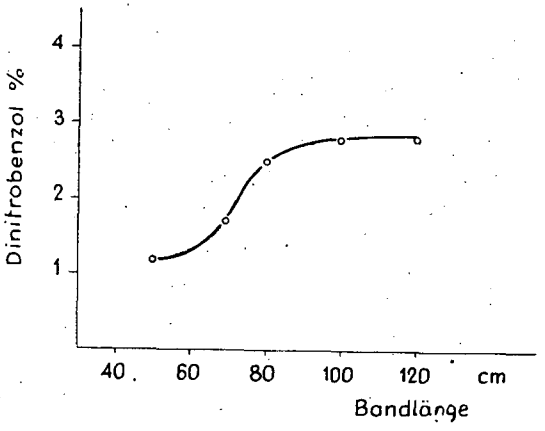

Abb. 4. Abhängigkeit des Dinitrobenzolgehaltes von der Bandlänge

erinnert an die Relationen von Bandlänge und Produktion im Falle von Nitrobenzol und Nitrotoluol.

Tab. I veranschaulicht auch deutlich, daß bei Nitrotoluol das Verhältnis der Isomeren bei den verschiedenen Bandlängen nahezu gleich ist.

Tabelle I

Abhängigkeit der Produktion von der Bandlänge bei Nitrierung von Benzol und Toluol

Nitriersäure	HNO_3/Benzol Molverhältnis	Dosierungsgeschwindigkeit Benzol cm^3/h	Dosierungsgeschwindigkeit Nitriersäure cm^3/h	Bandlänge cm	Nitrobenzolausbeute %	Dinitrobenzolgehalt %	
55 ml 65% HNO_3 65 ml cc. H_2SO_4	1,2	57,5	120	50	29,8	1,2	
				70	36,0	1,7	
				80	46,6	2,5	
				90	64,7	2,55	
				100	77,6	2,75	
				120	78,0	2,8	
					Nitrotoluolausbeute %	*o*-Nitrotoluolgehalt %	*p*Nitrotoluolgehalt %
35,2 ml 65% HNO_3 40,2 ml cc. H_2SO_4	0,9	58	75,5	40	31,6	73,3	26,6
				60	33,3	73,0	27,0
				80	48,1	73,6	26,4
				100	75,2	73,3	26,7
				120	76,2	72,8	27,2

In der nächsten Versuchsreihe wurde bei Verwendung eines 100 cm langen Bandes die Wirkung der Änderung der Dosierungsgeschwindigkeit auf die Produktion untersucht. Die Meßergebnisse sind in Tab. II dargestellt. Mit der Veränderung der Dosierungsgeschwindigkeit des Benzols wurde natürlich auch die Dosierungsgeschwindigkeit der nitrierenden Säure proportional geändert, um die Beständigkeit des HNO_3/Benzol-Molverhältnisses zu sichern.

Tabelle II

Abhängigkeit der Produktion von der Dosierungsgeschwindigkeit bei 100 cm Bandlänge

Dosierungsgeschwindigkeit cm^3/h		Nitrobenzolausbeute (%)
Benzol	Nitriersäure	
50	101,5	85,1
60	125	74,9
70	146	64,2
90	188	50,5
120	249	40,8
140	292	37,1

Aus dem Zusammenhang von Dosierungsgeschwindigkeit und Produktion (Abb. 5) ist ersichtlich, daß mit der Steigerung der Dosierungsgeschwindigkeit in dem von uns angewandten Benzoldosierungsintervall von 50—140 cm^3/h die Produktion nachläßt. Dies erklärt sich daraus, daß an einer gegebenen Bandoberfläche die größere Dosierungsgeschwindigkeit einen dickeren Film, eine größere Laufgeschwindigkeit zeitigt, wodurch die Intensität der Mischung und die Verweil-

zeit am Bande verringert werden, also das Ausmaß der Umwandlung kleiner wird.

Die Ergebnisse zusammenfassend ist zu sagen, daß der Bandreaktor zur Verwirklichung von Nitrierungsreaktionen gut verwendbar ist. In jedem Falle muß im Interesse der Erzielung einer maximalen Umwandlung die optimale Länge und Dosierungsgeschwindigkeit ermittelt werden.

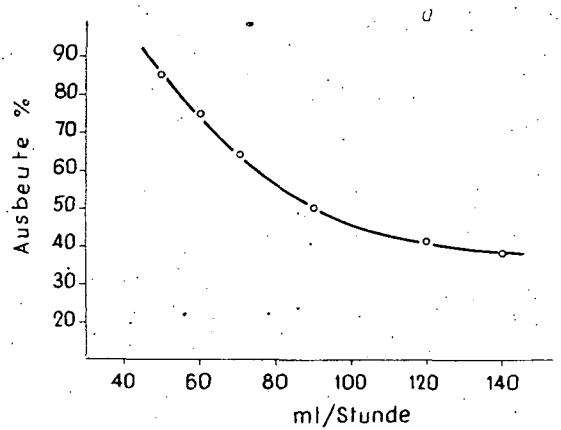

Abb. 5. Abhängigkeit der Produktion von der Dosierungsgeschwindigkeit bei Benzolnitrierung

Literatur

[1] *Szabó, M., L. Mészáros, Z. Baumann:* Acta Phys. et Chem. Szeged **20,** 177 (1974).
[2] *Mészáros, L., S. A. Gilde:* Acta Phys. et Chem. Szeged **15,** 67 (1969).
[3] *Mészáros, L., S. A. Gilde:* Fette, Seifen, Anstrichmittel **71,** 559 (1969).
[4] *Mészáros, L., F. Sirokmán, S. A. Gilde:* Acta Phys. et Chem. Szeged, Supplement, im Druck.
[5] *Újhidy, A., B. Babos:* Filmbepárlók, Filmreaktorok (Filmverdunster, Filmreaktoren, in Ungarisch), Műszaki Könyvkiadó, Budapest, 1967.
[6] *Dahmen, E. A. M.:* Chem. Weekbland **38,** 275 (1941).
[7] *Sohár, I., L. Mészáros:* Vortrag am V. Internationalen Kongress über Oberflächenaktivität. A Quimica de los Agentes Tensio-Activos. Barcelone, 9th to 13th Sept. 1968. A III 232, 7. p.: Compt. rend, 1969

ИЗУЧЕНИЕ НИТРОВАНИЯ В ЛЕНТОЧНОМ РЕАКТОРЕ

М. Сабо, Л. Месарош, Ж. Урбанич

Из серии новых типов реакторов, созданных нами за последние годы, увеличением размеров нитевого реактора изготовлен ленточный реактор. Если нитевой реактор пригоден для микропрепаративных лабораторных целей, то ленточный и пленочный реакторы могут служить для препаративных лабораторных и производственных процессов. В настоящее время применяются эти реакторы в промышленном масштабе при производстве органических эфиров фосфорной и угольной кислот. В данной работе рассмотрено применение ленточного реактора в процессах нитрования бензола и толуола.

ANWENDUNG EINES NEUARTIGEN, MIT MIKRODOSIERUNG ARBEITENDEN FADENREAKTORS BEI NITRIERUNGSREAKTIONEN

Von

M. SZABÓ, L. MÉSZÁROS und Z. BAUMANN

Institut für Angewandte Chemie der Attila-József-Universität Szeged,

(Eingegangen am 20. November 1973)

Im Laufe unserer technologischen Forschungen haben wir eine Filmreaktorenfamilie entwikkelt, zu dem auch der in der vorliegenden Arbeit beschriebene Fadenreaktor gehört. Dieser kontinuierliche Mikroreaktor ist zur Herstellung von 0,5—2,0 g Substanz pro Stunde geeignet. Die Reaktionskomponenten treten an der Fadenoberfläche unter Bildung eines feinen Films miteinander in Berührung. Mit diesem Reaktor lassen sich chemische und physikalische Prozesse in der heterogenen Phase im Mikromaßstabe verwirklichen. Es wird die Verwendbarkeit des Reaktors bei Nitrierungsreaktionen untersucht.

Aufbau und Funktion des Fadenreaktors

Der Reaktor besteht aus zwei Y-förmig zusammengedrehten Fäden, die in der Längsachse eines temperierbaren, doppelwandigen Glasrohres Platz nehmen (Abb. 1). Probenentnahme in verschiedener Höhe des Fadens ist im Falle der in Abb. 2 ersichtlichen Zusammenstellung möglich.

Der Fadenreaktor [1—4] ist reaktortechnisch als eindimensionaler kontinuierlicher Filmreaktor zu betrachten. Als eindimensional, weil der Durchmesser des Fadens im Verhältnis zu seiner Länge zu vernachlässigen ist und so die physikalischen und chemischen Erscheinungen — einen stationären Betrieb vorausgesetzt — sich nur entlang der Längsache ändern; als kontinuierlich, weil die Reaktionskomponenten und die entstandenen Produkte ohne Unterbrechung zugeführt, bzw. aus dem System entfernt werden können. Die Strömung ist ständig, ohne Materialanhäufung. Ein Filmreaktor ist er insofern, als die in Reaktion tretenden Stoffe an der Oberfläche des Fadens unter Bildung eines dünnen Films miteinander in Kontakt treten.

Zwecks gleichmäßiger Zuführung der Reaktionskomponenten haben wir eine Mikrodosier-Bürette konstruiert. An der Oberfläche der in der Mikrobürette befindlichen Flüssigkeit kann durch einen vorher einstellbaren Reduktor ein Luft- oder Inertgas-Überdruck von 0,1—2,0 At hergestellt werden. Am unteren Teil endet die Bürette in einer Kapillare, die die in der Bürette enthaltene Flüssigkeit auf den Y-förmigen Faden dosiert und eine gleichmäßige Zuführung von 0,1—4,0 ml pro Stunde sichert. Durch gesonderte oder simultane Änderung von Druck, Kapillarenlänge und Kapillarenquerschnitt läßt sich die gewünschte Dosierungsgeschwindigkeit reproduzierbar einstellen. Durch hydrostatische Druckänderungen wird die gelichmäßige Dosierung nicht wahrnehmbar beeinflußt.

Im Reaktor sind Reaktionen in der Flüssigkeit—Flüssigkeit- und in der Flüssigkeit—Gas-Phase gleichermaßen durchführbar.

Das Material des Fadens kann stets der Natur der jeweiligen chemischen Reaktion entsprechend gewählt werden: er kann aus Glas, imprägniertem Glas, Textilie, Quarz und Keramik bestehen.

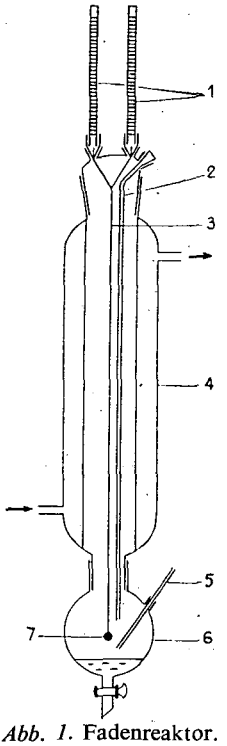

Abb. 1. Fadenreaktor. 1: Mikrodosier-Bürette; 2: Gasableitungsrohr; 3: Glasfaden; 4: Doppelwandiger Reaktorkörper aus Glas; 5: Kapillare zur Probenentnahme des Produkts; 6: Sammelkolben mit Ablaßhahn; 7: Glaskugel zum Fixieren des Fadens

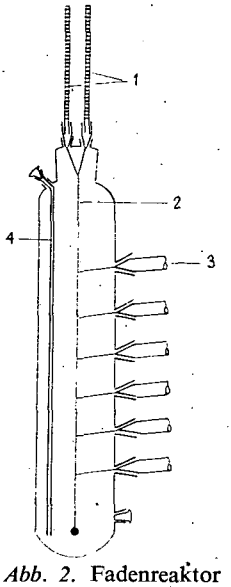

Abb. 2. Fadenreaktor mit Probenentnahme-Kapillaren in verschiedenen Höhen. 1: Mikrodosier-Bürette; 2: Glasfaden; 3: Probenentnahme-Kapillaren: 4: Gasableitungsrohr

Im Reaktor spielt der Faden eine sehr wichtige Rolle; deshalb ist es im Interesse der Reproduzierbarkeit der Reaktionen zweckmäßig, folgende Eigenschaften konstant zu halten:

a) die chemische Zusammensetzung des Fadenmaterials (um Änderungen eventueller heterogener katalytischer Wirkungen zu vermeiden)

b) die physikalischen und geometrischen Eigenschaften des Fadens (Festigkeit, Zwirnung, Fadenlänge und -dicke, Rauheit der Oberfläche), die hinsichtlich der Kontaktdauer, des Diffusionsquerschnittes sowie der Stabilisierung des Vermischungsgrades wesentlich sind.

Im Falle von nicht mischbaren Flüssigkeiten konnten wir anhand mikroskopischer Untersuchungen feststellen, daß am Faden eine vorwiegend laminare Strömung zustandekommt [5].

Wir haben die Anwendbarkeit des Reaktors in chemischen Reaktionen erprobt und bei den Versuchen einen Glasfaden benutzt, der aus 100 Einzelfäden von je 20—30 µm Durchmesser bestand. Die Länge des Fadens wurde der optimaler Umwandlung entsprechend gewählt.

Nitrierung von Chlorbenzol am Fadenreaktor

Der Fadenreaktor ist — seinem Mikrofilm-Reaktor-Charakter entsprechend — besonders zur Durchführung von stark exothermischen Reaktionen in heterogener Phase, wie z. B. Nitrierung und Sulfonierung, geeignet. Als Modellverbindung bei der Untersuchung der Nitrierungsreaktion wählten wir Chlorbenzol.

Die Versuche wurden bei verschiedenen Temperaturen und Dosierungsgeschwindigkeiten, sowie bei Verwendung von zwei HNO_3/Chlorbenzol-Molverhältnissen unternommen. Die Reaktion wurde von dem Zeitpunkt verfolgt, als im Reaktor und am Faden der stationäre Zustand erreicht war, d.h. als ein dem thermodynamischen Gleichgewicht entsprechend zusammengesetztes Reaktionsgemisch den Reaktor verließ.

Die zum Erreichen des Gleichgewichtes erforderliche Zeit wird vor allem von dem Verhältnis der Reaktionskomponenten, von ihrer Mischbarkeit, im Falle von nicht-mischbaren Flüssigkeitsphasen von der Größe der Berührungsfläche der Phasen und von der Zuführungsgeschwindigkeit bestimmt.

Bei Erhöhung der Dosierungsgeschwindigkeit des Chlobenzols wurde auch die Zufuhr der Nitriersäure proportional erhört. Das quantitative Verhältnis der *ortho*- und *para*-Isomeren im Reaktionsgemisch wurde mittels IR Spektroskopie bestimmt.

Die Länge des bei den Versuchen benutzten Fadens betrug 44 cm.

Die verwendete Nitriersäure hatte folgende Zusammensetzung: 1 ml konz. HNO_3 (spez. Gew.: 1,54) und 1,2 ml konz. H_2SO_4. Meßergebnisse sind in Tab. I und II zusammengefaßt. Die Ausbeutewerte wurden auf Chlorbenzol bezogen berechnet.

Wie die Tabellen I und II deutlich zeigen, nimmt bei Erhöhung der Temperatur und des HNO_3/Chlorbenzol-Molverhältnisses die Ausbeute zu, bei Steigerung der Dosierungsgeschwindigkeit dagegen ab. Letzteres erklärt sich daraus, daß mit höherer Dosierungsgeschwindigkeit der Film dicker wird, das Material schneller am Faden entlang rinnt und so die Komponenten einender kürzere Zeit berühren, was einen geringeren Umwandlungsgrad zur Folge hat.

Aus Tabelle II geht hervor, daß das Verhältnis der Isomere unter den von uns angewandten Versuchsbedingungen unverändert blieb, aber von den in der Literatur angegebenen Mengen [6] — nämlich 30,1% *o*-Nitrochlorbenzol und 69,9% *p*-Nitrochlorbenzol — abwich.

Tabelle I

Produktion bei einem HNO_3/Chlorbenzol Molverhältnis von 1:3 und verschiedenen Dosierungsgeschwindigkeiten und Reaktionstemperaturen

Reaktionstemperatur °C	Dosierungsgeschwindigkeit		Reaktionsdauer Min.	Gewicht des isolierten Nitrochlorbenzols g	Ausbeute %
	Chlorbenzol cm^3/h	Nitriergemisch cm^3/h			
25	2	2,4	30	0,6211	40,7
	1,7	2	35	0,6623	41,9
	1,5	1,8	40	0,7004	43,1
	1,3	1,6	45	0,7012	43,4
	1,2	1,44	50	0,7125	44,1
40	2	2,4	30	0,7475	48,5
	1,7	2	35	0,7595	49,7
	1,2	1,4	50	0,7805	50,7
60	2	2,4	30	0,8495	55,0
	1,5	1,8	40	0,8688	56,4
	1,2	1,4	50	0,8717	57,1

Tabelle II

Produktion im Falle eines HNO_3/Chlorbenzol Molverhältnisses von 2,5 und verschiedenen Temperaturen und Dosierungsgeschwindigkeiten

Reaktionstemperatur °C	Dosierungsgeschwindigkeit		Reaktionsdauer Min	Gewicht des Nitrochlorbenzols g	Ausbeute %	Gehalt des Produktes an	
	Chlorbenzol cm^3/h	Nitriersäure cm^3/h				*o*-Nitrochlorbenzol %	*p*-Nitrochlorbenzol %
25	2	4,4	30	0,7817	51,3	20,65	75,54
	1,3	2,9	45	0,8613	55,8	21,52	74,58
	1,2	2,6	50	0,8939	58,11	—	—
40	2	4,4	30	0,9247	60,1	21,62	74,48
	1,7	3,8	35	0,9617	62,3	22,1	75
	1,5	3,3	40	0,9981	64,8	—	—
60	1,7	3,8	35	1,1586	75,2	21,5	75,2
	1,5	3,3	40	1,1738	76,2	22,09	74,01
	1,2	2,6	50	1,2569	81,6	—	—

Die durchgeführten Versuche beweisen, daß der Fadenreaktor zur kontinuierlichen Nitrierung von Mikromengen geeignet ist und bei optimaler Auswahl der Reaktionsparameter die Umwandlung sich im gewünschten Maß erreichen läßt.

Literatur

[1] *Mészáros, L., I. Mészáros:* Fette, Seifen, Anstrichmittel **70**, 940 (1968).
[2] *Mészáros, L.:* Fette, Seifen, Anstrichmittel **72**, 549 (1970).
[3] *Mészáros, L., I. Mészáros:* Chemia Analityczna **14**, 235 (1969).
[4] *Mészáros, L.:* A specifikus felületnövelés hatása folyamatos kémiai átalakulásokra. Komplett katalitikus laboratóriumok, II. (Einfluß der Steigerung der spezifischen Oberfläche auf kontinuierliche chemische Umwendlungen, in Ungarisch) Acta Phys. et Chem. Szeged **16**, Supplementum I. (1970).
[5] *Mészáros, I.:* Doktor-Dissertation, Szeged, 1968.
[6] *Groggins, P. H.:* A szintetikus szerves vegyipar alapeljárásai. (Die Grundverfahren der synthetischen organisch-chemischen Industrie, in Ungarisch). Műszaki Könyvkiadó, Budapest, 1958, S. 12.

ПРИМЕНЕНИЕ НИТЕВОГО РЕАКТОРА, ИМЕЮЩЕГО МИКРОДОЗАТОР НОВОЙ КОНСТРУКЦИИ, В РЕАКЦИЯХ НИТРОВАНИЯ

М. Сабо, Л. Месарош, З. Бауман

При исследовании технологии химических процессов разработана серия реакторов нового типа. Описанный в данной работе нитевой реактор, является одним из представителей этой серии. Этот микрореактор беспрерывного действия пригоден для получения 0,5—2 г. вещества в час. Компоненты реакции приходят в соприкосновение на поверхности нити в образующейся тонкой пленке. Реактор пригоден для проведения гетерогенных физических и химических процессов в микроразмерах. В данной работе рассмотрено применение реактора в процессе нитрования.

VERWENDUNG DER FADENCHROMATOGRAPHIE ZUR TRENNUNG VON ^{14}C- UND ^{3}H-MARKIERTEN VERBINDUNGEN

Von

F. SIROKMÁN, E. KÖVES, M. SZABÓ und L. MÉSZÁROS

Institut für Radiochemie, Pflanzenphysiologie und Angewendte Chemie der Attila-József-Universität, Szeged

(Eingegangen am 2. März 1974)

Auf Glasplatten mit verschieden großen Trogmulden gelang die Trennung eines Konjugates aus ^{14}C-markierten Indol-3-Essigsäure-Metaboliten und ^{3}H-markierter Asparaginsäure mittels Silikagel-Fadenchromatographie. Bei Trennung eines Materialgemisches von 1 μg war autoradiographisch eine Aktivität von 10^{-4} μCi nachweisbar.

Das Ziel der Entwicklung der Materialisolierungsmethoden ist, einerseits die Trennung verschiedener Verbindungen auch im Falle von chemisch geringfügig erscheindenden Unterschieden immer wirksamer zu gestalten, anderseits durch mikroanalytische Methoden auch den Nachweis und die Trennung geringster Materialmengen zu ermöglichen. Die benutzten Methoden sind oft einfach and genau. Das als Fadenchromatographie bezeichnete Verfahren hat erstmalig EDSTRÖM [1] für fadenelektrophoretische Zwecke verwandt. MÉSZÁROS und MÉSZÁROS [2] arbeiteten ein Verfahren aus, das die chromatographische Trennung geringster Mengen verschiedener Stoffe gestattet. Die Verfasser stellten verschiedene Trägerfäden her, teils indem sie auf Glasplatten parallele Rinnen ausätzten und diese mit dem entsprechenden Reagens bzw. mit der festen Phase beschickten. Als eine weitere Möglichkeit zur Ausgestaltung der Trägerfäden beschreiben sie die Anwendung von zwischen Glasrahmen gespannten Fäden aus verschiedenem Material (Glas, Polyester usw.), mit dem Träger versehen, oder u.U. auch ohne Träger [3].

Mit Hilfe der Fadenchromatographie läßt sich die Trennung kleiner Materialmengen, u. zw. nach Literaturangaben [4—6] bis zu 1—5 μg herab, erreichen. Die Anwendbarkeit der Methoden haben wir im Falle von radioaktiv markierten Verbindungen untersucht. Es wurden Glasplatten mit Rinnen verschiedener Größe benutzt, in denen das geeignete Adsorbent mit den bei der Dünnschichtchromatographie üblichen Methoden angewandt wurde. Die kleinsten trennbaren Isotopen-Konzentrationen wurden mittels der autoradiographischen Röntgen-Filmtechnik kontrolliert. Im Falle der ^{3}H-markierten Verbindungen benützten wir die Methode von LÜTHI und WASER [7], wonach Silikagel und Anthracen zuvor in einem Gemisch von 1:1 homogenisiert und als Adsorbent verwendet wird. Um die Verteilung des Materials am Faden zu verfolgen, verwandten wir zuerst einen Packard'schen Tricarb-Chromatogramm-Scanner, doch erwies sich zur Messung der kleinen Aktivitäten die

Autoradiographie als empfindlicher. Bessere Resultate waren durch Eluierung und Flüssigkeits-Scintillationsmessung der aktiven Flecken zu erreichen.

Bei Benutzung der autoradiograpischen Meßtechnik ergab sich die Nachweisbarkeitsgrenze zu $4 \cdot 10^{-4}$ μCi. Zur Bestimmung wurden Serien von ^{14}C-markierter Verbindungen mit bekannter Aktivität bei einwöchiger Expositionsdauer benützt. Bei der Anwendung markierter Verbindungen mit hoher spezifischer Aktivität war aufgrund der Nachweisgrenzen-Aktivität das Separieren und der Nachweis von Mengen bis zu etwa 10^{-9} g möglich.

Die Anwendbarkeit des Verfahrens in biologischen Systemen wurde mittels der Trennung der Metabolite der 2-^{14}C-Indol-3-essigsäure aus pflanzlichem Material geprüft. In früheren Untersuchungen mit Papier- und Dünnschichtchromatographie [8] gelang uns mit größeren Materialmengen nur der Nachweis von insgesamt drei radioaktiven Metaboliten, während mit der Fadenchromatographie fünf Stoffe mit R_f-Werten von 0,07, 0,35, 0,36, 0,75 bzw. 0,80 zu unterscheiden waren. Die Methode ist somit nicht nur von größerer Empfindlichkeit, sondern sichert auch eine bessere Trennung als die Papier- bzw. die Dünnschitchchromatographie.

In weiteren Versuchen wurden Pflanzenbestandteile mit ^{3}H-Asparaginsäure inkubiert. Bei der Fadenchromatographie der Metabolite gelang es, das *in vivo* entstandene Konjugat der Indol-3-essigsäure und der Asparaginsäure, die radioaktive Indol-3-acetyl-asparaginsäure, nachzuweisen, was mit der Dünnschichtchromatographie nicht zu erreichen war.

Literatur

[1] *Edström J. E.:* Nature **32**, 809 (1951).
[2] *Mészáros L., I. Mészáros:* Fette, Seifen, Anstrichmittel **70**, 486 (1968).
[3] *Lenk H. P., H. Gruber:* Mikrochim. Acta (Wien) **1972**, 646.
[4] *Mahon J., A. A. Benedetti—Pichler:* Mikrochim. Acta (Wien) **1960**, 831.
[5] *Mészáros L.:* Fette, Seifen, Anstrichmittel **72**, 870 (1970).
[6] *Tichonov G. S.* und *I. A. Tichomirov:* Z. Anal. Chim. **24**, 1258 (1969).
[7] *Lüthi U., P. F. Waser:* Nature **205**, 1190 (1965).
[8] *Köves E., F. Sirokmán:* Biochem. Physiol. Pflanzen **164**, 276 (1973).

ПРИМЕНЕНИЕ ФИБРИЛЛЯРНОЙ ХРОМАТОГРАФИИ ДЛЯ РАЗДЕЛЕНИЯ ВЕЩЕСТВ МЕЧЕНЫХ ^{14}C И ^{3}H

Ф. Широкман, Е. Кевеш, М. Сабо, Л. Месарош

С применением силикагельной фибриллярной хроматографии удалось провести разделение смеси индол-3-уксуснокислых метаболитов и аспарагиновой кислоты, меченых ^{14}C и ^{3}H соответственно. Применяя смеси веществ в количестве 1 μg, авторадиографически можно было обнаружить 10^{-4} μCi.

TOMI PRIORES

Acta Chemica, Mineralogica et Physica,	Tom.	I,	Fasc.	1—2,	1928—29.
Acta Chemica, Mineralogica et Physica,	Tom.	II,	Fasc.	1—2,	1932.
Acta Chemica, Mineralogica et Physica,	Tom.	III,	Fasc.	1—3,	1934.
Acta Chemica, Mineralogica et Physica,	Tom.	IV,	Fasc.	1—3,	1934.
Acta Chemica, Mineralogica et Physica,	Tom.	V.	Fasc.	1—3,	1937.
Acta Chemica, Mineralogica et Physica,	Tom.	VI,	Fasc.	1—3,	1938.
Acta Chemica, Mineralogica et Physica,	Tom.	VII,	Fasc.	1—3,	1939.
Acta Chemica et Physica,	Tom.	I,	Fasc.	1—2,	1942.
Acta Chemica et Physica,	Tom.	II,	Fasc.	1—6,	1948—50.
Acta Physica et Chemica, Nova series	Tom.	I,	Fasc.	1—4,	1955.
Acta Physica et Chemica, Nova series	Tom.	II,	Fasc.	1—4,	1956.
Acta Physica et Chemica, Nova series	Tom.	III,	Fasc.	1—5.	1957.
Acta Physica et Chemica, Nova series	Tom.	IV,	Fasc.	1—2,	1958.
Acta Physica et Chemica, Nova series	Tom.	IV,	Fasc.	3—4,	1958.
Acta Physica et Chemica, Nova series	Tom.	V,	Fasc.	1—2,	1959.
Acta Physica et Chemica, Nova series	Tom.	V,	Fasc.	3—4,	1959.
Acta Physica et Chemica, Nova series	Tom.	VI,	Fasc.	1—4,	1960.
Acta Physica et Chemica, Nova seties	Tom.	VII,	Fasc.	1—2,	1961.
Acta Physica et Chemica, Nova series	Tom.	VII,	Fasc.	3—4,	1961.
Acta Physica et Chemica, Nova series	Tom.	VIII,	Fasc.	1—2'	1962.
Acta Physica et Chemica, Nova series	Tom.	VIII,	Fasc.	3—4,	1962.
Acta Physica et Chemica, Nova series	Tom.	IX,	Fasc.	1—2,	1963.
Acta Physica et Chemica, Nova series	Tom.	IX,	Fasc.	3—4.	1963.
Acta Physica et Chemica, Nova series	Tom.	X,	Fasc.	1—2,	1964.
Acta Physica et Chemica, Nova series	Tom.	X,	Fasc.	3—4,	1964.
Acta Physica et Chemica, Nova series	Tom.	XI,	Fasc.	1—2,	1965.
Acta Physica et Chemica, Nova series	Tom.	XI,	Fasc.	3—4,	1965.
Acta Physica et Chemica, Nova series	Tom.	XII,	Fasc.	1—2,	1966.
Acta Physica et Chemica, Nova series	Tom.	XII,	Fasc.	3—4,	1966.
Acta Physica et Chemica, Nova series	Tom.	XIII,	Fasc.	1—2,	1967.
Acta Physica et Chemica, Nova series	Tom.	XIII,	Fasc.	3—4.	1967.
Acta Physica et Chemica, Nova series	Tom.	XIV,	Fasc.	1—2'	1968.
Acta Physica et Chemica, Nova series	Tom.	XIV,	Fasc.	3—4.	1968.
Acta Physica et Chemica, Nova series	Tom.	XV,	Fasc.	1—2,	1969.
Acta Physica et Chemica, Nova series	Tom.	XV,	Fasc.	3—4,	1969.
Acta Physica et Chemica, Nova series	Tom.	XVI,	Fasc.	1—2,	1970.
Acta Physica et Chemica, Nova series	Tom.	XVI,	Fasc.	3—4,	1970.
Acta Physica et Chemica, Nova series	Tom.	XVII,	Fasc.	1—2,	1971.
Acta Physica et Chemica, Nova series	Tom.	XVII	Fasc.	3—4,	1971.
Acta Physica et Chemica, Nova series	Tom.	XVIII	Fasc.	1—2,	1972.
Acta Physica et Chemica, Nova series	Tom.	XVIII	Fasc.	3—4,	1972.
Acta Physica et Chemica, Nova series	Tom.	XIX	Fasc.	1—2,	1973.
Acta Physica et Chemica, Nova series	Tom.	XIX,	Fasc.	3,	1973.
Acta Physica et Chemica, Nova series	Tom.	XIX,	Fasc.	4,	1973.

A kiadásért felelős: Dr. Leindler László
1974
A kézirat a nyomdába érkezett: 1974. márc. 6. Megjelenés: 1974. augusztus
Példányszám: 550 Ábrák száma: 81 Terjedelem: 16,5
Készült monó szedéssel, íves magasnyomással, az MSZ 5601—54 és az MSZ 5602—50 A szabványok szerint
74-1091 — Szegedi Nyomda